THE UNIVERSITY
of EDINBURGH

Thesis Title: Acute and chronic effects of systemic inflammation on P301S tau mouse model of neurodegeneration

Megan Torvell

Doctor of Philosophy The University of Edinburgh 2017

Contents

Tables

Figures

List of Abbreviations

AD	Alzheimer's Disease
AGD	Argyrophilic Grain Disease
Aldh1l1	Aldehyde Dehydrogenase 1 Family, Member L1
ALS	Amyotrophic Lateral Sclerosis
ANOVA	Analysis of Variance
APC	Antigen Presenting Cells
Apoe	Apolipoprotein E
APP	Amyloid Precursor Protein
ATP	Adenosine Triphosphate
AUC	Area Under the Curve
Axl	Gene Encoding Tyrosine Kinase Receptor
Aβ	Amyloid -B
BBB	Blood Brain Barrier
BDNF	Brain-Derived Neurotrophic Factor
BIC	Bayesian Information Criteria
BrdU	Bromodeoxyuridine
C57BL/6J	Control Mice - Background Strain of P301S Mice - Referred To Throughout As "C57BL/6"
CAM	Confusion Assessment Method
CaMKII	Ca2+/Calmodulin-Dependent Protein Kinase II
CBD	Corticobasal Degeneration
CCL19	Chemokine (C-C Motif) Ligand 19
CCL21	Chemokine (C-C Motif) Ligand 21
CD11b	Complement Receptor 3 (CR3)
CD14	TLR4 Co-Stimulator
CD200	Cluster of Differentiation 200
CD200R	Cluster of Differentiation 200 Receptor
CD28	Cluster of Differentiation 28 - T Cell Costimulation

CD4	Cluster of Differentiation 4
CD45	Cluster of Differentiation 45
CD68	Cluster of Differentiation 68
CD80/CD86	MHCI /II Co-Stimulator
CDK5	Cyclin-Dependent Kinase 5
cDNA	Complimentary DNA
CI	Confidence Interval
Clec7a	Gene, Encoding Pattern Recognition Receptor Dectin-1
CMVO	Circumventricular Organs
CNS	Central Nervous System
COX-1 or -2	Cyclooxygenase 1 Or 2
Csf1	Gene Encoding Macrophage Colony-Stimulating Factor
CT	Cycle Threshold Value
C_T(GOI)	The C_T Value of The Gene of Interest
C_T(HK)	The C_T Value of The House Keeper
CX3CL1	Fractalkine
CX3CR1	Fractalkine Receptor
CXCL12	C-X-C Motif Chemokine Ligand 12
Cybb	Gene Encoding Pro-Inflammatory Oxidase Nox2
DAB	3′,3′-Diaminobenzidine
DAMPs	Danger-Associated Molecular Pattern
dcLN	Deep Cervical Lymph Nodes
DCX	Neuronal Migration Protein Doublecortin
DNA	Deoxyribonucleic Acid
DRS-R98	Delirium Rating Scale - Revised - 98
EAE	Experimental Autoimmune Encephalomyelitis
EPM	Elevated Plus Maze
ERK6	A Mitogen-Activated Protein (MAP) Kinase-Related Serine/Threonine Kinase
FTD	Frontotemporal Dementia

FTDP-17	Frontotemporal Dementia and Parkinsonism Linked to Chromosome 17
GABA	Gamma-Aminobutyric Acid
GFAP	Glial Fibrillary Acidic Protein
GLAST	Glutamate-Aspartate Transporter
GLT-1	Glutamate Transporter-1
Gly	Glycine
GS	Glutamine Synthetase
GSK3	Glycogen Synthase Kinase 3
GTO	Granular Tau Oligomers
HMGB1	High-Mobility Group Box-1 Protein
HPRT	Hypoxanthine-Guanine Phosphoribosyltransferase
Hsp27	Heat Shock Protein
IBA1	Ionized Calcium-Binding Adapter Molecule 1
IFNγ	Interferon Gamma
Ig	Immunoglobulin
IL-10	Interlukein-10 (Or Cytokine Synthesis Inhibitory Factor CSIF)
IL-12	Interlukein-12
IL-1β	Interlukein-1β
IL-4	Interlukein-4
IL-6	Interlukein-6
IMC	Information-Memory-Concentration (Subtest of The Blessed Dementia Rating Scale)
ISEL	In Situ End Labelling
ITAMs	Immunoreceptor Tyrosine-Based Activation Motifs
itgax	Gene Encoding CD11c, A Subunit of Complement Component 3 Receptor
ITIMs	Immunoreceptor Tyrosine-Based Inhibition Motifs
JNK	C-Jun N-Terminal Kinases

ki67	Also Known As MKI67, Is A Cellular Marker For Proliferation
LBP	LPS Binding Protein TLR4 Co-Stimulator
LPS	Lipopolysaccharide
MAP	Microtubule Associated Protein
MAPK	Mitogen Activated Protein Kinase
MAPT	Microtubule Associated Protein Tau (Gene Name)
MARK	Microtubule-Affinity Regulating Kinase
MCAO	Middle Cerebral Artery Occlusion
MCP-1	Monocyte Chemoattractant Protein 1 (Also Known as CCL2)
MCSF	Macrophage Colony-Stimulating Factor
MD-2	TLR4 Co-Stimulator
MHC class I/II	Major Histocompatibility Complex - I or II
MHV	Mouse Hepatitis Virus
MMSE	Mini-Mental State Exam
MND	Motor Neurone Disease
MS	Multiple Sclerosis
MWM	Morris Water-Maze
NeuN	Is A Specific Marker of Neuronal Cells
NeuroD	Neurogenic Differentiation 1 - Transcription Factor
NFT	Neurofibrillary Tangles
NFκB	Nuclear Factor Kappa-Light-Chain-Enhancer of Activated B Cells
NK-cells	Natural Killer Cells
NLR	NOD-Like Receptors
NLRP3-inflammasome	NACHT, LRR And PYD Domains-Containing Protein 3 - Inflammasome
NO	Nitric Oxide
NOS / iNOS	Nitric Oxide Synthase / Inducible Nitric Oxide Syntase

NSAIDS	Non-Steroidal Anti-Inflammatory Drugs
ONS	Office for National Statistics
p21Cip1 and p27Kip1	Cyclin-D-CDK4 Complex Inhibitors
p25	Cleaved Fragment of P35
P301L	Proline to Leucine Mutation Position 301 Of Tau Protein
P301S	Proline to Serine Mutation Position 301 Of Tau Protein
p35	The Constitutively Expressed Co-Activator of CDK5
p38	Mitogen-Activated Protein Kinases
PAMPs	Pathogen Associated Molecular Pattern
PBBS	Peripheral Benzodiazepine Binding Sites
PBS	Phosphate Buffered Saline (See Solutions for Details)
PCNA	Proliferating Cell Nuclear Antigen
PD	Parkinson's Disease
PDPKs	Proline-Directed Protein Kinases
PFA	Paraformaldehyde (See Solutions for Details)
PGD_2	Prostaglandin D2
PGE2	Prostaglandin E2
PGE2	Prostaglandin E2
PHF	Paired-Helical Filaments
PiD	Pick's Disease
PKA	Cyclic-AMP-Dependent Kinase
PO/AH	Preoptic Area and The Anterior Hypothalamus
PP2A/2B	Phosphatase Proteins 2A/2B
PrP	Prion Protein
Pro	Proline
PRRs	Pattern Recognition Receptors
PSP	Progressive Supranuclear Palsy
PTX3	Pentraxin-Related Protein
qPCR	Quantitative Polymerase Chain Reaction

R406W	Arginine to Tryptophan Mutation at Position 406 Of Tau Protein
RANTES	T-Cell Chemoattractant Chemokine
Rb tract	Rubrospinal Tract
RNA	Ribonucleic Acid
ROS	Reactive Oxygen Species
RQ	Relative Quantity
SAPK4	Stress-Activated Protein Kinases
Ser	Serine
SF	Straight Filaments
SOD1	Superoxide Dismutase
STEAP4	Six-Transmembrane Epithelial Antigen of Prostate 4 - Metalloreductase
TCA cycle	Tricarboxylic Acid Cycle
TCR	T-Cell Receptor
TDP43	Transactivation Response Element (TAR) DNA-Binding Protein-43 (TDP-43)
TGF-β	Transforming Growth Factor Beta
Thr	Threonine
Thy 1.2	Otherwise Cluster of Differentiation 90 (CD90)
TLR2	Toll-Like Receptor 2
TLR4	Toll-Like Receptor 4
TNFR	TNF-A Receptor
TNF-α	Tumour Necrosis Factor
TNS	Tris Non-Saline Solution
TRADD	TNF-Receptor Associated Death Domain Protein
TRAF	TNF Receptor Associated Factor 2 Protein
TREM2	Triggering Receptor Expressed on Myeloid Cells 2
TSEs	Transmissible Spongiform Encephalopathies
TSPO	Translocator Protein

TUC-4	(TOAD/Ulip/CRMP) Family Of Proteins Involved In Growth Cone Signaling
TUNEL	Terminal Deoxynucleotide Transferase Mediated Dutp Nick-End Labelling
USVs	Ultrasonic Vocalisations
VEGFR3	Vascular Endothelial Growth Factor Receptor 3
YFP	Yellow Fluorescent Protein
YM1	Chitinase-3-Like Protein 3

Declaration

I declare that this thesis has been composed solely by myself and that it has not been submitted, in whole or in part, in any previous application for a degree. Except where states otherwise by reference or acknowledgment, the work presented is entirely my own.

_____

Megan Torvell

Acknowledgements

First, I would like to thank Prof Siddharthan Chandran, Prof Alasdair MacLullich and Dr Colm Cunningham for the opportunity to work on this project, a topic which is so close to my heart. Your diverse backgrounds and the breadth of your collective experience have helped broaden my understanding and approach to the topic.

I would like to thank Dr David Hampton for showing me the ropes and then untangling them when I wound them up in knots.

Dr Pete Connick for all of your help with the statistics, your endless patience, and for your kind, encouraging words when they were really needed.

Thank you to all the lovely people in the March unit; Jenni, Kerry (for the photos too!), Jamie, Lynn for brightening up my days and for all your hard work.

Thank you to members of the Chandran lab for their help, support and friendship; David Story, Sachin, Navneet, Bhuvaneish. I am especially grateful to my wonderful friends from the lab Ghazal, Elaine, and Sam – I hope for science's sake that you all continue to be the strong and capable women in science that you already are. Thank you for being there when it got tough!

Thank you to Jane Saffell for setting me off on this path. Graham, for always existing nearby. Thank you, Annelies for being you and for reminding me about work-life-balance. Thank you to Jamie and Rhi for adopting me early on. Mélissa for Image J/Fiji help. Edel for the instant friendship and (on-going!) moral support.

Thank you to my Weird Pocket Lovers for providing a constant soundtrack to my life.

To my family: I would not be where I am without your continual guidance and unwavering support. Thank you to my mum Holly; my dad Matt; my sister Boo; my ETOD Brandon; my granny Joan. Thank you to the Beauts.

Finally, I would like to thank my best friend Peter. He is my rock.

I would like to dedicate this thesis to my beautiful and kind hearted Grandma Betty Lilian Hannam. I wrote this for you.

Abstract

Systemic inflammation is thought to be an important driver in chronic neurodegeneration. During systemic infection, the inflammatory status of the periphery is communicated to the brain and conserved sickness behaviours initiated. However, in the context of dementia the same inflammatory stimulus might trigger delirium.

Delirium is a severe, transient neuropsychiatric condition characterised by altered levels of arousal, inattention, cognitive deficits and psychoses. Delirium and systemic inflammation exacerbate the trajectory of pre-existing dementia, and are associated with increased risk of future dementia.

Accumulating experimental studies suggest microglia are "primed" by chronic neurodegeneration, such that a subsequent inflammatory insult – central or systemic – induces an increased inflammatory response which manifests as exaggerated sickness behaviours. To date there have been no studies of microglial priming in the context of pure tau pathology, without amyloid pathology, and none investigating acute sickness behaviour in such a model. The overarching aim of this thesis is to address this gap in the literature and further our understanding of the interactions between systemic inflammation, neuroinflammation and neurodegeneration in the context of tauopathy.

The P301S mouse over-expresses human mutant tau protein under the Thy1.2 promoter. It develops hyperphosphorylated and insoluble tau accumulations and progressive neuronal loss. Consequently, P301S mice develop progressive hind limb paralysis. This study identified the horizontal bar task, a test of motor control and coordination, conducted at weekly intervals from 8-22 weeks of age, as a non-invasive measure of disease progression. In addition, a detailed temporal profile of pathological hallmarks at 8, 9, 10, 11, 12, 16 and 20 weeks of age was determined. Key results presented here demonstrate progressive, superficial neuronal loss in the cortex of P301S mice, with associated astrogliosis and surprisingly this occurs in the

absence of apparent cortical microgliosis. In stark contrast, there is progressive microgliosis in the spinal cord of P301S mice.

On this background, lipopolysaccharide (LPS), a chemical moiety found on the outer surface of gram-negative bacteria, was used to mimic a systemic bacterial infection. P301S mice and C57BL/6 control mice were injected, at 10 or 16 weeks of age, intraperitoneally with 500 μg/kg LPS or saline and were monitored in the following hours and weeks.

Acutely, P301S mice showed signs of an exaggerated, longer lasting sickness response. Importantly, exaggerated acute symptoms extended beyond those typically associated with sickness behaviour; LPS induced an exaggerated acute impairment of horizontal bar performance in P301S mice and not C57BL/6 mice – a function which is known to be impaired in P301S mice later in disease. Impairments were age-dependent in terms of timing of injection. These data suggest an interaction between acute infection and existing CNS vulnerability leading to acute neurological dysfunction that is not a feature observed in sickness in a normal animal. LPS-injected P301S mice also showed, again age-dependent, increased rate of decline in motor performance compared with controls.

There was no evidence of microglial priming in P301S mice. LPS caused an acute increase in AT8-positive phospho-tau however this did not persist until end stage. At 22 weeks of age there was significant disease-associated cortical neuronal loss in the vehicle-injected P301S mice, and additional superficial cortical neuronal loss in LPS-injected P301S mice and control mice. There was significant IBA1-positive microgliosis in the spinal cord of P301S mice at end stage which was further increased in LPS-injected P301S mice.

Taken together these data indicate a clear and clinically relevant interaction between systemic inflammation and tau-associated neuropathology with acute and long-term functional consequences. In the absence of evidence of microglial priming, future work will explore potential mechanisms.

Lay Summary

You will recognise from personal experience that common symptoms of illness or infection include feeling antisocial, lethargic, and feverish. This is because when you get an infection, it is detected by immune cells, which are like soldiers patrolling the body looking for foreign invaders, and these "soldiers" send chemical and electrical signals to the brain which tell it about the infection. The brain then initiates the "sickness behaviours", including those described above. These behaviours have evolved over time to aid our recovery and reduce the risk of further spread of the infection.

However, when somebody who has dementia suffers from a similar infection they might experience delirium. Delirium is a disturbed state of mind where the sufferer may feel confused and unable to focus their attention; they might hallucinate and often fluctuate between being hyperactive and unresponsive. Delirium usually only lasts a matter of days but it can be very distressing and it can have long-term impacts on the brain; it can make the dementia worse, and increase the rate of cognitive decline of dementia patients.

How does this happen? It is thought that, in someone with dementia, when the chemical and electrical signals reach the brain, it over-reacts. The predominant theory in the field is that the immune "soldier" cells stationed in the brain – called "microglia" – which are normally very tightly controlled, can detect that something is awry in a brain with dementia and become "primed". This might be akin to turning off their weapons' safety catches, so that when they later receive the signals from the patrolling cells that there is an infection in the body, they over-react with negative consequences. This over-reaction is thought to underpin delirium and might also cause permanent damage leading to the observed long-term impacts.

This work aimed to test this theory using genetically modified mice with dementia-like features and injecting them with a compound which mimics a bacterial infection.

A genetic mutation that caused dementia in humans was identified in the gene that encodes a protein called "tau" and this faulty gene was turned on in the nerve cells of mice to create "mutant-tau" mice. As these genetically modified mice age the faulty tau protein accumulates in "tangles" in the nerve cells. The nerve cells in the brain and spinal cord are then no longer able to function properly and eventually those nerve cells die. Some of them are important for controlling movement and coordination so as those nerve cells die the mice develop movement problems.

This thesis demonstrated that a behavioural task, the horizontal bar task, that measures muscle control and coordination in mice, can be used as a non-invasive way to measure disease severity. Secondly, this thesis determined a detailed time course for nerve cell death in the brains of mutant-tau mice and investigated markers of inflammation in the brain and spinal cord.

When the mice were still young, before they developed symptoms, they were injected with a chemical compound called lipopolysaccharide (LPS) which is recognised by the patrolling immune cells as a bacterial infection. These experiments demonstrated, for the first time, that in the hours following injection with LPS, mutant-tau mice were much sicker than normal mice and in the longer-term, mutant-tau mice that received LPS showed an increased rate of decline compared with those that were injected with a control solution. These experiments mimic the situation in dementia patients following an infection.

Importantly, when the brain and spinal cord were studied there were no signs of "primed" microglia. Therefore, future work will explore potential mechanisms to explain how infection increases the rate of decline of dementia.

1 Chapter 1: Introduction

1.1 Introduction Part 1: Dementia and Tauopathies

1.1.1 Dementia

1.1.1.1 Dementia definition

Dementia, is now referred to in the Diagnostic and Statistical Manual of Mental Disorders (DSM)-5 as Major Neurocognitive Disorder and is diagnosed based on "*Evidence of significant cognitive decline from a previous level of performance in one or more cognitive domains*" which include learning and memory, language, executive function, complex attention, perceptual-motor and social cognition. In order to meet the diagnostic criteria the cognitive deficits must cause impairment in personal, social or occupational functioning, impact on independence in everyday activities, cannot be better explained by another mental disorder (e.g., major depressive disorder, schizophrenia) and must not occur exclusively in the context of delirium (American Psychiatric Association).

Dementia is the clinical manifestation of neuronal damage and dysfunction hence symptoms include memory loss, emotional or mood changes and problems with communication and reasoning. Dementia is also often associated with impaired motor function. Together these deficits often make it impossible for sufferers to live independently, especially as the disease progresses (Buchman et al., 2011).

1.1.1.2 Dementia prevalence and cost

In 2015 Dementia and Alzheimer's disease replaced ischaemic heart disease as the leading cause of death registered in England and Wales, accounting for 11.6% of all deaths registered in 2015 according to the Office for National Statistics (ONS, 2016). Dementia accounted for 21.2% of deaths in 2015 among women aged 80 and over and 13.7% of deaths in males of this age group (ONS, 2016). There are currently approximately 850,000 people living with dementia in the UK today and with the

rapidly expanding and ageing population that figure is predicted to reach 1 million by 2025 and over 2 million by 2050 (ARUK – Defeat Dementia Policy Report 2014).

The cost to society in the UK was £26 billion per year, according to a 2014 report by Alzheimer's Society, this includes social care (£10bn) and healthcare (£4bn). An estimated 670,000 people in the UK act as primary carers for people with dementia saving the state £11bn a year, but often have to leave work in order to care full-time; by 2030 the estimated cost to business is £3bn per year (ARUK – Defeat Dementia Policy Report 2014).

Government funding for dementia research was approximately £66m in the year 2014/2015 and in February 2015 then-Prime Minister David Cameron published The Prime Minister's Challenge on Dementia 2020 which pledged to double research funding by 2025 (2015).

The Prime Minister's Challenge on Dementia states "it is estimated that if there was a disease-modifying treatment from 2020 that delayed the onset of Alzheimer's disease by five years, by 2035 there would be 425,000 fewer people with dementia, with accumulated savings from 2020 of around £100 billion.", there is a powerful argument for the economic benefit of even just *delaying the onset* of dementia by a few years, since there would be fewer dementia sufferers to treat, fewer sufferers in care homes or hospitals, fewer carers forced to leave work and vastly improved quality of life for would-be patients and carers.

Dementia is a collective term describing a legion of diseases including Alzheimer's disease (AD, 62%), vascular dementia (17%), and Frontotemporal Dementia (FTD, 2%), Parkinson's Disease (PD, 2%), Dementia with Lewy Bodies and Motor Neuron Disease to name a few. Dementia is a clinical syndrome caused by multiple pathologies which often overlap and interact; the heterogeneous clinical presentations are the result of variation in underlying disease pathology; which neuronal and/or glial populations are impacted and how. For example, AD is

associated with accumulation of amyloid-β (Aβ) protein deposits and tau protein in the form of neurofibrillary tangles (discussed below), and significant loss of cholinergic and glutamatergic neurons, and resulting early episodic memory impairments and later semantic memory impairments (Grand et al., 2011). Whereas frontotemporal dementia describes a variety of non-Alzheimer's clinical syndromes, with behavioural, personality, language and sometimes motor disturbances associated with accumulation of tau protein, and degeneration of anterior hemispheres (Grand et al., 2011). Vascular dementia (VaD), on the other hand results from the effects of cerebrovascular disease. Multi-infarct dementia (post-stroke dementia) occurs when multiple infarcts are caused by occlusion of large vessels e.g. by atherosclerotic thrombosis or cardiac embolization. Patients present with severe deficits in specific domains while other domains remain intact (Grand et al., 2011). Dementia is usually progressive, however with such distinct aetiologies there is marked heterogeneity in the speed of decline; occlusion of blood vessels in VaD causes a sudden decline, compared with the gradual decline of AD.

Although distinct neurodegenerative diseases are characterised by accumulation of specific proteins, in actual fact it is more complicated. Mis-accumulation of proteins associated with neurodegeneration does not necessitate disease; plaques and tangles have been observed in non-demented cases at autopsy (Price et al., 1999, Bennett et al., 2006) and there is often overlap between pathologies among diseases. Aggregated proteins including Aβ, tau, TDP-43 and α-synuclein can interact with each other, causing mis-localisation, dysregulation of post-translational modifications and cross-seeding of aggregates of other protein species. In a study of pathological cohorts at different ages Aβ deposits were found in 80% of all autopsy cases over 80 years of age and tau deposits were found in almost 100% of cases in the same age group (Spires-Jones et al., 2017).

1.1.1.3 **Drug Treatments**

Drug treatment for dementia is currently limited to symptomatic treatment with acetylcholinesterase (AChE) inhibitors, including rivastigmine, donepezil and galantamine (Allgaier et al., 2013) and treatment of behavioural and psychological symptoms of dementia (BPSD) with antipsychotics and other agents (Zdanys et al., 2016). Acetylcholine is a neurotransmitter in the CNS. Positron emission tomography (PET) studies indicate that increasing cortical acetylcholinesterase inhibition in AD correlates with an increase in cognitive rescue (Bohnen et al., 2005). Cholinergic dysfunction is a consequence rather than a cause of neurodegeneration however AChE blockers aim to rebalance cholinergic neurotransmission by prolonging the action of ACh at the synaptic cleft. Memantine is the only approved AD drug which targets the glutamatergic system instead. The glutamatergic system is affected by the impaired glutamate uptake by glial cells which results in elevated background glutamatergic "noise". Memantine, an N-methyl-D-aspartate (NMDA) receptor antagonist is a fast, voltage dependent blocker (Francis et al., 2012). Currently available treatments are often ineffective and are not disease-modifying.

1.1.1.4 **Dementias as proteinopathies**

Diagnoses of specific dementias are made based on clinical presentation; cognitive and motor tests have been designed to scrutinise the CNS regions affected by disease. However, it is not until post mortem that diagnoses can be confirmed.

Insoluble protein deposits are consistent hallmarks of neurodegenerative conditions. Alois Alzheimer observed senile plaques, now known as amyloid-β (Aβ) plaques, aggregates composed of misfolded amyloid protein and neurofibrillary tangles (NFTs), aggregates composed of filamentous hyperphosphorylated tau protein in a patient with early onset Alzheimer's disease over a century ago. Since then several additional mis-folded proteins have been identified in neurodegeneration (**Table 1**). some of which are implicated in multiple diseases, for example tau protein, which

will be discussed in more detail later. These proteins have proved useful indicators of the pathways implicated in disease aetiology.

Discovery of mutations in hundreds of the genes encoding these pivotal proteins as well as the enzymes involved in their processing have continued to focus research attention towards this aspect of pathology and have enabled the development of animal models of neurodegeneration (sections 1.1.5 and 1.1.6).

Protein	Disease
Amyloid β (Aβ)	• Alzheimer's disease (AD) • Dementia with Lewy bodies
Tau	• AD, • Fronto-temporal dementia with parkinsonism (FTDP), • Progressive supranuclear palsy (PSP), • Corticobasal degeneration (CBD),
Huntingtin	• Huntington's disease
α-synuclein	• Parkinson's disease, • Multiple systems atrophy, • Dementia with Lewy bodies
Prion protein (PrP)	• Transmissible spongiform telencephalopathies
Super-oxide dismutase (SOD1)	• Familial Amyotrophic lateral sclerosis (fALS)
TAR DNA binding protein 43 (TDP-43)	• FTD • ALS
Ubiquitin 2	• FTD • ALS

Table 1 – Proteins commonly accumulated in neurodegenerative diseases

1.1.2 Tau Protein and its Role in Dementia

Tau protein is the main component of neurofibrillary tangles (NFTs) (Grundke-Iqbal et al., 1986) which are the defining feature of a myriad of neurodegenerative diseases

including Alzheimer's disease and inherited frontotemporal dementias (Spillantini et al., 2013) (discussed further in section 1.1.4).

Discovery of mutations in tau protein which are responsible for inherited tauopathies indicate that tau dysfunction is sufficient to cause dementia on its own (Clark et al., 1998, Hutton et al., 1998, Poorkaj et al., 1998, Spillantini et al., 1998) however the mechanisms leading from mutation to neurodegeneration are not clearly defined.

The following section will first introduce tau protein and its normal role in the healthy brain before discussing the role of tau protein in neurodegeneration, animal models of tauopathy and finally it will introduce the P301S tau mouse model used in my thesis.

1.1.3 Tau Protein

Tau is a microtubule-associated protein (MAP) which consists of an N-terminal projection domain and a C-terminal microtubule binding domain. In humans, there are 6 different isoforms of tau all encoded by one gene (MAPT) (Neve et al., 1986, Goedert et al., 1989a). Tau is 55–74 kDa in size (depending on splice variant and phosphorylation status). Multiple isoforms arise from a single gene via alternative splicing (see **Figure 1**) and they differ from each other by inclusion or not of exons 2 (orange) and 3 (green) in the N-terminal half and exon 10 (dark yellow) at the C-terminus. Exon 10 contains a Pro-Gly-Gly-Gly microtubule binding motif. Tau lacking this insert contains three microtubule binding motifs (yellow) and is referred to as three-repeat (3R) tau, and tau including this insert is referred to as 4R tau. The inclusion of this microtubule binding domain influences the microtubule binding affinity. Splicing of tau is developmentally regulated, only 3R tau is found in foetal

brain whereas adult brain contains a 1:1 ratio of 3R and 4R tau (Goedert et al., 1990). 4R tau promotes microtubule assembly 2.5- to 3-fold faster than 3R tau.

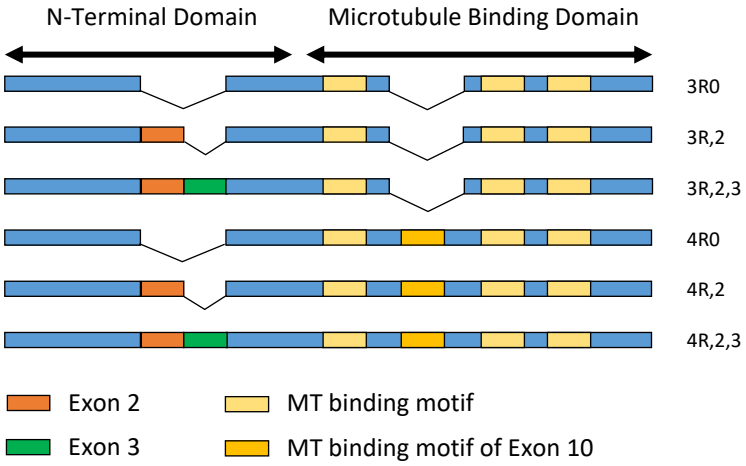

Figure 1 – Tau Isoforms: *Alternative splicing generates 6 isoforms of tau with or without Exons 2, 3, and 10. Exon 10 contains an additional microtubule binding domain hence alternative splicing influences MT-binding affinity. Isoforms excluding this domain are referred to as 3-repeat or 3R tau and isoforms including this domain are referred to as 4R tau.*

1.1.3.1 Role of Tau protein in healthy CNS

Tau binds reversibly to the microtubules of the cytoskeleton in order to stabilise them. Microtubules are a key component of the cytoskeleton – they are long hollow fibres made up of tubular subunits which can be added and removed dynamically to allow the cytoskeleton to grow and collapse in response to its environment (Lodish et al., 2000).

The cytoskeleton is important in all cells for cell division, maintaining cell structure, enabling cell migration and transport of nutrients and waste around the cell, hence the proper function of the cytoskeleton is important for cell survival (Fletcher et al., 2010). The successful regulation of cytoskeletal stability by tau and other MAPs is even more critical in neurons than other cell types due to their specialised morphology and function.

Tau binding is dynamic and its binding affinity is largely dependent on post-translational modifications, including, importantly its phosphorylation state (Drechsel et al., 1992, Biernat et al., 1993). Hence it is subject to second messengers,

protein kinases such as mitogen activated protein kinases (MAPKs), glycogen synthase kinase 3 (GSK3), cyclin dependent kinase 5 (CDK5) and phosphatases (phosphatase proteins 1, 2A and 2B). Tau protein is hyperphosphorylated during mitosis (Kanemaru et al., 1992, Brion et al., 1993, Pope et al., 1994, Illenberger et al., 1998) and during hibernation (Zhou et al., 2001, Arendt et al., 2003) where it is associated with neuronal plasticity. It is important to recognise that tau hyperphosphorylation is not necessarily pathological but is a normal feature of tau regulation.

1.1.4 Tau protein is implicated in Dementia

Neuronal death and dysfunction underpin all dementias. Alzheimer's disease is characterised by accumulation of amyloid-β protein into Aβ-plaques and hyperphosphorylated tau into NFTs. Multiple mutations have been identified in the Aβ processing pathway and although Aβ is thought to be the main initiator of AD (Hardy et al., 2002) , the extent of misfolded tau protein correlates more closely with neuronal loss and cognitive dysfunction (Arriagada, 1992, Bancher et al., 1993, Bierer et al., 1995, Gomez-Isla et al., 1997, Giannakopoulos et al., 2003, Guillozet et al., 2003, Ingelsson et al., 2004). NFTs are a consistent hallmark of AD and tau protein is recurrently implicated in sporadic neurodegenerative conditions.

Tau pathology is not exclusively found in association with amyloid pathology. Dementias where tau is implicated as the main cause are known as tauopathies. Importantly several inherited tau mutations have been discovered which demonstrate that tau mutations are sufficient to cause dementia. Rare genetic forms of tauopathy dementia share pathology with the more common sporadic forms of disease and have been pivotal in our understanding of the pathology of dementias.

1.1.4.1 Frontotemporal dementia

Frontotemporal dementia (FTD) is the second most common dementia affecting people in middle age, after AD and accounts for almost 20% of presenile dementias

(Snowden et al., 2002). Symptoms of FTD include social behavioural changes such as a lack of empathy, disinhibition, agitation and loss of social etiquette, as the disease progresses symptoms including cognitive decline, memory loss and in some cases motor symptoms develop. FTD is classified into different neuropathologic subtypes based on the predominance of: tau pathology, i.e., FTLD-tau; TDP43 pathology, i.e., FTLD-TDP; or other accumulated proteins including fused-in-sarcoma (FUS) protein, i.e., FTLD-FUS. FTLD-tau encompasses corticobasal degeneration (CBD), progressive supranuclear palsy (PSP), Pick's disease (PiD) and argyrophilic grain disease (AGD). These diseases are all characterised by the accumulation of pathological tau protein in neurons, astrocytes and oligodendrocytes.

1.1.4.2 **Disease associated tau mutations**

At the time of writing this thesis more than 100 tau mutations have been sequenced in 150 families worldwide (http://www.alzforum.org/mutations/). Mutations in the MAPT gene encoding tau protein account for approximately 5% of cases of FTD and tau protein is implicated in sporadic FTD.

1.1.4.3 **Pathological Tau hyperphosphorylation**

Tau protein is normally unfolded, soluble and monomeric, however, in tauopathies it becomes hyperphosphorylated and forms insoluble filaments. There are seventy-nine serine (Ser) or threonine (Thr) phosphorylation sites on the longest tau isoform in the brain. In the normal healthy brain for every mole of tau there is approximately 1.9 moles of phosphate, however in AD the ratio shifts to 1 mole of tau to 6-8 moles of phosphate (Ksiezak-Reding et al., 1992). Abnormal hyperphosphorylation of tau results in both loss of normal function of tau and gain of toxic function of tau.

As previously discussed (section 1.1.3.1) phosphorylation, and even hyperphosphorylation of tau protein can occur in the normal, healthy brain. In the diseased brain, however there is excessive hyperphosphorylation which renders tau unable to bind to microtubules.

Tau phosphorylation status depends on the relative activity of protein kinases and phosphatases, many of which have been implicated in neurodegenerative diseases. Most of the kinases involved in tau phosphorylation are proline-directed protein kinases (PDPKs). *In vitro* studies have suggested a potential role of several PDPKs in phosphorylation of tau in tauopathies, including MAPK (Drewes et al., 1992, Vulliet et al., 1992), GSK3 (Hanger et al., 1992, Zheng-Fischhöfer et al., 1998), cyclin-dependent kinases cdc2 (which was physically associated with paired helical filaments (PHF) from Alzheimer's disease brains), CDK5 (Baumann et al., 1993, Liu et al., 1995) and activated protein kinases ERK6 and SAPK4, p38, p38β and JNK1 (Goedert et al., 1997, Reynolds et al., 1997, Kumagae et al., 1999).

Outside of the PDPK family, other protein kinases capable of phosphorylating tau include microtubule-affinity regulating kinase (MARK) (Drewes et al., 1997), Ca2+/calmodulin-dependent protein kinase II (CaMK II) (Baudier et al., 1987), cyclic-AMP-dependent kinase (PKA) (Johnson, 1992) and casein kinase II (Greenwood et al., 1994).

The increased hyperphosphorylation of tau might also be the result of a shift in activity of phosphatases such as phosphatase proteins 2A and 2B (PP2A and PP2B) whose activity is decreased in AD (Gong et al., 1995, Ladner et al., 1996).

1.1.4.4 **Tau aggregation in disease**

While tau hyperphosphorylation may occur in the native developing brain as well as the pathological brain, aggregation of tau into filaments and then tangles does not occur during development. This suggests that further post-translational modifications are required for aggregation. These modifications may include further hyperphosphorylation at pathology-specific sites, glycosylation (Sasaki et al., 1998) ubiquitination (Mori et al., 1987) and truncation.

Monomeric tau usually exists in a random coil conformation under normal physiological conditions. Tau may form dimers, trimers and small soluble oligomers

(Sahara et al., 2007). Granular tau oligomers (GTOs) are densely packed soluble tau polymers which have been isolated from AD brains and are composed of approximately 40 monomers of tau (Maeda et al., 2007).

Healthy monomeric tau does not form filaments, hence a "prion-like" seeding event is required. Aggregation is concentration-dependent hence aberrant tau expression might be a sufficient trigger. Post-translational modifications including truncation and phosphorylation might also be sufficient to cause conformational changes required to seed aggregation.

Tau can form different types of filaments depending on the isoforms recruited and these different tau filaments are associated with different tauopathies. Paired-helical filaments (PHFs) are twisted ribbons of 10–20 nm width, with aperiodicity of ~80 nm, associated with AD; all six tau isoforms are present in PHFs in the brains of patients with AD (Goedert et al., 1992) whereas in CBD and PSP tau tends to form straight filaments (SFs), 15-nm-wide filaments that lack periodicity and are composed of 4R tau only (Ksiezak-Reding et al., 1994, Delacourte et al., 1996). In Pick's disease tau forms filamentous, non-fibrillar aggregates called Pick's bodies which are approximately the size of the nucleus and are composed of disorganised bundles of 3R tau filaments (Goedert, 1998). Argyrophilic grains of AGD are much smaller and are composed of bundles of 4R tau-containing SFs and smooth tubules. (Braak et al., 1989). Tau filaments may also exist as twisted ribbons or rope-like filaments. PHFs and SFs form large fibres which bundle together into 'flame-shaped' neurofibrillary tangles (NFTs) in cell bodies, neuropil threads within neuronal processes, and neuritic plaques which are associated with dystrophic neurites (Buée et al., 2000).

As well as being comprised from different isoforms, tau pathology is found in neurons and glial cells in different ratios depending on the disease (Kahlson et al., 2015). Tau forms coiled cytoplasmic bodies in oligodendrocytes prominent in PSP, CBD, PiD and in fibrous and protoplasmic astrocytes in PiD (Kahlson et al., 2015).

The degree of tau pathology correlates with cognitive decline, however it remains unclear which is the toxic tau species – soluble tau, monomeric, small oligomeric, insoluble or fibrillary tau and whether tau toxicity is due to loss of function or gain of toxic function.

1.1.4.5 **Tau Spread**

Once it has begun, tau aggregation is an energetically favourable, self-propagating process, with a "prion-like" recruitment of tau into pathological tau filaments. Hyperphosphorylated, truncated or mutated tau is recruited more rapidly than endogenous tau. Interestingly 3R tau can recruit 4R tau but 4R tau cannot recruit 3R tau (Dinkel et al., 2011); this might be an important consideration when designing animal models since the rodent brain contains only 4R tau.

In AD tau pathology tends to spread according to the Braak progressive stages of tau pathology which range from I to VI (Braak et al., 2006):

> *"Stage I: Lesions develop in the transentorhinal region (locus coeruleus, magnocellular nuclei of the basal forebrain)...*
>
> *Stage II: Lesions extend into the entorhinal region…*
>
> *Stage III: Lesions extend into the neocortex of the fusiform and lingual gyri…*
>
> *Stage IV: The disease process progresses more widely into neocortical association areas…*
>
> *Stage V: The neocortical pathology extends fanlike in frontal, superolateral, and occipital directions, and reaches the peristriate region…*
>
> *Stage VI: The pathology reaches the secondary and primary neocortical areas and, in the occipital lobe, extends into the striate area…"*

There have been several *in vivo* studies indicating a trans-synaptic spread of tau pathology through the brain. Stereotaxic injection of brain homogenate from mice over-expressing human mutant P301S pathological tau into mice expressing human wild-type tau induced recruitment of wild-type tau into filaments and propagation of tau pathology to neighbouring brain regions (Clavaguera et al., 2009). Multiple studies in transgenic mice over-expressing human mutant tau restricted to the entorhinal cortex (EC) showed progression of tau pathology from transgene-expressing neurons of the EC to neighbouring cells, and then to synaptically connected neurons in the dentate gyrus, and CA1 of the hippocampus (de Calignon et al., 2012, Harris et al., 2012, Liu et al., 2012b). *In vitro* experiments have shown the release of intracellular tau into the medium and uptake by recipient cells thus demonstrating trans-synaptic spread of tau protein from cell to cell (Frost et al., 2009, Kfoury et al., 2012) tau filaments were then able to induce fibrillization in naïve cells (Kfoury et al., 2012) offering a mechanism for the spread of tau pathology to distal but synaptically-connected regions.

1.1.5 Rodent models of tauopathy

The discovery of rare inherited mutations in tau protein capable of causing dementia has enabled the development of animal models to investigate the mechanisms of tau driven neurodegeneration. These are summarised in Table 2 and discussed below.

The idiosyncrasies of specific models are dependent on the background strain of the animal model, the promoter used to drive tau expression, the isoform of tau expressed and the mutation introduced, if any. Despite these variables several rodent models have been generated with robust and overlapping characteristics which recapitulate key hallmarks of tauopathies including hyperphosphorylation of tau and accumulation into filaments and NFTs, associated gliosis and upregulation of inflammatory markers, synaptic changes, neuronal loss and associated phenotypes include cognitive and motor changes (Table 2).

Transgene expression varies considerably between models, from 1 to 13-fold endogenous tau levels, dependent on the promoter, the copy number and location of integration (Table 2).

Unlike humans, adult mice express only 3 isoforms of tau, all of which include 4 microtubule repeats (4R tau) rather than the 6 isoforms (3R or 4R) expressed in the human brain. Over-expression of normal human wild-type tau can cause pathological tau changes (Ishihara et al., 1999, Spittaels et al., 1999, Probst et al., 2000, Andorfer et al., 2003) hence care must be taken when interpreting mechanistic data from transgenic mice since some tau pathology might be attributed to over-expression *per se* or a shift in isoform ratio rather than human dementia relevant tau pathology.

Mice expressing a transgene for all 6 isoforms of human tau under the mouse tau promoter on top of the endogenous mouse tau (8c mice) showed no signs of tau pathology (Duff et al., 2000) (Table 2). However when the same mice were crossed with tau knock-out mice to produce hTau mice, expressing exclusively human tau, these mice demonstrated pathological tau phosphorylation and accumulation which authors attribute to a shift in tau isoforms (Andorfer et al., 2003). In line with this, rodents expressing only 3R isoforms of tau or pathological truncated tau found in AD both developed pathological tau filaments with associated hind limb paralysis (Ishihara et al., 1999, Zilka et al., 2006, Zilka et al., 2009).

Tau mouse models often display a progressive motor phenotype (11 of the 26 lines described in Table 2); when lifted by the tail mutant tau mice clasp their hind limbs rather than splay them out and they show impaired performance on the rotarod task – a test of motor coordination where mice are placed on a rotating rod (with constant or increasing speed depending on the protocol) and time taken to fall from the rod is recorded (see Table 2 for multiple references). This progressive hind limb phenotype might reflect cell specific vulnerability of motor neurons of the spinal cord to tau pathology; different cell types express different isoforms of tau (Goedert et al., 1989b) which might influence the recruitment of endogenous tau into NFTs or perhaps the

long axonal projections of motor neurons make them more susceptible to disruption of microtubule stability. Alternatively, it might reflect cell specificity of the promoter driving transgene expression.

In order to circumvent the problems associated with hind-limb deficits, researchers have developed models with region specific and inducible promoters (Table 2 – Column 1). Transgenic mice expressing the full length R406W mutant tau under the CaMK-II promoter showed very little human tau expression in the spinal cord and had no apparent motor deficits (Tatebayashi et al., 2002). However, another model expressing the P301L mutant tau under the same promoter still displayed the clasping reflex and weight loss typical of mutant tau mice (Ramsden et al., 2005) hence the phenotype cannot be attributed to the promoter driven expression alone.

Because AD is the most common type of dementia, animal models which recapitulate AD-associated tau pathology are desirable and hence models have been engineered with promoters which drive predominantly hippocampal and cortical expression of tau. These models often display spatial impairments in the Morris water maze or radial arm maze which can be attributed to hippocampal pathology (Ramsden et al., 2005, Murakami et al., 2006, Rosenmann et al., 2008, Flunkert et al., 2013).

There has been a great deal of discussion about the pathological substrates of behavioural deficits seen in animal models of tauopathy. The rTg4510 mouse model over-expresses P301L mouse tau under the CaMK-II promoter and develops progressive tau pathology associated with forebrain atrophy, hippocampal neuronal loss, spatial working memory deficits in the Morris water maze, as well as the phenotypic weight loss and hind limb paralysis typical of mutant tau lines (Ramsden et al., 2005). Studies in these mice indicated that different lines expressed different dosage of mutant tau and the rate at which mice developed neurofibrillary pathology was directly related to the amount of tauP301L expression. Suppression of tau transgene rescued spatial memory and neuron numbers but NFTs continued to

accumulate indicating that NFTs are not sufficient to cause cognitive decline or neuronal death (SantaCruz et al., 2005).

Yoshiyama et al. (2007 – Table 2) showed that the PS19 mouse line (over-expressing human P301S tau under the mouse prion promoter at 5-fold greater levels than endogenous mouse tau) had median survival of around 9 months. Tau was hyperphosphorylated and formed insoluble, randomly oriented tau filaments in the neocortex, amygdala, hippocampus, brain stem and spinal cord. There were early defects in axonal transport in PS19 mice which resulted in axonal degeneration. Microtubule destabilisation, impaired axonal trafficking, and axonal degeneration are associated with the decreased binding affinity of tau protein and are recurrent features of animal models (Table 2) (Ishihara et al., 1999, Spittaels et al., 1999, Tatebayashi et al., 2002, Zhang et al., 2004, de Calignon et al., 2012, Gilley et al., 2012). Tau mutations destabilise microtubules and affect axonal transport (Cuchillo-Ibanez et al., 2008, Dixit et al., 2008, Morfini et al., 2009) and it is thought that the disturbance in axonal transport impairs essential trafficking to the distal parts of the cell resulting in 'dying back' (whereby synaptic regions gradually degenerate toward the intact cell body).

Yoshiyama et al. (2007) also demonstrated early synaptic loss and reduced synaptic function which preceded NFT formation, these are recurrent hallmarks of dementias (Table 2) (Terry et al., 1991, Selkoe, 2002, Ingelsson et al., 2004). The literature on the role of tau protein in synaptic deficits is contradictory (Kopeikina et al., 2013). The predominant view is that tau results in regional synaptic loss in vulnerable cells however overall synaptic density is preserved, which is likely due to compensatory increases in synaptic density in other neuronal populations (Kopeikina et al., 2013) and several of the models in Table 2 indicate this regional synaptic loss or dysfunction (David et al., 2005, Murakami et al., 2006, Schindowski et al., 2006, Rosenmann et al., 2008, Hoover et al., 2010, Alldred et al., 2012, de Calignon et al., 2012, Koss et al., 2016).

Tau pathology in PS19 mice also correlates regionally and temporally with microgliosis and astrogliosis in PS19 mice (Yoshiyama et al., 2007). Astrogliosis and microgliosis are recurrent hallmarks of tauopathy dementias and are also associated with tau pathology in animal models expressing human mutant tau protein. These will be discussed further in section 1.2.5.1.

Mutation (Name) ***Isoform*** **Promoter**	**p-Tau**	**Insoluble tau**	**NFTs Width (nm)**	**Motor & Cognitive deficits**	**Neuronal loss**	**Synaptic loss**	**Axonal degeneration transport deficits**	**Astrogliosis**	**Microgliosis**	**Reference**
WT Tau *4R,2,3* Thy 1	✓ - Transgenic tau 5-fold endogenous mouse tau - Hippocampus, DG, CA	X	X							(Gotz et al., 1995)
WT Tau (ALZ17) *4R,2,3* Thy 1.2	✓ - No NFTs - 1.5-fold endogenous tau in the brain - 10-fold endogenous tau in spinal cord. - Human tau in neurites and synapses not cell bodies. - Human tau in somatodentritic compartment	✓	X	- Dystonic posture, clasping and limb retraction when lifted by the tail - Progressive decline in rotarod performance.	- No neuronal loss		- Axonal degeneration in brain and spinal cord - Axonal dilations	✓	✓	(Spittaels et al., 1999, Probst et al., 2000)
WT Tau hWT $23^{+/-}$ *4R,2,3* Mouse prion promoter (MoPrP)	✓ - Heterozygous tau ~8- to 10-fold over endogenous m-tau - 1 to 6 mo - diffuse perikayal tau in cortex, hippocampus, cerebellum, and spinal cord - Over 18 mo - occasional tau-positive filaments	X	X	- No motor impairments						(Zhang et al., 2004)

Mutation (Name) ***Isoform*** **Promoter**	**p-Tau**	**Insoluble tau**	**NFTs Width (nm)**	**Motor & Cognitive deficits**	**Neuronal loss**	**Synaptic loss**	**Axonal degeneration transport deficits**	**Astrogliosis**	**Microgliosis**	**Reference**
WT Tau *3R,2,3* mouse Tα1 α-tubulin promoter	✓ - Human tau 5.5-fold higher than endogenous mouse tau - Tau immunoreactivity in neurons and glia - Progressive phosphorylation and accumulation	✓	✓	- Progressive motor weakness, impaired ability to stand on a slanted surface - Dystonic movement of the hindlimbs and sometimes forelimbs when lifted by tail	✓ - Progressive neuronal loss (also early oligo loss)			GFAP - Elevated but then progressive loss		(Higuchi et al., 2002)
WT Tau *3R,0* MoPrP	✓ - 10–20 nm diameter - Straight filaments (randomly arranged) - Spinal cord > cortex and brainstem	✓	✓	- Motor weakness			- Diminished microtubules - Radiolabelled tau showed reduced axonal transport in ventral roots	GFAP		(Ishihara et al., 1999, Ishihara et al., 2001)
WT Tau (8c) *All 6 isoforms* Tau promoter	- All six isoforms represented in brain - mRNA and protein. - 3R expression > 4R - No obvious tau pathology			- No motor abnormalities						(Duff et al., 2000)

Mutation (Name) *Isoform* Promoter	**p-Tau**	**Insoluble tau**	**NFTs Width (nm)**	**Motor & Cognitive deficits**	**Neuronal loss**	**Synaptic loss**	**Axonal degeneration transport deficits**	**Astrogliosis**	**Microgliosis**	**Reference**
WT Tau (hTau) *All 6 isoforms* Tau promoter mTau KO	✓ - All 6 isoforms of human tau, but do not express mouse tau - 3R expression > 4R	✓ ~15 nm diameter filaments - Age related increase in tau phosphorylation - ent. cortex, hippocampus, ventromedial hypothalamus, medial septum	✓		- Some evidence of apoptosis, DNA fragmentation but not caspase activation. - Upregulation of markers of cell cycle re-entry	- Altered morphology (decrease in some areas, compensation in others) - Down regulation of synaptic-related genes			- IBA1 positive progressive microgliosis - Elevated levels of cleaved CX3CL1	(Andorfer et al., 2003, Dickstein et al., 2010, Alldred et al., 2012)
P301L (JNPL3) *4R0 (human)* MoPrP	✓ - 10−30 nm diameter - Straight or twisted ribbon - Astrocytes and oligodendrocytes contain filamentous tau - Cerebellum and hippocampus > thalamus > hypothalamus > spinal cord > brainstem > cortex.	✓	✓	- Progressive motor disturbances	- 48% loss of motor neurons - Apoptosis -Downregulation of inhibitors of apoptosis		- Progressive white matter pathology in the spinal cord	- GFAP		(Lewis et al., 2000, Lin et al., 2005) (Ho et al., 2001)

Mutation (Name) ***Isoform*** **Promoter**	**p-Tau**	**Insoluble tau**	**NFTs Width (nm)**	**Motor & Cognitive deficits**	**Neuronal loss**	**Synaptic loss**	**Axonal degeneration transport deficits**	**Astrogliosis**	**Microgliosis**	**Reference**
P301L *4R,2,3* Syrian hamster prion promoter	✓ - 12-22 nm diameter - Straight filaments criss-crossing herring-bone like structure - NFTs in the frontotemporal cortex, hippocampus, amygdala, basal forebrain nucleus, locus ceruleus, and substantia nigra	✓	✓	- Impaired spatial memory in MWM and radial arm maze. - Impaired memory on taste aversion test.	- Severity of degeneration paralleled the frequency of NFTs	-Hippocampus		- GFAP preceded tau accumulation	- Iba1, Mac1, F4/80RCA1 lectin and MHC II - Microgliosis regionally correlated with severity of tau pathology (AT8 staining)	(Murakami et al., 2006, Sasaki et al., 2008)
P301L *4R,2,3* Thy 1.2	✓ ∼15 nm diameter - Expression levels of human tau were high in hippocampus, fornix fimbriae, amygdala, spinal cord, and cortex.	✓	✓	- 6 months – no difference on rotarod but increased total number of activity state changes in openfield. Enhanced taste aversion in P301L mice. - 11 months – increased total dist travelled in openfield and elevated O-maze, more visits to inner zone in openfield.	- Apoptosis	- Compensat-ory increase in synapse related proteins due to synaptic loss		- GFAP		(Götz et al., 2001, Pennanen et al., 2004, David et al., 2005, Pennanen et al., 2006)

Mutation (Name) ***Isoform*** **Promoter**	**p-Tau**	**Insoluble tau**	**NFTs Width (nm)**	**Motor & Cognitive deficits**	**Neuronal loss**	**Synaptic loss**	**Axonal degeneration transport deficits**	**Astrogliosis**	**Microgliosis**	**Reference**
P301L (rTg4510) *4R,0* CaMK-II induced with tetracycline suppressed w. doxycycline	✓ - Straight tau filaments - NFT pathology in the neocortex > hippocampus > limbic structures with increasing age	✓	✓	- Phenotypic weight loss and dystonic posture, clasping and limb retraction when lifted by the tail - 4 months onwards – progressive spatial memory impairments in MWM	- Gross forebrain atrophy & hippocampal CA1 - (no mechanism identified)	- Mislocalized tau enriched in PSD - Synaptic dysfunction - Decreased AMPA and NMDA		- GFAP		(Ramsden et al., 2005, SantaCruz et al., 2005, Hoover et al., 2010)
P301L (rTgTauEC) *4R,0* CaMK-II induced with tetracycline expressed under Neuropsin promoter	✓ - Straight tau filaments - Ent. cortex and hippocampus. - Trans-synaptic spread of tau with axonal transport through connected but distal brain regions.	✓	✓		- 42% neuronal loss in ent. cortex	✓	✓	- GFAP - PHF1-positive tau was taken up by astrocytes	- IBA1	(de Calignon et al., 2012)

Mutation (Name) ***Isoform*** **Promoter**	**p-Tau**	**Insoluble tau**	**NFTs Width (nm)**	**Motor & Cognitive deficits**	**Neuronal loss**	**Synaptic loss**	**Axonal degeneration transport deficits**	**Astrogliosis**	**Microgliosis**	**Reference**
P301L *All 6 isoforms* Tau (knock in)	- Total tau = same as controls with expected ratio of 0N4R, 1N4R and 2N4R - No change in insoluble tau, or hyperphosphorylated tau			- No motor decline measured by rotarod - Increased locomotor activity - Normal social transmission of food preferences (STFP) test			- Reduced MT binding - Altered anterograde mitochondrial transport (no change in retrograde transport)			(Gilley et al., 2012)
P301L *4R,2,3* Thy 1.2	✓	✓	✓	- Progressive motor impairments						(Terwel et al., 2005)
	- 4-fold higher than endogenous mouse tau - Human protein tau in layers II, V, and VI of neocortex, in layer III of the entorhinal cortex, in the basolateral amygdala, hippocampus, zona incerta of the thalamus, brain stem nuclei, deep cerebellar nuclei, and spinal cord									

Mutation (Name) ***Isoform*** **Promoter**	**p-Tau**	**Insoluble tau**	**NFTs Width (nm)**	**Motor & Cognitive deficits**	**Neuronal loss**	**Synaptic loss**	**Axonal degeneration transport deficits**	**Astrogliosis**	**Microgliosis**	**Reference**
P301S *4R,0* Thy1.2	✓ - 5 mo – half-twisted ribbons and AD-like PHFs ~2 fold endogenous levels - Brainstem and spinal cord > frontal and temporal cortices, cerebral cortex and hippocampal formation	✓	✓	- PND 3, 5 and 7 - pups increased ultrasonic vocalisations (USVs) - 8 weeks – enhanced exploratory activity in MWM and in the openfield task - no deficit in cognitive performance. - 3 months onwards – progressive decline in rotarod performance	- Non-apoptotic nerve cell loss in the cortex and the spinal cord - Denervation of hind-limb skeletal muscle			- GFAP	- CD11b and MHCII in the spinal cord - Bushy morphology	(Allen et al., 2002, Bellucci et al., 2004, Hampton et al., 2010, Scattoni et al., 2010)
P301S (PS19) *4R,2* MoPrP	✓ - 12–20 nm diameter - Randomly oriented filaments - NFTs in neocortex, amygdala, hippocampus, brain stem and spinal cord - Immunosuppression reduces hyperphosphorylated and insoluble tau burden	✓	✓	- Clasping and limb retraction when lifted by the tail at 3 mo - Paralysis at 7–10 mo; - Median survival ~9 mo	- 8 mo onwards- progressive neuron loss in hippocampus - 12 mo amygdala, neocortex, ent. cortex (No mechanism identified.)	- Synaptic loss at 3 mo precedes NFTs - Reduced LTP at 6 mo	- Early defect in axonal transport - Axonal degeneration	- GFAP in hippocampus, amygdala, ent. cortex, and spinal cord at 6 mo	- 3-4 mo MHC's and cd11b especially in hippocampus, amygdale, and ent cortex. - Bushy - Precedes astrogliosis	(Yoshiyama et al., 2007)

Mutation (Name) ***Isoform*** **Promoter**	**p-Tau**	**Insoluble tau**	**NFTs Width (nm)**	**Motor & Cognitive deficits**	**Neuronal loss**	**Synaptic loss**	**Axonal degeneration transport deficits**	**Astrogliosis**	**Microgliosis**	**Reference**
R406W *4R,2,3* CaMK-II	✓ ~10 nm nm diameter - Straight filament - Inclusions in forebrain - Hippocampus > neocortex > olfactory bulb > striatum > thalamus >> midbrain, cerebellum, spinal cord.	✓	✓	- Associative memory (fear conditioning) impairment without obvious sensorimotor deficits			- Microtubule disruption			(Tatebayashi et al., 2002)
R406W *4R,2,3* Syrian hamster prion protein promoter	✓ - 15 to 30 nm diameter - Straight filaments ~1.2-fold endogenous tau - Progressive accumulation in hippocampus & amygdala >> cortices and subcortical areas >> caudate putamen, white matter, and cerebellar cortex - Tau was phosphorylated, ubiquitinated, argyrophilic, and sarkosyl-insoluble. - GSK-3β and CDK5 activation (but not PS9, GSK-3α, MAPK)	✓	✓	- Age related motor disturbances (rotarod) 10 to 12 mo - No difference in step-through passive avoidance test but decreased retention time for the avoidance reaction				- GFAP amygdala and hippocampus	- F4/80 neocortex, amygdala and hippocampus	(Ikeda et al., 2005)

Mutation (Name) ***Isoform*** **Promoter**	**p-Tau**	**Insoluble tau**	**NFTs Width (nm)**	**Motor & Cognitive deficits**	**Neuronal loss**	**Synaptic loss**	**Axonal degeneration transport deficits**	**Astrogliosis**	**Microgliosis**	**Reference**
R406W *4R,2,3* MoPrP	✓ - 10-15 nm diameter - Straight filaments ∼8- to 10-fold over endogenous mouse tau. - Neocortex, amygdala, hippocampus, brainstem, and spinal cord - Somato-dendritic compartment of neurons FTDP-17 like NFTs	✓	✓	- Progressive motor weakness - Dystonic movements of hindlimbs when lifted by tail			- Reduced binding to MTs - Tau transport reduced [35S]-labelled methionine radiolabelled tau	GFAP		(Zhang et al., 2004)
P301L + R406W *4R,2,3* murine CaMKIIα	✓ - 24-fold below that of endogenous murine Tau levels	X	X	- No motor impairments (balance beam) - No change in spatial acquisition in MWM. - Increased swim speed. - Impaired STFP - Less time in open arms of EPM - Electroencephalographic investigations indicated altered vigilance		- Reduction in efficacy of synaptic transmission - No change in synaptic plasticity				(Koss et al., 2016)

Mutation (Name) ***Isoform*** **Promoter**	**p-Tau**	**Insoluble tau**	**NFTs Width (nm)**	**Motor & Cognitive deficits**	**Neuronal loss**	**Synaptic loss**	**Axonal degeneration transport deficits**	**Astrogliosis**	**Microgliosis**	**Reference**
G272V and P301S (THY-Tau22) *4R,2,3* Thy1.2	✓ ~20 - 30 nm filament diameter - NFT like inclusions, rare ghost tangles and PHF-like filaments - Abnormal tau species in neocortex, hippocampus striatum, olfactory bulb, occipital cortex, amygdala, ventral thalamic nuclei, and deep layers of entorhinal cortex	✓	✓	- No motor deficits on rotarod or changes in total motor activity - Impaired anxiety (more time spent in open arms of EPM) - Delayed learning from 3 months, and reduced spatial memory at 10 months in MWM	- Decrease density of pyramidal CA1 cell layer - 12 months - 34% decrease in pyramidal neurons	- Decrease in hippocampal synaptic excitability (excitatory postsynaptic potentials - EPSPs) in old age but no change in LTP		- GFAP - Spatio-temporally correlated with hippocampal tau pathology	- Lectin, CD11b, CD68 - Spatio-temporally correlated with hippocampal tau pathology	(Lim et al., 2001, Schindowski et al., 2006)
V337M *4R,2,3* (PDGF)-b	✓ - Expression levels 1/10th endogenous levels - 11 mo - hippocampal CA1, CA2, and CA3 neurons	✓	✓	- Time spent in the open arms of EPM and extent of locomotor activity were significantly different - No difference in MWM	- Neuronal cell death after accumulation of p-tau and RNA - Fragmentation & blebbing of nucleus and cytoplasm were not present. - No increased TUNEL staining					(Tanemura et al., 2001, Tanemura et al., 2002)

Mutation (Name) ***Isoform*** **Promoter**	**p-Tau**	**Insoluble tau**	**NFTs Width (nm)**	**Motor & Cognitive deficits**	**Neuronal loss**	**Synaptic loss**	**Axonal degeneration transport deficits**	**Astrogliosis**	**Microgliosis**	**Reference**
V337M and R406W *4R,2,3* mThy1	✓ ~2-fold increased expression	X	X	- No motor deficits - Impaired spatial learning in MWM						(Flunkert et al., 2013)
K257T and P301S *4R,0* rat tau promoter	✓ ~15–20 nm twisted filaments - 5–10% expression relative to the endogenous tau cortex, hippocampus and brainstem	✓	✓	- No obvious motor deficit - Impaired spatial memory in radial arm maze - Excessive urination and defecation – anxiety		- Deficit in hippocampal plasticity		- GFAP in the cortex, hippocampus and brainstem		(Rosenmann et al., 2008)
G272V, P301L, and R406W *4R,2,3* Thy1	✓ - 2 - 5 nm thin filaments - Twisted filaments (2 x thin filaments) -Thick straight filaments ~8nm - Tau expressed in cortex and hippocampus > striatum > spinal cord - Increase in the number of lysosomal complexes in neurons with associated increase in acid phosphatase activity	✓	✓							(Lim et al., 2001)

Mutation (Name) ***Isoform*** **Promoter**	**p-Tau**	**Insoluble tau**	**NFTs Width (nm)**	**Motor & Cognitive deficits**	**Neuronal loss**	**Synaptic loss**	**Axonal degeneration transport deficits**	**Astrogliosis**	**Microgliosis**	**Reference**
Truncated tau (t151-391) Thy 1	X	✓	X	- Hunched posture, muscular weakness, bradykinesia and paraparesis					- cd11b - Microgliosis colocalised with tau pathology - CD68 indicates phagocytosis of tau (AT8) - Upregulation of CD11a, CD11b, CD18, CD4, CD45	(Zilka et al., Hrnkova et al., 2007, Zilka et al., 2009)
	Transgenic rats: - Expression levels 2–5-fold over endogenous tau in the isocortex, hippocampus, diencephalon, brain stem and the spinal cord - Decreased life span - Neurological impairment,									

Table 2 – Models of tauopathy. *Summarises key findings from studies on animal models of tauopathy including; the mutation expressed (if any), the isoform of tau, the promoter driving expression, whether or not rodents had phosphorylated, insoluble tau, neurofibrillary tangles, motor or cognitive deficits, neuronal loss, synaptic loss, axonal degeneration or transport impairments, astrogliosis, microgliosis. Abbreiviations: CA - Cornu Ammonis; DG – Dentate Gyrus; EPM – Elevated Plus Maze; Ent. Cortex – Enthorinal Cortex; MoPrP – Mouse prion promoter; MWM – Morris Water Maze; NFT – Neurofibrillary Tangle; PSD – Post Synaptic Density; p-Tau – Phosphorylated tau protein; STFP – Socially Transmitted Food Preferences; USVs – ultrasonic vocalisations.*

1.1.6 Other models of tauopathies

Other models of inherited human tauopathy include *Caenorhabditis elegans* and *Drosophila melanogaster*. In a *C. elegans* model expressing P301L and V337M tau there was hyperphosphorylation and accumulation of insoluble tau, a presynaptic defect in cholinergic neurotransmission and neurodegeneration (Kraemer et al., 2003).

Overexpression of wild-type human tau (0N3R) in *Drosophila* led to impaired axonal transport but not cell death. Transport impairments were visualised by vesicle aggregation and loss of locomotor function. These impairments were rescued by co-expression of constitutively active glycogen-synthase kinase-3β (GSK-3β) and the rescue reversed by GSK-3β inhibitors indicating a role of tau phosphorylation in impaired transport (Mudher et al., 2004).

In vitro studies using cell lines expressing AD truncated tau (AT tau, 151-391 4R) or full length tau (Tau 40) showed that overexpression of either tau reduced metabolic activity of the cells indicative of slowing of cell proliferation. AT tau was more toxic, and cell death appeared to occur via apoptosis; there was cell shrinkage, nuclear, and DNA fragmentation. However, there was no activation of executive caspases involved in the initiation of apoptosis or the caspase cleavage products (PARP and fodrin) (Zilkova et al., 2011).

Contrary to these findings, it has even been suggested by some that tau hyperphosphorylation might in fact be neuroprotective; the surprising lack of evidence tying tau hyperphosphorylation to apoptosis has led some to postulate that tau hyperphosphorylation causes abortion of apoptosis. Tau-expressing cell lines exposed to different types of pro-apoptotic factors, including staurosporine, camptothecin, hydrogen peroxide, ER stress, Aβ, death associated protein kinase-1, and GSK-3β, unexpectedly showed reduced apoptosis compared with controls (Li et al., 2007, Wang et al., 2010b, Liu et al., 2012a). Authors of an interesting review (Wang et al., 2014) postulate that tau hyperphosphorylation prevents apoptosis by substrate

competition, preventing Bcl-2 phosphorylation and thus preventing the release of cytochrome-c from mitochondria into the cytosolic fraction, while also inhibiting Bax expression and caspase-9/3 activity. Instead they postulate that the mechanism of cell-death in neurodegeneration does not occur via apoptosis or any alternative previously described pathway but is in fact a distinct type of cell death which they call "neurodegenerasis".

1.1.7 The P301S Tau Family

It was originally thought that CBD and FTD were two distinct entities based on the clinical presentation and gross pathology; FTD patients suffer emotional, behavioural and intellectual decline before developing motor symptoms, whereas CBD patients present with dystonic limb, progressing to rigidity but retain cognitive faculties until later in disease.

However, the P301S mutation was encoded in 1999 in a father and son who suffered FTD and CBD respectively therefore demonstrating that this tau mutation is sufficient to trigger neurodegeneration and dementia (Bugiani et al., 1999), while also demonstrating that CBD and FTD are distinct clinical phenotypes of a single disease.

The father and son were both in their late twenties when they began to experience symptoms which included depressive mood changes, memory loss, personality changes, and both experienced motor deficits and rigidity (Bugiani et al., 1999).

The mutation was sufficient to induce hyperphosphorylation of tau; antibodies against AT8, AT100 and AT180 labelled most neurons in the cortex as well as axons and dispersed grains and threads. Cells contained abundant filamentous structures, which appeared to be straight filaments, width ~10 nm, sometimes forming filament bundles. Tau pathology was associated with gliosis often including tufted astrocytes. Tau pathology was sufficient to cause nerve cell loss, vacuolation and gliosis in the cortex, caudate nuclei, substantia-nigra and locus coerulus.

DNA sequence analysis identified a C-to-T transition in the first base of codon 301 of the tau gene resulting in a proline-to-serine mutation in tau.

1.1.8 The history of the P301S Tau Mouse

The P301S mouse over-expresses human mutant P301S tau under neuronal promoter Thy 1.2 on a C57BL/6J background. P301S homozygous mice were generated in the Goedert laboratory as previously described (Allen et al., 2002). Briefly, the P301S mutation was introduced by site directed mutagenesis to cDNA encoding the shortest of the 4R tau isoforms (4R0). The mutant tau cDNA was cloned into a genomic expression vector containing the thy1.2 promoter sequence prior to pronuclear injection. Founders were generated and cross breeding generated a line with expression of human mutant tau at twice the levels of endogenous tau.

The original paper on the P301S mouse sought to demonstrate that this animal model recapitulates key hallmarks of disease; they showed by immunoblotting that there is indeed successful expression of the 4R0 isoform of human tau at approximately two-fold endogenous mouse tau levels in both brain and spinal cord tissue of mice aged 5-6 months, and that it is hyperphosphorylated. There is strong labelling of hyperphosphorylated tau in nerve cell bodies and processes, in layers 2, 4, and 5 of the frontal and temporal cortices, in the hippocampal formation, and predominantly in the brainstem and spinal cord. By electron microscopy it was shown that there were large numbers of abnormal ribbon-like tau filaments which positively labelled with hyperphosphorylated tau antibody, AT8. Sarkosyl-insoluble tau filaments were predominantly "half-twisted" ribbons as is commonly found in FTDP-17 and a minority of filaments were more like Alzheimer-paired helical filaments.

The P301S mouse develops a neurological phenotype dominated by a severe paraparesis at 5 – 6 months of age hence they investigated the lumbar spinal cord; they found a 49% motor neuron loss in the ventral grey matter of the spinal cord at 6 months of age compared with control mice, and the skeletal muscle fibres showed

signs of denervation atrophy. Thus, as in human tauopathies, the accumulation of hyperphosphorylated tau correlated with neuronal loss. This nerve cell loss is also associated with GFAP-positive astrogliosis and denervation of hind-limb skeletal muscle (Allen et al., 2002). The mechanism of neuronal loss was not determined; authors were unable to demonstrate apoptosis by in situ end labelling (ISEL) or staining for caspases.

There is also microgliosis in the spinal cord of P301S mice at end stage as indicated by a bushy morphology and expression of CD11b – a receptor involved in migration and complement recognition – and MHCII proteins involved in antigen presentation and interaction with T-cells. There was also co-localisation of IL-1β and COX-2 with cells of neuronal morphology, although the cells producing the IL-1β were not formally identified (Bellucci et al., 2004).

In 2010 Hampton et al. expanded on the original work, demonstrating significant cortical neuronal loss which was specific to the superficial layers of the cortex, as seen in FTD. By immunohistochemistry there was a significant loss of cresyl-violet positive cells, NeuN positive neurons and GABA-ergic neurons in the superficial cortex and not in the deeper layers of the cortex and qPCR showed a decrease in superficial marker reelin and not cux-1 a marker of deeper neurons. This neuronal loss was progressive; there was no significant difference between P301S mice and control mice at 8 weeks of age but there was significant neuronal loss at 12 weeks of age and more so at 20 weeks of age. There was also progressive astrogliosis in the same area of the cortex.

P301S tau mice were crossed with YFP-H mice expressing yellow fluorescent protein in a subset of cortical neurons and long-term two-photon *in vivo* imaging was used to follow the fate of individual dendritic spines in 4-month-old P301S mice. Dendritic spines were lost and replaced in control mice at equal rates such that there was no overall change in synaptic density, however in P301S mice more dendritic spines were lost than gained resulting in an overall decrease in spine density (Hoffmann et

al., 2013). By immunohistochemistry there was little overlap between phospho-tau (AT8) and YFP expressing neurons or NFTs and YFP, and no AT8 staining was observed in the dendritic spines hence authors conclude it is unlikely that the cells imaged *in vivo* contained phospho-tau which otherwise might account for dendritic spine abnormalities.

A behavioural study by Scattoni et al. (2010) investigated early phenotypic markers of disease in P301S mice and demonstrated enhanced motor and exploratory activity in P301S mice at 8 weeks of age in the Morris water-maze and in the openfield task without any deficit in cognitive performance. A later study demonstrated impaired learning in the Morris water maze at 10 weeks of age; control mice repeatedly exposed to the MWM showed decreased latency to find the platform whereas P301S mice showed a significant impairment in platform acquisition over 5 days (Xu et al., 2014) however this finding directly contradicts that of Scattoni et al. (2010). This apparent deficit occurred at a time when tau pathology was detected in the hippocampus by MC1 (conformational epitope) and CP13 (pSer202) as well as reduced average spine density, length, area and volume compared to wild type mice at 2.5 months of age (Xu et al., 2014). They also found lower spine density and larger spine size in P301S mice at 5 months which might be indicative of impaired synaptogenesis or synapse elimination (Xu et al., 2014).

Scattoni et al. (2010) also showed that P301S mouse pups emitted more ultrasonic vocalisations (USVs) than controls at postnatal days 3, 5 and 7; a pup is taken away from its mother and placed in a sound-attenuating Styrofoam box to record emitted sounds. USVs are reportedly related to emotional development (Scattoni et al., 2009, Wöhr et al., 2015).

P301S mice were also able to acquire the rotarod task aged 1 month, however there was a progressive decline in rotarod performance which appeared in the 3rd month of age.

Unpublished data from our lab shows that at 10 weeks of age, in the elevated plus maze (EPM) P301S mice cover significantly less distance in total and in the open arms of the maze, compared with control mice. This is at an age where P301S mice show no signs of hind limb phenotype and are hyperactive in the openfield and MWM. Taken together with the increased activity in the openfield and MWM and increased USVs, this indicates that the mechanisms regulating how P301S mice respond to novelty are perturbed.

1.1.9 Conclusion of Part 1

Here I have introduced dementia and more specifically tauopathy dementias, I have provided background information on the role of tau protein in the healthy and diseased CNS and have introduced various tauopathy mouse models including the P301S tau mouse model of neurodegeneration that will be the subject of my experiments.

On that background, the aim of this thesis is to determine the effect of acute illness on tauopathy disease and vice versa, hence, in the next section I will introduce the broad topic of inflammation: inflammation in the periphery and in the central nervous system, as well as the interactions between the two, in health and in CNS disease.

1.2 Introduction Part 2: Inflammation

1.2.1 Inflammation

Part 1 introduced the concept of dementia as a group of proteinopathies, with accumulation of different proteins and with a whole host of complex aetiologies and neurodegenerative processes, however one significant hallmark all dementias have in common is inflammation in the CNS.

A major part of this thesis is to study how peripheral inflammation influences central inflammation in the context of neurodegenerative disease. In order to understand the relationship between dementia and systemic inflammation it is first necessary to discuss peripheral and central inflammation, their similarities, their differences and ultimately their interactions.

1.2.2 Peripheral Immunity

The ability to mount an immune response is essential for survival of any organism. The inflammatory immune response is the series of events whereby the body is able to:

1. Detect tissue damage or the presence of foreign bodies (e.g. bacterial or viral)
2. Recruit the appropriate cellular – and with them molecular – components to the site of damage or infection in order to...
3. Isolate and destroy the foreign bodies
4. Initiate repair and restore homeostasis

The immune response occurs in two waves; first is the innate immune response which is immediate and short lived. This is followed by the adaptive response which is more specific, takes longer to initiate (Lyman et al., 2013) and generates immunological memory.

Here I will focus primarily on the innate immune response because it is the innate tissue-resident immune cells that underpin the main differences between central and peripheral inflammation. It is likely that the adaptive immune system also plays an important role in neurodegenerative diseases too, especially given the breakdown of the blood brain barrier in disease context, however the field is not quite there yet, hence my decision to focus predominantly on innate immunity.

1.2.3 Innate Immunity in the Periphery

1.2.3.1 Key Players in Innate Immunity

The key players in innate immunity are: the endothelial and epithelial cells, which provide the first line of defence by forming a barrier to keep pathogens out, and the white blood cells or "leukocytes" some of which reside in tissue – macrophages and dendritic cells – and some of which circulate in the blood and lymph vessels – these include neutrophils, eosinophils, basophils, monocytes and natural killer cells (NK cells).

1.2.3.2 Initiating the innate immune response – DAMPs, PAMPs and PRRs

The initiation of the innate immune response depends on the recognition of conserved molecular signatures called danger- or pathogen- associated molecular patterns (DAMPs or PAMPs, respectively) by pattern recognition receptors (PRRs).

DAMPs and PAMPs are chemical moieties associated with tissue damage (DAMPs) or bacterial and viral infections (PAMPs). DAMPs are usually intracellular molecules which are externalised when a cell is ruptured e.g. adenosine triphosphate (ATP) and high-mobility group box-1 protein (HMGB1). PAMPs include chemical moieties such as mannose-rich oligosaccharides and peptidoglycans often found on the outer surfaces of bacteria, and double stranded RNA, which is released by viruses.

PAMPs are evolutionarily conserved structures; this characteristic has allowed coevolution of appropriate receptors on host cells. PRRs are expressed by innate

immune cells such as epithelial and endothelial cells, macrophages, dendritic cells and NK cells. PRRs include toll-like receptors (TLRs), NOD-like receptors (NLRs) and scavenger receptors. PRRs can be membrane bound or cytosolic and intra- or extra-cellular, as required; bacteria tend to exist in the extracellular milieu whereas viral PAMPs are often inserted into the cytoplasm of host cells – PRRs are positioned accordingly.

PRR binding triggers a rapid intracellular signalling cascade, leading ultimately to the synthesis of diverse and pleiotropic inflammatory mediators; chemokines, cytokines (IL-1β, TNF-α, IL-6, IL-12) and acute phase proteins.

1.2.3.2.1 LPS and TLR4

Lipopolysaccharide (LPS) – often used to experimentally mimic a bacterial infection – is a PAMP found on the outer surface of many gram-negative bacteria such as *Escherichia coli*. LPS consists of three parts: lipid A (the main PAMP), a core oligosaccharide, and an O side chain (see **Figure 2**). It can cause systemic inflammation and at high doses can cause sepsis. LPS stimulates the PRR TLR4 through interactions with LPS binding protein (LBP), CD14 and MD-2 (Lu et al., 2008). LBP is a soluble protein which binds to LPS and facilitates binding of LPS to CD14 which then passes the LPS on to the TLR4:MD2 complex (Wright et al., 1989, Wright et al., 1990). Binding of LPS causes oligomerization of TLR-4 bringing the Toll-interleukin-1 receptor (TIR) domains into proximity; the TIR domains recruit several signal transduction adaptor proteins including MyD88 (myeloid differentiation primary response gene 88), TIRAP (TIR domain-containing adaptor protein), TRIF (TIR domain-containing adaptor inducing IFN-β) and TRAM (TRIF-related adaptor molecule) (Lu et al., 2008). Signalling via MyD88 dependent or independent pathways results in NFκB and IRF-3 or -5 (interferon regulatory factor 3 or 5) mediated transcription of proinflammatory cytokines, chemokines and immune receptors.

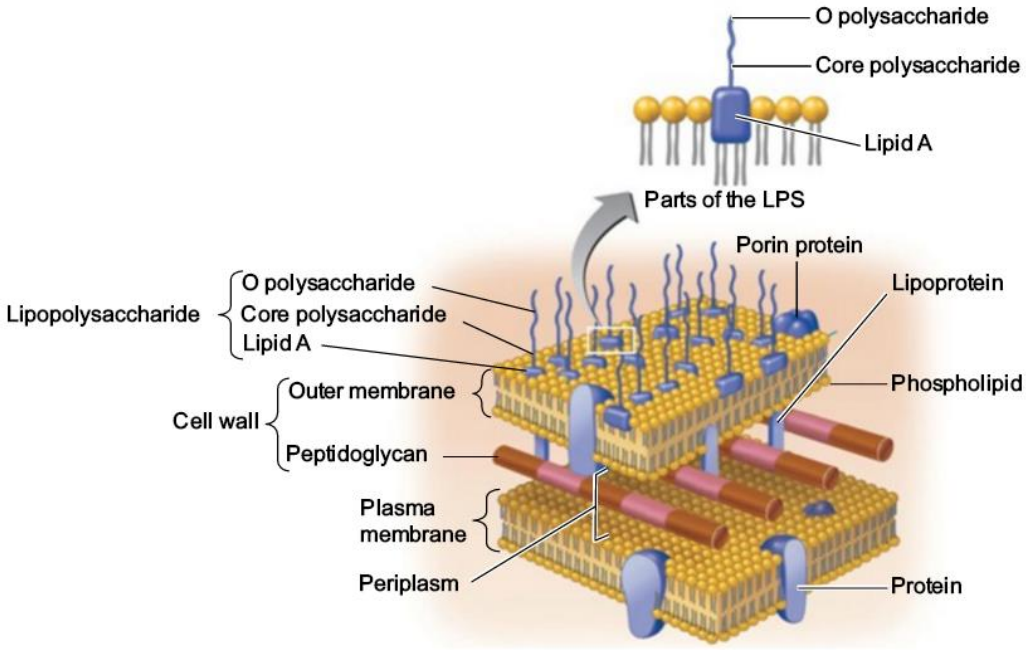

Figure 2 – Lipopolysaccharide (LPS) schematic. *LPS is a chemical moiety found on the outer surface of gram negative bacteria, consisting of three parts: lipid A (the main PAMP), a core oligosaccharide, and an O side chain. Borrowed from ©2016 Pearson Education, Inc.*

1.2.3.3 **Scavenger Receptors**

Another type of PRR - the scavenger receptor - found on the surface of macrophages and dendritic cells - allows cells to bind, phagocytose and degrade pathogens. These cells may become antigen presenting cells (APCs); they degrade the pathogen and present "non-self" peptides bound to major histocompatibility complex (MHC) receptors, along with co-stimulatory molecules expressed on their cell surface, which, together, interact with T-cell receptors (TCRs) to activate T – cells of the adaptive immune response.

1.2.3.4 **Chemokines and Cytokines**

Chemokines are chemotactic factors which recruit cells with the correct chemokine receptors to the site of damage or infection – cells of the innate and adaptive immune systems which may be pro- or anti-inflammatory.

Cytokines are secreted proteins which may have pro- or anti- inflammatory effects. Cytokines bind to their specific cytokine receptors and in doing so they stimulate further cytokine production, as well as proliferation, activation and differentiation of adaptive immune cells which themselves might be pro- or anti-inflammatory. For example, pro-inflammatory cytokine TNF-α binds TNF receptor 1 which initiates a signalling cascade whereby NFκB- and JNK-signalling regulate apoptosis and inflammation. TNF-α also signals through the fas-associated death domain triggering caspase-8 which is involved in IL-1β production. IL-1β activates mitogen-activated protein kinase (MAPK) and resulting in further proinflammatory cytokine production.

IL-10 on the other hand used to be known as cytokine synthesis inhibitory factor (CSIF) and it also downregulates expression of MHCII costimulatory molecules CD80/CD86 (Moore et al., 2001).

More than one type of cytokine is present at any one time, and each is present in different concentrations. These varying combinations, which show dynamic changes, are extremely important in orchestrating the amplitude, polarity and duration of immune responses.

1.2.3.5 **Complement System**

Another important component of innate immunity is the complement system – a group of more than 30 complement proteins. Through a tightly coordinated series of events complement proteins recognise and bind to the surface of bacteria and then two things can happen. Complement proteins completely coat the bacteria – a process called opsonisation - enabling recognition by immune cells with complement receptors. Those immune cells can then bind, engulf and destroy the pathogen. Alternatively, the complement proteins recruit more complement proteins which are able to insert into the bacterial cell membrane and form a pore, killing the cell in the process.

1.2.4 Resolution and regulation

The resolution and regulation of inflammation is essential to avoid tissue damage. Phagocytic cells involved in clearing up the aftermath of inflammation phagocytose pathogens and debris, which stimulates release of regulatory cytokines including IL-10 and TGF-β which are involved in dampening the immune response and resolution of the inflammation including by inhibition of cytokine synthesis, downregulation of costimulatory receptors.

The importance of a well-balanced immune response was underscored by an infamous phase 1 clinical study in 2006; six healthy volunteers were injected with a CD28 superagonist TGN1412 – the CD28 superagonist was supposed to activate T-regulatory cells which are useful in the treatment of autoimmune diseases. Just a few minutes after injection all six volunteers suffered severe cytokine release syndrome which lead to multiple organ failure (Suntharalingam et al., 2006).

Dysregulation of the immune response also causes autoimmune diseases such as rheumatoid arthritis and multiple sclerosis where the immune system is activated by self-antigens. On the other hand, failure to mount an immune response leaves hosts vulnerable to infection.

The peripheral immune response must therefore be carefully regulated at many stages in order to minimise damage to bystander host cells. To discuss all the regulatory mechanisms of the immune response is beyond the scope of this thesis but it is important to highlight that there are many mechanisms in place. Examples which are relevant for central immunity include: inhibitory molecules which prevent destruction of host cells; regulatory immune cells which release cytokines involved in suppressing the immune response; feedback inhibition in the production of proinflammatory cytokines.

1.2.5 CNS Immunity

Since most neurons of the central nervous system are post-mitotic and must last a lifetime, the immune response must be even more tightly regulated than in the periphery since any inappropriate immune reaction would be extremely costly. One key difference between the central and peripheral immune response is the cellular components.

1.2.5.1 Key Components in CNS Immunity

The key players in immunity in the CNS are the astrocytes, paraventricular macrophages and microglia; the resident macrophage cells of the brain. Neurons and epithelial cells are also capable of expressing cytokines and receptors at low levels.

1.2.5.1.1 Endothelial Cells of Blood Brain Barrier

The central nervous system was previously thought to be completely isolated from circulating peripheral inflammatory mediators by the blood brain barrier (BBB) – a specialised endothelial layer with tight junctions. It is now understood that circulating pro-inflammatory cytokines such as TNF-α, IL-6, and IL-1β – all of which are elevated in dementias – can influence BBB permeability (Wong et al., 2004). The BBB actively transports cytokines such as TNF-α and IL-1β (Gutierrez et al., 1993, Gutierrez et al., 1994) and can also be stimulated to release proinflammatory mediators and allow extravasation of leukocytes into the brain parenchyma (Laflamme et al., 1999, Terrando et al., 2011).

1.2.5.1.2 Brain lymphatic system

Two groups independently discovered the existence of a brain lymphatic system in 2015, which will have huge implications for the field (Aspelund et al., 2015, Louveau et al., 2015). The lymph vessels express markers of lymphatic endothelial cells including lymphatic vessel endothelial hyaluronan receptor 1 (Lyve-1) and vascular endothelial growth factor receptor 3 (VEGFR3). They run alongside blood vessels in

the meninges and drain into deep cervical lymph nodes (dcLN). Genetic ablation of the vessels or ligation of lymph vessels near the dcLN blocks drainage of dyes to the dcLN and led to an increase in T-cell density in the vessels. This discovery contradicts what was previously thought to be true about T-cell circulation in the brain. There is still, however, no evidence for a cell which exists in the normal brain parenchyma and is capable of antigen presentation *and* migration from the CNS to the lymph nodes for stimulation of T- and B- lymphocytes, as is seen in the periphery. This difference is likely to be key in the immune-privilege status of the CNS.

1.2.5.1.3 Astrocytes

Astrocytes, so called because of their often star-like morphology, make up ~70% of cells in the cerebral cortex. Astrocytes play an important role in maintaining homeostasis in the CNS and are also involved in CNS immunity.

1.2.5.1.3.1 Astrocytes - Role in the healthy brain

Astrocytes found in grey matter are "protoplasmic" and have lots of shorter branches, whereas astrocytes of the white matter are "fibrous" and have longer unbranched processes. Astrocytes form syncytial networks around neurons to provide physical support and enable provision of energy and removal of toxic waste as required.

Generation of an action potential by neurons is extremely metabolically demanding; astrocytes are the only cells in the brain capable of "energy storage" in the form of glycogen, which can be rapidly converted into glucose, astrocytes can convert glucose to lactic acid which is subsequently taken up by neurons and converted to pyruvate for energy metabolism (Danbolt, 2001). Astrocytes make contact via end-feet-processes with capillaries and with the Node of Ranvier and the synapse of neurons and in this way they are able to provide neurons with energy and remove waste.

Astrocytes contribute to a tripartite-synapse, where they maintain neurotransmitter concentrations; they take up glutamate, GABA and glycine thus avoiding over-

stimulation and resulting neurotoxicity. Astrocytes contain glutamate transporters GLT-1 (glutamate transporter-1) and GLAST (glutamate-aspartate transporter) which allow glutamate uptake, thereby avoiding glutamate induced neurotoxicity, and glutamine synthetase which enables conversion of glutamate back into glutamine for uptake by presynaptic neurons which can then convert glutamine back into glutamate for reuse (Martinez-Hernandez et al., 1977).

Astrocyte end feet make contact with synapses and also with brain vasculature thus modulating blood flow in an activity dependent manner; glutamate activates metabotropic glutamate receptors on astrocytes, and downstream signalling results in local release of calcium, prostaglandins, and nitric oxide which regulate capillary dilation (Hirase, 2005).

Astrocytes also provide neurotrophic support for neurons (Zhou et al., 1994, Friedman et al., 1998), maintain pH, ion homeostasis, and help to maintain proper functioning of the BBB (Fuller et al., 2010).

Emerging evidence suggests that astrocytes release signals which induce expression of complement C1q protein by synapses, thereby labelling them for synaptic pruning by microglia (Stevens et al., 2007).

1.2.5.1.3.2 Astrocytes – Role in Immunity

The phenomenon of immune activation of astrocytes is referred to as astrogliosis. Astrocytes detect change in their environment and switch to a "reactive" phenotype, i.e. they proliferate and undergo morphological changes. Reactive astrogliosis can be triggered by a whole host of molecules including cytokines (IL-6, LIF, CNTF, TNF-α, INF-γ, IL-1α/β, IL-10, TGF-β, FGF-2), TLR ligands (e.g. LPS), neurotransmitters, ATP, ROS, NOS, products of neurodegeneration (Aβ) (Sofroniew, 2009).

Glial fibrilliary acidic protein (GFAP) is the key astrocyte-specific intermediate filament protein which mediates the cytoarchitectural changes during reactive

astrogliosis. During mild reactive astrogliosis there is little proliferation of astrocytes but there is upregulation of GFAP in cells which did not previously express GFAP giving the impression of increased numbers. There is very little overlap between astrocytes, and the lack of reorganization of tissue means that astrocytes may return to their previous appearance once the initial trigger of gliosis is resolved. In severe astrogliosis there is vast upregulation of GFAP and mature astrocytes re-enter the cell cycle, proliferate and invade the site of injury where they switch to a reactive morphology with lots of overlapping and interaction between densely packed astrocytes in a bid to isolate the damaged area; this is called a glial scar. This concentrates inflammatory cells where they are needed and prevents spread to surrounding healthy tissue. Glial scar formation also prevents the spread of demyelination.

GFAP is such a consistent marker of reactive astrogliosis that it is often used alone to demonstrate astrogliosis in pathological context giving the false impression that astrogliosis is a homogenous event. In reality increased GFAP expression, is a universal response of astrocytes to environmental changes such as injury and disease, but astrogliosis is a spectrum of molecular, cellular and functional changes of astrocytes in response to injury or disease; different stimuli initiate different astrocyte expression profile and thus the role of reactive astrocytes varies and can be damaging or beneficial (Zamanian et al., 2012). These differences are not discriminated by GFAP.

Cluster analysis of GeneChip expression profiling data from astrocytes isolated from mice following either middle cerebral artery occlusion (MCAO) to induce ischemia or LPS-injection showed an increase in several genes common to both insults but also indicated that the different injuries produced different patterns of reactive astrocyte gene expression (Zamanian et al., 2012). LPS mostly fails to cross the BBB (Banks et al., 2010) and thus exerts its effects by proinflammatory cytokine signalling downstream of TLR4 activation whereas in MCAO all cell types are exposed to ischemia, and astrogliosis is triggered by dying cells, hypoxia, acidosis, direct trauma,

and pro-inflammatory cytokines. LPS-induced reactive astrocytes upregulated genes involved in the antigen presentation and complement pathway activation and are therefore considered detrimental, whereas MCAO reactive astrocytes expressed genes involved in increased metabolic activity, cell-cycle genes, transcription factors and neurotrophic factors and appear to be neuroprotective (Zamanian et al., 2012).

These deleterious and neuroprotective astrocyte profiles have since been referred to as A1 and A2 astrocytes respectively (Liddelow et al., 2017), in line with (now out-dated) terminology used to refer to polarised microglial subtypes (discussed in section 1.2.5.1.4.2 Microglia – Role in immunity) .

Astrogliosis can have dual role in CNS inflammation, the switch towards reactive astrocytes with a proinflammatory profile can result in loss of previously described essential functions of astrocytes leading to loss of homeostasis in the brain. Astrocytes can inhibit axonal regeneration following spinal cord injury (McKeon et al., 1991, Fitch et al., 2008) and are also capable of producing molecules which can exacerbate CNS inflammation including proinflammatory cytokines and chemokines (Brambilla et al., 2005).

However astrocytes have several beneficial roles in pathological conditions including: protection from cytotoxic effects of glutamate by glutamate uptake; protection from oxidative stress; facilitation of BBB repair; restoration of homeostatic water levels and ion concentrations and more (Faulkner et al., 2004, Sofroniew et al., 2010).

Activated astrocytes upregulate a whole host of molecules involved in cell adhesion, antigen presentation, growth factors and their receptors, cytoskeletal proteins (vimentin, GFAP), molecules involved in calcium signalling (Eddleston et al., 1993). Astrocytes are capable of producing pro- and anti-inflammatory cytokines depending on their context; astrocytes close to lesion sites are more likely to acutely produce

proinflammatory cytokines however astrocytes distal to lesion site, or after some time produce anti-inflammatory cytokines.

1.2.5.1.4 Microglia

Microglia are ubiquitous tissue resident innate immune cells. They enter the CNS very early in embryonic development before formation of the BBB where they make up ~10% of the adult brain cell population (Lawson et al., 1990). They play a role in development and homeostasis but they are also the macrophages of the brain and therefore have an important role in neuroinflammation.

1.2.5.1.4.1 Microglia – Role in the healthy brain

Microglia exist relatively evenly spaced throughout the brain parenchyma and with very little overlap between cells. There is evidence to suggest different populations of microglia exist within different regions of the CNS (Elkabes et al., 1996, Ren et al., 1999, Sriram et al., 2006, Grabert et al., 2016).

Microglia are important during development for synaptic pruning. In normal conditions microglia exist in a ramified morphology; they have a relatively small soma and they extend long, motile processes which are constantly palpating and detecting changes in their microenvironment, as was seen using two-photon microscopy (Nimmerjahn et al., 2005). These processes make contact with dendrites and synapses of neighbouring neurons where they are able to detect synaptic dysfunction and remove dysfunctional synapses by phagocytosis.

Microglia also release growth factors; for example, insulin-like growth factor 1 which is involved in layer V cortical development (Ueno et al., 2013) and BDNF which is involved in learning-dependent synapse formation. Resting microglia are also involved in the removal of debris and apoptotic cells during development.

1.2.5.1.4.2 Microglia – Role in immunity

However, microglia are also the tissue-resident innate immune cells – the macrophages of the brain. Many useful parallels can be drawn between macrophage and microglial biology.

There is a great deal of discussion around microglial and macrophage phenotypes. Historically peripheral macrophages were understood to be *either* pro- or anti-inflammatory. Macrophages were thought to be "classically activated" by pro-inflammatory cytokines such as IFN-γ or TNF-α, resulting in a pro-inflammatory, M1 cytokine profile including interlukin-1β (IL-1β), IL-6, IL-12 and tumour necrosis factor a (TNF-α); or "alternatively activated" by IL-4, inducing an anti-inflammatory M2 profile including IL-10, and TGF-β expression. However, in recent years it has become apparent that there is in fact a subtler spectrum of activation states rather than two polarised states. Macrophages respond to extracellular factors and can simultaneously express pro- and anti-inflammatory mediators.

Since microglia are the macrophages of the brain this begs the question, does this spectrum of activation also apply to microglia? The quick answer is "Yes". Microglia are extremely dynamic and their morphology and expression profile is dependent on their microenvironment. When microglia detect a change in their environment they too are capable of phenotypic switching.

Experiments where microglia are artificially exposed to LPS or IL-1β show that they are indeed capable of an M1-like proinflammatory state (Herrera et al., 2000, Hauss-Wegrzyniak et al., 2002). However, since neurons are mostly post-mitotic and an over-zealous immune response in the central nervous system would be extremely costly, microglial activation is in actual fact repressed.

While the CNS is not completely isolated by the BBB, microglial cells are, for the most part, sheltered from circulating serum proteins and the extracellular milieu in the

healthy brain is generally anti-inflammatory with relatively high levels of TGF-β and anti-inflammatory prostaglandin E_2 (PGE_2).

The activation (or not) of microglia depends on their relative expression of activating and inhibiting receptors, which have either immunoreceptor tyrosine-based activation motifs (ITAMs) or immunoreceptor tyrosine-based inhibition motifs (ITIMs) on their intracellular domain.

Microglia express CD200R a receptor with an inhibitory motif. CD200R binds CD200, a neuronal membrane bound protein which inhibits microglial activation (Barclay et al., 2002, Koning et al., 2009). Microglia from CD200 deficient mice have an exaggerated response to TLR2 and TLR4 stimulation (Costello et al., 2011) and real-time PCR indicated increased CD11b, MHCII and CD40 expression in hippocampus of CD200 deficient mice (Denieffe et al., 2013). Fractalkine (CX3CL1) is a neuronal secreted protein which binds to microglial fractalkine receptor (CX3CR1) (Harrison et al., 1998) to elicit a "quiescent" phenotype (IL-10, TGF-β). TREM2 (Triggering receptor expressed on myeloid cells 2) is another microglial protein which belongs to the immunoglobulin (Ig) superfamily of receptors is involved in phagocytosis and downregulation of pro-inflammatory cytokines. There is also evidence that microglial cells express neurotransmitter receptors and are repressed by neurotransmitters e.g. acetylcholine and gamma-aminobutyric acid (GABA) and hence neuronal activity is important in microglial activation (Pocock et al., 2007). In this way neuronal loss in neurodegenerative diseases might lead to progressive microglial activation.

Microglia are therefore not only sensitive to DAMPs, PAMPS and cytokines as seen in peripheral macrophages but are also responsive to small changes in their micro-environment; the absence of neuronally-expressed inhibitors (CD200 and CX3CL1, neurotransmitters) due to neuronal dysfunction, or presence of serum proteins (fibrinogen binds CD11b) due BBB breakdown can activate microglial cells.

Microglial activation occurs within hours of injury or proinflammatory stimulus. Activated microglia upregulate surface receptors including chemokine receptors (enables chemotaxis), complement receptors and Fc receptors (enables phagocytosis of opsonised antigen), MHC proteins and accessory proteins (enables antigen presentation and interaction with infiltrating T-cells). They produce ROS, NO, along with release of proinflammatory cytokines which influence BBB permeability and allow recruitment of adaptive immune cells to the site of infection.

When microglia are activated they withdraw their long processes and adopt a bushy morphology with thickening of proximal processes, there is visible membrane ruffling as they become migratory in response to chemokine expression at the site of infection (Lively et al., 2013). Microglia are capable of phagocytosis of pathogens and cellular debris. This phagocytosis results in expression of anti-inflammatory cytokines (Fadok et al., 1998, Huynh et al., 2002) which together with regulatory T-cells help to dampen the local inflammatory response and in this way the acute immune response is self-limiting and ultimately leads to repair and restoration of homeostasis.

1.2.6 CNS Inflammation associated with Dementias

Neuroinflammation is often described as a double-edged sword; in section 1.2 I described the inflammatory response as an adaptive sequence of events which aims to remove pathogens, repair damage and restore homeostasis, however I have also highlighted the importance of regulation of the immune response.

Chronic inflammation in the central nervous system (CNS) is a consistent hallmark of all dementias. CNS inflammation can be beneficial when it is acute and transient as discussed above, however chronic inflammation associated with CNS disease can become deleterious.

Astrogliosis and microgliosis were both described in post-mortem AD by Alois Alzheimer over a century ago. These and other hallmarks of inflammation have been

described in most neurodegenerative conditions since then; including AD, PD, amyotrophic lateral sclerosis (ALS), multiple sclerosis (MS), and Wallerian degeneration.

The vast literature on the role of neuroinflammation in neurodegeneration predominantly focuses on AD where studies suggest that Aβ-plaques provide a proinflammatory stimulus for astrocytes and microglia (Giulian et al., 1996, McDonald et al., 1998, Liu et al., 2012c). For extensive reviews on the role of neuroinflammation in neurodegeneration, in particular AD, see (Akiyama et al., 2000, Schwab et al., 2010, Cunningham, 2013).

However little attention is focused on the role of neuroinflammation in the context of pure tauopathies in the absence of Aβ. Here I will introduce what is currently understood on the subject.

There are notable differences between microglia in AD and in pure tauopathies; in AD brain there are greatly elevated numbers of microglial cells even in areas lacking Aβ-deposition, whereas in a pure tauopathy such as Pick's Disease there were relatively fewer microglial cells, and microglial activation was seen only in areas of extreme tau pathology (Paulus et al., 1993). This is in line with several other studies showing regional association of microglial activation with tau pathology in post-mortem tissue from pure tauopathies including PSP and CBD (Kida et al., 1992, Sheng et al., 1997, Ishizawa et al., 2001, Sasaki et al., 2008). This regional association has also been observed in patients diagnosed with FTLD, CBD and PSP visualised by positron emission tomography using [11C](R)-PK11195, a marker of peripheral benzodiazepine binding sites (PBBS) expressed by activated microglia (Cagnin et al., 2004, Henkel et al., 2004, Gerhard et al., 2006).

The regional association of microglia with tau pathology has been recapitulated in many transgenic models of tauopathies. A study in a P301L tau transgenic mouse showed that microglial activation correlated with the degree of tau pathology and

that where there was only mild tau pathology there was no microglial activation. Interestingly where there was tau pathology and associated increase in IBA1-positive microglia they did not cluster around cells containing AT8-positive structures such as NFTs, pretangles and neuropil threads as is often the case with Aβ-laden cells and immune-electron microscopy using IBA1 showed lysosomal dense bodies but no filamentous structures corresponding with NFTs (Sasaki et al., 2008).

The role of microglial cells in CNS disease is not clear cut. As mentioned before, experiments which attempt to model microglial activation by artificially exposing microglia to IL-1β and LPS do not realistically model microglia found in CNS disease where they often adopt an activated morphology but do not express the full complement of typically proinflammatory cytokines.

A study of transgenic rats expressing pathological truncated tau indicated that NFTs were associated with upregulation of complement receptor 3, CD4 and CD45. Furthermore, double immunofluorescence staining showed co-localisation of phospho-tau (AT8) with microglial marker of lysosomal degradation - glycoprotein CD68 indicative of phagocytosis of tau protein (Zilka et al.).

In CNS disease, neuronal damage and the accumulation of mis-folded proteins provide a persistent trigger for inflammation and since the immune response cannot successfully remove the threat as it could if it were an invading pathogen, there is no resolution of the inflammatory response. It is likely that the chronic nature of CNS diseases combined with the immune-suppressive environment of the brain might provide persistent and conflicting signals.

There are examples indicating that microglia have both beneficial and detrimental effects in CNS disease (Hanisch et al., 2007), for example, microglia are capable of phagocytosis with concomitant expression of anti-inflammatory cytokines (Magnus et al., 2001). Loss of TREM2 leads to impaired phagocytosis and increased production of proinflammatory cytokines and rare polymorphisms in TREM2 are a risk factor for

AD and FTD (Guerreiro et al., 2012, Jonsson et al., 2013, Singaraja, 2013). CCL2, also known as monocyte chemoattractant protein 1 (MCP1), is a chemokine for microglial activation and monocyte attraction and is upregulated in AD (Sly et al., 2001). Depletion of Ccr2, the chemokine receptor on microglial cells, in Tg2576 AD mice impaired microglial accumulation, accelerated Aβ accumulation and increased mortality (El Khoury et al., 2007). Microglia transplantation led to improved Aβ-clearance (Takata et al., 2007). However, it seems that microglia are surprisingly poor at phagocytosis in the context of CNS disease (Wisniewski et al., 1991).

Yoshiyama et al (2007) demonstrated early microgliosis which preceded tangle formation in the PS19 mouse. Microgliosis was visualised by staining for MHCs and CD11b and also by radiograms using radiotracer [3H]-DAA1106. Microglial activation corresponded with regions of tau pathology and was characterized by bushy, thickened and branched processes. Astrogliosis visualised by GFAP staining, was demonstrated in the same areas.

Interestingly, immunosuppression with FK506 increased the life span of PS19 mice, dramatically rescued neuronal counts, attenuated markers of inflammation (CD11b, and neuronally expressed Cox-2 and IL-1β) and reduced hyperphosphorylated and insoluble tau burden (Yoshiyama et al., 2007). Authors attribute these beneficial effects to repressed *microglial* activation, although FK506 functions through binding calcineurin which is also expressed in T-cells, astrocytes and neurons (Ho et al., 1996, Solà et al., 1999, Furman et al., 2014). The effect of FK506 on T-cells might be significant since in a similar model and in a P301L tau FTD patients there was infiltration of CD8+ T-cells into the brain parenchyma (Laurent et al., 2016). However, the point stands that immunosuppression was beneficial in this instance.

As previously described, there is age related phosphorylation and accumulation of tau protein in the hTau mouse model (section 1.1.5 and (Andorfer et al., 2003)) the accumulation of tau in this model is associated with neuronal loss and progressive microgliosis (IBA1) (Bhaskar et al., 2010). Microglia from hTau mice showed elevated

levels of cleaved fractalkine (CX3CL1), inducible nitric oxide synthase (NOS2) and MCP1, however TNF-α, INF-γ, IL-1β and IL-6 levels remained unchanged.

Since fractalkine is essential in modulating microglial activation, hTau mice were crossed with fractalkine knock out mice to determine the effect of dysregulation of microglia on disease pathology. hTau-CX3CR1$^{-/-}$ mice displayed increased microgliosis compared with age matched hTau-CX3CR1$^{+/+}$ mice, determined by increased IBA1 staining with thickened, bushy microglial morphology as well as increased CD68, CD11b and iNOS staining. This increased microgliosis was associated with elevated levels of pathological hyperphosphorylated and insoluble tau compared with hTau-CX3CR1$^{+/+}$ mice. Further mechanistic studies identified p38-MAPK as the responsible kinase involved in the increased microglial mediated tau phosphorylation.

Astrogliosis is another recurrent hallmark of tauopathy dementia and has been repeatedly demonstrated in transgenic mutant tau animal models of tauopathies (discussed in section 1.2.5.1.3.2 and summarised in Table 2).

Astrogliosis in CNS disease is typically characterised by hypertrophy, proliferation and GFAP expression (Sajja et al., 2016) and, as with microgliosis, the degree of astrogliosis correlates with the degree of tau pathology (Sheng et al., 1997).

Astrocytes in tauopathies often have tau positive inclusions and the profile of those glial inclusions correlates with the type of tauopathy; astrocytic tufts of abnormal fibres are found in PSP, astrocytic plaques in the distal dips of glial cells and dense glial threads are seen in CBD and ramified astrocytes and small Pick body-like inclusions in PiD (Feany et al., 1995, Komori, 1999, Broe et al., 2004). It is likely that the intracellular tau deposits result from glial expression of aberrant tau protein since there is no evidence of tau uptake by glia. This is supported by the lack of astrocytic tau in animal models expressing tau under neuronal promoters.

Astrocytic tau deposits result in loss of neuroprotective astrocyte function in disease. Animal models expressing tau under the GFAP promoter develop astrocytic tau inclusions typical of tauopathies and have reduced glutamate transporter (GLT-1 and GLAST l) expression as was also reported in CBD post-mortem tissue (Dabir et al., 2006).

Some loss of neuroprotective function will come from phenotype switching to reactive astrocytes. Indeed in our own model of P301S tau there is progressive reactive astrogliosis detected by GFAP and transplantation of astrocytes and progenitor cells which differentiated into astrocytes led to astrocyte-mediated neuroprotection perhaps, but not exclusively, by increased secretion of neurotrophic factors (Hampton et al., 2010).

In addition to microgliosis and astrogliosis, there is evidence of T-cell infiltration in AD tissue (Itagaki et al., 1988, Rogers et al., 1988, Togo et al., 2002). However there has been limited research into the role of infiltrating adaptive immune cells in tauopathy dementia.

THY-Tau22 mice express full length mutant tau (G272V and P301S) under the thy 1.2 promoter; tau is hyperphosphorylated and develops into NFT like inclusions, rare ghost tangles and PHF-like filaments. Tau pathology is spatiotemporally associated with astrogliosis (GFAP) and microgliosis (lectin, CD11b, CD68, IBA1) and recent studies indicate CD8+ T-cell infiltration. T-cell depletion improved performance on the Y-maze but did not alter tau expression, truncation or phosphorylation. T-cells were also present in the brain parenchyma of P301L tau FTD patients (Laurent et al., 2016).

1.2.7 Dementia and systemic inflammation

There is a body of evidence which suggests that systemic illnesses with an inflammatory component such as diabetes, increase the risk of dementia (Engelhart et al., 2004, Yaffe et al., 2004, Perry et al., 2007, Tobinick, 2008).

Numerous inflammatory medical conditions are associated with increased risk of dementia, including stroke, diabetes, midlife hypertension, midlife obesity and midlife hypercholesterolaemia. A case-control study of patient records from the General Practice Research Database, with 9954 valid cases, and 9374 valid controls, showed an increased risk of dementia diagnosis following infection (Dunn et al., 2005). A population-based prospective cohort study, demonstrated an association between plasma levels of inflammatory proteins (α-antichymotrypsin, IL-6, and C-reactive protein (CRP)) and increased risk of dementia (Engelhart et al., 2004).

In a prospective study of 300 subjects with mild to severe AD, patients were cognitively assessed using the Alzheimer's Disease Assessment Scale (ADAS-COG), carers provided details of incident systemic inflammatory events and a blood sample was collected. Patients were followed up at 2, 4, and 6 months. Increased circulating TNF-α at baseline was associated with a 4-fold increase in the rate of cognitive decline over the 6-month follow-up period. Acute systemic inflammatory events were associated with increased circulating TNF-α and a 2-fold increase in the rate of cognitive decline over a 6-month period. Subjects with elevated TNF-α at baseline and subsequent acute systemic inflammatory events had a 10-fold increased rate of cognitive decline during the 6-month period compared with subjects with low TNF-α and no acute inflammatory events (Holmes et al., 2009). Infection and raised serum IL-1β levels are also associated with increased rate of cognitive decline in patients with AD (Holmes et al., 2003).

There is evidence that long term exposure to non-steroidal anti-inflammatory drugs (NSAIDs) is protective against AD and Parkinson's disease (PD) (Rogers et al., 1993, Breitner, 1996, Weggen et al., 2001, Sastre et al., 2003, Szekely et al., 2004, Chen H et al., 2005) which is regularly quoted as evidence that *neuro*inflammation has a causative role in progression of disease with no mind to the fact that the NSAIDS were prescribed to treat *systemic* illness.

1.2.7.1 Systemic inflammation and the CNS: Sickness Behaviour

There was a long-held misconception that the CNS is an immune-privileged region, isolated from circulating inflammatory mediators of the peripheral immune system by the BBB. We now know however that isolation of the brain is not absolute; there are a number of pathways which allow deliberate communication of the systemic inflammatory state with the CNS.

While circulating pro-inflammatory cytokines are too large to cross the BBB themselves, they are able to communicate across the BBB via a number of means; they are able to initiate expression of cytokines and cyclooxygenase (COX) enzymes by endothelial cells (Matsumura et al., 2004); enter the brain via the circumventricular organs (CMVOs) where there are no tight junctions between endothelial cells (Blatteis et al., 1983); and they stimulate afferents of the vagus nerve (Blatteis et al., 1998, Konsman et al., 2002, Romanovsky, 2004, Szekely et al.), subdiaphragmatic vagotomy attenuates the fever response to systemic LPS (Roth et al., 2001).

The pathways of communication between peripheral immunity and the CNS enable systemic inflammation to initiate fever and sickness behaviours including anorexia, decreased locomotor activity and decreased social interaction, all of which are coordinated by the CNS (Dantzer, 2001).

These sickness behaviours are adaptive and serve to reduce the risk of further spread of the pathogen however it is thought that an aberrant sickness response to systemic inflammation arises when systemic inflammatory signals are superimposed onto CNS disease and this aberrant response might be the biological substrate of delirium caused by systemic inflammation with dementia (Cunningham et al., 2013).

1.2.8 Delirium

Delirium is a common and profound neuropsychiatric condition, characterized by altered levels of arousal, inattention, cognitive deficits and psychoses with a

fluctuating pattern as described by the Delirium Rating Scale - Revised - 98 (DRS-R98) or the Confusion Assessment Method (CAM). It is a short-term, reversible condition, with acute onset.

Delirium is an extremely complex condition with a vast range of predisposing and precipitating factors; it is usually caused by a combination of factors and hence teasing apart mechanisms is complicated. However, elderly people and those with pre-existing dementia are particularly susceptible to delirium compared with non-demented counterparts (Fick et al., 2002).

1.2.8.1 **Dementia as a risk factor for Delirium**

In 1986 a study of two-thousand medical inpatients found that 41.4% of demented patients experienced delirium compared to only 12.4% of non-demented patients (Erkinjuntti et al., 1986).

In a population-based longitudinal study Davis et al. (2015) showed that increased dementia severity, determined by Mini-Mental State Exam (MMSE) correlated with increased risk of delirium; for every MMSE point lost the risk of delirium increased 5% (Davis et al., 2015).

Still relatively little is known about how different types of dementia impact on the likelihood of delirium. After an extensive search of the literature for examples of "delirium" or "confusion" in the context of different types of dementia I found only one relatively small study from 1997 of 175 patients with AD, vascular AD and FTD which indicated a higher rate of delirium in patients with late onset AD (LAD – 57%) than early onset AD (EAD – 14%) or FTD (19%) and higher rates in VAD (40%) than EAD (Robertsson et al., 1998). The differences could not be explained by age. There was a relationship between disease severity (mild, moderate or severe) and occurrence of delirium but authors suggested the different rates of delirium between different types of dementia might relate to the areas of the brain affected, since EAD

and FTD are predominantly cortical whereas pathology is more widespread in LAD and VAD.

1.2.8.2 **Delirium has long-term cognitive impacts**

Delirium is not just a benign and transient state of confusion as was previously thought. A population-based cohort study showed that delirium increases the risk of incident dementia and it exacerbates the severity and trajectory of pre-existing neurodegenerative conditions (Davis et al., 2012).

A large prospective cohort study of the Massachusetts Alzheimer's Disease Research Centre's patient registry showed that delirium accelerates the rate of cognitive decline measured by the Information-Memory-Concentration (IMC) subtest of the Blessed Dementia Rating Scale. Prior to delirium dementia patients showed a decline in IMC performance of 2.5 points per year, following delirium the average decline was accelerated to 4.9 points per year. There was no change in the rate of decline seen in patients who did not experience delirium (Fong et al., 2009).

The duration of follow up in this study was unclear, however, another study of hospitalised patients with AD showed that the rate of decline in patients prior to hospitalisation did not differ, whereas, in the 5-year period following hospitalisation the rate of decline in patients who developed delirium during their stay was double that of those who did not experience delirium during their stay (Gross et al., 2012).

Not only does delirium increase the risk and trajectory of long term cognitive impairment but there is also evidence that longer duration of delirium is associated with worse long term cognitive impairment (Pandharipande et al., 2013).

A meta-analysis of studies published between January 1981 and April 2010 with minimum follow-up of 3 months found that delirium is also associated with increased risk of permanent institutionalisation, dementia and death (Witlox et al., 2010).

Importantly it is estimated that delirium could be prevented in up to a third of hospital inpatients (Inouye et al., 1999).

It is thought that delirium is the result of an aberrant psychoneuroimmunological response to systemic inflammatory signals caused by the already inflammatory environment within the CNS during neurodegeneration (Cunningham et al., 2013); more specifically it is thought to be underpinned by microglial priming.

1.2.9 Microglial priming

The microglial priming hypothesis describes the phenomenon whereby microglia in the diseased brain exist in an altered state of activation such that a subsequent inflammatory insult – central or systemic – induces an exaggerated inflammatory response.

Pioneering work in the ME7 prion disease mouse model of chronic neurodegeneration showed that during CNS neurodegeneration microglia exist in an atypical state of activation (Cunningham et al., 2003).

Prion diseases, otherwise known as transmissible spongiform encephalopathies (TSEs), are a group of infectious progressive neurodegenerative diseases where the infectious agent is mis-folded prion protein which cannot be broken down. Pathological mis-folded prion protein seeds self-propagating mis-folding and recruitment of prion protein (Prusiner, 1982) leading ultimately to the demise of neurons with associated neuronal dysfunction, neuroinflammation, and clinical phenotype. The transmissible nature of prion disease makes it a useful tool for creation of animal models of neurodegeneration, including the ME7 prion disease mouse model which is created by injection of ME7-infected C57BL/6 brain homogenate into the brain.

This model recapitulates key hallmarks of prion disease including extracellular amyloidosis, synaptic loss, microglial activation, neuronal death and mice show

progressive cognitive decline. Microglia were initially thought to be in pro-inflammatory M1 state in prion disease, based on their morphology and the expression of inflammatory markers such as MHCI and CR3. There is a 10-fold increase in the number of microglia in the hippocampus of ME7 mice 23-weeks post-inoculation compared with control animals. There were also CD8+ve T-lymphocytes and associated astrogliosis (Betmouni et al., 1996). However, elevated levels of anti-inflammatory cytokine TGF-β were found along with very limited expression of archetypal pro-inflammatory cytokines IL-1β, IL-6, TNF-α (Cunningham et al., 2003, Cunningham et al., 2005).

Cunningham et al. (2009) showed that subsequent peripheral injection with lipopolysaccharide, which mimics bacterial infection, resulted in exaggerated sickness behaviour in prion diseased mice compared with injected controls. This sickness behaviour was associated with dramatically exaggerated LPS-induced production of pro-inflammatory mediators by microglia, including IL-1β, IL-6 and TNF-α; there was also increased iNOS expression, increased neutrophil infiltration and increased apoptosis. However, the peripheral cytokine response was the same in prion diseased mice and control mice hence the exaggerated central pro-inflammatory response to LPS and resulting sickness behaviours must be determined within the CNS. The increased proinflammatory capacity of microglia due to neurodegeneration is termed "microglial priming" (Perry et al., 2007, Cunningham et al., 2009).

The group also found that the degree of underlying disease pathology at the time of systemic inflammation influences the severity of the deficits induced by the same inflammatory insult; mice challenged with LPS 16-weeks post-ME7-inoculation had a significantly worse transient cognitive deficit than mice exposed to LPS just 12-weeks post-ME7-inoculation (Davis et al., 2015).

More recently research from the same group indicated astrocyte priming in ME7 mice. There was astrogliosis visualised by increased GFAP expression in ME7 mice

and astrocytes in ME7 mice given intra-hippocampal IL-1β or TNF-α showed increased nuclear localization of p65 indicative of NFκB activation. This was associated with vast increase in astrocytic production of CCL2 and neutrophil chemoattractant CXCL1. TNF-α also induced T-cell chemoattractant chemokine RANTES (Hennessy et al., 2015). This indicates a "primed" neuroinflammatory state of the brain in general, not just in microglia, during neurodegeneration.

The priming hypothesis is not just a peculiarity of systemic LPS insult, since peripheral viral infections also trigger exaggerated sickness in ME7 mice and in this case primed microglia produce an elevated type 1 interferon response (Field et al., 2010). Nor is it a peculiarity of ME7 prion disease since microglial priming has now been demonstrated in alternative models of ageing (Chen et al., 2008) and CNS disease including models of AD, PD, tauopathies, and Wallerian degeneration (Sly et al., 2001, Lee et al., 2002, Kitazawa et al., 2005, Palin et al., 2008, Lee et al., 2010, Sy et al., 2011) (summarised in ***Table 3*** and discussed below).

Microglial priming is a functional definition, hence in 2015 Weighted Gene Co-expression Network Analysis (WGCNA) was used to investigate microglial gene expression in mouse models of aging, Alzheimer's disease (AD), and amyotrophic lateral sclerosis (ALS) and compared with microglia isolated from mice 4-hours post-intraperitoneal LPS-injection in order to investigate whether or not microglial priming might be a homogeneous phenotype with a specific transcriptional signature (Holtman et al., 2015). The study demonstrated a transcriptional signature of microglial priming which was distinct from that of acutely LPS-induced microglia. Both LPS-induced and primed microglia showed increases in genes associated with immune and stress responses (innate immune receptor *Tlr2*, proinflammatory cytokine *Il-1β*, and chemokine *Cxcl10*). LPS-induced microglia were enriched with NFκB factor p65 (RelA) and genes associated with TLR and NLR signalling whereas primed microglia had a signature associated with Alzheimer's disease signalling (*Apoe*), antigen presentation (MHC proteins), lysosomes and phagosomes suggesting that neurodegenerative conditions initiate a phagocytic microglial phenotype

(Holtman et al., 2015). Specifically, genes enriched in primed microglia included: *Axl*, a tyrosine kinase receptor involved in dampening the immune response, regulating cytokine secretion, clearing apoptotic cells and debris, and maintaining cell survival (Weinger et al., 2011, Chiu et al., 2013); *Clec7a* gene, encoding pattern recognition receptor dectin-1, a transmembrane receptor with intracellular immunoreceptor tyrosine-based activation (ITAM)-like motif – this receptor is associated with phagocytosis and increased cytokine and chemokine production (Tsoni et al., 2008); *itgax*, encoding CD11c, a subunit of complement component 3 receptor (Chiu et al., 2013); *Lgals3* (also known as *Galectin-3* and *Mac2*) which is involved in phagocytosis (Rotshenker, 2009); *Cybb*, encoding pro-inflammatory oxidase Nox2 (Chiu et al., 2013); and finally *Csf1* encoding macrophage colony-stimulating factor (M-CSF) – a cytokine involved in microglial proliferation in chronic neurodegenerative conditions (Smith et al., 2013, Holtman et al., 2015). Microglial CD14 expression has also been associated with microglial priming in AD; it is capable of binding amyloid protein and LPS and is upregulated in AD (Fassbender et al., 2004, Liu et al., 2005).

Mouse brain tissue from rTg4510 mice over expressing human P301L mutant tau transgene downstream of the tetracycline inducible CaMKIIα promoter indicated significant overlap with genes identified as markers of primed microglia (Holtman et al., 2015) although not described in detail.

Studies in old mice indicate age-related neuroinflammation. Microgliosis was characterised by altered morphology stained with tomato lectin, increased MHCII expression, and elevated IL-1β and TNF-α expression. LPS-injection impaired T-maze performance in mice at all ages but had a greater impact on older mice. Working memory deficits were associated with LPS-induced IL-1β, IL-6, IL-10, TNF-α and TLR2 expression which were all elevated in older LPS-injected mice compared with younger LPS-injected mice. It was later shown that CX3CL1 protein was reduced in older mice and that LPS insult enhanced CX3CR1 expression in young mice but caused a marked decrease in CX3CR1 in aged mice. Impaired CX3CL1–CX3CR1 signalling corresponded with delayed recovery from sickness behaviour, prolonged

IL-1β induction and decreased TGF-β expression. Impaired CX3CL1–CX3CR1 mediated regulation, resulting in microglial activation, thus contributed to the exaggerated sickness response in aged mice compared with younger mice following peripheral LPS challenge (Henry et al., 2009, Wynne et al., 2010).

Studies in Tg2576 mice which express mutant amyloid precursor protein (APP - K670N/M671L) showed mild microglial activation and pro-inflammatory cytokine expression in 6-month-old transgenic mice and more severe microglial activation in 16-month-old transgenic mice compared with controls – the degree of microglial activation correlated with Aβ-plaque load. Intravenous LPS induced over-production of IL-1β in the brains of 16-month transgenic animals but not 6-month-old animals suggesting that the degree of microglial priming depends on the degree of underlying disease pathology. LPS-induced inflammation lead to an increase in Aβ burden (Sly et al., 2001), a result which has since been replicated in alternative models of AD (Sheng et al., 2003, Lee et al., 2008).

An APP/PS1 model was crossed with a Col1-IL-1β^{XAT} Cre-inducible model of osteoarthritis, a common medical condition with known inflammatory component which is associated with increased risk of dementia (Huang et al., 2015). The systemic inflammation associated with the model of osteoarthritis was sufficient to increase microglial activation and amyloid deposition, and the APP/PS1 x Col1-IL-1β^{XAT} Cre inducible model had no detectable circulating IL-1β which might explain this result (Kyrkanides et al., 2011).

Mice with presenilin 1 M146V knock-in mutation have increased soluble Aβ, though there are no deposits of aggregated Aβ, no differences in cytokine profile and no differences in the number of microglia in the hippocampus compared with wild-types at baseline. Peripheral LPS injection induced an exaggerated cytokine response; IL-1β, TNF-α, IL-6 levels and iNOS expression were all elevated in PSmutK1 mice following LPS injection compared with LPS injected wild-types. Authors attribute the

exaggerated cytokine response to the expression of mutant PS1 in microglia rather than amyloid pathology (Lee et al., 2002).

Intracerebral injection of LPS was seen to induce reduction of amyloid burden in mouse models of amyloidopathy. Reduced amyloid burden correlated with the dose of LPS (DiCarlo et al., 2001, Herber et al., 2004). This was likely due to increased phagocytic properties of LPS-induced microglia, these findings highlight the poor phagocytic capacity of microglia in the context of AD and highlight the important differences between central and peripheral LPS-injection.

Taken together studies from amyloid models of AD indicate that amyloid pathology is sufficient to prime microglia; primed microglia are not fully activated and are inefficient at phagocytosis but subsequent inflammatory insult causes a dramatic over production of proinflammatory cytokines, especially IL-1β and is generally associated with increased disease amyloid pathology – but what about tau pathology?

Kitazawa et al. characterised the temporal profile of the triple transgenic (3xTgAD) mouse model of AD (with APP $_{K670N, M671L}$, PS1 $_{M146V}$, Tau $_{P301L}$ mutations). The 3xTgAD mouse develops age-related Aβ plaques and NFTs composed of hyperphosphorylated tau and shows progressive microglial activation which correlated with extracellular Aβ deposition. LPS was administered at 4 months of age by intraperitoneal injection twice per week for 6 weeks (500 μg/kg) and tissue analysed 24 hours after the final injection. This chronic LPS regime dramatically increased microglial burden and induced 5-fold IL-1β expression in 3xTgAD mice compared with PBS treated counterparts. Levels of amyloid precursor protein (APP) and Aβ deposition were unaffected, however, LPS-treatment significantly impacted tau hyperphosphorylation – total tau levels were unchanged but staining with phosphorylation specific antibodies AT8 and AT180 was increased two-fold (Kitazawa et al., 2005). Further probing of the mechanism indicated that LPS-induced tau phosphorylation might be mediated by cdk5 through increased expression of co-

activator protein p25. p25 is a cleaved fragment of p35, the constitutively expressed co-activator of CDK5 which exists near the plasma membrane and has a very short half-life whereas p25 is cytosolic and has a longer half-life. Elevated p25 levels and resulting cdk5 deregulation have been reported in post-mortem AD brain tissues (Patrick et al., 1999). The chronic LPS-induced phosphorylation of tau was reversed with cdk5-specific inhibitor Roscovitine.

The same lab went on to investigate the effects of the same LPS protocol later in disease, when mice were 12 months old rather than 4 months. LPS-injection similarly did not alter Aβ-deposition but was associated with increased neuroinflammatory markers, increased phosphorylated and insoluble tau burden and working memory impairments measured by MWM. Increased tau phosphorylation at this late stage in disease was attributed to GSK-3β activation. Inhibition of GSK-3β rescued tau pathological markers without impacting neuroinflammatory markers (Sy et al., 2011).

Hence studies in the 3xTgAD mouse model have demonstrated that systemic-LPS-induced microglial activation increases tau pathology, however the acute neuroinflammatory response of 3xTgAD mice was not compared with that of LPS-injected non-transgenic mice. Authors did comment that this chronic LPS regime was sufficient to induce tau pathology in control mice however data is not shown and therefore cannot be compared with 3xTgAD mice – hence this LPS-induced increase in tau pathology might be a response to neuroinflammation and not dependent on microglial priming.

Furthermore, viral infection of the same 3xTgAD mice and wild type mice by injection of neuroadapted JHM strain of mouse hepatitis virus (MHV) into the hippocampus caused microglial activation and infiltration of macrophages and T-cells. There was no difference in acute immune response between transgenic and control mice however there were long term impacts: 4-weeks post-infection there was an increase in tau pathology in MHV-infected compared to sham-injected 3xTgAD mice

however, again, results were not compared with infected non-transgenic mice (Sy et al., 2011).

Another study in the rTg4510 mouse, carrying the P301L mutation in tau, demonstrated age-related microgliosis (CD45-positive) in the cortex and hippocampus compared with control mice. Intracerebral LPS induced equivalent CD45-positive and Arginase-1-positive microgliosis in rTg4510 mice compared with control mice, however there was increased expression of microglial marker YM1. YM1 historically was associated with "M2 -alternatively activated" macrophages but it has also been known to display chemotactic activity for T lymphocytes, bone marrow cells, and eosinophils the precise function of this lectin is still unclear (Zhao et al., 2013, Rőszer, 2015). LPS also exacerbated tau pathology, further supporting the claim that a proinflammatory environment drives tau pathology in rTg4510 mice and not control mice. It remains to be seen whether this increased tau pathology reflects a difference in the neuroinflammatory response in rTg4510 mice compared with controls, as indicated by increased YM-1 expression or whether it is a result of increased vulnerability of mutant-tau-positive neurons to inflammation-induced tau phosphorylation. This study also used intracerebral injection of LPS rather than peripheral injection and hence does not tell us about the effects of *systemic* inflammation on tau pathology (Lee et al., 2010).

As previously described (section 1.1.5 and 1.2.6) hTau mice show progressive accumulation of insoluble phospho-tau and associated microgliosis with increased levels of fractalkine, iNOS and CCL2. CD45-positive microgliosis was later shown to correlate spatially and temporally with the spread of tau pathology in the hippocampus and with memory deficit (Maphis et al., 2015b). hTau mice were crossed with fractalkine knock out mice to generate hTau-CX3CR1$^{-/-}$ mice which displayed exacerbated microgliosis and tau pathology. Intraperitoneal LPS injection (1 mg/kg or 10 mg/kg) resulted in a dose dependent increased tau phosphorylation at the phospho-thr231 (TG3) and AT8 epitopes in hTau mice compared with non-transgenic control mice and a further increase in tau phosphorylation in hTau-

Cx3cr1$^{-/-}$ mice. (Bhaskar et al., 2010). In a further study the group went on to show that adoptive transfer of purified microglia derived from hTau-*Cx3cr1*$^{-/-}$ mice was able to induce tau hyperphosphorylation in recipient non-transgenic mice, which could be blocked by an IL-1R agonist.

Hence these data indicate that microglia are activated in tauopathy dementia but that they are still subject to immune-modulation by CX3CL1–CX3CR1 signalling. LPS induced increased tau phosphorylation in transgenic mice but not non-transgenic mice which was mediated via microglia and exacerbated by further microglial activation by ablation of CX3CL1–CX3CR1 signalling however the magnitude of the LPS-induced inflammatory response in hTau mice was not compared to that of non-transgenic mice and hence, again, it remains unclear whether the increased tau hyperphosphorylation in mutant tau mice is the result of a differential inflammatory response or increased vulnerability of mutant tau-positive neurons.

Animal Model	Insult	Mode	Dose	Dosing regime	Sac	WT + Inflammatory Challenge	Disease related Pathology	Disease + Inflammatory Challenge	Reference
ME7 8 wk post inoculation	LPS	i.p.	10 µg	Single	6 h	Hypothermia Hypoactivity (openfield)	Normothermia Normal activity (openfield)	Equivalent hypothermia Hypoactivity (openfield)	(Combrinck et al., 2002)
ME7 19 wk post inoculation	LPS	i.p.	10 µg	Single	6 h	Hypothermia Hypoactivity (openfield) I.C. IL-1β production	Normothermia Normal activity (openfield) Negligible IL-1β	Exaggerated hypothermia Exaggerated hypoactivity (openfield) Exaggerated I.C. IL-1β production	
ME7 19 wk post inoculation	LPS	i.c	2 µg	Single	6 or 18h	Ramified microglia (tomato lectin) IL-1β staining near injection site and from infiltrating neutrophils Negligible iNOS	Dense microgliosis, active morphology Negligible IL-1β Negligible iNOS	Equivalent dense microgliosis, active morphology Exaggerated IL-1β (ipsilateral and contralateral) Exaggerated iNOS expression	(Cunningham et al., 2005)
ME7 19 wk post inoculation	LPS	i.p.	500 µg/kg	Single	6, 9, 13, 18h	Increased IL-1β, TNF-α and IFN-β	Negligible IL-1β, TNF-α and IFN-β	Equivalent dense microgliosis, active morphology Exaggerated IL-1β, TNF-α and IFN-β production Increased endothelial expression of COX-2 Increased apoptosis (TUNEL and caspase-3)	

Animal Model	Insult	Mode	Dose	Dosing regime	Sac	WT + Inflammatory Challenge	Disease related Pathology	Disease + Inflammatory Challenge	Reference
ME7 12 wks post innoculation	LPS	i.p.	100 µg/kg	Single	2h	Impaired burrowing Hypoactivity (openfield) Normothermia Increased IL-1β, TNF-α and IL-6 No effect on Y-maze performance	Normal burrowing Normal activity (openfield) Normothermia Negligible IL-1β, TNF-α and IL-6	Longer lasting impaired burrowing Exaggerated hypoactivity (openfield) Hypothermia Exaggerated IL-1β, TNF-α and IL-6 production Induced microglial COX-2 expression Impaired learning in Y-maze	(Cunningham et al., 2009)
	LPS	i.p.	500 µg/kg	Single		Impaired horizontal bar and inverted screen performance 6 h but not longitudinally (16-20 weeks)	Normal horizontal bar and inverted screen performance @ 6 h but impaired longitudinally (16-20 weeks)	Exaggerated impairment of horizontal bar and inverted screen performance 6 h and longitudinally (16-20 weeks)	
ME7 18 wks post innoculation	RNA poly I:C	i.p.	12 mg /kg	Single	3, 4, 6, 15 h	Increased plasma IFN-α/β Increased CNS IFN-α/β and IL-1β Hyperthermia Impaired Horizontal Bar and Inverted Screen tasks acute	Horizontal Bar and Inverted Screen tasks neurodegenerative decline	Equivalent increased plasma IFN-α/β Exaggerated increase in CNS IFN-α/β and IL-1β Hypothermia No change in PrP Increased Apoptosis Horizontal Bar and Inverted Screen tasks showed exaggerated sickness response and worse neurodegenerative decline	(Field et al., 2010)
	RNA poly I:C	i.p.	12 mg /kg	3 times, 2 weeks apart	3, 4, 6, 15 h			Each response worse than the one before and lasted longer	

Animal Model	Insult	Mode	Dose	Dosing regime	Sac	WT + Inflammatory Challenge	Disease related Pathology	Disease + Inflammatory Challenge	Reference
ME7 Young 12wk Old 16wk	LPS	i.p.	100 µg/kg	Single			Young: Synaptic loss Old: More synaptic loss	Young ME7 + LPS: Acutely impaired T-maze alternation Old ME7 + LPS: More impaired T-maze alternation	(Davis et al., 2015)
BALB/c	LPS	i.p.	0.33 mg/kg	Single injection	4 h post LPS	Young (3-6 mo) LPS induced IL-1β, IL-6, and TNF-α mRNA	Aged (22-24 mo) Increased IL-1β and TNF-α IL-6 not affected by age Microgliosis with age (tomato lectin) Slowed rate of acquisition of the task	Aged (22-24 mo) Exaggerated IL-1β, IL-6, and TNF-α mRNA levels Working memory deficits (under water radial arm maze)	(Chen et al., 2008)
BALB/c	LPS	i.p.	0.33 mg/kg	Single injection	4 or 8 h post LPS	Young (3-6 mo) LPS induced circulating and microglial expression of IL-1β and IL-10 Increased TLR2 on microglia No change in microglial MHCII	Aged (22-24 mo) Increased microglial expression of MHCII associated with age	Aged (22-24 mo) LPS induced circulating IL-1β levels equivalent to young But exaggerated CNS IL-1β and IL-10 expression and Microglial TLR2 No change in microglial MHCII	(Henry et al., 2009)
BALB/c	LPS	i.p.	0.33 mg/kg	Single injection	4 or 8 h post LPS	Young (3-6 mo) CX3CL1 protein was unaltered by LPS injection CX3CR1 was enhanced	Aged (22-24 mo) CX3CL1 protein was reduced	Aged (22-24 mo) CX3CL1and cd11b were unaltered Decrease CX3CR1 Corresponded with: Delayed sickness behaviour recovery Prolonged IL-1β induction Decreased TGF-ß expression	*(Wynne et al., 2010)*

Animal Model	Insult	Mode	Dose	Dosing regime	Sac	WT + Inflammatory Challenge	Disease related Pathology	Disease + Inflammatory Challenge	Reference
C57BL/6J	LPS	i.p.	250 µg/kg	1 per day for 5 days 1) 1 LPS + 4 x saline 2) 5 x LPS 3) 5 x Saline		Young (2 mo) Normal MWM activity	Aged (12 mo) Longer latencies, greater distances, and slower swim speeds in MWM	No significant main effects of LPS treatment (or treatment condition × age interactions) were found on any of the retention testing Swimming thigmotaxis observed in aged animals exposed to 5 x LPS injection	(Sparkman et al., 2005)
Tg2576 AD (APP_{695} K670N/ M671L) 6 mo	LPS	i.v.	25 µg	Single			Astrogliosis Microgliosis Impaired learning and memory β-Amyloid (Aβ) plaques Elevated TNF-α	IL-1β = control levels Significantly elevated Aβ1-40 in cortex at 4 and 6h	(Sly et al., 2001)
Tg2576 AD (APP_{695} K670N/ M671L) 16 mo	LPS	i.v.	25 µg	Single		Elevated IL-1β	Astrogliosis and Microgliosis Impaired learning and memory β-Amyloid (Aβ) plaques Elevated TNF-α, (IL)-1α (2.2-fold), IL-1β (3.4-fold), TNF-α (3.9-fold), CCL2 (2.5-fold), GFAP C1qA and C3	Exaggerated IL-1β >2-fold in cortical and hippocampal tissue (but not cerebellar) IL-1β increased progressively from 1 to 6h Significantly elevated Aβ1-40 and Aβ1-42 in cortex at 2, 4 and 6h	

Animal Model	Insult	Mode	Dose	Dosing regime	Sac	WT + Inflammatory Challenge	Disease related Pathology	Disease + Inflammatory Challenge	Reference
APPswe Tg mice	LPS	i.p.	150 µg	/mouse /week for 12 weeks		Not assessed	Microglial activation correlates with APP and Aβ expression	3 fold increased Aβ1-42 and 1.8 fold increased APP (ELISA, Western blots and IP–MS ProteinChip analysis) Increase in the number + size of both microglia (F4/80) and astrocytes (GFAP) in LPS-treated mice	(Sheng et al., 2003)
Tg2576	LPS	i.c.	1, 4 or 10 µg	Single injection	1, 3, 7, 14 or 28 days	Not assessed	Aβ accumulation Microgliosis (CD45) Astrogliosis (GFAP)	Reduced Aβ burden (correlates with dose and time post LPS) Increased microgliosis (CD45, FcγR) with altered morphology Increased astrogliosis (GFAP)	(Herber et al., 2004)
APP/PS1 mice APP_{SWE}, $PS1_{M146L}$	LPS	i.c.	2 µg or 4 µg	once	3 or 7 days	Not assessed		Reduced Aβ burden Microgliosis (MHCII)	(DiCarlo et al., 2001)
PSmutK1 PS 1_{M146V}	LPS	i.p.	50 µg in 100 µL	Single injection	2, 6 16 & 20 h	Increased TNF-α, IL-1β, IL-6, IL-1α, IL-1ra Increased MAC1 positive microglia in hippocampus increased	Increased TNF-α, IL-1R, IL-10, IL-1α/β, IL-1ra, IL-6	Exaggerated IL-1β, TNF, IL-6, IIL-1α, IL-1RI, IL-1ra, and IL-10 Exaggerated increase in MAC1 positive microglia in hippocampus iNOS expression Equivalent cytokines in Spleen	(Lee et al., 2002)

Animal Model	Insult	Mode	Dose	Dosing regime	Sac	WT + Inflammatory Challenge	Disease related Pathology	Disease + Inflammatory Challenge	Reference
3xTgAD (APP_{SWE}, $PS1_{M146V}$, Tau_{P301L}) 4 mo	LPS	i.p.	500µg /kg	2x /week for 6 weeks	24h post final injection	Not assessed	Progressive accumulation of Aβ, tau pathology, microgliosis and astrogliosis Some IL-1β	No effect on Aβ deposition or APP processing Increased microgliosis, IL-1β Increased tau hyperphosphorylation (AT8 and AT180) mediated by p25-cdk5 activation and reversed by roscovitine.	(Kitazawa et al., 2005)
3xTgAD	LPS	i.p	500µg /kg	2x /week for 6 weeks (age 12mo)	48h	Not assessed	As above	No change in Aβ pathology. Increased tau pathology (AT8, AT100, PHF1) associated with GSK-3β activity and blocked by lithium. MWM activity impaired	(Sy et al., 2011)
	MHV	i.c.	500 units	Single	2 & 4 wk			No change in Aβ pathology. Increased tau pathology associated with GSK-3β and p25-cdk activation.	
rTg4510	LPS	i.c.	10µg	Single injection	7 days	LPS induced CD45, YM-1 and Arg1 positive microglia	Age related p-tau age related increase in microglial expression of CD45, MHCII but not YM1	LPS induced exaggerated YM1 Equivalent CD45 and Arg1 LPS induced tau phosphorylation but not accumulation into insoluble tau	(Lee et al., 2010)

Animal Model	Insult	Mode	Dose	Dosing regime	Sac	WT + Inflammatory Challenge	Disease related Pathology	Disease + Inflammatory Challenge	Reference
hTau	LPS	i.p.	1 mg/kg	Single	24 h	No change in tau phosphorylation	Progressive tau phosphorylation and aggregation neuronal loss Progressive microgliosis (IBA1) Elevated levels of cleaved CX3CL1, NOS2 and CCL2 But TNF-α, INF-γ, IL-1β, IL-6 remained unchanged	Increased tau phosphorylation at the phospho-thr231 (TG3) and AT8 epitopes	(Bhaskar et al., 2010)
hTau-Cx3cr1$^{-/-}$	LPS	i.p.	1 mg/kg	Single	24 h	Cx3cr1$^{-/-}$ + LPS Increased AT8 positive tau	hTau-Cx3cr1$^{-/-}$ Impaired spontaneous alternation Microgliosis more than hTau (IBA1, CD45 and CD68)	hTau-Cx3cr1$^{-/-}$ + LPS Further elevated levels of p-tau in hTau-Cx3cr1$^{-/-}$ mice	

Table 3 – Systemic inflammation in animal models *Summarises key findings from studies investigating the effects of an inflammatory insult in animal models of neurodegeneration; details include the name of the animal model, the inflammatory stimulus, the site of injection, dose, dosing regime, when mice were sacrificed relative to the injection, the effect of the inflammatory stimulus in control animals, the disease associated pathology, the combined effect of disease and inflammatory stimulus. Abbreiviations: i.p. – Intraperitoneal; i.c.- intracerebral; IP–MS – immunoprecipitation–mass spectrometry; MHV – Mouse hepatitis virus; MWM – Morris water maze; poly I:C – poly inosine:cytosine (viral mimetic).*

1.3 Conclusions

In conclusion, dementia is a major public health problem. The estimated global cost of dementia in 2015 was 818 billion US dollars and set to reach 1 trillion USDs by 2018 (Wimo et al., 2017). In the absence of disease modifying treatments and with the rapidly ageing population this burden will only intensify.

Tau protein is a microtubule associated protein which is implicated in many dementias where it becomes hyperphosphorylated and forms insoluble aggregates referred to as neurofibrillary tangles. The precise role of tau protein in neurodegeneration is unclear. However, the discovery of causative inherited mutations in the gene encoding tau protein indicate that tau dysfunction alone is sufficient to cause dementia. Identification of inherited mutations has also enabled the development of animal models of tauopathy dementia including the P301S mouse used here.

Neuroinflammation is a robust hallmark of all dementias including tauopathy dementias. There is evidence that systemic inflammation is associated with increased risk of dementia. Those with dementia are prone to an exaggerated sickness response. Systemic inflammation, for example caused by infection, can cause delirium in patients with pre-existing dementia which might be underpinned by microglial priming in the brain. Evidence suggests that systemic inflammation and/or delirium exacerbate the rate of decline of dementia. Infection and systemic inflammation are potentially modifiable. Even just delaying the onset of dementia will have a huge positive impact in terms of reducing the socioeconomic burden and improving quality of life for sufferers and their families.

1.3.1 Project Aims & Objectives

This project aims to use a known model of neurodegeneration which recapitulates key hallmarks of tauopathies including accumulation of hyperphosphorylated tau, neuronal loss and gliosis, to explore the effect of systemic inflammation on disease progression in a mutant tau mouse model of neurodegeneration with both pathological and behavioural outcomes.

The hypothesis I will be testing is that over-expression of mutant tau protein is sufficient to influence the inflammatory status of the CNS and that this will in turn affect the response to systemic inflammatory insult.

In order to address this hypothesis in the P301S mice, I will first characterise the temporal pathological profile as well as identify a behavioural measure of disease progression before examining the pathological and behavioural impact of intraperitoneal LPS-injection at two timepoints.

2 Chapter 2 – General Methods

All analyses were blinded to genotype and intervention unless otherwise specified.

2.1 Animals

All procedures were performed in compliance with the UK Animals (Scientific Procedures) Act 1986 and University of Edinburgh regulations. Mice were bred, maintained and terminated in compliance with project license 60/4240. Animals were group-housed in environmentally-enriched cages within humidity and temperature controlled rooms, with a 12-hour light dark cycle, and access to food and water *ad libitum*.

The P301S mouse line was originally generated in Cambridge as previously described (Allen et al., 2002). P301S mice over-expresses human mutant P301S tau under neuronal promoter Thy 1.2 on a C57BL/6J background. Mice were maintained as a homozygous colony. The same C57BL/6J strain were used as control mice throughout this thesis and will be referred to as 'C57BL/6' or 'control' mice. This is important since genomic and phenotypic analysis of different C57BL/6 strains have identified a number of genetic and phenotypic differences among strains, including SNPs in genes involved in CNS degeneration (Mekada et al., 2009, Simon et al., 2013). For behavioural tasks, age-matched control C57BL/6J mice were transferred to the home room at least two weeks prior to experiments in order to allow acclimatisation. All mice were earmarked prior to behavioural testing.

Only female mice were used for all experiments to avoid fighting and injury since this is likely to influence performance on behavioural tasks and might also have an impact on pathology. Unpublished data from the lab has also demonstrated significant sex differences in the behaviour and pathology of P301S mice.

The main phenotype of P301S mice is a progressive hind limb paralysis that is driven by loss of ventral spinal cord motor neurons. Animals were terminated when 20% body weight loss persisted for 48 hours and/or a phenotypic score of 4 was attained, as shown in Table 4.

Score	Description
0	Normal
1	Beginning of phenotype (typically observed from 4 months onwards). Animals develop a wobble in their movement and/or may show hind limb clasping reflex when hind end lifted, but no problems with feeding or drinking and still active. Begin weighing every 2-3 days.
2	Movement is slower but still able to reach food and water. Start feeding mash and or gel. Continue weighing every 2-3 days
3	Wobbling is pronounced, walking speed is slow. Weakness/poor motor control in one or both hind limbs. Tremor may be present and weight loss may now be evident. Still has righting reflex and still reach food. Begin daily weighing.
4	Hind limb paralysis
5	Mouse not walking at all, lost control/movement of both hind limbs and trembling. Marked loss of weight and possible eye inflammation. No righting reflex and the mouse cannot stand upright therefore unable to reach food and/or water

Table 4 - P301S hind limb paralysis phenotype scoring system

2.2 Behaviour

Assessment of burrowing was performed in the home room. For all other behavioural tasks, mice were taken to an 'experimental room' 15 minutes prior to the task so that they could acclimatise to the new environment.

2.2.1 Spontaneous Alternation T-maze

The spontaneous alternation task has previously been used to detect working memory and spatial memory deficits. Measurement of spontaneous alternation in the T-maze relies on an innate reproducible behaviour of mice; when mice are placed at the start arm of a T-shaped maze (Figure 6A), mice will explore the maze, they will

travel towards the two goal arms and either turn left or right. When replaced in the maze, seconds to minutes later, their natural tendency is to explore the previously un-explored arm of the maze, assuming successful recollection of their previous visit and this is recorded as a correct alternation (Dember, 1989, Deacon et al., 2006). Spontaneous alternation relies on working memory and spatial memory, and the alternation task has been used previously to detect lesions of the hippocampus (Roberts et al., 1962), septum (Douglas et al., 1966), and prefrontal cortex (Divac et al., 1975).

2.2.1.1 **Apparatus**

The apparatus is a plastic T-shaped maze with black walls 20 cm high and a white base. The arms are 30 cm length by 7 cm width (see Figure 6A). There is a removable central partition and two guillotine doors. Bedding taken from a cage of mice of the opposite sex was spread in the goal arms to increase motivation to explore.

2.2.1.2 **Acclimatisation**

During the acclimatisation period, mice were first taken to the experimental room and handled for five minutes each. The next day mice were introduced to the apparatus for the first time with cage mates to encourage exploration. The following day mice underwent a single trial run prior to testing.

2.2.1.3 **Protocol**

Mice were tested weekly between 8 and 22 weeks of age through application of the following protocol.

"Decision trial": With the central partition in place, the mouse was placed at the base of the start arm always facing away from the goal arms. The mouse travelled down the start arm and either turned left or right; the guillotine door was closed and the mouse was allowed to explore the first goal arm for 30s. Then the mouse was removed

and placed in a holding cage for a 20 second interval. The central partition and the guillotine doors were removed. The first goal arm was recorded, that is, left or right.

"Alternation trial": The mouse was returned to the starting position for a second trial, travelled up the starting arm and the decision to turn left or right was recorded before returning the mouse to the home cage. If on the alternation trial the mouse chose the arm not visited before this was recorded as a correct alternation. The decision to turn was only counted once all four paws cross the line of the goal arm. This whole protocol was repeated 5 times per animal per session.

2.2.1.4 Statistics

The number of correct alternations made by each mouse were converted into percentage correct alternations and a mean determined for each group using this formula:

$$= \left(\sum \left(\frac{Number\ of\ correct\ alternations}{Total\ number\ of\ alternation\ trials} \right) x\ 100 \right) /n$$

The percentage of correct alternations made by individuals was used for T-test comparison of the C57BL/6 within-time-point mean performance to the overall mean of the performance at all other time points.

2.2.2 Burrowing

Burrowing is another innate behaviour in mice and one that is often impaired during CNS disease. In the wild, mice create burrows by displacing soil; the burrowing task quantifies this behaviour by measuring displacement of food from a tube. Burrowing is reduced by acute illness (LPS) and the burrowing task has previously been used to detect hippocampal and medial prefrontal cortex lesions (Deacon et al., 2002, Deacon et al., 2003, Deacon, 2006).

2.2.2.1 **Apparatus**

A tube measuring 6.8 cm diameter and 20 cm length, with one closed end, was filled with 425g of dried food pellets. The open end of the tube was elevated 3 cm. The tube was placed in the back, right corner of a cage along the longest edge with wood chippings on the cage floor and bedding in the back-left corner (see Figure 6C for experimental set up). Mice were provided with water *ad libitum*.

2.2.2.2 **Acclimatisation**

For the first two nights of the acclimatisation phase mice were allowed to explore the apparatus along with their cage mates. This was followed by several nights of individual burrowing acclimatisation.

2.2.2.3 **Protocol**

Each mouse had its own experimental cage and was returned to the same cage for each trial; the chippings on the cage floor were not changed so that the mouse would recognise its own scent. Burrowing cages were kept on a cage rack in the same room as home cages to minimise disturbance. Mice were transferred to their experimental cage with burrowing apparatus at 5pm. The dark cycle begins at 7pm and ends at 7am. At 9am mice were returned to their home cage. The cage lid was used to filter the food pellets from the chippings of the cage floor and chippings were returned to the cage floor. The food pellets remaining in the tube and food pellets displaced from the tube after the over-night burrowing session were weighed, recorded and returned to the tube. Both measurements were recorded as a mistake-proofing precaution. Any food that had been eaten overnight was replaced, then the tube was topped up to 425g and replaced in the cage ready for the next session.

2.2.2.4 Statistics

The total weight of food burrowed from the tube measured in grams was converted to a percentage of the total weight and group averages calculated using the formula:

$$= \left(\sum \left(\frac{Weight\ Burrowed\ (g)}{425} \right) x\ 100 \right) / n$$

"Percentage burrowed" data was used for statistical analysis. Initial inspection of the longitudinal change in burrowing behaviour identified three distinct phases (see Figure 6D): an initial phase of improving performance (phase 1), a second phase of stable performance (phase 2), and a final phase of declining performance (phase 3). Piecewise mixed effects linear regression was therefore used to evaluate genotype and age (weeks) with random effects for individual animals. Cut points were as follows: phase 1, 8-12 weeks of age; phase 2, between 12-17 weeks of age; phase 3, between 17-22 weeks of age.

2.2.3 Horizontal Bar Task

The horizontal bar task is a physical task which gives a measure of muscle strength and coordination (Cunningham et al., 2005).

2.2.3.1 Apparatus

The apparatus consists of a metal bar 0.2 cm in diameter, 26 cm long, which is elevated 19.5 cm between two plastic pillars. There is a metal mesh on the platforms to enable grip. See photograph Figure 6E. The horizontal bar task was carried out in a large chamber with 25cm high walls.

2.2.3.2 Acclimatisation

During the acclimatisation period, mice were taken to the experimental room and were handled for 5 minutes each. The next day mice were introduced to the apparatus. Pilot data from the first cohort demonstrated an initial difference in

performance between P301S mice and controls. Mice in every experiment thereafter were subjected to 'training exposures' as required to minimise this initial difference. During these training sessions, mice were first placed with all four paws on the bar facing a platform and were encouraged to crawl along the bar whilst supported by the tail. Later, mice were placed with only fore-paws on the bar and were encouraged to raise their hind limbs.

2.2.3.3 **Protocol**

Mice were suspended by the tail above the metal bar and allowed to grip the bar with their forelimbs and the tail was gently released leaving them suspended in the centre of the bar, hanging by their forelimbs. Mice then had to crawl along the bar to reach one of the platforms at either end. A maximum of 60 seconds was allowed to complete the task. A healthy mouse will complete this task in approximately 3 seconds (once it has learned the optimal way to cross the beam) however as the P301S mice develop hind limb paralysis the task becomes more difficult, they take longer to complete it and eventually they are unable to complete the task and fall off the bar. The time taken for the mouse to either reach the platform or fall from the bar was recorded using a stop clock and converted to a score between 1-10 according to the criteria described in Table 5.

A previously published horizontal bar scoring method recorded only the time spent on the bar prior to falling up to a maximum of 60 seconds. If the mouse did not fall because it reached a supporting column, it attained the maximum score of 60 (Cunningham et al., 2005). Here the scoring method was modified to increase sensitivity. Whereas all mice that reached the platform in the published method attained the same score, here the time taken for mice to reach the platform was also recorded and used as part of the score such that the quicker mice reached the platform, the higher their score. The horizontal bar task was repeated three times per mouse per session. Horizontal bar performance of P301S mice was assessed weekly from 9 weeks of age until they were sacrificed at 20-22 weeks of age.

Score	Time to Fall (s)
0	0-5
1	6-10
2	11-20
3	21-40
4	41-59
5	60

Score	Time to Platform (s)
10	0-5
9	6-10
8	11-20
7	21-30
6	31-59
5	60

Table 5 - Horizontal bar task scoring system

2.2.3.4 **Statistics**

For each trial the time taken to reach the platform or time taken to fall from the bar were converted to a score as described above (Table 5) and the mean score for that session was calculated for each mouse (three trials per session). This "within animal" mean was used as the primary data in statistical analysis. Piecewise linear regression was used with random intercept for ID to compare the trajectory of the longitudinal performance of the two or four groups.

2.3 Histochemistry

2.3.1 Tissue Collection for Histochemistry

Mice were sacrificed by a lethal intraperitoneal injection of 0.3 ml/100 g body weight of sodium pentobarbital (euthetal). They were transcardially perfused with 30-50 ml of 1% phosphate buffered saline (PBS) using a peristaltic infusion pump. Animals were then perfused with 50-100 ml 4% paraformaldehyde (PFA) in 1% PBS. Brains and cervical spinal cords (c5-c7) were removed and post fixed in 4% PFA over night before cryoprotection in 25% sucrose in PBS solution. Brains and spinal cords were frozen and cut on a cryostat at 25μm and 16 μm respectively (Leica CM1950). Sections were mounted onto superfrost slides (VWR, UK) and stored at -20 °C whilst being collected and then transferred to -80 °C for long term storage.

2.3.2 Cresyl stain

Slides were defrosted and air dried for 1 hour. Serial dehydration in 70%, 95% and then 100% ethanol (5 minutes each), was followed by 20 minutes in 50/50 chloroform/ethanol to de-fat sections. Slides were then rehydrated in 95%, then 70% ethanol, and then distilled water (5 minutes each). Sections were stained in cresyl violet (Fisher Scientific) for 2 hours. Before the stain was differentially removed to achieve optimal staining and dehydrated in 70% then 95% ethanol (2.5 minutes each), then 100% ethanol (3 minutes) and finally xylene (5 minutes) before mounting with DPX (Fisher Scientific).

2.3.3 Fluorescent Staining

Slides were allowed to defrost and air dry, then a hydrophobic barrier was drawn around the section (*PAP pen, molecular probes, UK*) before two ten minute washes in 1% PBS, on a shaker. Sections were blocked and permeabilised with 3% normal serum (goat or horse depending on secondary antibody, S-1000 or S-2000, Vector Laboratories) and 0.2% Triton-X (X-100, Sigma) as required, in PBS (~300µl per slide) for 1 hour. They were incubated with primary antibodies (see relevant chapters for details) with 1% blocking serum in 1% PBS or 0.2% Tx-PBS, as required over-night. Three ten minute washes in 1% PBS on a shaker were followed by a 1.5-hour incubation with secondary antibodies (see relevant chapters for details), with 1% blocking serum and Bis-benzamide (1:4000, B1155, Sigma Aldrich) in 1% PBS. If a biotinylated secondary was used, bis-benzamide was omitted from the secondary antibody step and included instead with the tertiary antibodies (see relevant chapters for details). Slides were washed in PBS, as before, to remove secondary antibodies and then incubated with a tertiary antibody and bis-benzamide in 1% PBS for 1.5 hours. Slides were washed twice in 1% PBS (10 minutes) and then twice in TNS (Tris non-saline solution) for 10 minutes, and then stayed in TNS until mounting in fluorosave reagent (345789, Millipore). Slides were stored in the dark at 4 °C.

2.3.4 DAB Staining

Slides were defrosted and air dried before quenching of endogenous peroxidase in 1% H_2O_2 in methanol followed by two five minute washes in 1% PBS. For antigen retrieval slides were incubated in citric acid solution (2.1g in 1L ddH2O, pH 6) for 10 minutes. Following two five minute washes in 1% PBS, sections were blocked with 10% normal goat or horse serum in 1% PBS (~300µl per slide) for 1 hour. They were incubated with primary antibody as required (see relevant chapters for details), with 10% NHS in 1% PBS over-night. Three ten minute washes in 1% PBS on a shaker were followed by incubation with biotinylated secondary antibody for 1.5 hours (see relevant chapters for details). Three ten minute washes in PBS were followed by incubation in ABC-peroxidase solutions containing Reagent A (1: 200, Avidin DH solution) and Reagent B (1: 200, biotinylated enzyme), both also from the VECTASTAIN UNIVERSAL Elite ABC Kit (Vector Laboratories, PK-6200) in 1% PBS for 45mins.

After thorough washing the reaction product was visualized using avidin-biotin and 3′,3′-diaminobenzidine (DAB) as the chromagen (DAB kit, Vector Laboratories). Slides were serially dehydrated in 70%, 80%, 95% and then 100% alcohol (5 secs, 5 secs, 5 secs and 30 secs respectively) followed by two 2 minute washes in xylene. Slides were mounted with DPX mounting media. Slides were stored at room temperature.

2.4 Imaging of Brain and Spinal Cord

A Zeiss upright A1 microscope was used in conjunction with Axiovision 4.8 software and a digital camera unless otherwise stated.

When imaging the brain, the camera was rotated such that the surface of the brain was aligned with the edge of the image (see **Figure 3**). Images of the superficial layers of the motor cortex were taken 0.75-1.25 mm from the midline of sections identified

as 0.5-2.3 mm rostral of bregma. Multiple hemispheres were imaged per animal; specific details are given below or within each relevant section.

Lamina 9 of the spinal cord was identified using anatomical features and reference to the online Allen Brain Atlas, which includes a mouse spinal cord reference atlas (see **Figure 3**). The camera was aligned with the white- / grey-matter boundary.

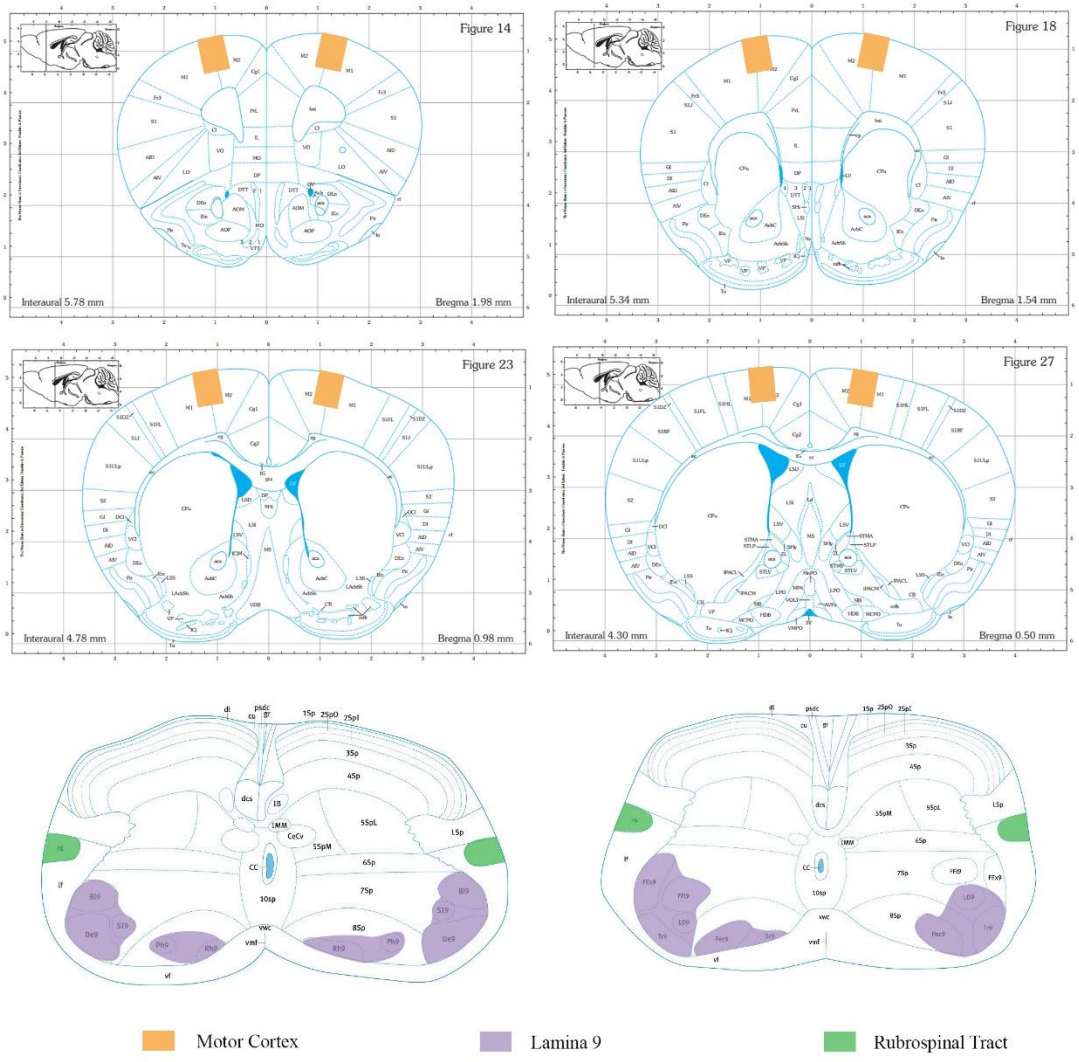

Figure 3 – Anatomical schematic of motor cortex, and lamina 9 and rubrospinal tract of the spinal cord.

2.5 Automated Image Processing and Data Acquisition using ImageJ/Fiji software – Percentage area containing positive signal

ImageJ/Fiji software (Schindelin et al., 2012, Schneider, 2012) was used for automated image analysis. ImageJ is commonly used image analysis software and Fiji is a version of ImageJ with additional plugins, which is freely available to download.

A template macro (a kind gift from Dr Mélissa Cizeron) was used to batch process images. The template macro included steps for recognising and opening all ".tif" files within a specified input folder, duplicating them and saving the duplications with a new name in a chosen output folder such that any modifications to the images during the processing did not overwrite the original images.

The macro was edited to include the following additional steps: 1) Subtract the background from the duplicated images; 2) Impose an intensity threshold; 3) Create a binary mask; 4) Select an area of interest; 5) Determine the percentage of the selected area containing positive signal.

The "Subtract backround" tool removes smooth continuous background based on a "rolling ball" algorithm. If one were to plot the coordinates of a cross section of the image (x axis) against the grayscale intensity (y axis) as illustrated in Figure 4 (Image J/FIJI documentation - https://imagej.nih.gov/ij/docs/guide/user-guide.pdf) and if one were able to roll a ball of a given radius along the profile of the plot, then the troughs reachable by the ball are the background to be subtracted. Subtraction of the background minimises the false positives detected when using of the threshold tool.

The threshold tool sets upper and lower grey-scale threshold values (between 0-255) and allows creation of a binary image or "mask".

An area of interest was selected and the percentage area positive signal was determined (defined in Analyze > Set measurements > Area Fraction).

Parameters were determined by iterative optimisation on a sample of randomly selected images prior to batch processing.

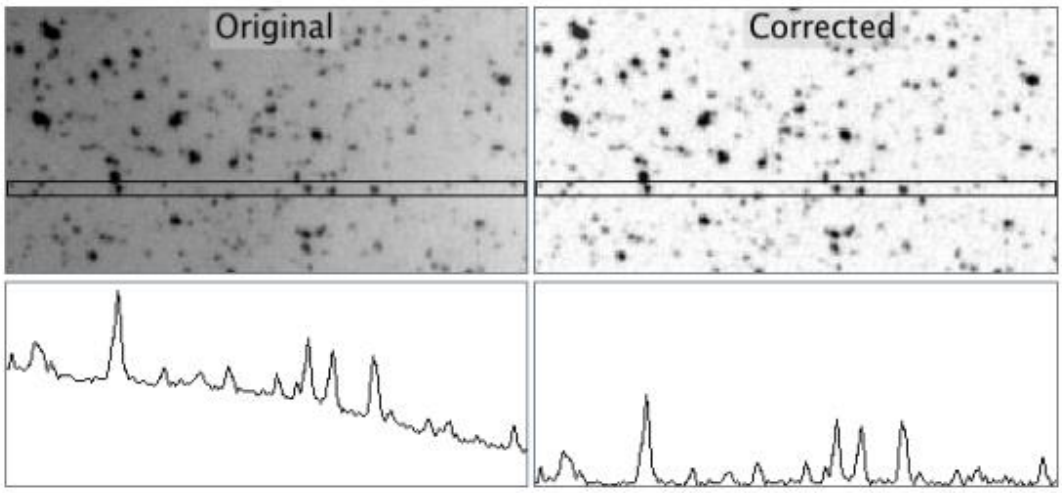

Figure 4 - "Subtract Background: This command uses a 'sliding paraboloid' or a legacy 'rolling ball' algorithm that can be used to correct uneven illuminated background as shown in the profiles (Analyze. Plot Profile [k]) below each image. Rolling ball radius should be set to at least the size of the largest object that is not part of the background." Image and caption accredited to Image J/FIJI documentation (https://imagej.nih.gov/ij/docs/guide/user-guide.pdf

2.6 qPCR

2.6.1 Tissue collection for qPCR

C57BL/6 and P301S mice were sacrificed at 16 weeks of age 4-hours post intraperitoneal injection with LPS or saline solution. Mice were euthanized by a lethal intraperitoneal injection of 0.3 ml/100 g body weight of sodium pentobarbital (euthetal). Blood samples were immediately collected by cardiac puncture whilst the heart was still pumping – a 23-gauge needle attached to a 2-ml syringe was inserted into the right atrium with the bevelled edge down and the atrium gently lifted to encourage blood flow. Blood samples were spun at 6,000 rpm to remove cells. Pellet and supernatant were separated and instantly frozen on dry ice. Meanwhile, brain and spinal cord (c5-c7) were rapidly removed. Brains were cut along the midline and then the cortex carefully dissected out, using a scalpel. Approximately 30 µg of

cortical and spinal tissue was collected. Samples were placed in Eppendorf tubes and frozen on dry ice and were stored in the -80°C freezer. Brain and spinal cord samples were used for gene expression assays.

2.6.2 RNA Isolation

The frozen samples and labelled Precellys lysing tubes were placed on dry ice. Samples were weighed to ensure each lay in the range of 20–40 mg and transferred immediately to lysis tubes. Samples were lysed and homogenised in 1ml of QIAzol Lysis Reagent (Cat No./ID: 79306, Qiagen, Crawley, UK) using the Precellys ®-24 high-throughput tissue homogenizer – brain samples were spun at 5000 rpm for 15 second twice, and spinal cords were spun four times because of the high fat content. Samples were left at room temperature for 5 minutes and then transferred to new labelled tubes.

Total RNA was extracted from brain and spinal cord samples using Qiagen RNeasy Mini Kit (Cat No./ID: 74104 Qiagen, Crawley, UK) in accordance with manufacturer's instructions. 200µl chloroform was added and samples shaken for 15 seconds before resting at room temperature for 2-3 minutes. Samples were centrifuged at 12000 x g for 15 minutes at 4°C and then the clear aqueous phase was transferred to a new tube. 600µl of 70% ethanol was added to the sample and vortexed. 700µl of the sample was transferred to a labelled RNeasy mini spin column with a 2-ml collection tube. Columns were centrifuged for 15 s at 8000 x g and flow-through discarded. This was repeated with the remaining sample and flow-through discarded again. 700µl of Qiagen Buffer RW1 was added to the column, centrifuged for 15 s at 8000 x g and flow through discarded as before. 500µl Qiagen Buffer RPE was added, centrifuged for 15 s at 8000 x g and flow through discarded. This step was repeated and the second-time columns were spun for 2 mins to dry. Columns were placed into a new collection tube, 30µl of RNase-free water was added and columns were centrifuged at 8000g for 2 minute to elute RNA. The eluate was then added onto the column again and centrifuged again to increase the yield.

2.6.3 DNase Digestion

TURBO DNA-free™ Kit, (Ambion Life Technologies), was used to remove DNA contamination. 3µl DNase buffer and 1µl DNase 1 (TURBO DNA-*free*™ Kit, AM1907) was added to each 30µl sample for DNase digestion at 37 °C for 30 minutes on the heat-block. 6µl of DNase inactivation reagent was added and samples left at room temperature for 5 minutes. Samples were centrifuged at 10,000 rpm for 5 minutes and supernatant was transferred to a fresh tube. RNA yields were determined by spectrophotometry using the NanoDrop® ND-1000 (Thermo Scientific). Quantified RNA was stored at −80°C until cDNA synthesis and PCR assay.

2.6.4 Reverse Transcription – RNA to cDNA

Thermo Scientific DyNAmo cDNA Synthesis Kit was used for reverse transcription as per kit instructions. 500ng of RNA is required for the reaction (for IL-1β 750ng RNA was converted); the volume of sample required was calculated from the concentration and made up to a final volume of 6µl with nuclease free water. 2µl of 80 µg/µl Random Hexamers was added. Samples were incubated in a BioRad PCR machine for 5 minutes at 65°C and then placed on ice for 2 minutes.

12µl master mix (containing 10µl of 2 x RT Buffer and 2µl M-MuLV RNase H+ reverse transcriptase) was added to samples. PCR tubes were placed in a C1000™ Thermal Cycler PCR machine (Bio-Rad Laboratories, Inc). Dynamo cycling conditions as follows: Hot lid 105°C 30s, 25°C for 10 minutes, 37°C for 40 minutes, 85°C for 300 seconds. Samples were held at 4°C until collection and then stored at −20°C until assay.

2.6.5 Gene Expression Assay by Taqman

96-well plates were used for quantitative (q)-PCR of brain and spinal cord tissue from C57BL/6 and P301S mice treated with either saline or LPS by real-time PCR with TaqMan gene expression assay. There were 4 groups (C57BL/6 + Saline, C57BL/6 +

LPS, P301S + Saline and P301S + LPS) and 6 animals per group. Brain and spinal cord tissue was analysed from each animal and triplicates of each sample were required hence samples were split across two plates. Plate design is illustrated in Figure 5.

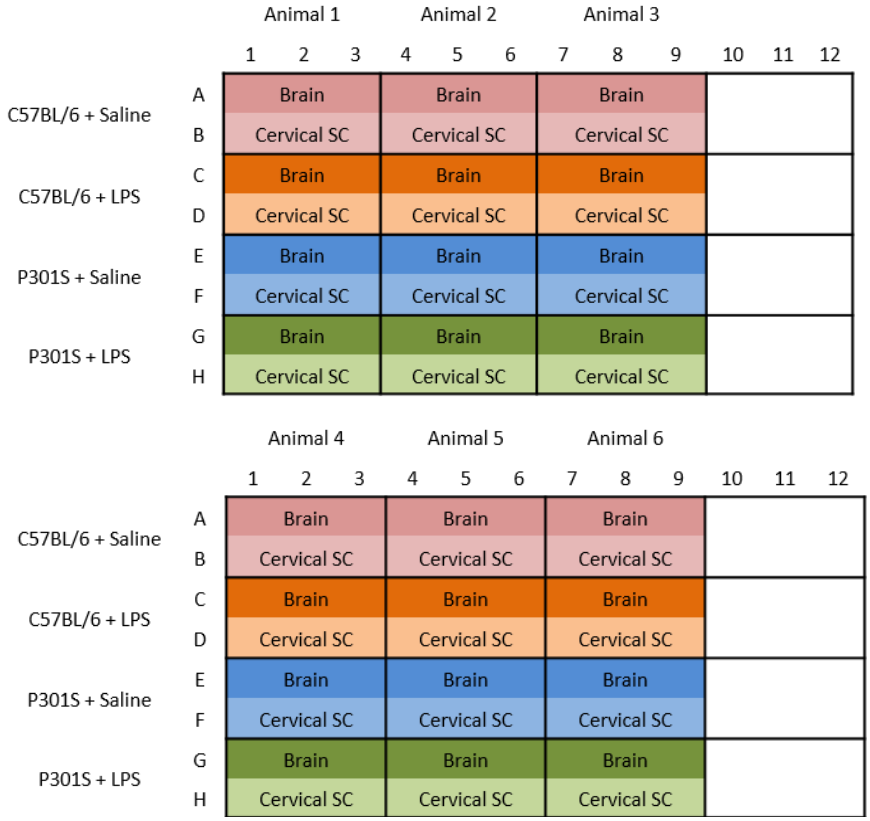

Figure 5 - Gene expression assays - plate design. Brain and spinal cord tissue from C57BL/6 and P301S mice injected with saline or LPS were used for gene expression assays to detect changes in GFAP, CD11b and IL-1β expression.

The following gene expression assays were used (Thermo Fisher Scientific): GFAP, (Mm01253033_m1), CD11b (Mm00434455_m1) and IL-1β (Mm00434228_m1). The levels of GFAP and CD11b mRNA were determined relative to the endogenous control gene HPRT (Mm01545399_m1) in duplex reactions. However, due to the relatively low abundance of IL-1β mRNA levels were compared to HPRT in singleplex gene expression assays.

For duplex reactions, each well had 20µl total volume which included: 10µl Taqman iQ Supermix (Cat. no:1708862, BioRad; iQ Supermix contains dNTPs, 6 mM $MgCl_2$, 50 U/ml hot-start iTaq™ DNA polymerase); 1µl of target gene expression assay; 1µl

of HPRT gene expression assay; 7µl of PCR water; and 1µl cDNA. For singleplex IL-1β gene expression assay 1µl of HPRT assay was replaced with an additional 1µl of PCR water, and for singleplex HPRT assay 1µl of target gene expression assay was replaced with an additional 1µl of PCR water.

A master-mix was made including all components apart from the cDNA. The master-mix was then pipetted into labelled tubes; 57µl per tube – enough for triplicates. 3µl cDNA was added to each tube. The cDNA sub-master-mix was pipetted up and down to mix and was then pipetted into triplicate wells.

An adhesive film was used to seal the plate before qPCR was performed using Bio Rad CFX96 Real-Time PCR Machine. Forty cycles were run with the following conditions: 3 minutes at 95°C and for each cycle 15 seconds at 95°C to denature and 50 seconds at 60°C for transcription.

2.6.6 Quantification of gene expression

The relative abundance of mRNA in the four groups was calculated by the comparative C_T method as follows:

$$RQ = 2^{(-\Delta\Delta C_T)}$$

$$RQ = 2^{-(\Delta C_T(GOI) - \Delta C_T(HPRT))}$$

$$\mathrm{RQ} = 2^{-((C_T(GOI)_{Sample\ A} - C_T(GOI)_{Ref} - (C_T(HPRT)_{Sample\ A} - C_T(HPRT)_{Ref})}$$

Where RQ is the relative quantity or fold change, C_T(GOI) is the C_T value of the gene of interest, C_T(HK) is the C_T value of the house keeper or internal control, $C_T(\ )_{Sample\ A}$ refers to the C_T value of an individual and $C_T(\ )_{Ref}$ refers to the average C_T value of the C57BL/6 + Saline reference group. The RQ value was used in statistical testing.

2.6.7 Statistics

Data clean-up: rodents were excluded where the C_T(HK) was more than 3 SD from the mean of the group but the C_T(GOI) was not as this implies a technical error. Mixed effects linear regression with random intercept for ID was used for primary analysis of RQ values. To investigate the potential influence of outliers a sensitivity analysis was run. Individuals with RQ more than 3 SDs from the mean were excluded, new $C_T(GOI)_{Ref}$ and $C_T(HK)_{Ref}$ were determined and the RQ recalculated.

2.7 Solutions

PBS: 137mM NaCl; 2.7mM KCl;10mM Na_2HPO_4; 1.8mM KH2PO4; pH=7.4 adjusted with HCL

PFA: 4% Paraformaldehyde in 1% PBS

TNS: 50mM Trizma base, pH 7.4 with Nitric acid

3 Chapter 3 – Characterising the P301S mouse

3.1 Introduction

Dementia and Alzheimer disease (AD) were the leading cause of death in England and Wales in 2015 (ONS, 2016). Tau protein is implicated in AD. In tauopathy dementias such as frontotemporal dementia (FTD), corticobasal degeneration (CBD), progressive supranuclear palsy (PSP) and Pick's disease (PiD) tau becomes hyperphosphorylated, forms insoluble intracellular aggregates and ultimately leads to the demise of neurons. The realisation that mutations in tau protein are sufficient to cause dementia (Clark et al., 1998, Hutton et al., 1998, Poorkaj et al., 1998, Spillantini et al., 1998) led to the development of animal models of tauopathy (discussed in section 1.1.5), including the P301S mouse model used in this thesis, which expresses human mutant tau under neuronal Thy 1.2 promoter.

Previous work using this model demonstrated that the P301S mouse accurately recapitulates many of the pathological features of tauopathy, including hyperphosphorylation and aggregation of pathological tau throughout the CNS and neuronal loss, astrogliosis and microgliosis in the spinal cord (Allen et al., 2002, Bellucci et al., 2004) along with age-related, region specific cortical neuronal loss (Hampton et al., 2010). Abnormal ultrasonic vocalisations (USVs) have also been identified in P301S mice as early as postnatal day 3 and enhanced motor and exploratory activity in the openfield at 8 weeks of age (Scattoni et al., 2010). P301S mice develop a gradual hind-limb paralysis as a result of neuronal loss in the spinal cord.

Here I aimed to determine a detailed temporal profile of disease-associated behavioural and pathological changes: firstly to identify an appropriate behavioural task which would accurately and non-invasively reveal the progressive trajectory of the disease in P301S mice; secondly to use this task to determine the longitudinal behavioural profile of the P301S mouse compared with control mice; thirdly to

investigate key pathological hallmarks – neuronal loss, astrogliosis and microgliosis at multiple time points throughout the trajectory of the disease.

These experiments will provide key details that will inform the timing of interventions in future experiments.

3.2 Methods

3.2.1 Behaviour

This chapter aimed to identify a behavioural task that would provide a non-invasive tool to monitor the trajectory of the disease in P301S mice. To detect a disease-related decline in performance of P301S mice it is necessary to identify an appropriate behavioural task which meets the following criteria: control mice must be able to maintain a steady baseline performance so that any difference in performance between controls and P301S mice is necessarily the result of the disease; P301S mice must be able to achieve a steady initial baseline performance; the task must reliably and reproducibly expose a disease-related decline in performance in P301S mice compared with control mice.

In order to identify an appropriate behavioural task to capture the longitudinal profile of the P301S mice, three behavioural cohorts were tested on two of three different behavioural tasks (see Table 6; methods described in section 2.2).

Age in Weeks	Spontaneous Alternation in T-maze (n)		Burrowing Task (n)		Horizontal Bar Task (n)	
Genotype	**C57BL/6**	**P301S**	**C57BL/6**	**P301S**	**C57BL/6**	**P301S**
<20	14	16	15	17	15	15
21	14	16	12	14	12	12
22	14	16	7	9	7	7

Table 6- Animals used in chapter 3 - characterising the longitudinal behavioural profile of P301S mice.

3.2.2 Histochemistry

Cresyl violet neuronal staining was performed on brain sections as described in section 2.3.2. Immunohistochemistry was performed for GFAP-positive astrocytes and IBA1-positive microglia in brain and spinal cord tissue as described in sections 2.3.3 and 2.3.4 and either visualised by fluorescent antibodies or by DAB staining. Details of antibodies used are given in Table 7.

3.2.3 Imaging, Quantification and Statistics

3.2.3.1 NeuN in the Brain

3.2.3.1.1 Imaging

Fluorescent images were taken of two NeuN-stained cortical hemispheres per animal as described in section 2.4, at 20x objective.

3.2.3.1.2 Quantification

Cell counts were conducted in each hemisphere using Zen 2011 software; two digital areas 150 μm x 150 μm were carefully aligned with the pial membrane such that counts were conducted in the first 150 μm of the superficial motor cortex. The "Events" tool was used to keep track of counted cells. Where the border of the counting area bisected a cell only cells with more than half of the soma inside the area were counted.

3.2.3.1.3 Statistical Analysis

Cell counts were converted to cells per mm^2 in Excel and this "Cells per mm^2" data was used for statistical analysis. Mixed effects linear regression with random intercept for animal ID was used for within time-point comparison of P301S mice with pooled C57BL/6 mice. C57BL/6 n=9, P301S 8wk n=4, 12wk n=6, 20wk n=3.

Antibodies used

Tissue	Primary Antibody	Dilution	Cat. #	From	Secondary Antibody	Dilution	Cat. #	From	Method
Brain	Mouse monoclonal anti - NeuN	1:400	MAB377 B	Merk Millipore	Streptavidin Conjugated Alexa 488	1:1000	S32354	Thermo Fisher Scientific	Fluorescent
Brain	Rabbit polyclonal anti-GFAP	1:1000	ZO334	DAKO	Goat anti-Rabbit IgG (H+L) Alexa Fluor 488	1:1000	A11008	Thermo Fisher Scientific	Fluorescent
Spinal Cord	Rabbit polyclonal anti-GFAP	1:1000	ZO334	DAKO	Biotinylated universal horse anti mouse/rabbit IgG (H+L)	1:200	BA-1400	Vector laboratories	DAB
Brain and Spinal Cord	Rabbit polyclonal anti-IBA1	1:1000	MP-290-CR05	A. Menarini Diagnostics	Biotinylated universal horse anti mouse/rabbit IgG (H+L)	1:200	BA-1400	Vector laboratories	DAB

Table 7 - Antibodies used in chapter 3 - characterising the longitudinal pathology of the P301S mouse.

3.2.3.2 **Cresyl Stain in the Brain:**

3.2.3.2.1 Imaging

Brightfield images of cresyl violet-stained sections were taken as described in section 2.4 at 20x objective, with an exposure 12 ms.

3.2.3.2.2 Quantification

Counts were conducted in the first 150 µm using Zen 2011 software as described for NeuN-positive cell counts. Both hemispheres from a minimum of 2 sections were counted per animal (total of 4 hemispheres were imaged per animal).

3.2.3.2.3 Statistical Analysis

Raw cell counts were converted to cells per mm^2 in Excel. The summary data indicated three possible options for the trajectory of decline in cell density in P301S mice:

1) a linear decline in cell numbers between 8 and 20 weeks;

2) a bi-phasic decline, whereby there is a steady phase up until 10 weeks of age followed by a progressive decline until 20 weeks;

3) a tri-phasic decline whereby there is a steady stage from 8 to 10 weeks followed by a progressive neuronal loss from 10 to 12 weeks and this is followed by a plateau between 12-16 weeks. Three linear mixed effects models with random effects for individual animals were fitted in order to test these three models and the Bayesian Information Criteria (BIC) was used to indicate the appropriateness of the model. Comparison of the three models using the BIC was done by Dr Pete Connick using STATA software. C57BL/6: n=4, P301S: 8wk n=5, 9wk n=7, 10wk n=7, 11wk n=4, 12wk n=5, 16wk n=5 20wk n=5.

3.2.3.3 Astrogliosis in the Brain: GFAP Stain

3.2.3.3.1 Imaging

Fluorescent images of the motor cortex from brain sections stained for glial fibrillary acidic protein (GFAP) – a marker of reactive astrocytes – were taken with 20x objective and 810 ms exposure.

3.2.3.3.2 Quantification

Manual cell counts were conducted, using Axiovision 4.8 software. A digital area 150 μm x 300 μm was carefully aligned with the pial membrane such that counts were conducted in the first 150 μm of the superficial motor cortex. Both hemispheres from a minimum of 2 sections were counted per animal. Counts were converted to cells per mm^2 and these data used for statistical analysis (See section 3.2.3.7). C57BL/ 6; pooled n=8 (8 weeks n=2, 12 weeks n=1, 20 weeks n=5), P301S; 8 weeks n=5, 9 weeks n=5, 10 weeks n=5, 11 weeks n=5, 12 weeks n=5, 16 weeks n=5, 20 weeks n=4.

3.2.3.4 Astrogliosis in the Spinal Cord: GFAP Stain

3.2.3.4.1 Imaging

Bright field images were taken of lamina 9 of GFAP stained spinal cord sections, visualised by DAB. Sections were imaged at 20x objective. An average of 4 images were taken per animal (min = 3, max = 5).

3.2.3.4.2 Quantification

GFAP-positive cell counts were conducted using Zen 2011 software. A digital area 400 μm x 200 μm was positioned in the centre of the image and counts conducted therein using the "Events" tool used to keep track of counted cells. Cell counts were converted to cells per mm^2 in Excel and this data used for statistical analysis (See section 3.2.3.7). C57BL/6 n=8, 8 weeks n=4, 9 weeks n=4, 10 weeks n=3, 11 weeks n=4, 12 weeks n=5, 16 weeks n=5, 20 weeks n=4.

3.2.3.5 Microgliosis in the Brain: IBA1 Stain

3.2.3.5.1 Imaging

Brightfield images were taken of IBA1-DAB stained motor cortex. Both hemispheres from a minimum of 2 sections (total 4 hemispheres) were imaged per animal.

3.2.3.5.2 Quantification

Cell counts were conducted using Zen 2011 software, within two digital areas each 200 x 200 μm. Cells were only counted if there was a clear cell body. Cell counts were converted to cells per mm^2 and these data used for statistical analysis (See section 3.2.3.7). C57BL/6 n=13, 8 weeks n=6, 9 weeks n=4, 10 weeks n=6, 11 weeks n=5, 12 weeks n=5, 16 weeks n=6, 20 weeks n=6.

3.2.3.6 Microgliosis in the Spinal Cord: IBA1 Stain

3.2.3.6.1 Imaging

Images of the whole IBA1 DAB-stained spinal cord were generated by taking multiple brightfield images at objective 20x and exposure 1 ms using the Panavision tool in Axiovision 4.8 software and manually stitching them together.

3.2.3.6.2 Quantification

IBA1-positive cell counts were conducted using Zen 2011 software in three digital areas 200 μm x 200 μm positioned over lamina 9 of the ventral horn. Microglial cells were counted if there was a clear cell body. Cell counts were converted to cells per mm^2 and these data used for statistical analysis (See section 3.2.3.7). (C57BL/6 n=15, 8 weeks n=4, 9 weeks n=3, 10 weeks n=7, 11 weeks n=4, 12 weeks n=3, 16 weeks n=5, 20 weeks n=4).

3.2.3.7 Statistical Analyses

Mixed effects linear regression with random intercept for animal ID was used for within time-point comparison of P301S mice with pooled C57BL/6 mice.

To investigate the trajectory of astrogliosis and microgliosis in P301S mice mixed effects linear regression with random intercept for animal ID was used and a dummy variable was created for age in weeks to re-centre data.

3.3 Results

This project aims to use the P301S mouse as a model of neurodegeneration, to determine whether systemic inflammation can influence the trajectory of disease progression. In order to answer this question, a robust understanding of the usual trajectory of disease progression in this mouse model is required, hence, an appropriate behavioural task must be identified, and appropriate pathological readouts defined.

3.3.1 Behaviour

3.3.1.1 Spontaneous alternation

Spontaneous alternation of P301S and C57BL/6 mice in the T-maze was tested weekly. Most animals alternated in the T-maze at above chance levels, although visual inspection of weekly performance among C57BL/6 mice showed marked apparent variability (**Figure 6**B). Comparing the C57BL/6 within-time-point mean performance to the overall mean of the performance at all other time points, statistically significant differences were seen at weeks 9, 12, 13, 14 and 16 (**Figure 6**B) The lack of any temporal patterning suggests low test-retest reliability. In order to test this formally a repeated-measures one-way ANOVA was performed, confirming differences in percentage alternation in the control group over the 15 weeks of the experiment, $F(14, 182) = 3.51$, $p < 0.00005$.

Alternation in this apparatus is typically a spontaneous behaviour in mice and the reason for this failure to establish stable alternation in normal animals is not clear but lack of stability of performance among control mice makes conclusions about working memory in these animals unreliable and suggests that spontaneous

alternation in the T-maze was not a suitable model to determine whether there is any significant disease-related difference between P301S mice and controls or in which to test interventions.

In any case, P301S mice also showed no decline over time; indeed, at 22 weeks of age P301S mice were still able to attain 80.0 ± 5.6% successful alternation compared with 59.3 ± 8.0% for the control mice.

3.3.1.2 **Burrowing**

Overnight burrowing performance of P301S and C57BL/6 mice was tested weekly. Comparison of the grand means shows that across the whole longitudinal period, P301S mice burrowed significantly less than control mice (48.0 ± 1.9% and 54.2 ± 2.0% respectively Holm-Sidak ANOVA, p=0.022) (**Figure 6**D). However, analysing the data as one epoch may be misleading because there appear to be three distinct phases to the burrowing behaviour of P301S mice; phase 1, 8-12 weeks of age; phase 2, between 12-17 weeks of age; and phase 3, between 17-22 weeks of age (see **Figure 6**D).

At the outset of phase 1 there was an apparent reduction in performance of P031S mice compared with controls although this did not reach statistical significance at α= 0.05 (difference in initial performance -17.1%; p = 0.067; 95% CI -35.5 to 1.29).

C57BL/6 mice showed no evidence of change in their burrowing performance during phase one of the experiment (weekly change in percent burrowing -0.5%; p = 0.540; 95% CI -2.3 to 1.2). In contrast P301S mice, who initially burrowed less, showed an improvement in their performance during phase 1 (weekly change 4.5%; p < 0.001; 95% CI 2.1 to 6.9). During Phase 2 neither control mice nor P301S showed any change in burrowing performance (C57BL/6 weekly change in percentage burrowed 1.1%; p = 0.117; 95% CI -0.3 to 2.5; P301S weekly change in percentage burrowed 0.0%; p = 0.968; 95% CI -2.0 to 1.9). During the phase 3 control mice appeared to show a slight downward trend, but this did not reach significance at α=0.05 (weekly change -0.8%;

p = 0.397; 95% CI -2.8 to 1.1), whereas P301S mice showed a significant, progressive decline (weekly change -4.1%; p = 0.003; 95% CI -6.7 to -1.4).

3.3.1.3 **Horizontal bar task**

While horizontal bar task performance of control mice remained constant throughout the experiment, visual inspection of horizontal bar performance of P301S mice over time showed two obvious distinct phases (**Figure 6**F): the stable phase (phase 1; 9-15 weeks) and the declining phase (phase 2; 15-22 weeks). At the outset of phase 1 there was a very slight reduction in performance of P301S mice compared with controls (difference in initial performance -0.7; p = 0.001; 95% CI -1.1 to -0.3). During phase 1 control mice and P301S mice showed a subtle improvement (C57BL/6 weekly change in horizontal bar score 0.1; p = 0.007; 95% CI 0.0 to 0.1; P301S additional weekly change in horizontal bar score 0.0; p = 0.760; 95% CI -0.1 to 0.1).

During phase 2 control mice maintained a steady baseline performance (C57BL/6 weekly change in horizontal bar score 0.0; p = 0.694; 95% CI -0.1 to 0.1) whereas P301S mice showed an age-related decline in horizontal bar score (P301S weekly change -0.8; p < 0.001; 95% CI -0.9 to -0.6). The apparent improvement in performance at 22 weeks compared with 21 weeks is artefactual, arising because several mice with the most severe hind limb phenotype had to be sacrificed after 20 and 21 weeks of age in line with Home Office regulations.

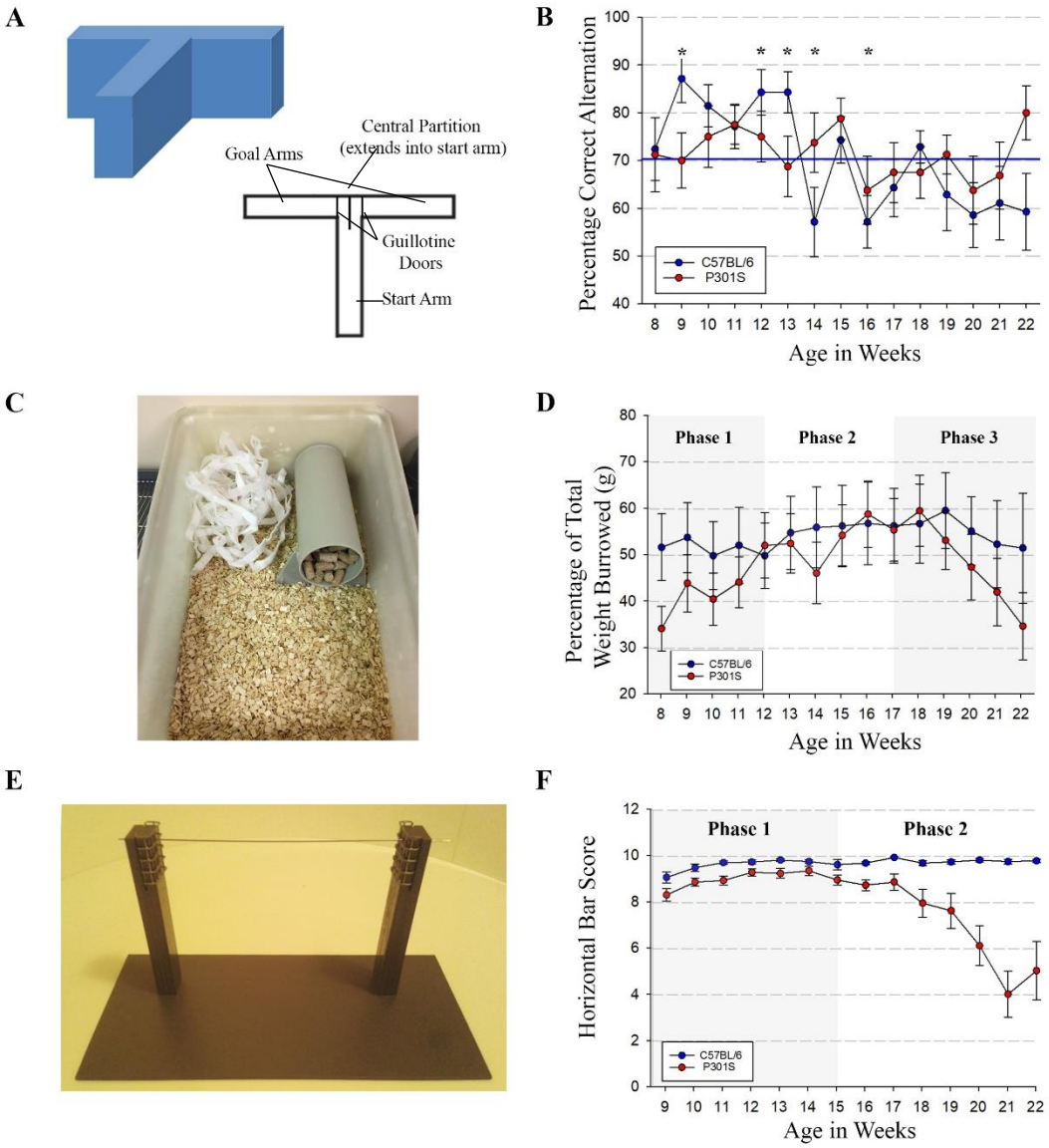

Figure 6 – Behavioural tasks: Longitudinal burrowing and horizontal bar behavioural tasks detect progressive decline in performance of the P301S mouse. *Three behavioural tasks are shown, spontaneous alternation in the T-maze, burrowing and horizontal bar task. Tasks were first evaluated for stable performance of controls, where this was met the temporal chance in P301S mice was explored. A) Diagram of spontaneous alternation apparatus – the T-shaped maze has arms 30 cm x 7 cm with walls 20 cm high, removable guillotine doors and a central partition. B) Spontaneous-alternation T-maze results - Percentage of correct alternations made by C57BL/6 mice (blue, n=14) and P301S mice (red, n=16), tested weekly from 8-22 weeks of age. Highly variable performance was seen for the control group (significant differences on t-test comparing within-time-point means vs. grand mean (blue line), indicated by *p<0.05). This task was therefore rejected for comparison of P301S vs controls. C) Photograph of filled burrowing tube in-situ prior to burrowing session.(Photograph by Kerry Lavin Thomson). D) Burrowing results - Percentage of total weight burrowed over-night (12h) by C57BL/6 and P301S mice, tested weekly from 8-22 weeks of age. Stable performance of control mice was seen throughout. P301S mice displayed three distinct temporal phases: learning phase (8-12 weeks); stable phase (12-17 weeks); and declining phase (17-22 weeks) (see results for further details). E) Photograph of horizontal bar apparatus: a 26 cm bar is suspended between two pillars at height 19.5 cm. Scores were assigned 0-10 (see methods). F) Horizontal bar results - C57BL/6 performance stable throughout 9-22 weeks. P301S mice displayed 2 phases: stable phase (phase 1; 9-15 weeks), declining phase (phase 2; 15-22 weeks) (see results for further details).*

3.3.2 Pathology

Tissue from control mice sacrificed at 8, 12, and 20 weeks of age was stained, imaged and quantified alongside P301S tissue. There was no age-related change in any of the markers quantified in control mice, hence in every experiment data from control mice of all ages were pooled and P301S mice sacrificed at 8, 9, 10, 11, 12, 16 and 20 weeks of age were compared to this pooled group.

3.3.2.1 **Progressive Neuronal loss in the Motor Cortex of P301S Mice**

Previous work demonstrated significant superficial, frontal, cortical neuronal loss in M2 of the motor cortex of P301S mice at 12 weeks of age and end stage (20-24 weeks) compared with controls (Hampton et al., 2010). Previous findings were first verified and then a more detailed temporal profile of this neuronal loss was determined.

Fixed brain sections collected from C57BL/6 and P301S mice at 8, 12 and 20 weeks of age were stained with an antibody against neuronal nuclei (NeuN) (Figure 7A-D), a neuronal specific nuclear protein in vertebrates (Mullen et al., 1992).

At 8 weeks of age, NeuN positive cell counts conducted in the superficial layers of the motor cortex indicated that there was no difference between control mice (818.8 cells per mm^2; $p < 0.001$; 95% CI 688.7 to 948.9) and 8-week-old P301S mice (-68.8 cells per mm^2; $p = 0.53$; 95% CI -302.5 to 164.8). There was a decline in cell density, which was significant at 12 (-361.8 cells per mm^2; $p = 0.001$; 95% CI -538.1 to -185.5) and 20 weeks of age (-390.5 cells per mm^2; $p = 0.036$; 95% CI -750.4 to -30.7) (Figure 7I).

In order to determine when the decline in cell density in the P301S mouse began and investigate the functional form of the decline, coronal sections from mice aged 8, 9, 10, 11, 12, 16, and 20 weeks were stained with cresyl violet and cells were counted in the superficial layers of the motor cortex, up to a sub-pial depth of 150 μm (Figure 7 E-H).

Previously published work by Hampton et al. (2010) demonstrating that neuronal density of control mice did not vary between 8 and 20 weeks was verified, and hence cell density of P301S mice at each time point was compared to cell density of C57BL/6 mice age 20 weeks.

Cresyl-positive cell density in P301S mice was different from control mice at 11 weeks of age (see **Table 8** for details of estimated difference in mean cell counts compared with controls).

P301S Age in Weeks	Cells per mm^2	Δ Cells per mm^2	p (comparison to C57BL/6)	95% Confidence Interval	
C57BL/6	1437.8	-	< 0.001	1077.4	1798.2
8	1202.1	-235.7	0.289	-719.9	248.5
9	1091.2	-346.6	0.160	-858.6	165.4
10	1342.6	-95.2	0.559	-451.4	261.1
11	923.6	-514.2	**0.036**	-982.0	-46.3
12	468.0	-969.8	**0.000**	-1328.1	-611.5
16	469.0	-968.8	**0.001**	-1369.3	-568.3
20	405.7	-1032.1	**0.000**	-1425.0	-639.1

Table 8 - Change in cresyl-positive cell density in P301S mice compared with C57BL/6. *The first term represents Cresyl-positive cells per mm^2 for the reference group: C57BL/6 mice. The following terms test for an independent effect of genotype by within time-point comparison of P301S mice with C57BL/6 mice.*

Visual inspection of the summary data in Figure 7 J suggests three possible models of the decline in cresyl-positive cell density: the first - linear decline throughout the experiment; second - a bi-phasic course, initially stable up to week ten followed by a period of linear progressive neurodegeneration and finally a tri-phasic course, stable up to week 10 followed by a period of rapid neurodegeneration up to week 12 and then a period of relative stability until week 20.

In order to test these three competing models, linear mixed effects models with random effects for individual animals were fitted to raw data cell counts per mm^2 and we evaluated "goodness-of-fit" using the Bayesian Information Criteria (BIC). For the

bi- and tri-phasic models these were piece-wise with cut points at 10 and 12 weeks of age. For the single linear model, BIC was 4347.9, for the biphasic model BIC was 4347.9, for the tri-phasic model BIC was 4333.0, the difference in BIC of 14.9 comparing linear to tri-phasic model provides very strong support that the tri-phasic model is a better fit to the observed data (Raftery, 1995 - Table 6).

Thus cresyl-positive superficial neuronal cell counts in P301S mice indicate a stable phase, from 8 until 10 weeks of age, followed by a decline phase from 10 to 12 weeks and then a stable phase from 12 weeks until 20 weeks of age.

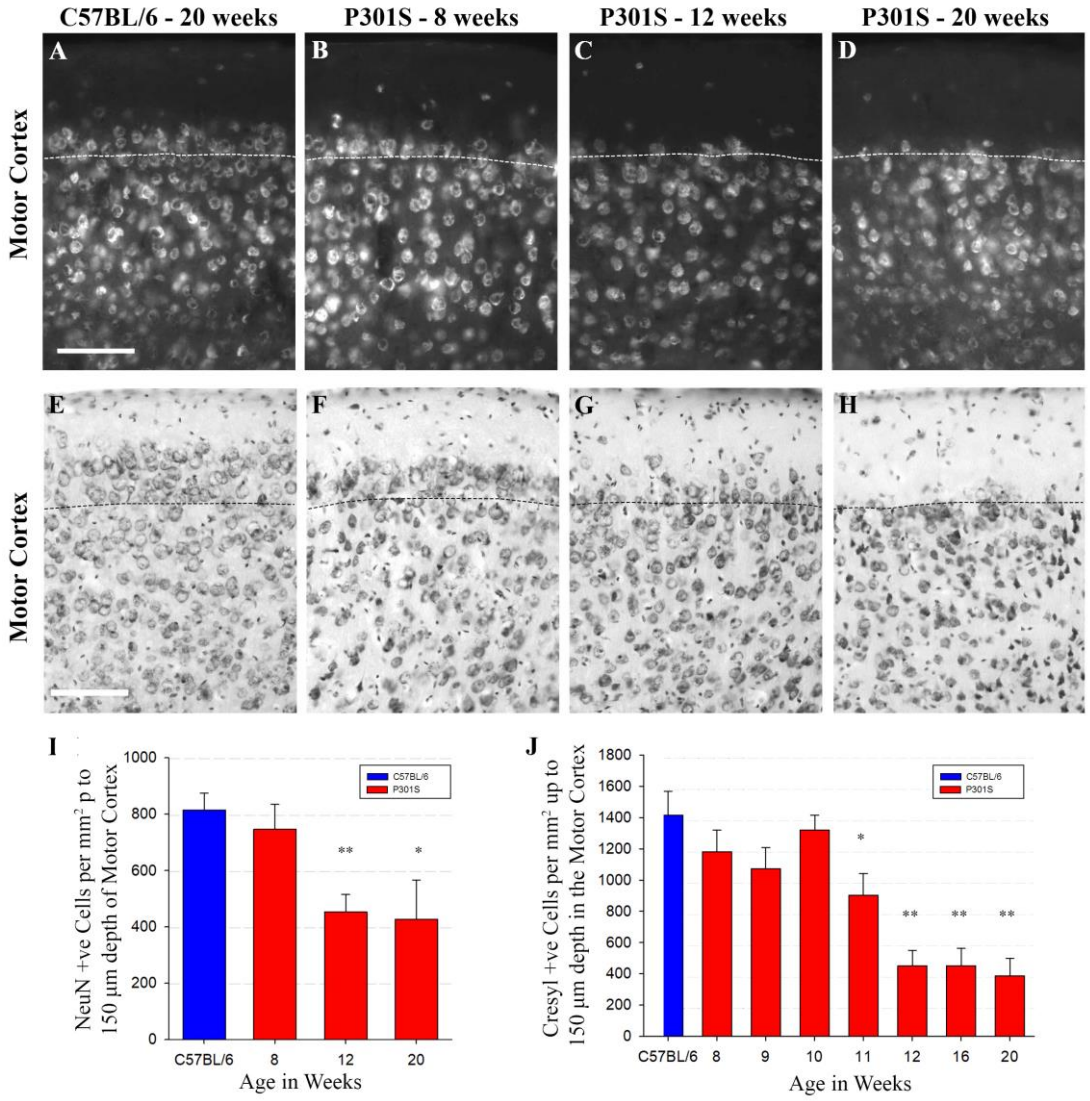

*Figure 7 - NeuN-positive and cresyl-positive cell counts show progressive reduction in cell density within the superficial layers of the cortex. A-D) Representative examples of NeuN stained 20 week old C57BL/6 mouse (A) and P301S mice at 8 (B), 12 (C) and 20 weeks of age (D). E-H) Representative examples of cresyl-stained 20 week old C57BL/6 mouse (E) and P301S mice at 8 (F), 12 (G) and 20 weeks of age (H). Scale bars 100 µm (A-D, E-H). I) NeuN positive cell counts in the motor cortex (to sub-pial depth of 150 µm) from control (blue) and P301S (red) mice showed neuronal loss in P301S mice from 12 weeks onwards (mixed effects linear regression, indicated by *p<0.05) (C57BL/6 n=9, P301S 8wk n=4, 12wk n=6, 20wk n=3). J) Cresyl positive cell counts indicate neuronal loss from 11 weeks onwards (mixed effects linear regression, indicated by *p<0.05, **p≤0.001). The temporal course of neuronal loss was evaluated by piecewise mixed effects linear regression. Optimum fit to the observed data was achieved with a tri-phasic model (see results for further details); stable phase (phase 1; 8-10 weeks), declining cell density phase (phase 2; 10-12 weeks) and stable phase (phase 3; 12-20) (see results section* 3.3.2.1 *for details). (C57BL/6 n=4, P301S 8wk n=5, 9wk n=7, 10wk n=7, 11wk n=4, 12wk n=5, 16wk n=5 20wk n=5).*

3.3.2.2 **Progressive Astrogliosis in the Motor Cortex of P301S Mice**

Hampton et al. (2010) showed that astrogliosis was absent in the cortex of P301S mice at 8 weeks of age compared with controls but there was astrogliosis in the P301S mice at 12 weeks which progressed further at 20 weeks of age. Astrogliosis was visualised with an antibody against glial fibrillary acidic protein (GFAP) - an intermediate filament protein which is upregulated in reactive astrocytes (Figure 8 A-D).

Here a more detailed temporal profile of astrogliosis in the cortex has been determined. There was no change in astrogliosis in control mice at 8, 12 or 20 weeks of age, hence C57BL/6 mice were grouped.

GFAP-positive cell counts indicated that there was already astrogliosis in P301S mice at 8 weeks of age, the youngest age examined, compared with controls (see Figure 8 I and see **Table 9**).

P301S Age in Weeks	Cells per mm²	Δ Cells per mm²	p (comparison to C57BL/6)	95% Confidence Interval	
C57BL/6	9.7	-	0.326	-10.4	29.8
8	70.0	+60.3	**0.001**	31.3	89.3
9	36.6	+26.9	**0.033**	2.6	51.3
10	65.5	+55.8	**0.000**	31.9	79.8
11	95.5	+85.8	**0.003**	34.1	137.6
12	140.0	+130.3	**0.000**	78.1	182.4
16	132.3	+122.5	**0.000**	74.2	170.8
20	175.0	+165.3	**0.000**	129.7	200.9

Table 9 - Progressive increase in GFAP-positive cell density in the cortex of P301S mice. *The first term represents GFAP-positive cells per mm² for the reference group: C57BL/6 mice. The following terms test for an independent effect of genotype by within time-point comparison of P301S mice with C57BL/6 mice.*

Astrogliosis was progressive, as indicated by the increasing estimated means and the increasingly significant p-values across time. This was confirmed by mixed effects linear regression, which indicated that there was a weekly increase in GFAP-positive cell counts of 10.4 cells per mm² ($p < 0.001$; 95% CI 6.2 to 14.6).

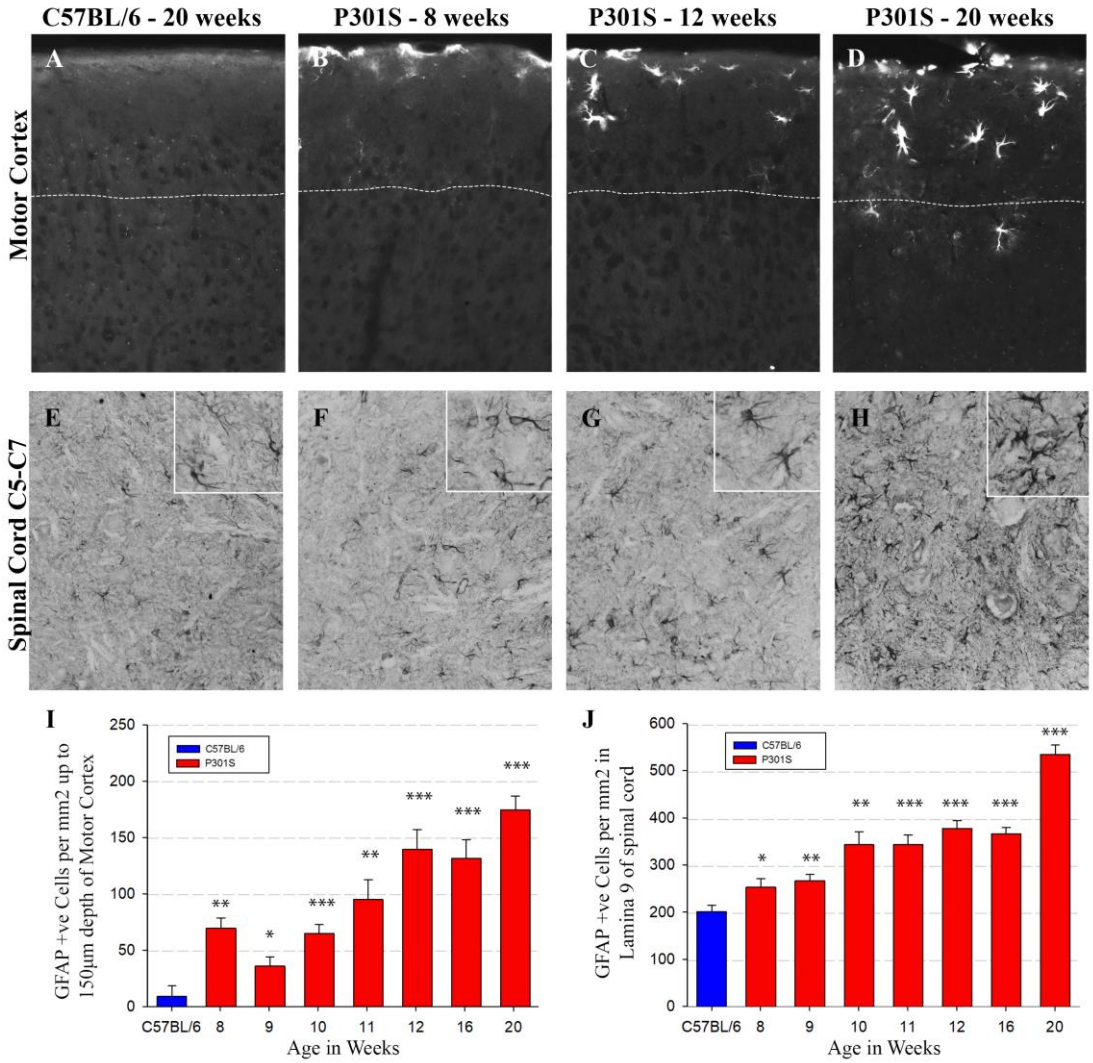

*Figure 8 - GFAP positive reactive astrocytes in the brain and spinal cord indicate regional and progressive astrogliosis. A-D) Representative examples of GFAP stained cortical tissue from C57BL/6 at 20 weeks, and P301S at 8, 12 and 20 weeks. E-H) Representative examples of GFAP stained spinal cord (lamina 9 of c5-c7) from C57BL/6 at 20 weeks, and P301S at 8, 12 and 20 weeks. Scale bar 100 µm (A-H). I) GFAP-positive cell counts conducted in the motor cortex (to sub-pial depth of 150 µm) of C57BL/6 (blue) and P301S mice (red) showed astrogliosis in P301S mice from 8 weeks onwards (mixed effects linear regression, indicated by; *p<0.05, **p≤0.005, ***p<0.0001). The temporal course of astrogliosis was evaluated by mixed effects linear regression; astrogliosis is progressive (see results for further details). (C57BL/6 n=8, P301S 8wk n=5, 9wk n=5, 10wk n=5, 11wk n=5, 12wk n=5, 16wk n=5 20wk n=4). J) GFAP positive cell counts in lamina 9 of the spinal cord also showed astrogliosis already significant at 8 weeks (mixed effects linear regression indicated by; *p<0.05, **p<0.005, ***p<0.0001). Again, evaluation of the temporal course by mixed effects linear regression showed that astrogliosis in the spinal cord was progressive (see results for further details). (C57BL/6 n=8, P301S 8wk n=4, 9wk n=4, 10wk n=3, 11wk n=4, 12wk n=5, 16wk n=5 20wk n=4).*

3.3.2.3 **Progressive Astrogliosis in the Spinal Cord of P301S Mice**

Allen et al. (2002) focussed primarily on the spinal cord because spinal cord pathology dominates the phenotype of P301S mice ultimately leading to hind limb paralysis. They showed astrogliosis in the spinal cord of 20 week P301S mice compared with controls. However, previous observations of astrogliosis in the spinal cord have been at end stage only. It is important to have an understanding of the nature of the progression of pathology in the spinal cord since understanding the chronology of pathology might both improve our understanding of disease pathology *per se* and inform any future interventions, hence I determined a longitudinal profile of astrogliosis in the ventral horn of the spinal cord; specifically, in lamina 9 of the spinal cord where there is severe motor neuron loss in P301S mice (Figure 8 E-H).

GFAP-positive cell density in the ventral horn of the spinal cord was elevated in P301S mice compared with controls as early as 8 weeks of age and continued to increase with age (Figure 8 J and Table 10). Mixed effects linear regression of GFAP cell counts confirms progressive astrogliosis in the P301S spinal cord (weekly increase in cell counts 19.9 cells per mm^2; $p<0.001$; 95% CI 14.2 to 25.6).

P301S Age in Weeks	**Cells per mm^2**	**Δ Cells per mm^2**	**p (comparison to C57BL/6)**	**95% Confidence Interval**	
C57BL/6	204.0	-	< 0.001	174.1	233.9
8	255.4	+51.4	***0.048***	0.7	102.2
9	269.8	+65.8	***0.001***	30.2	101.5
10	345.8	+141.7	***0.002***	68.2	215.2
11	346.2	+142.2	***0.000***	84.7	199.8
12	380.5	+176.5	***0.000***	128.7	224.3
16	369.7	+165.7	***0.000***	132.7	198.8
20	537.8	+333.8	***0.000***	278.1	389.5

Table 10 - Progressive astrogliosis in the spinal cord of P301S mice compared with controls*. The first term represents GFAP-positive cells per mm^2 for the reference group: C57BL/6 mice. The following terms test for an independent effect of genotype by within time-point comparison of P301S mice with C57BL/6 mice.*

3.3.2.4 No Apparent Disease- Associated Microgliosis in the Motor Cortex of P301S Mice

Ionized calcium binding adaptor molecule (IBA1) is a cytoplasmic protein constitutively expressed by microglia, which is upregulated in inflammation. IBA1 is involved in cytoskeletal reorganization and actin cross-linking needed for cell migration and palpitation of processes (Ohsawa et al., 2004). It is widely used as a pan-microglial marker. IBA1 positive cell counts in the superficial layers of the cortex showed no difference between controls and P301S mice at any time point (Figure 9 A-D and I and **Table 11**) and there was no change in the number of IBA1 positive microglial cells across the lifespan of P301S mice (weekly change in IBA1-positive cell counts 1.3; p = 0.424; 95% CI -2.0 to 4.7).

P301S Age in Weeks	Cells per mm²	Δ Cells per mm²	p (comparison to C57BL/6)	95% Confidence Interval	
C57BL/6	260.4	-	< 0.001	236.1	284.8
8	272.9	+12.5	0.716	-87.0	111.9
9	254.9	-5.5	0.808	-54.7	43.7
10	265.8	+5.4	0.758	-32.3	43.2
11	280.5	+19.6	0.352	-25.3	64.5
12	267.3	+6.9	0.742	-38.2	52.0
16	270.1	+9.7	0.545	-24.4	43.8
20	284.8	+24.4	0.320	-27.3	76.2

Table 11 - IBA1-positive cell counts in the motor cortex indicate no microgliosis. *The first term represents IBA1-positive cells per mm² for the reference group: C57BL/6 mice. The following terms test for an independent effect of genotype by within time-point comparison of P301S mice with C57BL/6 mice.*

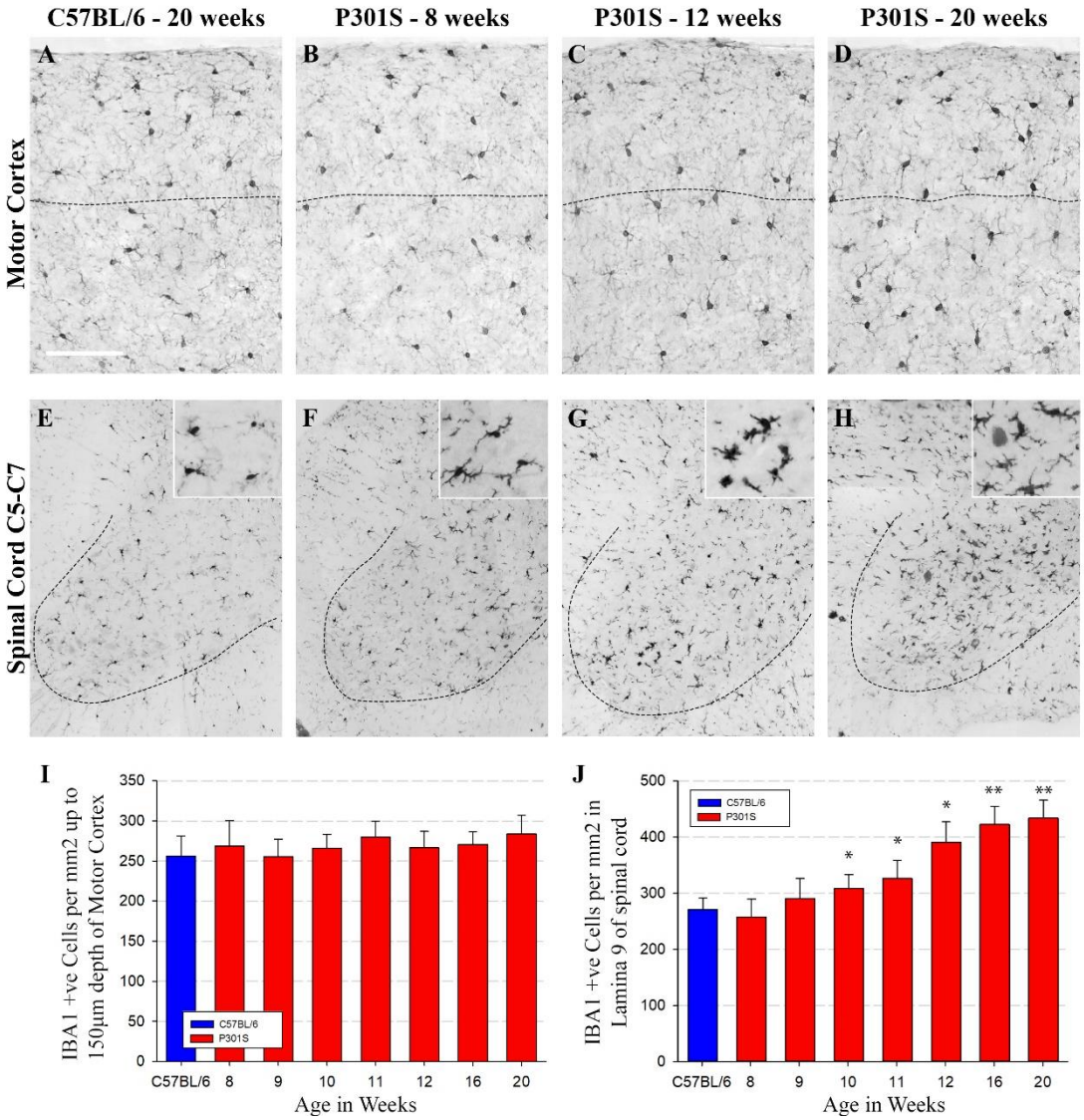

*Figure 9 -IBA1-positive microglial cell counts indicate progressive microgliosis in the P301S spinal cord but not in the brain. A-D) Representative examples of IBA1-stained cortical tissue from C57BL/6 at 20 weeks (A), and P301S at 8 (B), 12 (C) and 20 weeks (D). E-H) Representative examples of IBA1 stained spinal cord (lamina 9 of c5-c7) from C57BL/6 at 20 weeks (E), and P301S at 8 (F), 12 (G) and 20 weeks (H). Scale bar 100 µm (A-D). I) IBA1-positive cell counts conducted in in the motor cortex (to sub-pial depth of 150 µm) of C57BL/6 (blue) and P301S mice (red) showed no difference between C57BL/6 and P301S mice at any age and mixed effects linear regression showed no change over time. (C57BL/6 n=14, P301S 8wk n=4, 9wk n=3, 10wk n=5, 11wk n=5, 12wk n=5, 16wk n=6 20wk n=5). J) IBA1-positive cell counts in lamina 9 of the spinal cord indicated regional microgliosis in P301S mice from 10 weeks onwards (mixed effects linear regression indicated by; *p<0.05, **p<0.0001). The temporal course of microgliosis was evaluated by mixed effects linear regression; microgliosis in the spinal cord was progressive (see results section 3.3.2.5 for further details). (C57BL/6 n=15, P301S 8wk n=6, 9wk n=3, 10wk n=7, 11wk n=4, 12wk n=3, 16wk n=5 20wk n=4).*

3.3.2.5 **Progressive Microgliosis in the Spinal cord of P301S Mice**

Contrary to findings in the motor cortex, however, IBA1-positive cell counts in lamina 9 of the spinal cord indicated microgliosis in P301S mice compared with controls, apparent at 10 weeks of age (Figure 9 E-H and J and **Table 12**).

P301S Age in Weeks	Cells per mm²	Δ Cells per mm²	p (comparison to C57BL/6)	95% Confidence Interval	
C57BL/6	270.3	-	< 0.001	224.9	315.7
8	257.7	-12.6	0.702	-82.6	57.4
9	306.5	+36.2	0.334	-40.7	113.1
10	325.2	+54.9	**0.037**	3.7	106.0
11	342.7	+72.4	**0.038**	4.5	140.3
12	407.0	+136.7	**0.002**	59.4	214.1
16	439.1	+168.8	**0.000**	102.7	235.0
20	450.2	+179.9	**0.000**	112.5	247.2

Table 12 - Progressive microgliosis in the spinal cord indicated by IBA1 positive cell counts. *The first term represents IBA1-positive cells per mm² for the reference group: C57BL/6 mice. The following terms test for an independent effect of genotype by within time-point comparison of P301S mice with C57BL/6 mice*

IBA1 positive cell counts indicated progressive microgliosis in the spinal cord (weekly increase in IBA1 positive cell counts 15.5; 95% CI 11.1 to 19.8; $p < 0.001$). The increase in cell numbers was associated with a change in morphology from a senescent phenotype with a small cell body with long fine projections towards a thickened and bushy morphology (insets Figure 9 E-H).

3.4 Discussion

3.4.1 Behaviour

To capture the progressive decline of the disease it was important to identify a task that a young, pre-symptomatic P301S mouse could master and achieve a steady baseline performance, which would be progressively impacted as the disease progressed. Since the mice would be retested weekly throughout their lifespan, it was also important to identify a task which would not be complicated by test-retest variation; mice in a novel environment are usually very active and keen to explore, however activity generally decreases with repeated reintroduction into the same environment; hence a behavioural task such as openfield or novel object recognition might have been inappropriate. Another important consideration in choosing a behavioural task is that P301S mice develop a hind limb paralysis as they age, as a result of neuronal loss in the spinal cord, hence if a cognitive test is chosen which involves movement then this motor dysfunction might either contribute to, or mask any subtle changes in performance. This hind limb paralysis has been viewed by many as one of the major draw backs of the P301S mouse model, however the onset of paralysis in the P301S mouse is a robust and extremely consistent feature of the disease hence a task which measures the degree of motor dysfunction is ideal for tracking the progression of the disease.

3.4.1.1 Spontaneous alternation in the T-maze

Often the alternation in the T-maze is used as a learning and memory test; rodents are trained to alternate, by blocking off the alternative goal arm and by motivating correct alternation with a food treat in the goal arm or the temptation of escape from the T-maze into the safety of a home cage (Deacon et al., 2006). In that context, the task is used to test the ability to learn to alternate and to test working memory and if mice successfully acquire alternation it can be used to detect a decline or deficit in spatial and working memory. In this instance, however, the T-maze was used to test

spontaneous alternation, that is to say there is no motivation for mice to alternate, beyond their own innate curiosity of the previously unexplored arm.

The drive to explore a novel environment is strong and this test is able to detect hippocampal lesions in mice and rats however in this instance there was a huge degree of variability in performance of P301S mice *and* controls, potential explanations are discussed below.

This test depends on the desire of mice to explore a recently unexplored environment (Deacon et al., 2006) and it might be argued that the task therefore does not optimally lend itself to repeated retesting; mice are tested 5 times each week, from 8 until 22 weeks of age so very quickly the curiosity of the so called "previously unexplored arm" may decline.

This protocol requires handling of mice into and out of the maze. This can cause anxiety which might manifest as passivity or hyperactivity thus impacting the "decision making" capacity of mice. Handling of mice may also serve as negative reinforcement and therefore influence behaviour as observed by Gerlai (1998) who suggests an alternative continuous alternation protocol where mice are not removed from the maze between alternations but are allowed to return to the start arm after the decision trial where they are held until they are released for the next trial.

Thus, there are potential sources of variability across longitudinal testing but the most important factor in the rejection of this task is that it was unable to detect a progressive disease-associated decline in behaviour in the P301S mice. Exploration of novel environments, spatial learning and memory are all dependent on hippocampal function and this task is able to detect hippocampal lesions (Roberts et al., 1962). Hence this is suggests that hippocampal function is not significantly impacted by disease.

Pennanen et al. (2006) showed increased alternation in the Y-maze in mice expressing P301L human mutant tau under the Thy1.2 and authors put this increase down to

increased exploratory behaviour (Pennanen et al., 2006). P301S mice display increased exploratory behaviour in the openfield and increased interaction with novel objects; together these tasks indicate an impact on the pathways involved in reaction to novelty (Scattoni et al., 2010, Torvell et al., 2013). The fact that P301S mice are capable of 80% successful alternation at 22 weeks of age suggests there is no progressive decline in hippocampal function.

3.4.1.2 **Burrowing data**

Burrowing is another innate behaviour; the task was originally developed in an attempt to investigate hoarding tendencies of mice – a tube filled with food pellets was left in the cage and the next morning all of the food pellets had been displaced from the jar but they were haphazardly strewn across the cage floor not hoarded in any deliberate location. This behaviour also occurs with different substrates hence it is unlikely to be exclusively related to hoarding of food (Deacon, 2006). The reasons for burrowing activity remain unclear, in the wild animals create burrows to live in and escape predation and mice are often found with nesting materials in the tube the next day, however mice will still burrow in a full tube placed next to an empty tube (Deacon, 2006).

Here burrowing data showed three distinct phases. During phase 1 control mice showed no change in their performance, whereas P301S mice, who were initially lagging behind control mice, improved week on week. There are several possible explanations to explain why P301S mice were lagging behind; firstly, social facilitation is an important element of the acclimatisation phase – mice are introduced to the burrowing apparatus overnight alongside their littermates to encourage exploration of the apparatus – C57BL/6 mice were housed in cages of 7, 3 and 5 whereas P301S mice were housed in cages of 6, 3, 3 and 5. The group sizes may have affected the degree of social facilitation. Indeed, further analysis of the data shows that mice from smaller groups burrowed less during phase 1, and hence the smaller group sizes of P301S mice might therefore have introduced social facilitation bias.

P301S mice appear to be anxious compared with control mice; this might manifest as increased time taken to acclimatise to the burrowing apparatus. While P301S mice show increased exploration of novelty on some tasks (openfield and novel object) unpublished data from the lab indicates decreased exploration of open arms in the elevated plus maze (EPM) which is indicative of increased anxiety.

It is possible that phase 1 reflects a genuine developmental or learning delay in P301S mice; P301S mice are smaller than control mice; the initial difference in performance in phase 1 might reflect a physical developmental difference, which P301S mice must compensate for. Alternatively, since the tau transgene is expressed from as early as post-natal day 1 and this task has previously been able to detect lesions of the hippocampus and prefrontal cortex (Deacon et al., 2002, Deacon et al., 2003) it is plausible that this initial phase reflects a genuine developmental learning difference in P301S mice.

Irrespective of their slow start, P301S animals eventually burrow at similar rates to normal animals and continue to do so, throughout 'phase 2', until disease-related decline begins. Then during phase three P301S mice showed a gradual decline in burrowing performance whereas control mice do not. This decline in burrowing correlates with, and is likely to be the result of the progressive hind limb deficits. It is possible that there is an element of decline in performance that can be attributed to motivational or affective decline, however the neurological impacts cannot be teased apart from the muscle wastage that occurs as a direct result of neuronal loss and denervation.

3.4.1.3 **Horizontal Bar**

The horizontal bar task is a measure of motor strength and coordination; mice are suspended by their forelimbs from a bar; their innate response is to reach the platform at the end of the bar rather than fall – In similar studies, mice placed on a bar which is suspended from one end, facing the "open" end will spontaneously turn and travel

towards the supported end (Deacon, 2013). Hence this is a very simple "forced task" which measures physical ability and unlike many behavioural tasks horizontal bar task is not influenced by uncontrolled variables such as anxiety or test-retest variation.

The horizontal bar task has previously been published with a slightly different scoring method with "time spent on the bar" up to a maximum of 60 seconds as the variable and mice who reach the platform are given the maximum score of 60 seconds (Cunningham et al., 2005). Alternatively, the "time spent on the bar" was converted to an arbitrary score between 1 and 5 (*Falling between 1-5 sec = 1; Falling between 6-10 sec = 2; Falling between 11-20 sec = 3; Falling between 21-30 sec = 4; Falling after 30 sec = 5; Placing one forepaw on a bar support without falling = 5).* Here however the scoring method was modified slightly - a healthy mouse can reach the platform in under 3 seconds whereas P301S mice took much longer to reach the platform as disease pathology progressed. This difference in the time taken to reach the platform was not captured using the previous scoring methods and hence a new scoring method was designed around that fact, thereby improving the sensitivity of the task. Using this scoring method, the data demonstrated a progressive decline in horizontal bar performance of P301S mice.

Muscle weakness and muscle wasting associated with normal ageing is referred to as sarcopenia (Degens, 2007) and may be caused by 1) changes within the muscle (i.e. oxidation or glycation of the myosin filament), 2) changes in the environment which influence the regenerative capacity of skeletal muscles (i.e. elevated TNF-α which impairs myoblast differentiation), or 3) by denervation due to loss of alpha motor units from the spinal cord (Roubenoff, 2000, Degens, 2007). Muscle size and strength are proportional to usage hence denervation results in muscle wastage – denervation is also associated with loss of trophic signals from neurons (Roubenoff, 2000).

Importantly, there is a 49% motor neuron loss in the lumbar spinal cord (L2-L3) of P301S mice at 6 months of age which is associated with muscle denervation and

ultimately leads to hind limb wastage and paralysis (Allen et al., 2002). This is the most likely cause of decline in horizontal bar performance in P301S mice.

The time course of the motor neuronal loss in the spinal cord, however, remains to be determined. It is plausible that horizontal bar decline may precede α-motor neuronal loss. Firstly, because functional decline might result from neuronal dysfunction rather than death (e.g. synaptic dysfunction resulting from tau pathology). Secondly α-motor neurons receive inputs from upper motor neurons via corticonuclear, corticospinal and rubrospinal tracts, as well as sensory neurons and interneurons (Halliday et al., 2013), hence horizontal bar decline might be attributed to loss or dysfunction of any of these inputs. These inputs converge on the α-motor neurons which innervate muscles, hence death of motor neurons ought to cause immediate horizontal bar decline. However, there is plasticity in the system; neighbouring motor neurons are able to compensate for neuronal loss by "adoption" of muscle fibres (Roubenoff, 2000) hence motor neuron loss in the spinal cord might in fact precede horizontal bar impairment. Indeed very early evidence from rats indicated that weakness and atrophy were only detectable when 30% of motor neurons innervating a group of muscles was lost (Wohlfart, 1958).

The area assessed will be important in determining a relationship between motor neuronal loss and horizontal bar decline because the cord is organised in the rostral/caudal dimension such that cervical motor neurons innervate upper extremities and lumbar motor neurons innervate the lower extremities (Halliday et al., 2013).

This progressive hind limb phenotype is seen by many as a limitation of this and other rodent models of tauopathy dementia and has led to the development of transgenic models expressing tau under the control of inducible and cell- or region-specific promoters in order to generate mice with cognitive deficits, which mimic those seen in AD (As discussed in section 1.1.5)(Tatebayashi et al., 2002, Ramsden et al., 2005, Murakami et al., 2006, Rosenmann et al., 2008, Flunkert et al., 2013).

However here this disease-associated decline in motor function is exploited as a surrogate measure for disease severity. This task provides us with an excellent tool for following the trajectory of the disease; control mice and P301S mice are both capable of reaching and maintaining a consistent baseline score and the task sensitively and reproducibly picks up the gradual decline in performance and this decline in performance is a direct consequence of neuronal dysfunction in P301S mice.

3.4.2 Pathology

The P301S mouse expresses human mutant tau under the thy 1.2 promoter. This neuron-specific expression of mutant tau has previously been demonstrated sufficient to cause neuronal loss in the spinal cord and regional and progressive cortical neuronal loss with associated with astrogliosis.

3.4.2.1 Neuronal loss

Allen et al. (2002) focused on end point pathology in the spinal cord since there is hind limb paralysis and obvious spinal cord pathology; this paper demonstrated a 49% reduction in the number of motor neurons but was unable to demonstrate apoptosis by in situ end labelling (ISEL), caspase-3 or α-fodrin staining.

Hampton et al. (2010) later showed significant, progressive cortical neuronal loss in the superficial layers of the cortex at 12 weeks of age and at end stage by cresyl staining, immunohistochemistry for neuronal markers NeuN, GABA, and qPCR using neuronal marker Reelin.

A previous finding of progressive neuronal loss by NeuN staining at 8, 12 and 20 weeks of age was first replicated here and a more detailed temporal profile for the progressive cortical neuronal loss by cresyl staining was then conducted. The analysis indicated that neuronal loss followed a tri-phasic course; initially there was no significant difference between P301S mice and controls, between 10-12 weeks there was a rapid reduction in cell numbers followed by a period of relative stability at

which point there was roughly a 70% reduction in cresyl-positive cells in the area compared with control mice.

Hampton et al. (2010) indicated progressive neuronal loss such that there were fewer cells at end stage than at 12 weeks of age, whereas I have shown neuronal loss at 12 weeks of age which plateaus thereafter. It is likely that this disparity is due to the tissue used as well as the methods of analysis. Hampton et al. conducted cell counts in mice that were sacrificed at "end stage", which was determined by phenotype severity and ranged from 20 to 24 weeks whereas mice used here were sacrificed at exactly 20 weeks of age regardless of variation in the severity of phenotype. Hampton et al. conducted cell counts in the first 200 μm of the superficial layers of the cortex whereas I conducted cell counts in the first 150 μm – both factors which might contribute to loss of information between 12 and 20 weeks of age; cell counts in a larger area might detect ongoing neuronal loss.

Hampton et al. previously demonstrated, with immunohistochemistry and qPCR for superficial vs. deeper cortical neuronal markers, that neuronal loss in the P301S mice is restricted to the superficial cortex and not the deeper layers, hence in this instance only the first 150 μm were sampled. This approach is not ideal because it is plausible that an increase in the apparent size of layer one of the cortex, for instance due to superficial astrogliosis or due to the angle at which sections were cut, might cause an deceptive reduction in the cell numbers in the first 150 μm from the pial membrane, without genuine cell loss. This analysis might be improved by un-biased, random stereological sampling throughout the layers of the cortex in order to avoid introducing bias and demonstrate superficial neuronal loss which is absent in the deeper layers (West, 2012).

The cortical neuronal loss seen here precedes the decline in performance on the horizontal bar. Neurons in the motor cortex are arranged in layers (1-6) with a predominantly top—down excitatory organization (Weiler et al., 2008) such that axons of cells in the superficial layers arborise locally in layers 2/3 or synapse onto

layer 5 pyramidal and corticospinal neurons (Kaneko et al., 2000, Weiler et al., 2008, Anderson et al., 2010). Superficial pyramidal neurons receive inputs from the somatosensory cortex (Kaneko et al., 2000). Lesions in the somatosensory cortex impair acquisition of new motor skills without detectable changes in previously acquired skills (Sakamoto et al., 1989, Pavlides et al., 1993). The superficial motor cortical pyramidal cells thus integrate somatosensory and motor information and are involved in learning new motor skills (Kaneko et al., 2000) but are not directly involved in movement. This might explain the lack of correlation between superficial cortical neuronal loss and decline in horizontal bar performance.

Previously published work indicates faint staining of ring-like AT8-positive phospho-tau accumulations in the cortex at 8 weeks of age and an obvious increase in somato-dendritic accumulations by 12 weeks, there was a vast increase in AT8-positive cells at 20 weeks of age (Hampton et al., 2010). Unfortunately, there has been no temporal characterisation of the accumulation of NFTs in the P301S mouse so it is not possible to determine the relationship between different pathological tau species and neuronal loss, however the data do show progressive neuronal loss at a time when phospho-tau is accumulating in the somatodendritic compartment of neurons in the same region.

Although neuronal counts have showed progressive neuronal loss, the mechanism of cell death *per se* has not been identified. The original Allen et al., 2002 report suggested non-apoptotic neuronal loss in the spinal cord at 5-6 months of age on the basis of absence of in situ end labelling (ISEL) or caspase-3 staining. However, apoptosis at an individual cell level is a rapid event and ISEL only detects cell death which is on-going at the time of fixation. In certain models of severe, rapid and synchronous cell death this might be appropriate, however in a chronic slow-burning neurodegenerative condition there are likely to be very few cells dying at any given time. Indeed, if there is a tri-phasic course of neurodegeneration, as suggested here, it is possible that the time window to detect cell death was missed.

The exact mechanism of cell death in tauopathy dementia is unclear and widely debated. The most common form of cell death is apoptosis, otherwise known as programmed cell death. Apoptosis can be initiated by a cell-intrinsic or -extrinsic pathway and follows a well characterised sequence of events including activation of caspase proteins, chromatin condensation, DNA fragmentation, nuclear fragmentation, cell shrinkage and membrane blebbing. This controlled mechanism ensures that the contents of the cell are not exposed to the extracellular milieu, which would trigger an immune response. These well-characterised steps allow identification of apoptotic cells based on morphology, staining for activated caspases and labelling of 3'-OH ends of broken DNA. However, studies of human post mortem tissue fail to show any association between tau pathology and neuronal apoptosis (Gleckman et al., 1999, Atzori et al., 2001, Broe et al., 2004).

There is a large body of work focussing on cell-cycle re-entry as a mechanism of cell death in tauopathy dementias and indeed the inappropriate expression of many cell-cycle markers has been demonstrated in human dementias (Smith et al., 1995, McShea et al., 1997, Nagy et al., 1997a, Nagy et al., 1997b, Vincent et al., 1997, Arendt et al., 1998, Raina et al., 1999, Raina et al., 2000, Raina et al., 2001, Vincent et al., 2002, McShea et al., 2007, Previll et al., 2007, Lee et al., 2009). For review see Vincent et al 2003.

Cell cycle re-entry in the context of tauopathy is particularly interesting because of the role of tau and microtubules in spindle formation during cell division and the similarities between hyperphosphorylated tau during development and pathological tau found in dementias (Kanemaru et al., 1992, Brion et al., 1993, Brion et al., 1994, Pope et al., 1994, Illenberger et al., 1998). It has been postulated that mutant tau protein inhibits cell division by disrupting spindle formation. Pausing or disrupting mitosis results in cell death (Sorger et al., 1997) so not only are cells not being replaced but they also die – the mechanism of cell death is unclear but it is thought to resemble apoptosis.

Andorfer et al. (2005) investigated mechanisms of cell death in the hTau mouse model of tauopathy (described in section 1.1.5). Electron microscopy revealed neurons with morphological hallmarks of apoptosis including nuclear breakdown, chromatin condensation, membrane blebbing, however those cells with nuclear abnormalities did not contain tau aggregates, and cells which showed signs of DNA fragmentation (TUNEL staining) did not contain activated caspases. However, hTau brains showed a vast upregulation of cell-cycle regulating proteins including cyclin D_1, ki67 and PCNA – all of which are tightly regulated in the healthy brain but have been identified in AD brains. These proteins are associated with the early G_1/S-phase of the cell cycle and the absence of markers of the G_2/M transition (cyclin B an cdc2) indicate failure to complete mitosis and cell division (Andorfer et al., 2005).

Schindowski et al. (2008) investigated mechanisms of neuronal death in a mouse model of tauopathy, the THY-Tau22 mouse (described in section 1.1.5) which over expresses human tau mutated at G272V and P301S under the Thy1.2 promoter. Authors showed upregulation of cell cycle markers cyclin D1 (G_1/S-phase), Cyclin B1 (G_2/M-phase) and in young mice markers of neurogenesis and maturation (DCX, TUC-4 and NeuroD) and a BrdU-pulse indicated that the increase in cell cycle markers lead to the production of viable cells. Interestingly levels of cyclin D_1 increased with age, along with cyclin-D-CDK4 complex inhibitors p21Cip1 and p27Kip1, however there was a progressive decrease in markers of neurogenesis and maturation, suggesting dysregulation of the cell cycle with age (Schindowski et al., 2008).

This is particularly relevant since an attempt to determine the mechanism of neuronal loss in our P301S mice focussed on cell-cycle re-entry as a potential pathway to the demise of neurons (Delobel et al., 2006). Authors found that none of the activators or co-activators of the cell cycle assessed were over expressed or upregulated in 20-week old P301S mice, however cyclin-dependent kinase inhibitors p21Cip1 and p27Kip1 levels were elevated in brain and spinal cord tissue at end stage and were found in cells containing hyperphosphorylated tau inclusions. The presence of p21Cip1 and

p27Kip1 in P301S mice at 20 weeks of age might therefore be indicative of prior activation of markers of cell cycle re-entry.

It has also been suggested that neurodegeneration may occur by a distinct mechanism involving Wallerian degeneration-like dying-back of projections (Wang et al., 2014), the exact mechanism has not been provided but is tempting given the role of tau protein in axonal projections and the surprising lack of evidence for apoptosis in neurodegeneration.

The alternative to apoptosis is necrosis or necroptosis which involves rupturing of the cell membrane, releasing intracellular contents into the extracellular milieu and thus initiation of inflammatory events; this seems an unlikely cause of neuronal loss in this instance given the absence of microgliosis, which will be discussed further below.

In conclusion, here I provide evidence of progressive neuronal loss in the superficial layers of the motor cortex, but the mechanisms of cell loss remain unknown. The results I present here indicate that the most significant neuronal loss occurs between 10 and 12 weeks of age, although it is likely that neuronal loss continues after 12 weeks outside of the analysed field of view hence based on the literature and previous work in this mouse model it would be interesting to look for markers of apoptosis and cell-cycle re-entry in the cortex between 10 and 16 weeks of age.

3.4.2.2 **Astrogliosis**

Astrogliosis is a recurrent hallmark of tauopathy dementias (Bugiani et al., 1999, Broe et al., 2004). Astrogliosis in pure tauopathies is often associated with intracellular astrocytic tau deposits which vary in their appearance depending on the type of tauopathy (Komori, 1999). Thy 1.2-driven neuron-specific expression of tau in this P301S mouse model of tauopathy denies the opportunity to model astrocytic expression of mutant tau however it allows investigation of the impact of neuronal tau pathology on phenotypic switch to reactive astrocytes.

The data presented here demonstrated disease-associated reactive astrogliosis in the superficial cortex and in the spinal cord of P301S mice compared to controls, as determined by glial fibrillary acidic protein (GFAP)-positive cell counts, which were elevated in P301S mice compared with controls at every time point investigated. Furthermore, there was a progressive increase in the number of GFAP positive cells with age.

Progressive astrogliosis was present in other areas of the P301S brain and spinal cord. In line with similar P301S tau expressing mouse models astrogliosis was most apparent in the white matter (Yoshiyama et al., 2007) which is likely due to degeneration of white matter axons projecting from tangle-bearing neurons, however, here I aimed to identify pathological correlates of the neuronal loss seen in the superficial layers of the cortex and the previously published loss of motor neurons in the spinal cord (Allen et al., 2002).

GFAP is a marker of reactive astrocytes. In the pathological context it is up-regulated in cells where it was not previously expressed during health, hence, it remains to be seen whether this age-related increase in GFAP is the result of astrocyte proliferation or increased GFAP expression associated with phenotype switching. Recent findings from our group demonstrated that pan-astrocyte marker aldehyde dehydrogenase 1 family, member L1 (Aldh1l1) expression in the P301S spinal cord at 20 weeks was not altered at the mRNA or protein level compared with age-matched controls thus indicating that the increased GFAP signal in P301S mice is due to a switch in phenotype rather than proliferation of astrocytes (Hasel et al., 2017).

The increasing presence of GFAP-positive astrocytes indicates that they are indeed reacting to some pathological stimulus, however further characterisation is required to determine the nature of that reaction and therefore the role of astrocytes in the progression of the disease. There is evidence to suggest that reactive astrocytes may adopt different profiles similar to the observed spectrum of activated microglia and thus may be neuroprotective or deleterious (Zamanian et al., 2012).

Proteomic analyses of the spinal cord of the PS19 mouse model expressing P301S tau identified upregulation of astrocyte proteins believed to have neuroprotective effects in tauopathies, including heat shock protein Hsp27 (Yata et al., 2011). However, recently published work identified a host of astrocyte genes which are affected by the P301S mutation and indicate loss of normal function of astrocytes (Hasel et al., 2017). First, several astrocyte genes were identified as neuronally-regulated; they were upregulated when astrocytes were co-cultured with healthy neurons and *in vivo*. The expression of these astrocytic genes was then investigated in the spinal cord of P301S mice at 20 weeks of age and there was a significant decrease in expression of genes involved in glutamate and GABA transport and metabolism compared with age matched control mice. Hence these data indicate impaired neurotransmitter uptake and metabolism in astrocytes of the P301S mice at 20 weeks of age.

Previously published work from our lab indicated a neuroprotective effect of astrocyte transplant into P301S mice; although the mechanism of this neuroprotection was not determined there was a notable increase in neurotrophic factors following transplantation (Hampton et al., 2010).

In depth characterisation of the expression profile of astrocytes at different stages in disease progression might reflect a neuroprotective role or a proinflammatory pro-neurodegenerative role of astrocytes. There is important evidence that the expression profile and therefore function of reactive astrocytes is subject to changes in the environment. Reactive astrocytes may be either proinflammatory "A1" astrocytes, with increased expression of proteins involved in the antigen presentation pathway, complement pathway initiation, and cytokine and chemokine production, or they may be neuroprotective A2 astrocytes, a phenotype associate with increased production of neurotrophic factors (Zamanian et al., 2012). Importantly there is evidence that A1 astrocytes may be induced by microglia (Liddelow et al., 2017). Since the disease pathology in P301S mice is progressive and there are regional differences in microglial activation, there are likely to be important regional and temporal differences in astrocyte profile in P301S mice.

In conclusion, here I provided novel evidence for a progressive increase in GFAP-positive reactive astrocytes as a result of neuron-specific mutant tau transgene expression.

3.4.2.3 **Microgliosis**

Ionized calcium binding adaptor molecule 1 (IBA1) is a microglia/macrophage-specific calcium-binding protein whose expression increases with activation (Ito et al., 1998). Using this marker, I found evidence of progressive disease-associated microgliosis in the spinal cord of P301S mice. However, despite the progressive accumulation of phosphorylated tau protein, neuronal loss and astrogliosis observed in the superficial layers of the cortex, the data presented here demonstrated an *absence* of detectable microgliosis in the cortex of P301S mice. There was no change in the number of IBA1 positive microglia in the cortex at any time point analysed and cortical microglia maintained a ramified morphology throughout, contrary to the morphological changes seen in the spinal cord.

This is in line with work from human post mortem studies and animal models of tauopathy where the spatiotemporal correlation between microglial burden and pathological tau burden has been repeatedly observed and so too has the apparent lack of microglial activation in areas with only mild tau pathology (Kida et al., 1992, Paulus et al., 1993, Sheng et al., 1997, Ishizawa et al., 2001, Ikeda et al., 2005, Sasaki et al., 2008). A study of transgenic rats expressing pathological truncated tau commented "*Here we showed that activated microglia occurred in the same regions as AT8 immunoreactive tangles… but were conspicuously absent in areas with limited neurofibrillary degeneration such as thalamus, hypothalamus, striatum or cortex*" (Zilka et al., 2009).

The directionality of the association between tau pathology and microglial activation is unclear; the regional differences in microglial activation might be caused by the relatively mild pathological tau burden in cortex compared with the more severe tau

pathology in the spinal cord of P301S mice or conversely the tau pathology might depend on microglial activation.

In AD, following the death of tangle bearing neurons, NFTs remain in the extracellular space as "ghost tangles" (Spillantini et al., 2013) – which are capable of activating microglia (Morales et al., 2013), whereas in CBD, Pick's disease, PSP and other mutant tauopathies filamentous tau does not accumulate in the extracellular space (Spillantini et al., 2013). The intracellular deposition of tau is likely to curb the levels of microgliosis compared with neurodegenerative diseases associated with extracellular protein deposition. It is unclear at this stage what aspect of tau pathology triggers microglial activation, however, tau pathology as determined by tau phosphorylation and conformation-dependent staining is more extreme in the spinal cord of P301S mice compared with controls. There is AT8-positive tau pathology in the cortex of P301S mice but there is only very weak staining for NFTs in the cortex; AT8 binds tau protein phosphorylated at Ser 202 and Thr 205 which is a relatively early event, whereas NFT formation occurs later in pathology hence the cortical pathology is relatively mild (Allen et al., 2002, Hoffmann et al., 2013).

Interestingly, while there are regional differences in *pathological* tau between brain and spinal cord, at end stage total human mutant tau expression is 2-fold that of endogenous wild-type tau in the brain and the spinal cord of P301S mice (Allen et al., 2002). This indicates that differences in tau pathology between brain and spinal cord might result from different regional responses to tau expression rather than promoter-driven regional differences in mutant tau expression.

One explanation for the absence of microgliosis in the brain might be the regional heterogeneity in the immune-vigilance status of different microglial populations (Lawson et al., 1990, de Haas et al., 2008, Grabert et al., 2016). Genome-wide analysis of microglia from discrete mouse brain regions shows that microglia have distinct region-dependent transcriptional identities (Grabert et al., 2016). Microglia in the cortex are more stringently regulated than those in the cerebellum, which are, by

comparison, immune-vigilant. Genes involved in energy production (mitochondrial biogenesis, glycolysis, TCA cycle, electron transport chain and ATP synthesis) and genes encoding the cell surface sensing receptors with immunoreceptor tyrosine-based activation motifs (ITAMs) were more highly expressed in cerebellar microglia, whereas ITIM-containing inhibitory members were enriched in microglia of the cortex and striatum (Grabert et al., 2016). Fractalkine receptor (CX3CR1) was enriched in the cortex (Grabert et al., 2016). Fractalkine signalling reduces microglia reactivity to toxic stimuli, maintaining microglia in a modulated state; signalling reduces IL-1β levels and therefore minimises downstream damaging effects; modulates neuronal survival by increasing neurotrophic output; and influences phagocytic capacity (Limatola et al., 2014).

Studies in hTau mice indicated only very mild microgliosis in the dentate gyrus despite the accumulation of tau pathology (Bhaskar et al., 2010). hTau-*Cx3cr1*$^{-/-}$ mice were generated and immunohistochemistry for microglial markers IBA1, CD68, CD11b, CD45 and iNOS demonstrated increased microgliosis in hTau-*Cx3cr1*$^{-/-}$ mice compared with hTau mice or *Cx3cr1*$^{-/-}$ mice (Bhaskar et al., 2010).

Triggering receptor expressed on myeloid cells 2 (TREM2) was also enriched in the cortex (Grabert et al., 2016); which is a cell surface receptor of the immunoglobulin superfamily, involved in phagocytosis and downregulation of pro-inflammatory cytokines. Hence it is plausible that the pathological differences between brain and spinal tissue result from differences in regional immune regulation.

Here I demonstrated age-related increase in abundance of IBA1 positive cells in the spinal cord. The progressive increase in IBA1-positive cells seemed to begin at the earliest time points measured, but within time-point comparisons indicated that cell counts became significantly different compared with controls at 10 weeks of age.

IBA1 is a generic microglial marker and stains resting and activated microglia regardless of phenotype, giving no indication of their activation status other than by

morphological changes. The progressive increase in microglial counts was also associated with altered microglial morphology; shortening and thickening of microglial processes and enlarged soma typical of microglial activation. Un-published work from our lab also indicated a progressive increase in CD68-positive microglia in the brainstem, and absence of CD68 staining in the cortex – CD68 is a marker of phagocytic microglia. Microglia have previously been shown to phagocytose pathological tau aggregates *in vitro* and *in vivo* in the PS19 mouse which also expresses P301S tau and by phagocytosis and exocytosis microglia are thought to be involved in the propagation of tau pathology (Asai et al., 2015).

Microglial transcriptome profiling of animal models of aging and APP/PS1 and SOD1 models of neurodegeneration identified several genes which are thought to be part of a consistent transcriptional profile of primed microglia, including Axl, Clec7a, CD11b, CD11c, Cybb and Cfs1 (Chiu et al., 2013, Holtman et al., 2015) – discussed in Introduction section 1.2.9. The same microglial priming associated genes were also shown to be elevated in rTg4510 mice overexpressing human mutant P301L tau under an inducible regional promoter although there was no detailed summary of expression levels in the rTg4510 mice.

It will be interesting to investigate further the microglial expression profile in P301S mice in order to determine whether they demonstrate this signature primed microglia transcriptional profile. It would also be interesting to compare and contrast between brain and spinal cord tissue since there is an apparent difference in microglial activation.

It seems unlikely that phospho-tau, insoluble tau or even NFTs would be able to directly activate microglia since they are intracellular however microglia are known to interact with synapses; synaptic loss and axonal degeneration caused by loss of tau function might impact microglial-synaptic connections and thus might provide a stimulus for microglial activation. Indeed, synaptic loss and microglial activation were both early events in the pathology of PS19 mice (Yoshiyama et al., 2007).

Alternatively, Bellucci et al. (2004) showed that at end stage the microglia in the brain stem and spinal cord of P301S mice are clustered around IL-1β and COX-2 positive neurons containing pathological tau. There might be other tau pathology-induced neuronally-expressed microglial activating signals. Interestingly there were COX-2, but not IL-1β, positive neurons in the cortex of P301S mice, which might also contribute to differences in microglial activation. The presence of IL-1β and COX-2 stained neurons has however only been demonstrated at end stage and might be the result of neuroinflammatory changes rather than an early trigger of microgliosis.

In a later study the same author examined human post-mortem tissue from a patient with P301S tau mutation and found CD68 and MHCII positive cells of amoeboid morphology and also bushy morphology. As seen in P301S mice there was co-localisation of IL-1β and COX-2 with AT8-positive hyperphosphorylated tau. There were also COX-2 positive microglia (Bellucci et al., 2011). Together these results indicate a proinflammatory microgliosis in the brainstem and spinal cord of P301S mice with a phagocytic profile, certainly at end stage.

It is apparent that some aspect of tau pathology, directly or indirectly, causes microglial activation, and it has also been demonstrated that microglial activation drives tau pathology via proinflammatory cytokine signalling which activates intracellular kinases such as CDK5, GSK-3β and p38-MAPK (Li et al., 2003, Kitazawa et al., 2005, Bhaskar et al., 2010, Sy et al., 2011, Maphis et al., 2015b) hence tau pathology and microglial activation could be in a self-exacerbating loop.

Yoshiyama et al. (2007) demonstrated early microgliosis in PS19 mice, which preceded tangle formation and neuronal loss (details of PS19 mice discussed in Section 1.1.5 and summarised in Table 2). Unfortunately, the temporal profile of the aggregation of different types of tau pathology (oligomers, NFTs) and neuronal loss in the spinal cord of P301S mice remains to be determined.

The fact that tau pathology appears to start in the spinal cord and work its way up towards the brain and that the spinal cord phenotype limits the lifespan of mice has often been considered a limitation of this and other models of tau pathology when attempting to model cortical and hippocampal degeneration and associated cognitive changes. This spinal degenerative phenotype has previously been attributed to the Thy 1.2 driven expression of tau protein leading to the development of new inducible models. This has resulted in mouse models with controlled expression of tau under cell- and region-specific inducible promoters (See Table 2 and Section 1.1.5 for details).

However, the regional differences in the severity of pathology in these mouse models ought not to be set aside as artefacts of promoter driven expression; firstly, there is an equivalent 2-fold human mutant tau expression compared with endogenous mouse tau in the brain and spinal cord; secondly, there are regional differences in the immune-regulation of microglia such that microglia in the cortex tend to exist in a more stringently regulated state and it is known that microglia are capable of driving tau pathology; third, there are differences in the vulnerability of neuronal subpopulations to tau pathology.

In future, as well as investigating how microglia in the brain and spinal cord might be contributing to disease pathology in the brain compared with the spinal cord, it will be informative to investigate regulators of microglial activation such as microglial CX3CR1 and CD200R and corresponding ligands CX3CL1 and CD200, in order to ascertain how the micro-environment is influencing microglial activation.

3.5 Conclusions

Data presented here show that over-expression of human mutant P301S tau is sufficient to cause age-related neuronal loss, astrogliosis and microgliosis. Importantly there are regional differences in these pathologies which might reflect

variations in regional immune-vigilance, cell specific vulnerabilities, or might be attributable to thy 1.2 driven P301S tau expression.

The data presented here indicate that microgliosis is not necessary to drive neurodegeneration, at least in the cortex, and that tau pathology associated cortical neuronal loss occurs via a mechanism which does not robustly stimulate microglia. A reliable behavioural task has been identified, which can be used to reproducibly and non-invasively monitor disease progression. This is a valid model for studies relevant to understanding how systemic inflammation influences key markers associated with neurodegeneration.

4 Chapter 4 – The Phenotypic Effects of Systemic Inflammation in the P301S Tau Model of Tauopathy

4.1 Introduction

Systemic inflammation is a common comorbidity with age-related neurodegeneration and it is proposed to be a driver of chronic neurodegeneration (Perry et al., 2007). During infection, the systemic inflammatory status is communicated to the brain via neural routes and via inflammatory mediators, such as cytokines, in the circulation (Dantzer, 2009). When these signals reach the brain, they coordinate the conserved "sickness behaviours", characterised by fever, malaise, fatigue, depressed locomotor activity, decreased exploration and social activity, anorexia, increased threshold to thirst, and cessation of grooming (Hart, 1988, Dantzer, 2001).

It has been proposed that in the context of dementia the same systemic inflammation might interact with the ongoing neuroinflammation resulting in both acute and long term detrimental consequences (Cunningham et al., 2009). A systemic infection in a person with dementia can be sufficient to induce delirium, an acute neuropsychiatric condition which in some cases is thought to be the clinical manifestation of an exaggerated, aberrant sickness response (Cunningham et al., 2013). Delirium and systemic inflammatory illness are associated with increased risk of dementia, and can exacerbate or accelerate pre-existing dementia (Rockwood et al., 1999, Engelhart et al., 2004, Yaffe et al., 2004, Perry et al., 2007, Tobinick, 2008, Fong et al., 2009).

Several *in vivo* studies have used lipopolysaccharide (LPS), a chemical moiety found on the surface of gram-negative bacteria, to mimic a systemic infection. Studies modelling systemic inflammation superimposed onto rodent models of aging or neurodegeneration have successfully demonstrated exaggerated sickness behaviours and have been able to replicate advanced neurodegenerative decline (Chen et al., 2008, Cunningham et al., 2009). Recent experiments in rodent models of

neurodegeneration indicate that the degree of underlying disease pathology at the time of systemic inflammation influences the severity of the acute deficits induced by the same inflammatory insult (Davis et al., 2015).

Until now, studies of systemic inflammation and neurodegeneration have predominantly focussed on animal models with extracellular protein deposits and prominent microglial activation. There have been relatively few studies investigating the impact of systemic inflammation on animal models of pure tauopathy dementia (discussed in introduction section 1.2.11 (Kitazawa et al., 2005, Bhaskar et al., 2010, Sy et al., 2011)) and none investigating acute sickness behaviour in a pure tau model. It remains unclear whether tau pathology in the absence of amyloid-β is sufficient to induce microglial priming with subsequent increase in cytokine production following inflammatory insult and associated exaggerated sickness response.

Thus, this study aimed to use non-invasive phenotypic and behavioural measures to investigate the interaction between systemic inflammation and disease in a pure tau mouse model of neurodegeneration.

To test the prediction that P301S mice will show an exaggerated sickness response P301S mice and C57BL/6 control mice were injected intraperitoneally with 500 μg/kg of LPS or saline and the acute response was monitored. Mice were injected at either 10 or 16 weeks of age in order to determine whether the degree of underlying pathology at the time of injection influenced the severity of the sickness response. The previous chapter described the disease-associated trajectory of P301S mice compared with control mice, in terms of both behaviour and pathology, and identified the horizontal bar task as a suitable tool to follow the trajectory of the disease. In this chapter mice completed the horizontal bar task weekly until they were sacrificed at end stage in order to determine whether a superimposed single acute systemic inflammatory challenge influenced the trajectory of the decline associated with neurodegeneration.

The hypotheses being tested in these experiments are:

- *There will be an exaggerated acute behavioural response to systemic inflammation in P301S mice compared with controls.*
- *The degree of underlying pathology at the time of injection will determine the magnitude of this acute response to systemic inflammation; specifically, there will be an exaggerated acute response in mice injected at 16 weeks of age compared with mice injected at 10 weeks of age*
- *The systemic inflammation will influence the chronic end stage trajectory of the disease. This might be impacted by the age at the time of injection – 10 or 16 weeks of age.*

4.2 Methods

4.2.1 Experimental design

In order to determine the impact of systemic inflammation on P301S mice, intraperitoneal injection of LPS was used to mimic a bacterial infection (details below).

To our knowledge, this is the first study involving LPS-injection into P301S mice and hence cohort 1, injected at 10 weeks of age, was used as a pilot study to inform future experimental designs. This pilot study generated new information regarding the severity and duration of the sickness response in P301S mice and controls, and thus informed the timing and the type of behavioural experiments used in future studies. In the pilot study, only horizontal bar performance was assessed. However, in all follow up experiments, in addition to horizontal bar performance, during the acute phase mice were weighed, their temperature recorded, their open field activity assessed and an acute sickness score was completed as per the schematics in **Figure 10** and **Figure 13**.

Based on behavioural data from Chapter 3, mice were group housed in cages of equal size where possible. Animals were caged according to the four treatment groups:

C57BL/6 injected with saline; C57BL/6 injected with LPS; P301S injected with saline; and P301S injected with LPS (numbers in Table 13). Experimental cages were placed on a separate cage rack in the home cage room and I exclusively cared for these mice myself. Their food, bedding and water was changed weekly after behavioural testing to minimise the impact of disturbances affecting behavioural results.

	C57BL/6 + Saline	**C57BL/6 + LPS**	**P301S + Saline**	**P301S + LPS**
Mice Injected at 10 weeks				
Cohort 1	4	4	4	4
Cohort 2	5	5	5	5
Cohort 3	5	5	3	4
Mice Injected at 16 weeks				
Cohort 4	8 (2 cages of 4)	8 (2 cages of 4)	8 (2 cages of 4)	8 (2 cages of 4)

Table 13- Behavioural cohorts used in chapter 4

4.2.2 LPS Intraperitoneal Injection

Lipopolysaccharide (LPS; from *Salmonella enterica* serotype abortus equi, Sigma L5886, Poole, UK) was dissolved in 0.9% $NaCl_2$ solution to yield a 1mg/ml LPS stock solution which was aliquoted and frozen. On the day of injection stock solution was diluted further in 0.9% $NaCl_2$ to yield a final concentration of 0.05mg/ml. Mice were scruffed and injected intraperitoneally with 500 μg LPS per kg animal's weight or an equivalent volume of saline solution and were then returned to their cage. The chosen dose 500 μg/kg body weight is sufficient to elicit a significant sickness response without inducing sepsis in alternative animal models (Cunningham et al., 2005), however it remained to be seen how this response would manifest in P301S mice. They were monitored for signs of acute sickness.

4.2.3 Acute Sickness Score

While monitoring the acute sickness response of cohort 1 observations were recorded which included: hunched posture, piloerection, decreased responsiveness, and the

presence of a film of white ocular discharge. The time of onset for each of these criteria was recorded for cohort 2 and the severity scored, which enabled generation of a new chronological scoring system (Table 14). This Acute Sickness Scoring System was then applied to all future cohorts. Mice were scored at -1, 2, 4, 6, 12, 24 and 36 hours relative to i.p. injection.

Score	Appearance
0	Normal for a mouse of that phenotype
1	Slightly hunched posture when undisturbed. Slow to respond.
2	Hunched posture. Slow to Respond. Piloerection. Possible mild ocular discharge
3	Hunched posture. Slow to Respond. Piloerection. Film of white ocular discharge has developed around the eyes.
4	Hunched posture. Unresponsive – can touch the mouse with very minimal reaction; barely tries to move. Piloerection. Thick coating of ocular discharge. Diarrhoea.

Table 14 – Acute Sickness Score

4.2.3.1 **Statistics**

The score was plotted and the area under the curve (AUC) was calculated for individual mice and mixed effects linear regression of AUC data was used to compare the impact of LPS on P301S mice and controls at all time-points assessed.

4.2.4 Open field Activity - as a measure of acute sickness

4.2.4.1 Apparatus

Apparatus consisted of a purpose-built, circular, white acrylic open field chamber measuring 1 m in diameter, with walls 30 cm high. A digital camera was suspended above the open field chamber and was linked to Actimetrics Limelight 3 tracking software on a laptop.

4.2.4.2 Protocol

Mice were placed in the centre of the chamber, always facing the same direction and were allowed to explore for 3 minutes. Their activity was recorded via the digital camera using Actimetrics Limelight 3 tracking software, which traced the movement of mice and recorded their distance travelled. Mice were returned to their home cage after 3 minutes and the open field chamber was cleaned with ethanol and dried. Mice were tested 24-hours prior to injection and then 4-hours, and 24-hours post-injection in order to capture the acute response. The distance travelled was recorded for each mouse.

4.2.4.3 Statistics

The average distance travelled by saline-injected groups was determined. The distance travelled by individual LPS-injected mice was then expressed as a percentage of the average distance travelled by saline-injected counterparts and average was calculated for each group as shown below.

$$= \left(\sum \left(\frac{Dist.Travelled}{Average\ Dist.Travelled\ by\ Saline\ Counterpart} \right) x\ 100 \right) /n$$

The "percentage open field activity" data was used in statistical analysis. Mixed effects linear regression with random intercept for ID was used to compare within-time-point data.

4.2.5 Weight

Mice were weighed using a Sartorius Entris 8201i-1S Toploader Balance. Mice were weighed 24-hours, 12-hours and 1-hour prior to injection and 2, 4, 6, 12, 24 and 36-hours post-injection.

4.2.5.1 Statistics

The average pre-injection baseline weight for each mouse was determined by averaging the 3 recordings prior to injection. For every time point post-injection the weight (g) of each mouse was converted to a percentage of its own baseline weight. These "percentage of baseline weight" data were used in statistical analysis. Mixed effects linear regression with random intercept for ID was used to compare groups.

4.2.6 Body Temperature

Unfortunately, use of a rectal temperature probe or biometric chip was not stipulated in our project licence and hence temperature recordings were taken using a GM300 Digital Infrared IR Thermometer Temperature Laser Point Gun. Mice were scruffed and the temperature probe held at a consistent angle relative to the direction of the fur and at a consistent distance from the mouse. The mammary glands were used as a landmark to ensure recordings were taken from the same area each time. The average of three measurements was recorded. Temperature fluctuates throughout the course of the day, hence in order to see the effect of LPS the temperature for LPS-injected mice is expressed as a percentage of that of saline-injected counterparts. Temperature recordings were taken 24-hours prior to injection and then 4, 6 and 12-hours post-injection (in mice injected at 16-weeks temperature was recorded at 24-hours post-injection and not 12-hours post-injection).

4.2.6.1 Statistics

The temperature data were used to calculate the AUC for individual mice and mixed effects linear regression with random intercept for ID was used to compare groups.

4.2.7 Horizontal Bar Task

The horizontal bar task was conducted as described in section 2.2.3. Mice were trained from 6 weeks of age and their activity on the horizontal bar recorded from 8 weeks of age onwards in order to establish a steady baseline prior to injection.

On the week of LPS injection (10 or 16 weeks of age) mice were assessed 24-hours and 1-hour prior to injection and again 6-hours and 24-hours post-injection in order to capture the acute response to injection. Mice injected at 16 weeks of age had not all recovered by 24-hours post-injection hence horizontal bar performance was also assessed 36-hours post-injection.

As well as piecewise linear regression to compare the trajectory of decline in the stable and chronic phases additional statistical tests were required to probe the acute phase: mixed effects linear regression with random intercept for ID was used for within time point comparisons of the four groups 24-hours prior to injection and 6-hours, 24-hours and where required 36-hours post-injection.

4.3 Results

4.3.1 Early systemic inflammation

P301S and C57BL/6 mice were injected with LPS or saline solution at 10 weeks of age when there is mild cortical astrogliosis but cortical neuronal loss has not yet become apparent, importantly there is significant astrogliosis and microgliosis in lamina 9 of the spinal cord hence at 10 weeks of age subtle disease pathology has begun but mice are not symptomatic and they are on the precipice of neurodegeneration (see Chapter 3). Mice were closely monitored around the time of injection; locomotor activity in

the open field was assessed, observations were recorded enabling generation of an Acute Sickness Score, and weight and temperature were recorded during the hours and days around the time of injection as per the schematic in **Figure 10**. Horizontal bar performance was assessed weekly across the lifespan and multiple times during the acute sickness.

P301S mice showed an exaggerated sickness response to LPS compared with C57BL/6 mice; this was apparent by observation but was also reflected by the data from behavioural tasks, as follows.

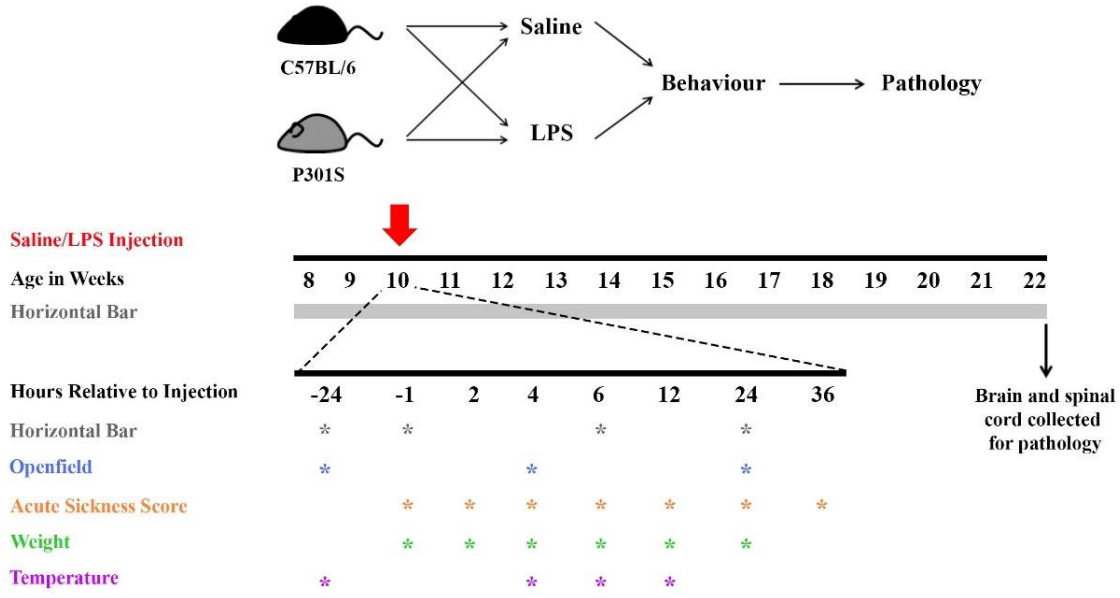

Figure 10 – Early systemic inflammation - Experimental design schematic. *C57BL/6 and P301S mice were tested on the horizontal bar weekly. They were injected with either Saline or LPS at 10 weeks of age and during the acute phase were tested on the horizontal bar and distance travelled in open-field, Acute Sickness Score, weight and temperature recorded at time points indicated.*

4.3.1.1 Exaggerated Acute Sickness Response in P301S mice

4.3.1.1.1 Prolonged reduction in locomotion in LPS treated P301S mice

The open field task is a simple task that records the innate exploratory behaviour of rodents with no need for training. Mice often display decreased locomotion during acute sickness (Bolivar, 2009). Mice were placed in the open field arena and their movement recorded 24-hours prior to injection, and then 4, 24 and 36-hours post-injection (**Figure 10**).

P301S mice are known to travel further than C57BL/6 mice in the open field (Scattoni et al., 2010) and when mice are repeatedly retested in an open field arena there is habituation – mice travel less as they become accustomed to the environment – this is true of even non-injected control mice. Therefore, to determine the influence of LPS on mice, without the variation due to genotype or re-testing, the distance travelled (cm) by LPS-injected mice was expressed as a percentage of within-genotype within-time-point saline-injected activity.

As expected 24-hours prior to injection there was no difference between saline and LPS treatment groups (C57BL/6 + LPS vs C57BL/6 + Saline: +19.6%; p=0.180; 95% CI -9.51 to 48.6; and P301S + LPS vs P301S + Saline: -7.4%; p=0.652; 95% CI -41.5 to 26.8) (Figure 11 A).

4-hours post-LPS-injection there was a 54.9% reduction in the distance covered by C57BL/6 mice compared with saline-injected counterparts (p=0.001; 95% CI -85.1 to -24.8). LPS-injected P301S mice travelled 88.0% less than their saline-injected counterparts (p<0.001; 95% CI -121.3 to -54.8). When formally tested the differential effect of LPS on P301S mice was not significant (-33.1%; p=0.139; 95% CI -77.7 to 11.4) (Figure 11 A).

By 24-hours post-LPS-injection C57BL/6 mice had recovered relative to saline-injected counterparts (-10.6%; p=0.534; 95% CI; -44.8 to 23.6). LPS-injected P301S mice, however, had still not yet recovered to the same activity as saline-injected

counterparts (-51.0; p=0.039; 95% CI -99.0 to -3.0) (Figure 11). When formally tested, the differential effect of LPS on P301S mice was not significant (-40.4%; p=0.113; 95% CI -90.9 to 10.1).

By 36-hours post-injection both LPS-injected groups had recovered compared to their saline-injected counterparts (C57BL/6 + LPS vs C57BL/6 + Saline: -20.6%; p=0.444; 95% CI -74.8 to 33.6; P301S + LPS vs P301S + Saline: -27.6%; p=0.374; 95% CI -91.4 to 36.2) (Figure 11 A).

Hence the open field task highlighted a potentially longer-lasting LPS-induced hypoactive sickness response in P301S mice compared with LPS-injected C57BL/6 mice.

4.3.1.1.2 Elevated Acute Sickness Score in P301S mice following LPS injection

LPS-injected mice were visibly unwell. Observations were recorded in chronological order and from this developed an Acute Sickness Score described in Table 14. Similar scoring techniques are used in the pharmaceutical industry to assess sickness in animal models (Irwin, 1968).

P301S and C57BL/6 mice that received a saline injection appeared "normal for their phenotype" and scored 0 throughout the experiment (Figure 11 B).

LPS-injected C57BL/6 mice were still phenotypically normal 2-hours post-injection but at 4-hours post-injection some had become hunched and slower to respond, scoring 1 on the acute sickness scale. This persisted until 12-hours post-injection but all C57BL/6 mice had recovered to normal activity by 24-hours post-injection (Figure 11 B).

LPS-injected P301S mice were phenotypically normal 2-hours post-injection but by 4-hours post-injection all the P301S mice scored 1 on the Acute Sickness Scale. By 6-hours P301S mice were hunched up and very slow to respond, their coats were unkempt and showing signs of piloerection and they showed signs of ocular

discharge. At 12-hours the inflammatory response had progressed to a thick coating of discharge around the eyes and in some cases mice showed signs of diarrhoea. 24-hours post-injection P301S mice were still slow to respond but by 36-hours post-injection P301S mice had fully recovered and appeared normal for their phenotype (Figure 11 B).

The area under the curve data indicated that LPS-injected P301S mice had a significantly more severe response than C57BL/6 mice overall (C57BL/6 + LPS: 1.9; p=0.006; 95% CI 0.6 to 3.2; P301S + LPS: 6.9; p<0.001; 95% CI 5.7 to 8.1). The differential effect of LPS was also greater in P301S mice than C57BL/6 mice when formally tested (differential 5.0; p < 0.001; 95% CI 3.0 to 6.9) (Figure 11 B).

4.3.1.1.3 Equivalent LPS-induced weight loss in P301S and C57BL/6 mice

Mice were weighed 24, 12 and 1-hour(s) prior to intraperitoneal injections (averaged to generate baseline weight) and 2, 4, 6, 12, 24 and 36-hours after injections (**Figure 10**). C57BL/6 mice weigh more than P301S mice hence the weight in grams was converted to weight as a percentage of baseline weight for each mouse.

There was subtle weight loss in saline-injected C57BL/6 (hourly change -0.1%; p=0.008; 95% CI -0.2 to 0.0) and P301S mice over time (additional 0.0%; p=0.876; 95% CI -0.1 to 0.1) (Figure 11 C). LPS induced an additional hourly loss of 0.3% of baseline body weight in C57BL/6 mice (additional -0.3%; p<0.001; 95% CI -0.4 to -0.2) which equates to approximately 10% of total body weight over the 36-hour recorded time-period. LPS induced an hourly loss of 0.2% of baseline body weight in P301S mice compared with saline-injected counterparts (-0.2%; p<0.001; 95% CI -0.3 to -0.1). There was no differential effect of LPS in P301S mice compared with C57BL/6 mice (additional 0.0%; p=0.671; 95% CI -0.1 to 0.2) (Figure 11 C).

4.3.1.1.4 LPS-induced Hypothermia in P301S mice

Temperature recordings were taken 24-hours prior to injection, and then 4, 6 and 12-hours post-injection. While the temperature of C57BL/6 mice appeared relatively

stable across the time-period of the experiment the temperature of P301S mice injected with LPS dipped at 4-hours and remained low at 6-hours before recovering at 24-hours. The area under the curve (AUC) was calculated for individual mice to compare their overall experience of temperature fluctuations during the experiment. Mixed effects linear regression of AUC data indicated that P301S mice were colder than C57BL/6 mice (ΔAUC: -4.4; p=0.008; 95% CI -7.5 to -1.4) (Figure 11 D). LPS did not impact the temperature of C57BL/6 mice (ΔAUC: -1.7; p=0.186; 95% CI -4.3 to 0.9) but LPS did cause a further decrease in temperature in P301S mice compared with saline-injected counterparts (ΔAUC: -4.4; p=0.026; 95% CI -7.9 to -0.8). The differential impact of LPS was not significant (-2.7; p=0.185; 95% CI -6.8 to 1.4) (Figure 11 D).

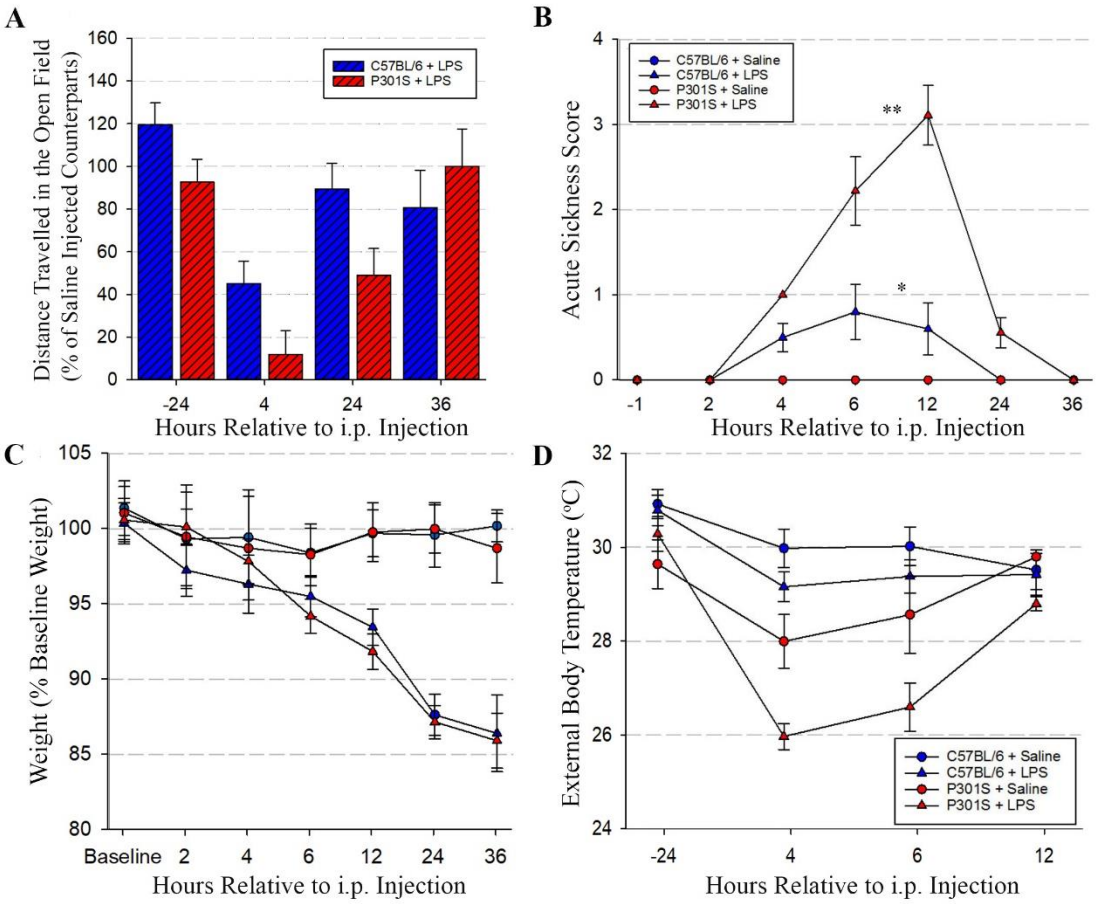

Figure 11 - Exaggerated impact of intraperitoneal LPS-injection in P301S mice compared with control mice. A) *Open field - distance travelled in an open field arena by C57BL/6 (blue) and P301S mice (red) was recorded 24h pre- and 4-, 24- and 36-hours post-injection with either saline or LPS. Distance travelled by LPS-injected mice is expressed as a percentage of distance travelled by saline-injected counterparts. 24h pre-injection groups travelled the same distance as their saline-injected counterparts. 4h post-injection LPS impacted open field activity of C57BL/6 and P301S mice (mixed effects linear regression, indicated by **p<0.001, **p<0.0001). 24-hours post-injection LPS-injected C57BL/6 mice had recovered compared with saline-injected counterparts, LPS injected P301S mice had not (indicated by *p<0.05). 36h post-injection all groups had recovered compared with saline-injected counterparts.* ***B)*** *Acute Sickness Score – the severity of the sickness response of C57BL/6 and P301S mice was scored regularly post-injection with saline or LPS (defined Table 14). The area under the curve (AUC) was calculated for individuals and mixed effects linear regression showed that LPS impacted C57BL/6 and P301S mice (indicated by * p<0.05, ** p<0.0001 respectively).* ***C)*** *Weight loss – P301S and control mice were weighed regularly following injection. LPS induced equivalent weight loss in C57BL/6 and P301S mice over the 24-hours post-injection (mixed effects linear regression). (**A-C:** C57BL/6 + Saline n=10, C57BL/6 + LPS n=10, P301S + Saline n=8, P301S + LPS n=9)* ***D)*** *External temperature – an infrared thermometer laser pointer gun was used to record temperature of C57BL/6 and P301S mice 24-hours pre-injection and 4-, 6- and 12-hours post-injection with either saline or LPS. The area under the curve (AUC) was calculated for individuals and mixed effects linear regression showed that P301S mice were colder overall (p<0.01) and LPS did not impact the temperature of C57BL/6 mice but caused a decrease in temperature in P301S mice compared with saline injected counterparts (p<0.05) (C57BL/6 + Saline n=5, C57BL/6 + LPS n=5, P301S + Saline n=3, P301S + LPS n=4).*

4.3.1.1.5 Exaggerated Acute Horizontal Bar Deficit in P301S mice

Prior to injection there was no initial difference in horizontal bar performance between genotypes or intervention groups and performance was stable throughout this phase of the experiment up to 10 weeks of age (see Figure **12** and Table 15 for details).

	Estimated mean	p (comparison to C57BL/6)	95% Confidence Interval	
Intercept				
Reference baseline score (C57BL/6 + Saline)	9.9	0.000	9.1	10.8
Δ Baseline P301S	-0.2	0.164	-0.6	0.1
Δ Baseline LPS	-0.2	0.138	-0.6	0.1
Δ Baseline P301S + LPS (interaction term)	-0.1	0.749	-0.5	0.4
Weekly rate of change				
Reference weekly change (C57BL/6 + Saline)	0.0	0.522	0.1	0.2
Δ Weekly change P301S	0.0	0.731	-0.1	0.2
Δ Weekly change LPS	0.0	0.863	-0.2	0.1
Δ Weekly change P301S + LPS (interaction term)	0.0	0.795	-0.2	0.2

Table 15 – Baseline horizontal bar score prior to injection (8-10 weeks) The first term represents baseline performance for the C57BL/6 group receiving saline. The following two terms test for an independent effect of genotype and intervention. The fourth term tests for a difference in the independent effect of LPS between genotypes. The last four terms can be interpreted in the same way but show differences in the weekly rate of change in performance.

On the week of injection mice were assessed 24-hours and 1-hour prior to injection and then 6-hours and 24-hours post-injection. Within time-point comparisons demonstrated the following.

24-hours prior to injection: All groups were at peak performance. There were no differences between genotype or LPS groups (See Figure **12** and Table 16 for details).

6-hours post-injection: Saline-injection had no effect on acute horizontal bar performance in P301S mice or controls; 6-hours post saline-injection C57BL/6 mice

could maintain a high score of 10.0 and saline-injected P301S mice were not significantly different (see Figure **12** and Table 16 for details). LPS injection did, however, influence horizontal bar performance; all LPS-injected C57BL/6 mice successfully completed the task but they were slower to complete the task and this was reflected in the score (see Figure **12** and Table 16 for details). Horizontal bar performance of LPS-injected P301S mice was also impaired; four of thirteen LPS-injected P301S mice failed the task at least twice thus LPS-injected P301S mice scored significantly less than saline-injected counterparts (-4.3; $p<0.001$; 95% CI -5.5 to -3.2). P301S mice also had a much more severe acute sickness response compared with LPS-injected C57BL/6 mice and this differential effect was reflected by interaction term (see Figure **12** and Table 16 for details).

24-hours post-injection: LPS-injected C57BL/6 mice had recovered to baseline performance 24-hours after injection (see Figure **12** and *Table 16* for details). LPS-injected P301S mice had almost but not fully recovered by this time compared with saline-injected counterparts (-0.5; $p=0.014$; 95% CI -0.9 to -0.1). The interaction term which formally tests the difference in the independent effect of LPS on C57BL/6 and P301S groups indicated no significant differential effect (see Figure **12** and Table 16 for details).

	24h Pre-injection				6h post-injection				24h post-injection			
	Estimated mean	**p**	**95% CI**		**Estimated mean**	**p**	**95% CI**		**Estimated mean**	**p**	**95% CI**	
Reference Score (C57BL/6 + Saline)	10.0	0.000	9.7	10.2	10.0	0.000	9.3	10.6	10.0	0.000	9.7	10.2
Δ Score P301S	-0.3	0.169	-0.6	0.1	-0.2	0.692	-1.1	0.7	0.0	0.759	-0.4	0.3
Δ Score LPS	-0.2	0.197	-0.6	0.1	**-1.0**	**0.020**	**-1.9**	**-0.2**	-0.1	0.363	-0.4	0.2
Δ Sore P301S + LPS (interaction term)	-0.1	0.839	-0.5	0.4	**-3.3**	**0.000**	**-4.5**	**-2.1**	-0.4	0.097	-0.8	0.1

Table 16 – Horizontal bar performance 24-hours pre-injection, 6-hours and 24-hours post-injection. The first term represents baseline performance for the C57BL/6 group receiving saline. The following two terms test for an independent effect of genotype and LPS treatment. The fourth term tests for a difference in the independent effect of LPS between genotypes

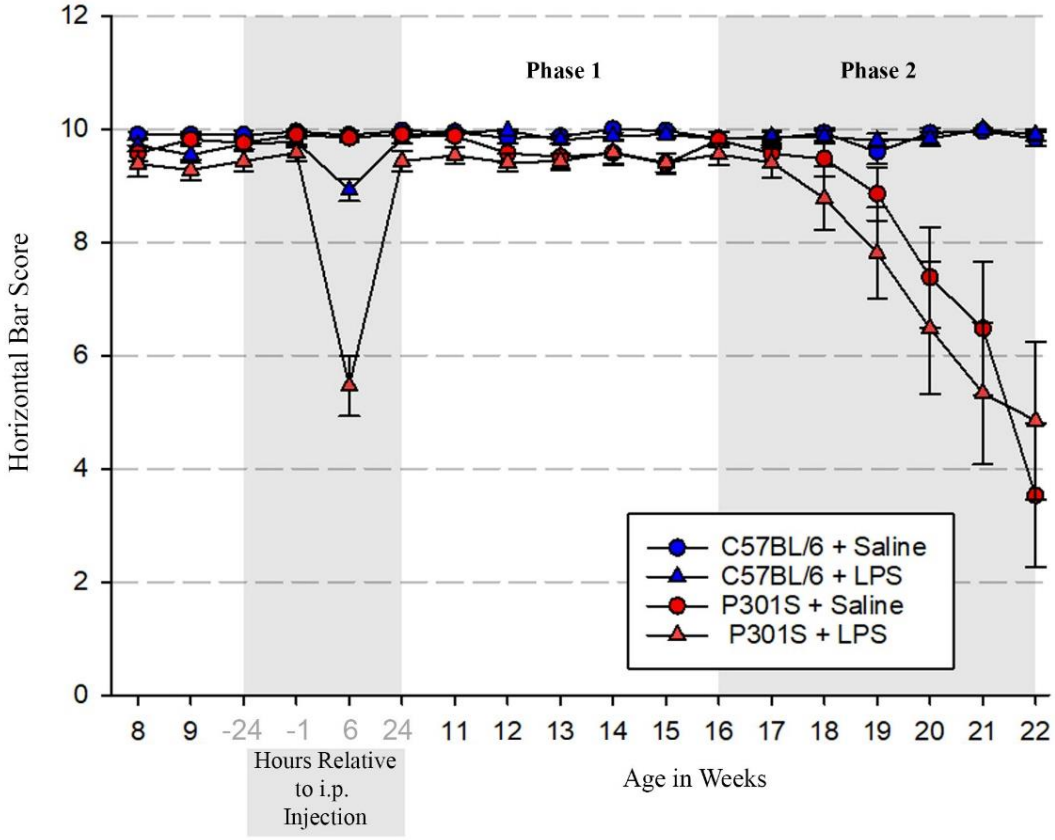

C57 + Saline	13	13	13	13	13	13	13	13	13	13	13	13	13	13	13	13	10	10
C57 + LPS	14	14	14	14	14	14	14	14	14	14	14	14	14	14	14	14	10	10
P301S + Saline	11	11	11	11	11	11	11	11	11	11	11	11	11	11	11	11	7	7
P301S + LPS	13	13	13	13	13	13	13	13	13	13	13	13	13	13	13	13	9	9

Figure 12 - Exaggerated impact of intraperitoneal LPS-injection on horizontal bar performance of P301S mice compared with control mice. *Horizontal bar task - performance of C57BL/6 (blue) and P301S mice (red) was tested weekly before and after intraperitoneal LPS (500 μg/kg) (triangle) or saline (circle) administration. During the acute period mice were tested 24-hours and 1-hour prior to injection and 6- and 24- hours post-injection (indicated by the grey area). 6-hours post-i.p.-injection LPS significantly impacted horizontal bar performance of C57BL/6 and P301S mice (mixed effects linear regression, indicated by *p<0.05, **p<0.0001). The impact of LPS on P301S horizontal bar performance was significantly greater than control mice (p<0.0001). All mice had recovered to baseline by 24h post-injection and continued to perform well until 16 weeks. Piecewise mixed effects linear regression showed that LPS administration at 10 weeks had no lasting effect on the trajectory of decline during the chronic phase (16-22 weeks). For details of n see below image.*

4.3.1.2 **Effect of early systemic inflammation on chronic horizontal bar performance**

All mice had recovered to peak performance following the acute sickness response. C57BL/6 mice maintained that healthy baseline performance throughout the rest of the experiment, regardless of whether they were injected with saline or LPS at week 10 (Figure **12**).

For P301S mice, however, there were two distinct phases: the stable phase (phase 1; 10-16 weeks) and the declining phase (phase 2; 16-20 weeks) (Figure **12**). During the stable phase both P301S groups maintained the steady baseline score (Figure **12** and Table 17). During the declining phase saline-injected P301S mice lost on average 0.8 points per week on the horizontal bar task (Figure **12** and Table 17). Mixed effects linear regression of the whole 16-to-22-week period indicates that LPS-injection at 10 weeks of age did not impact on the rate of decline in horizontal bar performance during the decline phase, however it should be noted that the first cohort of mice was sacrificed at 20 weeks of age and thus there was a loss of statistical power at 21 and 22 weeks of age (for details of n's see Figure **12**).

	Phase 1: Stable phase				Phase 2: Declining phase			
	Estimated mean	p	95% CI		Estimated mean	p	95% CI	
Intercept								
Reference baseline (C57BL/6 + Saline)	9.9	0.000	9.7	10.1	9.8	0.000	9.3	10.4
Δ Baseline P301S	-0.2	0.232	-0.4	0.1	-0.1	0.870	-0.9	0.8
Δ Baseline LPS	0.0	0.816	-0.3	0.2	-0.1	0.834	-0.9	0.8
Δ Baseline P301S + LPS (interaction term)	-0.2	0.231	-0.6	0.1	-0.5	0.409	-1.7	0.7
Weekly rate of change								
Reference weekly change (C57BL/6 + Saline)	0.0	0.780	0.0	0.0	0.0	0.908	-0.1	0.1
Δ Weekly change P301S	0.0	0.091	-0.1	0.0	-0.8	0.000	-1.0	-0.6
Δ Weekly change LPS	0.0	0.730	0.0	0.0	0.0	0.889	-0.2	0.2
Δ Weekly rate of change P301S + LPS (interaction term)	0.0	0.269	0.0	0.1	0.0	0.838	-0.3	0.2

Table 17 – Horizontal bar performance during stable phase and declining phase. The first term represents baseline performance for the C57BL/6 group receiving saline. The following two terms test for an independent effect of genotype and intervention. The fourth term tests for a difference in the independent effect of LPS between genotypes. The last four terms can be interpreted in the same way but show differences in the weekly rate of change in performance.

4.3.2 Late systemic inflammation

As described in the introduction, it is likely that the degree of underlying pathology in the P301S mouse will influence the extent of vulnerability to subsequent inflammatory challenge. This might manifest as heightened or longer lasting acute sickness and/or larger effects on the trajectory of the disease as measured by horizontal bar performance. To investigate this hypothesis further, mice were exposed to the same dose of LPS at 16 weeks of age instead of at 10 weeks and were monitored as per the schematic in **Figure 13**. At 16 weeks of age there is significant neuronal loss and more advanced astrogliosis in the cortex of P301S mice, there is astrogliosis and microgliosis in the spinal cord. They are also on the brink of the decline in motor function detected on the horizontal bar task.

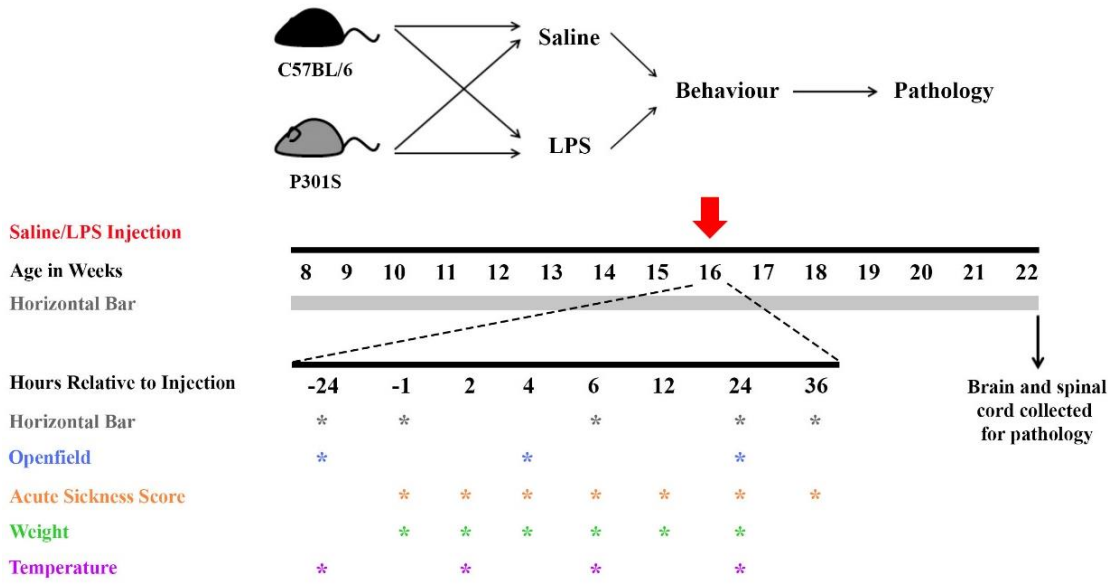

Figure 13 – Late systemic inflammation - experimental design schematic. *C57BL/6 and P301S mice were tested on the horizontal bar weekly. They were injected with either Saline or LPS at 16 weeks of age and during the acute phase were tested on the horizontal bar and distance travelled in open-field, Acute Sickness Score, weight and temperature recorded at time points indicated.*

4.3.2.1 Exaggerated Acute Sickness Response in P301S mice

4.3.2.1.1 Prolonged reduction in locomotion in LPS treated P301S mice

24-hours prior to injection there was no difference within genotypes between LPS and saline groups (C57BL/6 + LPS vs C57BL/6 + Saline: -9.4%; p=0.394; 95% CI -31.7 to 12.9; P301S + LPS vs P301S + Saline: 12.5%; p=0.260; 95% CI -10.4 to 35.4) (Figure 14A).

Again, LPS caused a decrease in activity in both groups of mice. At 4-hours post-injection LPS-injected C57BL/6 mice travelled significantly less than saline-injected counterparts (-72.1%; p<0.001; 95% CI -92.3 to -51.8) (Figure 14A). LPS-injected P301S mice also travelled significantly less than saline-injected counterparts (-75.2%; p<0.001; 95% CI -100.0 to -50.4). There was no differential effect of LPS on P301S mice (-3.1%; p=0.826; 95% CI -32.2 to 25.9) (Figure 14A).

24-hours post-LPS-injection C57BL/6 mice had recovered to normal activity compared with saline-injected counterparts (-0.5%; p=0.983; 95% CI -43.1 to 42.2). Whereas P301S mice had not (-43.9%; p=0.051; 95% CI -88.0 to 0.3) however when formally tested this differential effect of LPS on P301S mice was not significant (-43.4%; p=0.158; 95% CI -104.8 to 18.0) (Figure 14A).

By 36-hours post-LPS-injection both C57BL/6 mice and P301S mice had recovered to similar levels to saline-injected counterparts (C57BL/6 + LPS vs C57BL/6 + Saline: 0.0%; p=1.000; 95% CI -48.2 to 48.2; P301S + LPS vs P301S + Saline: 0.0%; p=1.000; 95% CI -51.4 to 51.4) (Figure 14A).

Comparison of open field data from mice injected at 10 weeks of age with mice injected at 16 weeks of age indicated that the LPS-induced decrease in locomotor activity 4-hours post-injection was not affected by the age of injection (16 week C57BL/6 + LPS vs 10 week C57BL/6 + LPS: -17.1%; p=0.363; 95% CI -54.6 to 20.3; 16 week P301S + LPS vs 10 week P301S + LPS: 12.8%; p=0.522; 95% CI -27.8 to 53.5) (Figure 11A and Figure 14A). This, and all future comparisons come with the caveat

that animals injected at 10 weeks and 16 weeks of age were not treated with LPS at the same time and so comparisons are across different experiments on different days.

The delayed recovery from LPS-injection measured 24-hours post-injection was also equivalent in mice injected at 16 weeks of age compared with mice injected at 10 weeks of age (16 week C57BL/6 + LPS vs 10 week C57BL/6 + LPS: 10.1%; p=0.704; 95% CI -42.8 to 63.0; 16 week P301S + LPS vs 10 week P301S + LPS: 7.1%; p=0.819; 95% CI -55.8 to 70.1) (Figure 11A and Figure 14A).

4.3.2.1.2 Elevated Acute Sickness Score in P301S mice following LPS injection

Mice were scored according to the Acute Sickness Scale (Table 14). As before saline-injected C57BL/6 and P301S mice were normal throughout the experiment and scored 0 (Figure 14B).

At 4 and 6-hours post-injection C57BL/6 mice injected with LPS were all hunched and slow to respond, scoring 1 on the acute sickness scale; at 12-hours post-injection they showed signs of piloerection and by 24-hours post-injection C57BL/6 mice had fully recovered (Figure 14B).

At 4-hours post-LPS injection P301S mice reacted the same as control mice, however by 6-hours post-injection P301S mice were extremely unwell and 7 of 8 mice scored a 4 – they were hunched and unresponsive when disturbed and showed signs of piloerection, inflammatory eye reaction and diarrhoea. This persisted at 12-hours post-injection. By 24-hours post-LPS-injection P301S mice had improved but still showed signs of an inflammatory response in the eye, piloerection and were slow to respond. By 36-hours post-injection LPS-injected P301S mice had still not fully recovered (Figure 14B).

Mixed effects linear regression comparing area under the curve data indicated that LPS-injected P301S mice had a significantly greater response than LPS-injected C57BL/6 mice (C57BL/6 + LPS: 3.9; p=0.001; 95% CI 1.7 to 6.1; P301S + LPS: 10.5;

p<0.001; 95% CI 7.3 to 13.7). The effect of LPS was also greater in P301S mice than C57BL/6 mice when formally tested (differential 6.6; p < 0.001; 95% CI 3.5 to 9.7).

Comparison of AUC data from mice injected at 16 weeks of age with those injected at 10 weeks of age indicated no differential LPS-induced acute sickness response in C57BL/6 mice (16 week C57BL/6 + LPS vs 10 week C57BL/6 + LPS: 2.0; p=0.106; 95% CI -0.4 to 4.4) but 16 week old P301S mice had a significantly worse experience than those injected at 10 weeks of age (16 week P301S + LPS vs 10 week P301S + LPS: additional 3.6; p=0.029; 95% CI 0.4 to 6.8) (Figure 11B and Figure 14 B).

4.3.2.1.3 Exaggerated LPS-induced weight loss in P301S compared with C57BL/6 mice

Mice were weighed 24, 12 and 1-hour(s) prior to injection (these were averaged to determine baseline weight) and 2, 4, 6, 12, 24 and 36-hours post-injection (Figure 14C). Mixed effects linear regression indicated that saline-injected C57BL/6 mice and P301S mice maintained their body weight over the 36-hour period (C57BL/6 + saline hourly change: -0.1%; p=0.133; 95% CI -0.2 to 0.0; P301S + saline hourly change: 0.1%; p=0.352; 95% CI -01 to 0.2).

LPS-injected C57BL/6 mice lost 0.4% of their baseline body weight every hour (additional hourly change: -0.3%; p<0.001; 95% CI -0.5 to -0.2). LPS-injected P301S mice lost on average 0.6% of their body weight every hour (additional hourly change vs P301S + saline: -0.6; p<0.001; 95% CI -0.8 to -0.4). The differential effect of LPS on P301S mice was significant when formally tested (-0.3; p=0.029; 95% CI -0.05 to 0.0) (Figure 14C).

Comparison of data from mice injected at 16 weeks of age with those injected at 10 weeks of age indicated no difference in the LPS-induced weight loss in C57BL/6 mice (additional hourly change 16 week C57BL/6 + LPS vs 10 week C57BL/6 + LPS: 0.0%; p=0.646; 95% CI -0.3 to 0.2) however there was an additional LPS-induced weight loss in P301S mice injected at 16 weeks compared with those injected at 10 weeks of age

(additional hourly change 16 week P301S + LPS vs 10 week P301S + LPS: -0.3; p=0.018; 95% CI -0.4 to 0.0).

4.3.2.1.4 Failure to detect LPS-induced hypothermia

External body temperature recordings were taken 24 hours prior to injection, as well as 4, 6 and 24-hours post-injection (Figure 14D). Comparison of AUC data for individual mice indicated that P301S mice might be slightly colder than C57BL/6 mice, although this did not reach significance at α= 0.05 (ΔAUC: -5.0; p=0.091; 95% CI -10.8 to 0.8). LPS had no significant impact on C57BL/6 mice (ΔAUC: -4.2; p=0.155; 95% CI -10.0 to 1.7) or on P301S mice (ΔAUC: -4.6; p=0.253; 95% CI -12.9 to 3.7) and there was no differential effect of LPS on P301S mice (ΔAUC: -0.5; p=0.910; 95% CI -8.7 to 7.8) (Figure 14D).

Comparison of temperature AUC data from mice injected at 16 weeks of age with that of mice injected at 10 weeks of age indicated no significant differences in the LPS-induced hypothermic response in control mice (16 week C57BL/6 + LPS vs 10 week C57BL/6 + LPS: -2.5; p=0.529; 95% CI -10.3 to 5.4) or P301S mice (16 week P301S + LPS vs 10 week P301S + LPS: -0.3; p=0.966; 95% CI -13.1 to 12.6).

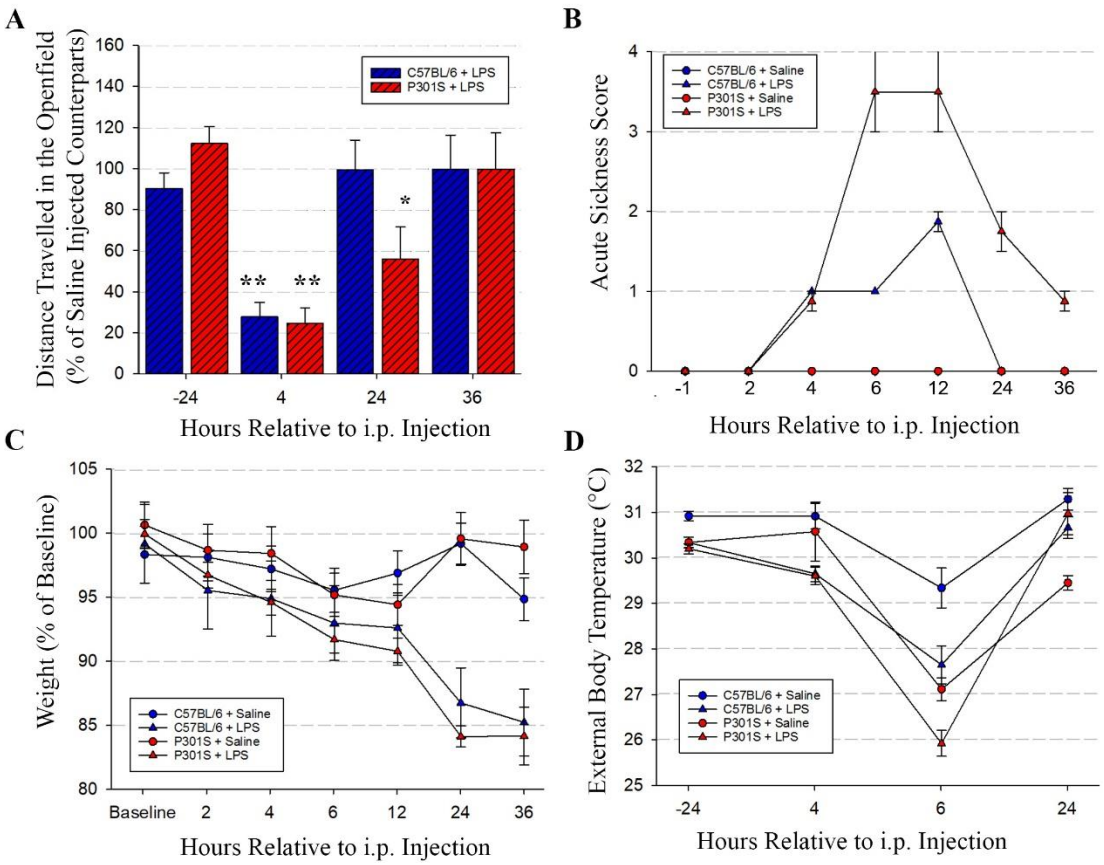

Figure 14 - Exaggerated impact of intraperitoneal LPS injection in P301S mice compared with control mice. A) *Open field - distance travelled in an open field arena by C57BL/6 (blue) and P301S mice (red) was recorded 24h pre-injection and 4- and 24- hours post-injection with either saline or LPS. Distance travelled by LPS-injected mice is expressed as a percentage of distance travelled by saline-injected counterparts. 24h pre-injection groups travelled the same distance as their saline-injected counterparts. 4-hours post-injection LPS impacted open field activity of C57BL/6 and P301S mice (indicated by **p<0.0001). 24h- post-injection LPS-injected C57BL/6 mice had recovered compared with saline-injected counterparts, LPS-injected P301S mice had not (indicated by *p<0.05). By 36h post-injection all groups had recovered compared with saline-injected counterparts.* ***B)*** *Acute Sickness Score – the severity of the sickness response of C57BL/6 and P301S mice was scored regularly post-injection with saline or LPS (defined Table 14). The area under the curve (AUC) was calculated for individuals and mixed effects linear regression showed that LPS had a significant impact on C57BL/6 and P301S mice (indicated by * p≤0.001 and ** p<0.0001 respectively).* ***C)*** *Weight loss – P301S and control mice were weighed regularly following injection. LPS induced weight loss in C57BL/6 and P301S mice over the 24-hours post-injection. LPS had a very slightly, but significantly, greater effect on P301S mice compared with controls (mixed effects linear regression, see results for more details).* ***D)*** *External temperature – an infrared thermometer laser pointer gun was used to record temperature of C57BL/6 and P301S mice 24-hours pre-injection and 4-, 6- and 12- hours post-injection with either saline or LPS. The area under the curve (AUC) was calculated for individuals and mixed effects linear regression showed that LPS had no significant effect on external temperature of C57BL/6 or P301S mice (**A-D:** C57BL/6 + Saline n=8, C57BL/6 + LPS n=8, P301S + Saline n=8, P301S + LPS n=7).*

4.3.2.1.5 Exaggerated Acute Horizontal Bar Deficit in P301S mice

As before all groups could achieve and maintain a steady baseline performance in the weeks prior to i.p. injection (see **Figure 15** and Table 18 for details). There was no impact of genotype or intervention group.

	Estimated mean	p (comparison to C57BL/6)	95% Confidence Interval	
Intercept				
Reference baseline (C57BL/6 + Saline)	9.9	0.000	9.8	10.0
Δ Baseline P301S	-0.1	0.118	-0.3	0.0
Δ Baseline LPS	0.0	0.904	-0.2	0.2
Δ Baseline P301S + LPS (interaction term)	0.1	0.342	-0.1	0.4
Weekly rate of change				
Reference weekly change (C57BL/6 + Saline)	0.0	0.397	0.0	0.0
Δ Weekly change P301S	0.0	0.369	0.0	0.0
Δ Weekly change LPS	0.0	0.842	0.0	0.0
Δ Weekly rate of change P301S + LPS (interaction term)	0.0	0.682	0.0	0.0

Table 18 - Baseline Horizontal bar performance prior to injection (8-10 weeks) The first term represents baseline performance for the C57BL/6 group receiving saline. The following two terms test for an independent effect of genotype and intervention. The fourth term tests for a difference in the independent effect of LPS between genotypes. The last four terms can be interpreted in the same way but show differences in the weekly rate of change in performance.

On the week of injection mice were assessed 24-hours and 1-hour prior to injection and then 6-hours, 24-hours and 36-hours post-injection. Within time-point comparisons demonstrated the following.

24-hours prior to injection: All groups were at peak performance. There were no differences between genotype or LPS groups (**Figure 15** and **Table 19**).

6-hours post-injection: Saline-injection did not influence horizontal bar performance of C57BL/6 or P301S mice at 6-hours post-injection (**Figure 15** and **Table 19**). LPS-

injection at 16 weeks impaired horizontal bar performance of C57BL/6 mice 6-hours post-injection. As before, all the LPS-injected C57BL/6 mice successfully reached the platform but they were slower to do so than saline-injected counterparts and thus they scored significantly less (**Figure 15** and **Table 19**). LPS-injection at 16-weeks had a more severe effect on P301S mice than on C57BL/6 mice. Just one of seven mice completed the task without falling from the bar, five of seven mice fell off twice or more and of the successful attempts, the average time taken to reach the platform was 31.8 seconds. Hence at 6-hours post-LPS-injection P301S mice scored significantly less than saline-injected counterparts (-5.1; $p<0.001$; 95% CI -6.0 to -4.1) and the differential effect of LPS was greater in P301S mice than C57BL/6 mice when formally tested (**Figure 15** and **Table 19**).

24-hours post-injection: LPS-injected C57BL/6 mice had fully recovered compared with saline-injected counterparts by 24-hours post-injection whereas P301S mice had not (**Figure 15** and **Table 19**); three of seven LPS-injected P301S mice fell from the bar at least once. Hence 24-hours post-injection LPS-injected P301S mice scored significantly less than saline-injected counterparts (-3.0; $p=0.018$; 95% CI -5.4 to -0.6). The differential effect of LPS on P301S mice compared to C57BL/6 mice was significant (**Figure 15** and **Table 19**).

36-hours post-injection: All groups had recovered to baseline performance; there were no impacts of genotype or LPS exposure (**Figure 15** and **Table 19**).

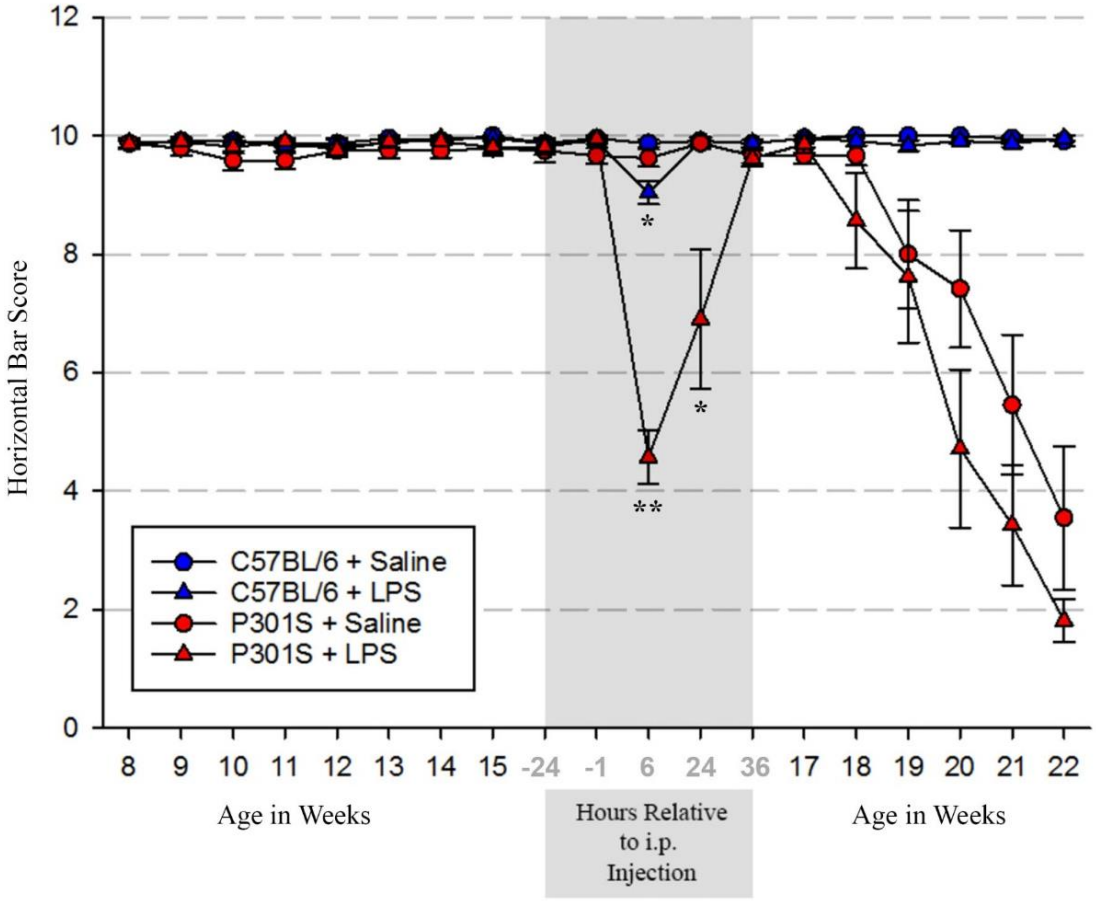

Figure 15 - Exaggerated impact of intraperitoneal LPS-injection on acute horizontal bar performance P301S mice compared with control mice and chronic performance compared with saline-injected group. *Horizontal bar task - performance of C57BL/6 (blue) and P301S mice (red) was tested weekly before and after intraperitoneal LPS (500 µg/kg) (triangle) or saline (circle) administration. During the acute period mice were tested 24 hours and 1 hour prior to injection and 6- 24- and 36- hours post-injection (indicated by the grey area). 6h post-injection LPS significantly impacted C57BL/6 and P301S horizontal bar performance (mixed effects linear regression, *p<0.05, **p<0.0001). The impact of LPS on P301S horizontal bar performance was significantly greater than control mice (p<0.0001). 24h post LPS-injection C57BL/6 mice had recovered but P301S mice had still not recovered to baseline performance (*p<0.05). By 36h post-injection all mice had recovered to baseline performance. Mixed effects linear regression showed that LPS administration at 16 weeks advances the decline in performance during the chronic phase (16-22 weeks) (p<0.001). (C57BL/6 + Saline n=8, C57BL/6 + LPS n=8, P301S + Saline n=8, P301S + LPS n=7).*

	24h Pre-injection				6h post-injection				24h post-injection				36h post-injection			
	Estimated mean	**p**	**95% CI**		**Estimated mean**	**p**	**95% CI**		**Estimated mean**	**p**	**95% CI**		**Estimated mean**	**p**	**95% CI**	
Reference Score (C57BL/6 + Saline)	9.9	0.000	9.6	10.2	9.9	0.000	9.4	10.4	9.9	0.000	8.8	11.0	9.9	0.000	9.7	10.1
Δ Score P301S	-0.1	0.515	-0.5	0.3	-0.3	0.462	-0.9	0.4	0.0	0.956	-1.6	1.5	-0.2	0.144	-0.5	0.1
Δ Score LPS	0.0	1.000	-0.4	0.4	**-0.8**	**0.019**	**-1.5**	**-0.1**	0.0	1.000	-1.5	1.5	0.0	1.000	-0.3	0.3
Δ Sore P301S + LPS (interaction term)	0.1	0.829	-0.5	0.6	**-4.2**	**0.000**	**-5.2**	**-3.2**	**-3.0**	**0.010**	**-5.2**	**-0.8**	0.0	0.813	-0.5	0.4

Table 19 - Horizontal bar performance 24-hours pre-injection, 6-hours, 24-hours and 36-hours post-injection. The first term represents baseline performance for the C57BL/6 group receiving saline. The following two terms test for an independent effect of genotype and LPS treatment. The fourth term tests for a difference in the independent effect of LPS between genotypes.

6-hours post-injection: The impact of LPS-injection on horizontal bar performance was not different when mice were injected at 16 weeks of age compared with mice injected at 10 weeks of age for C57BL/6 mice or P301S mice (16 week C57BL/6 + LPS vs 10 week C57BL/6 + LPS: 0.2; p=0.733; 95% CI -1.0 to 1.4; 16 week P301S + LPS vs 10 week P301S + LPS: -0.7; p=0.374; 95% CI -2.3 to 0.9) (**Figure 16**).

24-hours post-injection: P301S mice injected with LPS at 10 weeks of age had fully recovered whereas P301S mice injected with LPS at 16 weeks of age had not, hence there was a differential impact of age of injection for P301S mice but not C57BL/6 mice (16 week C57BL/6 + LPS vs 10 week C57BL/6 + LPS: 0.1; p=0.822; 95% CI -1.1 to 1.3; 16 week P301S + LPS vs 10 week P301S + LPS: -2.5; p=0.006; 95% CI -4.2 to -0.7) (**Figure 16**).

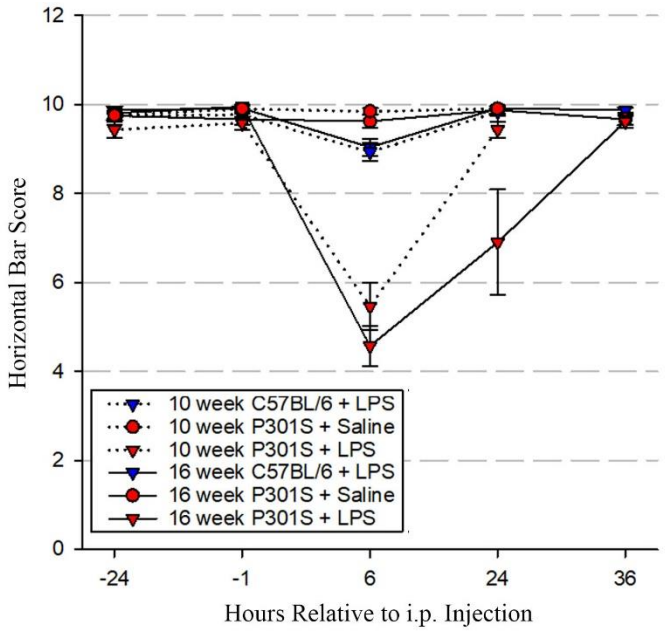

Figure 16 – Longer lasting impact of intraperitoneal LPS-injection on horizontal bar performance in 16 week old P301S mice compared with 10 week old mice. *C57BL/6 (blue) and P301S mice (red) were injected with LPS (i.p., 500 μg/kg) (triangle) or saline (circle) at 10 (dotted line) or 16 (solid line) weeks of age. Horizontal bar task - performance was tested 24-hours and 1-hour prior to injection and 6-, 24-, and 36- hours after injection. 6-hours post-injection the impact of LPS-injection on horizontal bar performance of P301S mice was not affected by age of injection. However, 24-hours post-LPS-injection there was a differential impact of age of injection for P301S mice (mixed effects linear regression, p<0.01). By 36-hours post-injection all mice had recovered to baseline performance. (10 week: C57BL/6 + LPS n=14, P301S + Saline n=11, P301S + LPS n=13, 16 week: C57BL/6 + LPS n=8, P301S + Saline n=8, P301S + LPS n=7).*

4.3.2.2 Effect of systemic inflammation on chronic horizontal bar performance

All groups fully recovered following the acute sickness response. C57BL/6 mice maintained a steady baseline for the remainder of the experiment regardless of whether they were exposed to saline or LPS at 16 weeks of age (**Figure 15** and Table 20). P301S mice however showed a progressive decline from 16 to 22 weeks of age. On average during the chronic phase saline-injected P301S mice lost 1 point per week. LPS-injection significantly increased the rate of decline in P301S mice (**Figure 15** and Table 20). The differential effect of LPS was greater in P301S mice than C57BL/6 mice when formally tested.

	Estimated mean	p	95% Confidence Interval	
Intercept				
Reference baseline (C57BL/6 + Saline)	9.9	0.000	9.1	10.8
Δ Baseline P301S	-0.2	0.675	-1.4	0.9
Δ Baseline LPS	-0.1	0.931	-1.2	1.1
Δ Baseline P301S + LPS (interaction term)	-0.3	0.747	-2.0	1.4
Weekly rate of change				
Reference weekly change (C57BL/6 + Saline)	0.0	0.936	-0.1	0.1
Δ Weekly change P301S	-1.0	0.000	-1.2	-0.9
Δ Weekly change LPS	0.0	0.985	-0.2	0.2
Δ Weekly rate of change P301S + LPS (interaction term)	-0.4	0.001	-0.6	-0.2

Table 20 - Horizontal bar performance during the declining phase. The first term represents baseline performance for the C57BL/6 group receiving saline. The following two terms test for an independent effect of genotype and intervention. The fourth term tests for a difference in the independent effect of LPS between genotypes. The last four terms can be interpreted in the same way but show differences in the weekly rate of change in performance

The chronic decline in horizontal bar performance of P301S mice injected at 10 weeks of age was compared with that of mice injected at 16 weeks. Mixed effects linear regression demonstrated no differences between any of the C57BL/6 groups regardless of age of injection or LPS exposure. There was no difference in the rate of decline of horizontal bar performance of saline-injected P301S mice between cohorts (16 week P301S + Saline vs 10 week P301S + Saline: additional weekly change -0.2; p=0.148; 95% CI -0.5 to 0.1). LPS-injection into 16-week-old, but not 10-week-old, P301S mice increased the rate of decline of horizontal bar performance compared with saline-injected counterparts, however, when formally tested, the differential impact of the age of LPS-injection was not significant at α=0.05 (additional weekly change -0.4; p=0.062; 95% CI -0.8 to 0.0) (see Figure 17).

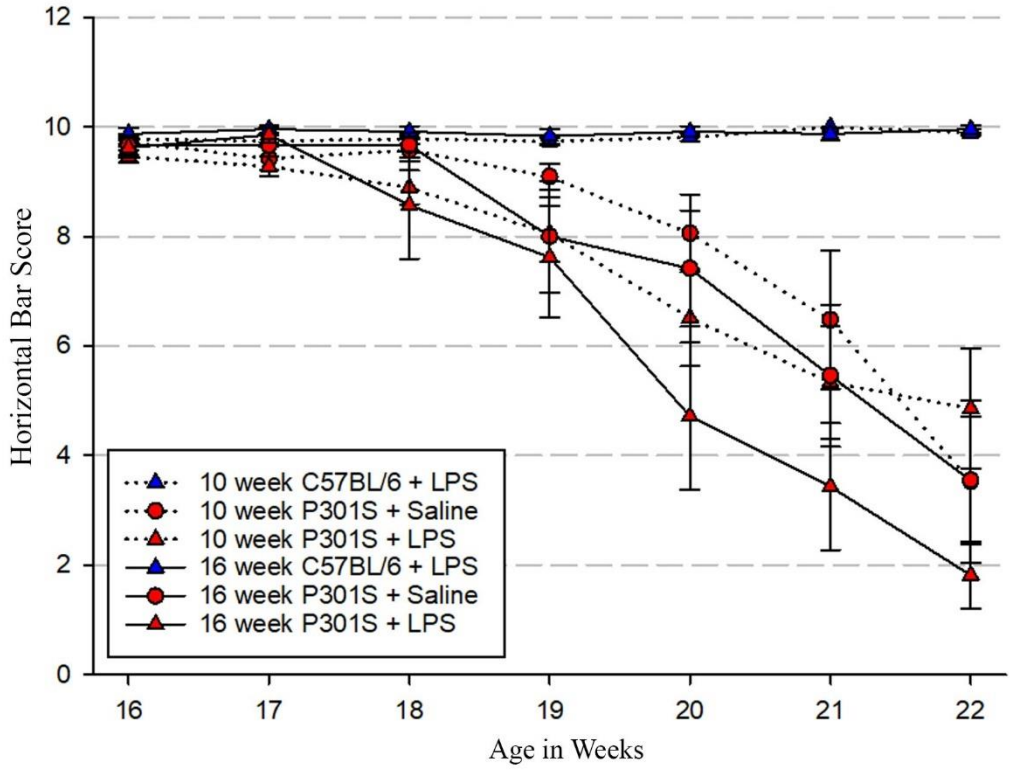

Figure 17 - LPS-injection into 16-week-old, but not 10-week-old, P301S mice increased the rate of decline of horizontal bar performance but the differential impact of age of LPS-injection was not significant. *C57BL/6 (blue) and P301S mice (red) were injected with LPS (i.p., 500 μg/kg) (triangle) or saline (circle) at 10 (dotted line) or 16 (solid line) weeks of age. Horizontal bar task performance was tested weekly from 16-22 weeks of age. Mixed effects linear regression showed that LPS injection at 16 weeks, but not 10 weeks of age, advances the decline in performance during the chronic phase (16-22 weeks) but when formally tested the differential impact of age of injection was not significant (p=0.062). (For details of 10 week n's see Figure* ***12****; 16 week: C57BL/6 + LPS n=8, P301S + Saline n=8, P301S + LPS n=7).*

4.4 Results Summary

The measures of the acute response to LPS discussed above are summarised in Table 21. The Acute Sickness Score indicated that P301S mice suffered more severe and longer lasting symptoms of LPS-induced sickness than C57BL/6 mice. They also took longer to return to normal open field activity compared with C57BL/6 mice, and while P301S mice injected at 10 weeks of age showed no difference in percentage weight loss compared with control mice, P301S mice injected at 16 weeks of age showed additional weight loss compared with age matched C57BL/6 mice or younger P301S mice. P301S mice injected at 10 weeks of age also showed signs of exaggerated hypothermia compared with C57BL/6 mice. The cause for the exaggerated response to LPS in P301S mice remains to be determined.

	10 week injection				16 week injection	
	Ref (C57BL/6 + Saline)	**C57BL/6 + LPS**	**P301S + Saline**	**P301S + LPS**	**C57BL/6 + LPS**	**P301S + LPS**
Open field activity @4h (% saline injected counterpart)	100.0	**-54.9**	100.0	-33.1	-17.1	12.8
Open field activity @24h (% saline injected counterpart)	100.0	-10.6	100.0	40.4	10.1	7.1
Acute Sickness Score (AUC)	0.0	**1.9**	0.0	**5.0**	2.0	**3.6**
Hourly weight loss (as % baseline)	-0.1	**-0.3**	0.0	0.0	0.0	**-0.3**
Hypothermia (AUC)	120.4	-1.7	**-4.4**	**-2.7**	-2.5	-0.3

Table 21 – The acute impact of LPS on phenotype of C57BL/6 and P301S mice at 10 and 16 weeks of age - summary table*: The Reference column shows the open field activity at 4- and 24-hours post-injection, Acute Sickness Score (AUC), hourly weight loss and temperature (AUC) of C57BL/6 mice injected with saline. The following two columns test for an independent effect of LPS or genotype on each of those measures. The fourth term tests for a difference in the independent effect of LPS between genotypes. The 5th column tests for a difference in the independent effect of LPS between 10 week and 16 week old C57BL/6 mice. The 6th term tests for a differential effect of LPS in P301S mice injected at 16 weeks compared with P301S mice injected at 10 weeks. Bold and underlined text indicates p<0.05. (AUC = Area under curve).*

4.5 Discussion

The current study demonstrates that an early systemic inflammatory insult in pre-symptomatic P301S tau mice (i.e. at 10 weeks of age) caused an exaggerated acute sickness response compared with age-matched control mice; LPS-injected P301S mice had a significantly higher sickness score than LPS-injected C57BL/6 mice (Figure 11 B). Importantly, exaggerated acute symptoms extended beyond those typically associated with the sickness behaviour; LPS induced an exaggerated acute impairment of horizontal bar performance (Figure **12**) in P301S mice compared with controls – a function which is known to be impaired in P301S mice later in disease and is associated with underlying disease pathology. These data suggest an interaction between acute inflammation and existing CNS vulnerability that brings about acute neurological dysfunction that is not a feature observed in sickness in a normal animal.

Additionally, the degree of underlying pathology at the time of injection seems to be important in determining the magnitude and duration of acute impairments. Although LPS-injection at 16 weeks of age had the same effect on C57BL/6 mice as injection at 10 weeks of age according to all observed outcomes, P301S mice injected at 16 weeks of age had a significantly higher Acute Sickness Score than those injected at 10 weeks of age (Figure 14 B). In addition, the acute horizontal bar performance of P301S mice injected with LPS at 16 weeks of age was significantly more impaired than LPS-injected C57BL/6 mice 6-hours post-injection, and unlike those injected at 10 weeks of age, LPS-injected P301S mice had still not recovered to baseline horizontal bar performance 24-hours post-injection (Figure **15**). These data are consistent with clinical studies showing that increased age and the presence of dementia confer greater vulnerability to delirium (Ahmed et al., 2014).

Furthermore, these data go on to demonstrate that an acute inflammatory event in pre-symptomatic mice with the P301S tau mutation was sufficient to negatively impact the disease-associated decline in performance of P301S mice and this effect

was greater in P301S mice injected at 16 weeks of age rather than at 10 weeks of age. Again, these data are consistent with clinical studies showing that episodes of delirium are a risk factor for chronic cognitive decline, and that prior neurodegeneration increases the strength of this relationship (Davis et al., 2017).

4.5.1 Exaggerated acute sickness response

Illness and infection induce well-characterised physiological and behavioural changes that are conserved in vertebrates; together they comprise an evolved, adaptive strategy that is beneficial in fighting infection. These coordinated behaviours exist to conserve energy required to mount an immune response and limit the spread of infection.

Mice were injected with LPS (500 μg/kg) or saline and were monitored over the following hours and days. During the pilot study observations were recorded in chronological order, allowing development of a semi-quantitative Acute Sickness Scoring System (see Table 14), which was then applied to all future cohorts at regular intervals. Recorded observations included hunched posture, piloerection, ocular discharge, diarrhoea and the degree of responsiveness when disturbed (Irwin, 1968, Grossberg, 2011).

The Acute Sickness Score demonstrated that P301S mice had a significantly more severe response than C57BL/6 mice (Figure 11B). At 10 weeks of age at the peak of sickness behaviour LPS-injected C57BL/6 mice had hunched posture and were slower to respond when disturbed, however these observations were short-lived, whereas P301S mice were significantly more affected than control mice and exhibited all the symptoms described above. The acute effects of LPS also persisted in P301S mice for longer than in control mice.

This impact of LPS on P301S mice Acute Sickness Score was even worse still when mice were injected at 16 weeks of age: P301S mice had still not fully recovered at the

final time point 36-hours post-injection. In hindsight, observations ought to have been carried out until mice had fully recovered.

It should be noted that the Acute Sickness Score is a semi-quantitative measurement based on subjective observations and blinding to genotype was not possible since mice are different colours. Blinding to treatment was also unrealistic since it was abundantly clear which mice had been exposed to saline versus LPS, nor age at which mice were injected since experiments were not run in parallel. Ideally Acute Sickness Scoring would have been conducted by an independent observer blind to all variables tested. This scoring method is in principle similar to the Grading System for Clinical Assessment of EAE (Fuller et al., 2004) whereby there is a chronological progression of symptoms which determines the severity of the score. Since the symptoms associated with sickness behaviour are not as chronologically conserved it might be worth modifying the scoring method to something more similar in structure to the Irwin Neurological Test Battery whereby criteria are rated independently based on presence or absence and in some cases severity and all the scores are added up.

Hypoactivity is another typically observed sickness behaviour, hence, the distance travelled by mice in an open field chamber was recorded at multiple time points following injection in order to identify any differences in activity (Figure 11A and Figure 14A). It has previously been demonstrated that 1) P301S mice have increased exploratory behaviour in the open field compared with control mice (Scattoni et al., 2010, Torvell et al., 2013), 2) regardless of genotype there is a significant experience-dependent decrease in distance travelled when mice are repeatedly retested in the open field arena; this happens as mice become habituated to this environment (Bolivar, 2009), and 3) open field activity fluctuates across the day (Gould et al., 2009). Hence here the distance travelled by LPS-injected mice was expressed as a percentage of the distance travelled by saline-injected counterparts at that time point.

LPS-injection induced equivalent hypoactivity in P301S and C57BL/6 mice compared with their saline-injected counterparts 4-hours post LPS-injection. This result is

typical of a 500 μg/kg dose of LPS (Combrinck et al., 2002), however by 24-hours post LPS injection C57BL/6 mice had recovered to equivalent activity compared with their saline-injected counterparts whereas P301S mice had not. This was true of mice injected at 10 or 16 weeks of age (Figure 11 A and Figure 14A).

It is plausible that decreased activity in the open field chamber might either reflect neurological motor impairments or alternatively decreased motivation to engage in non-essential activities and since P301S mice injected at 10 weeks of age demonstrated normal horizontal bar performance 24-hours post-injection it is likely that the decreased open field activity in P301S mice at this time point is a reflection of decreased motivation – a known characteristic of the sickness response. Hypoactivity is a known feature of sickness behaviours in rodents (Irwin, 1968, Combrinck et al., 2002) which aims to minimize muscle usage and thus conserve energy required to mount an immune response (Hart, 1988).

Anorexia is another known feature of sickness behaviours in rodents (Kluger, 1991) hence mice were weighed at regular intervals following injection. P301S mice and C57BL/6 mice injected with LPS at 10 weeks of age displayed equivalent weight loss throughout the experiment (Figure 11 C). In hindsight mice ought to have been weighed until full recovery (which in C57BL/6 mice given this dose of LPS ought to be approximately 5 days (Weiland et al., 2007)) in case there was a difference in the trajectory of recovery. However, the data here indicate no difference in LPS-induced weight loss between P301S and C57BL/6 mice in the first 36-hours. P301S mice injected at 16 weeks of age showed a subtle but significant additional weight loss compared with LPS-injected C57BL/6 mice and compared with P301S mice injected at 10 weeks of age (Figure 14 C).

Anorexia seems somewhat counterintuitive as an adaptive response to infection since fighting infection is so energetically costly. However, reduced food seeking behaviour in wild animals is beneficial for several reasons: decreased motivation for food and water facilitates decreased locomotion which minimizes risk of predation

and conserves energy by reduced muscular activity and reduced heat loss. Anorexia also reduces plasma iron and zinc levels – both elements are required by bacteria for replication and are sourced from host blood supplies, hence, during an infection iron is redistributed throughout the body (Kirby et al., 1982) and decreased food consumption helps reduce circulating iron levels and thus impairs replication of invading bacteria.

Systemic-inflammation-induced anorexia is mediated by central proinflammatory cytokines IL-1, IL-6 and TNF-α (Layé et al., 2000). Peripheral LPS administration increases proinflammatory cytokine levels in the hypothalamus of mice. Central IL-1 receptor agonist administration does not affect circulating cytokine levels but completely blocks IL-1β, IL-6 and TNF-α mRNA expression in the hypothalamus and is sufficient to partially abrogate LPS-induced anorexia (Layé et al., 2000). It is plausible that the increased weight loss in P301S mice exposed to LPS at 16 weeks of age related to disease-associated neuroinflammation.

LPS is known to cause hypothermia in C57BL/6 mice at ambient temperatures (Greer et al., 1978). Here I demonstrate an exaggerated LPS-induced hypothermia in P301S mice compared with LPS-injected C57BL/6 mice when mice were injected at 10 weeks of age (Figure 11 D) but not when they were injected at 16 weeks of age (Figure 14 D).

Multiple pro-inflammatory molecules have been implicated in mediating LPS-induced thermoregulatory responses, including key cytokines (IL-1β, TNF-α and IL-6) and prostaglandins (PGE_2, PGD_2) (Ueno et al., 1982, Derijk et al., 1994, Chai et al., 1996, Leon et al., 1998, Quan et al., 1999) and the anti-inflammatory cytokine IL-10 regulates the intensity and duration of the LPS-induced thermoregulatory response – IL-10 deficient mice have exaggerated and prolonged fever compared with wild type mice (Leon et al., 1999). It is conceivable that disease-associated dysregulation of these proinflammatory mediators are pivotal in producing an exaggerated hypothermic response in P301S mice.

Previous studies demonstrated an exaggerated hypothermic response to LPS (500 μg/kg) in the ME7 prion disease model of neurodegeneration (Combrinck et al., 2002, Teeling et al., 2010, Murray et al., 2011), which was reversed by blocking NFκB-dependent transcription of IL-1β and IL-6 with synthetic glucocorticoid dexamethasone-21-phopshate (Murray et al., 2011).

The downstream consequences of exaggerated hypothermia could be biologically significant in determining the severity of the acute response and the longer-term impacts of this acute insult. Hypothermia prolongs the activation of NFκB and increases production of pro-inflammatory cytokines IL-1β and TNF-α (Fairchild et al., 2004) which are key in determining the magnitude of the LPS-induced acute sickness response. Hypothermia is also associated with increased tau hyperphosphorylation through inhibition of phosphatase activity which persists 1 week later (Planel et al., 2007, Planel et al., 2009) and thus in a model of tauopathy it is plausible that LPS-induced hypothermia might increase tau pathology and thus influence the trajectory of the disease.

One major limitation of this experiment was that use of a rectal temperature probe was not permitted on our licence hence a non-contact infrared (IR) temperature point gun was used to record temperature of mice following i.p. injection of saline or LPS. The temperature changes typically associated with LPS-induced hypothermia in C57BL/6 mice are very small when measured using a rectal temperature probe; even the exaggerated hypothermic response of ME7 prion diseased mice saw temperatures of ~37.0°C in LPS-injected ME7 mice compared with ~37.6°C in saline-injected counterparts (Combrinck et al., 2002). In the current study, however, the recorded temperature prior to injection ranged from ~29 – 31°C and dropped to approximately 26°C following LPS. These absolute temperatures are comparable to those cited in the literature for the IR temperature probes compared with rectal or implanted temperature transponders (Stephens Devalle, 2005). IR thermometers detect the infrared radiation emitted from an object and deduce the surface temperature using Boltzmann's law which relates wavelengths of electromagnetic radiation to the

temperature; thus, IR thermometers detect only the surface body heat which is emitted through the fur rather than the true body temperature which explains why the temperatures recorded were so low. Not only this but emissivity of an object varies with colour and texture, hence coat colour and direction of fur might have introduced variability. In fact, it is plausible that coat colour may account for the observed temperature difference between saline-injected P301S mice and controls. External emitted temperature is also subject to changes in ambient temperature, altered vasodilation and cold-/warmth-seeking behaviours. It is because of the apparent flaws in the method of data collection that the AUC data rather than the absolute figures were analysed.

There were no significant differences in the AUC data between any of the groups injected at 16 weeks of age (Figure 14 D). The data suggest a dramatic hypothermic response in saline-injected mice as well as in LPS-injected mice. While it is known that there are stress-related thermoregulatory changes in mice following intraperitoneal injection *per se*, this generally manifests as a hyperthermic response and tends to last 30-120 minutes (Rudaya et al., 2005) and hence cannot explain the hypothermic response seen here at 4- and 6-hours post-saline-injection. This is likely due to use of an IR thermometer.

The data from the mice injected at 10 weeks suggest it is worth pursuing more accurate temperature recordings in the future. Alternative methods for monitoring the hypothermic response include: use of a rectal probe, however this method can cause stress-related temperature fluctuations which mask hypothermic responses (Dallmann et al., 2006); tympanic thermometers do not cause stress-related impacts on core body temperature, however there are contradictory results regarding the reliability (Stephens Devalle, 2005, Quimby et al., 2009). An implanted telemetry chip would be ideal in future experiments to ensure accurate recording of core body temperature –these devices, although expensive, can be transplanted in advance to avoid stress-related temperature changes interfering with data collection, by constant monitoring can allow detection of the peak temperature response and reflect core

body temperature rather than radiated temperature (Stephens Devalle, 2005, Quimby et al., 2009).

Peripheral LPS-induced inflammation communicates with the brain to initiate the conserved sickness behaviours via multiple routes. LPS is recognised in the periphery by local pattern recognition receptors expressed on monocytes, macrophages and liver Kupffer's cells (Dantzer, 2009), which induces NFκB-mediated transcription of pro-inflammatory cytokines (Dantzer, 2001, Dantzer, 2009). These cytokines are large hydrophilic peptides and cannot diffuse through the BBB, however they can influence the brain in several ways: 1) by stimulating afferent nerves, e.g. the vagal afferents which activate the brainstem, hypothalamus, and limbic structures (Goehler et al., 1997, Romanovsky, 2004); 2) circulating cytokines, or LPS itself, may act on endothelial cells of the BBB to induce active transport (Gutierrez et al., 1993, Gutierrez et al., 1994) or alternatively they stimulate synthesis of downstream mediators by endothelial cells themselves (Laflamme et al., 1999, Terrando et al., 2011); 3) cytokines may bypass the BBB entirely and act on macrophage-like cells via the circumventricular organs (CMVOs) which lack the tight junctions of the BBB (Blatteis et al., 1983, Dantzer et al., 2008). Electrical stimulation of the vagus nerve and cytokine signalling to endothelial cells and local macrophages then cause increased downstream production of cytokines and proinflammatory mediators such as nitric oxide (NO) and prostaglandins of the E2 series (PGE_2) by inducible cyclooxygenase - 2 (COX2) enzyme (Hosoi et al., 2000, Romanovsky, 2000). Cytokines and prostaglandins then enter the brain parenchyma by volume diffusion and act on the brain (Dantzer et al., 2008). This results in production of more proinflammatory mediators in the CNS by microglia; primarily IL-1α, IL-1β, IL-6 and TNF-α, as is seen in the periphery. Cytokines and other proinflammatory mediators work together to initiate sickness behaviours; use of cytokine receptor agonists and knock-out mice has shown that proinflammatory cytokines have overlapping functions, they potentiate and compensate for each other.

Sickness behaviours comprise conserved and coordinated behavioural responses to infection which aim to limit replication of the pathogen and conserve energy required by the host to fight infection. In this way sickness behaviours are a healthy and adaptive part of restoring homeostasis – the sickness response can however become maladaptive when it is exaggerated in intensity or duration. This can occur when: (1) there is over-production of proinflammatory cytokines, or cytokine production persists for longer than normal; (2) pro-inflammatory cytokines and cells are not downregulated in the usual way or; (3) the neuronal circuits that mediate sickness behaviour become sensitized.

Previous studies have shown exaggerated sickness behaviour in aged animals compared with young, associated with exaggerated neuroinflammation (Godbout et al., 2005) as well as in the ME7 prion disease model of neurodegeneration (Combrinck et al., 2002). In both instances the microglia were primed such that subsequent inflammatory challenge caused over-production of central proinflammatory cytokines including IL-1β, which is key in coordinating sickness behaviours. The over-zealous proinflammatory response in the CNS was deleterious in ME7 mice; it caused increased apoptosis, and exacerbated and accelerated the disease-associated decline in motor function (Cunningham et al., 2009).

Alternatively, rather than an over-zealous central inflammatory response in the CNS there might be an equivalent central inflammatory response but the neurons are in some way sensitised by the over-expression of mutant-tau such that they are unable to respond appropriately to an equivalent central cytokine response or there might be an exaggerated peripheral immune response in P301S mice with downstream effects on CNS inflammation. Thorough analysis of central and circulating pro- and anti-inflammatory markers following LPS-injection is required in order to better understand the cause of the exaggerated sickness response in P301S mice compared with control animals.

4.5.2 Exaggerated acute neurological deficit

The exaggerated acute deficits seen in the present experiments extend beyond those typically associated with sickness behaviours. In alternative models of neurodegeneration systemic inflammation appears to cause acute dysfunction in the already vulnerable neurocircuitry of the CNS, apparently propagated by microglia primed by the disease (Cunningham et al., 2005, Cunningham et al., 2009). This interaction of systemic inflammation and disease pathology results in acute deficits in disease-relevant faculties. In P301S mice there is a disease associated progressive decline in horizontal bar performance, hence this task was used to detect LPS-induced, acute, exaggerated neurological deficits in P301S mice compared with C57BL/6 mice, caused by an interaction between systemic inflammation and the underlying disease-pathology. LPS induced an exaggerated acute deficit in horizontal bar performance of P301S mice compared with C57BL/6 mice (Figure 12 and Figure 15). 6-hours post-injection LPS-injected C57BL/6 mice took longer to reach the platform than saline-injected counterparts, however all C57BL/6 mice successfully completed the task in under 30 seconds, whereas, in P301S mice LPS induced an exaggerated acute deficit in horizontal bar performance; several mice repeatedly failed the task and those that succeeded regularly took upwards of 30 seconds to reach the platform.

Furthermore, P301S mice injected at 16 weeks of age were more acutely impaired on the horizontal bar task than those injected at 10 weeks of age: mice injected at 16 weeks of age had still not recovered back to normal baseline performance by 24-hours post LPS injection whereas mice injected at 10 weeks of age had fully recovered by this time point (Figure 12 and Figure 15). The fact that LPS had a greater, longer lasting impact on horizontal bar performance of older P301S mice than younger mice, despite the mild response in C57BL/6 mice which was consistent regardless of age, supports the notion that the degree of underlying disease pathology predicts the magnitude of the observed exaggerated acute neurological deficits in P301S mice.

In epidemiological studies, dementia has often been treated as a binary condition; patients either have dementia or they do not. However, a recent study demonstrated that in humans, worse prior cognitive impairment, determined by Mini-Mental State Exam (MMSE), predicted increased susceptibility to acute deficits which manifest as delirium and in mice, worse disease pathology predicted the severity of the acute response to intraperitoneal LPS injection (Davis et al., 2015).

ME7 prion disease mice present with an exaggerated sickness response compared with wild-type mice when injected with LPS (Combrinck et al., 2002, Cunningham et al., 2005, Cunningham et al., 2009, Davis et al., 2015) and it has been suggested that the exaggerated response is underpinned by microglial priming (discussed in section 1.2.9). In ME7 prion diseased mice the pathology and primed microglial cells exist in the hippocampus and limbic system hence pathology is associated with functional deficits in tasks associated with these regions e.g. impaired T-maze performance (a predominantly hippocampal dependent task) (Betmouni et al., 1996, Guenther et al., 2001, Cunningham et al., 2005).

Since the neurocircuitry involved in T-maze alternation is known to be vulnerable in ME7 mice this task was used to demonstrate exaggerated acute hippocampal dependent cognitive deficits in the ME7 prion disease model following a systemic inflammatory event (Cunningham et al., 2009). These authors used this and other tasks to show that LPS induced a reversible, "acute onset, fluctuating, change in cognition not better accounted for by dementia" thus meeting the DSM-IV criteria for delirium (Davis et al., 2015). In animal models where there is microglial priming in the hippocampus and limbic systems, LPS appears to induce exaggerated deficits in hippocampal dependent tasks such as burrowing and impaired spatial memory in the underwater radial arm maze, Morris water maze and the "paddling" Y-maze task (Chen et al., 2008, Cunningham et al., 2009, Field et al., 2010, Sy et al., 2011, Davis et al., 2012).

However, P301S mice do not demonstrate disease-associated impairment of spontaneous-alternation in the T-maze with age. That does not necessarily mean that there is no disease-associated pathology in the region, and in any case the hippocampus receives cortical and sub-cortical inputs from regions with pathology (including the medial septum and amygdala) in the P301S mouse hence T-maze alternation during the acute phase might be an appropriate task for detecting exaggerated acute cognitive deficits in the P301S mouse. As of yet, no clear cognitive deficits have been identified in the P301S model of tauopathy. Disease pathology dominates in the spinal cord and the acute impairment of horizontal bar performance reflects this.

The horizontal bar task is used as a test of motor strength and coordination. It is possible that the exaggerated deficit in horizontal bar performance observed in P301S mice is not neurological, but might be the result of an exaggerated sickness response because this task does not allow distinction between malaise vs. motor dysfunction. However, inhibition of locomotion in the openfield was not significantly different between LPS-injected control mice and LPS-injected P301S mice and mice appeared to be trying hard to complete the horizontal bar task but were physically unable. Based on these observations and experience of watching mice during the chronic decline phase of disease I am inclined to speculate that this exaggerated acute deficit in horizontal bar task performance in P301S mice reflects an acute LPS-induced neurological impairment, rather than malaise.

In a case-controlled study of 60 patients with delirium or dementia, or both or neither (fifteen per group) patients had serial evaluations of motor control (Trunk Control Test – TCT) at 4 different time points. Results showed that delirium was associated with fluctuating motor performance whereas dementia was not (Bellelli et al., 2011). Delirium is also known to be associated with increased risk of falls; though there are multiple potential reasons for this, acute motor incoordination occurring as part of the syndrome is one plausible explanation (Babine et al., 2016).

It is unclear whether this neurological impairment might be due to increased production of proinflammatory mediators by microglia, as is the case in aged animals and prion diseased mice (Combrinck et al., 2002, Godbout et al., 2005), or whether this exaggerated response might be attributed to increased sensitivity of neurons in P301S mice. Indeed previous studies investigating inflammatory markers in P301S mice found IL-1β stained cells of neuronal morphology in the brainstem and spinal cord (Bellucci et al., 2004) hence it is plausible that P301S tau expression sensitizes neurons such that they respond differently to equivalent cytokine levels.

Regardless of the mechanism, these data indicate that there is an exaggerated acute deficit in the already vulnerable circuitry involved in horizontal bar performance in P301S mice, and worse disease pathology predicts increased vulnerability to the effects of LPS-induced systemic inflammation.

4.5.3 Long term impacts of systemic inflammation

There was no difference in the decline in horizontal bar performance of P301S mice injected with saline at 10 vs 16 weeks of age. P301S mice injected with LPS at 10 weeks of age showed no significant difference in the rate of decline compared with saline-injected counterparts, however the first pilot cohort of mice were sacrificed at 20 weeks of age, hence there is a loss of statistical power in the last two weeks which might have impacted on this result (see numbers in Figure **12**). P301S mice who were injected with LPS at 16 weeks of age, however, showed an accelerated and exacerbated decline in horizontal bar performance compared with saline-injected counterparts. These data, therefore, show that a single 500 μg/kg dose of LPS is capable of increasing the rate of disease-associated decline in motor function in P301S mice associated with permanent neurological dysfunction. Furthermore, the degree of pathology at the time of injection also affects the impact of LPS on the neurodegenerative decline such that worse disease pathology at the time of injection advances the decline.

The biological mechanism behind this altered trajectory of decline in horizontal bar performance remains to be determined. There is a known 49% reduction in motor neurons in the spinal cord of P301S mice at end stage (Allen et al., 2002) however the trajectory of that neuronal loss is unknown. Since tau protein is a microtubule associated protein found predominantly in the axon and tau pathology leads to microtubule destabilisation, declining horizontal bar performance might be associated with axonal degeneration or synaptic dysfunction (Spittaels et al., 1999). There is also progressive reactive astrogliosis and microgliosis in the P301S mouse which are thought to contribute to disease pathology through loss of neuroprotective and neurotrophic roles (Hampton et al., 2010) and gain of neuroinflammatory roles (Bellucci et al., 2004).

There are several ways in which LPS might exacerbate disease pathology and thus advance the decline in horizontal bar performance of P301S mice. LPS is also known to exacerbate tau pathology in mice. Evidence from triple transgenic 3xTgAD mice shows that a chronic systemic LPS regime increases tau pathology 24h and 48h post-injection (Kitazawa et al., 2005, Sy et al., 2011) and intracerebral mouse hepatitis virus (MHV) exacerbates tau pathology 2 and 4 weeks post-injection (Sy et al., 2011). Intracerebral LPS in the rTg4510 model of pure tauopathy caused an increase in tau pathology which persisted 1 week later (Lee et al., 2010). Systemic LPS also caused exacerbated tau pathology in the hTau mouse 24-hours post LPS which was further exacerbated in Cx3cr1 deficient hTau mice. Since CX3CR1 is involved in dampening the microglial response these data thus implicate microglial activation in the exacerbation of acute tau pathology (Bhaskar et al., 2010).

There is evidence that LPS can trigger a phenotypic switch in microglia and astrocytes away from neuroprotective and neurotrophic functions and towards a neurotoxic proinflammatory profile (Zamanian et al., 2012, Holtman et al., 2015, Liddelow et al., 2017). In an animal where there is mutant-tau-induced neuronal dysfunction and cell death, loss of neuroprotective function and gain of neurotoxic function is likely to be deleterious. As discussed, disease pathology might cause microglial priming such

that subsequent inflammatory LPS challenge causes exaggerated cytokine production. LPS is capable of inducing neuronal apoptosis (Semmler et al., 2005) e.g. via IL-1β induced p38-MAPK and JNK signalling (Lee et al., 2002, Xie et al., 2004). Apoptosis is a carefully controlled mechanism which depends on integration of pro- and anti-apoptotic signals – hence the expression of mutant tau under the Thy1.2 promoter might sensitise neurons such that they are more vulnerable to the effects of an inflammatory stimulus. All of these are mechanisms through which LPS might contribute to the observed advance in the decline of horizontal bar performance. These pathological correlates will be explored in more detail in Chapter 5.

4.6 Conclusion

The P301S mouse is a well-established model of progressive neurodegeneration which recapitulates key hallmarks of tauopathy dementia and by intraperitoneal injection of LPS it was possible to induce an acute and reversible sickness response.

In addition to typically observed sickness behaviours, the current study demonstrates that: 1) a single dose of LPS early in disease is sufficient to induce exaggerated acute impairments of motor strength and coordination in P301S tau mice compared with LPS-injected control mice; 2) acute motor function impairments were reversible and recovered with resolution of inflammation; 3) P301S mice injected at 16 weeks of age were more impaired and took longer to recover from the systemic inflammatory insult compared with mice injected with the same dose of LPS at 10 weeks of age; 4) importantly in P301S mice injected at 16 weeks systemic inflammation was sufficient to increase the rate of the chronic decline associated with neurodegeneration.

5 Chapter 5 – Acute and chronic pathological consequences of systemic inflammation in the P301S mouse

5.1 Introduction

As shown in experiments described in Chapter 4, P301S mice were more vulnerable to the acute effects of LPS compared with C57BL/6 mice. Symptoms extended beyond those usually associated with sickness behaviours – LPS-injected P301S mice showed exaggerated acute impairments of motor strength and coordination as measured by horizontal bar performance. The acute systemic inflammatory insult was also sufficient to exacerbate the trajectory of chronic decline in horizontal bar performance associated with neuronal dysfunction and neurodegeneration in the P301S mouse.

The exaggerated acute behavioural response seen in alternative animal models of neurodegeneration exposed to systemic LPS is suggested to be a consequence of microglial priming (Cunningham et al., 2005, Godbout et al., 2005). This is the phenomenon whereby microglia are in some way stimulated or disinhibited by ageing or disease such that subsequent inflammatory insult causes an exaggerated pro-inflammatory response typically with exaggerated production of cytokines, predominantly IL-1β (discussed in section 1.2.9).

The P301S mouse develops progressive neuronal loss and astrogliosis in the cortex in the absence of readily detectable microgliosis, and progressive astrogliosis and microgliosis in the spinal cord (Chapter 3). On that background this chapter aims to investigate the acute consequences of a systemic inflammatory challenge on key disease-relevant pathological hallmarks in the P301S mouse as well as those remaining at end stage.

P301S mice injected at 16 weeks of age were more vulnerable to the acute effects of LPS and the longer-term impacts on the decline in horizontal bar performance than

mice injected at 10 weeks of age which informed the decision to focus on the cohort of mice injected with LPS at 16 weeks in the following pathological studies.

5.2 Methods

In order to determine the acute and long term consequences of systemic inflammation on disease pathology mice injected intraperitoneally at 16 weeks of age with saline or LPS (500µg/kg – as previously described in section 4.2.2) were sacrificed 4-hours post-injection for qPCR, or 24-hours post-injection or at 22 weeks of age, for immunohistochemical pathological studies.

In every experiment, all of the tissue – acute and chronic tissue from C57BL/6 and P301S mice, exposed to either saline or LPS – was stained and imaged in a single batch.

5.2.1 Tissue Collection and Fluorescent staining

Fixed brain and spinal cord tissue was collected and processed as previously described in section 1.3.1. Numbers of animals quantified with each label are given in relevant sections.

Immunohistochemistry was performed for GFAP-positive astrocytes, IBA-1-positive microglia, AT8-positive hyperphosphorylated tau and NeuN-positive neurons as described in section 2.3.3 and using antibodies described in Table 22.

5.2.2 Imaging and Quantification

5.2.2.1 Astrogliosis in the motor cortex

5.2.2.1.1 Imaging

Fluorescent images of the motor cortex from GFAP-stained brain were taken as previously described in section 1.4, with 20x objective and 2300 ms exposure. Four hemispheres per animal were imaged and, as before, the camera was aligned with the surface of the motor cortex (see Figure 3).

1.1.1.1 **Antibodies used**

Tissue	Primary Antibody	Dilution	Cat. #	From	Secondary Antibody	Dilution	Cat. #	From	Tertiary Antibody	Dilution	Cat #	From
Brain & Spinal Cord	Rabbit poly anti-GFAP	1:1000	ZO334	DAKO	Goat anti-Rabbit IgG (H+L) biotinylated	1:1000	B2770	Thermo Fisher Scientific	Streptavidin Conjugated Alexa 568	1:1000	S11226	Thermo Fisher Scientific
Brain & Spinal Cord	Goat Poly anti-IBA1	1:1000	Ab5076	Abcam	Donkey anti-Goat IgG (H+L) Biotinylated	1:1000	A16003	Thermo Fisher Scientific	Streptavidin Conjugated Alexa 568	1:1000	S11226	Thermo Fisher Scientific
Brain & Spinal Cord	Mouse mono AT8	1:1000		Autogen Bioclear	Goat anti-Mouse IgG (H+L)	1:1000	A11004	Thermo Fisher Scientific	-	-	-	-
Brain	Mouse mono anti – NeuN	1:400	MAB377B	Merk Millipore	Streptavidin Conjugated Alexa 568	1:1000	S11226	Thermo Fisher Scientific	-	-	-	-

Table 22 - Antibodies used in chapter 5

5.2.2.1.2 Quantification by manual cell counts

GFAP-positive cell counts were counted manually using Zen 2011 software. An area 150 μm (sub-pial depth) x 300 μm length was pasted onto all images and counts conducted therein using the "Events" tool to quantify. Cell counts were converted to cells per mm^2 using Microsoft Excel™.

5.2.2.1.3 Automated quantification of percentage area containing GFAP signal

Fiji Image J software was used to determine the percentage of the selected area containing positive signal as described in section 2.5, with the following parameters: subtract background with rolling ball radius 50 pixels; set threshold (16, 255); select an area 150 μm by 333 μm; measure percentage area containing GFAP signal.

Statistical analyses are described in section 5.2.4. Acute tissue: C57BL/6 + Saline n=5, C57BL/6 + LPS n=5, P301S + Saline n=6, P301S + LPS n=6. Chronic tissue: C57BL/6 + Saline n=8, C57BL/6 + LPS n=8, P301S + Saline n=8, P301S + LPS n=8

5.2.2.2 Astrogliosis in lamina 9 of the spinal cord

5.2.2.2.1 Imaging

Fluorescent images of lamina 9 of GFAP-stained spinal cord were taken with 20x objective and 1200 ms exposure. Four sections per animal were imaged

5.2.2.2.2 Quantification of percentage area containing GFAP signal using Image J/ Fiji

Fiji Image J software was used to determine the percentage of the selected area containing positive signal as described in section 2.5. There was no need to subtract background from the image. The intensity threshold for chronic tissue was (55, 255). Astrogliosis was less severe in the acute tissue and hence the intensity threshold for acute tissue was modified to (45, 255).

Statistical analyses are described in section 5.2.4. Acute tissue: C57BL/6 + Saline n=3, C57BL/6 + LPS n=6, P301S + Saline n=6, P301S + LPS n=6 Chronic tissue: C57BL/6 + Saline n=8, C57BL/6 + LPS n=8, P301S + Saline n=8, P301S + LPS n=8

5.2.2.3 **Microgliosis in the motor cortex**

5.2.2.3.1 Imaging

Confocal z-stack images of the motor cortex from IBA1-stained brain were taken using a Ziess LSMZ10 confocal microscope with 15 slices per stack and 0.96 μm per slice. Four hemispheres were imaged per animal.

5.2.2.3.2 Quantification

IBA1-positive cells were counted manually using Zen 2011 software in the superficial layers of the cortex. Two areas both 150 μm (sub-pial depth) x 150 μm were copied across all images and counts conducted therein.

Cell counts were converted to cells per mm^2 in Excel. Statistical analyses described in section 5.2.4. Acute: C57BL/6 + Saline n=4, C57BL/6 + LPS n=6, P301S + Saline n=5, P301S + LPS n=6 Chronic: C57BL/6 + Saline n=6, C57BL/6 + LPS n=7, P301S + Saline n=6, P301S + LPS n=6

5.2.2.4 **Microgliosis in lamina 9 of the spinal cord**

5.2.2.4.1 Imaging

Fluorescent images were taken of lamina 9 and the rubrospinal (Rb) tract. When the Rb tract had been identified, the camera was adjusted to align the edge of the image with the edge of the spinal cord.

Images were taken of IBA1-stained spinal cord tissue, with 20x objective and 2300ms exposure.

5.2.2.4.2 Quantification by manual cell counts

IBA1-positive cells were counted in lamina 9 of the spinal cord using Zen 2011. An area 224 μm x 224 μm was copied across all images and cells counted therein. Cell counts were converted to cells per mm^2 in Excel.

5.2.2.5 Microgliosis in the white matter of the spinal cord

5.2.2.5.1 IBA1-positive cell counts using Image J/ Fiji

Automated IBA1-positive cell counts were conducted in the Rb tract using Image J/Fiji.

As with previous automation of image processing, in order to automate IBA1-positive cell counts one or two images were manually processed to determine parameters required, a template macro was then modified accordingly, the macro was tested on a small batch of approximately 10 representative images and parameters were optimised and then the images were batch processed.

As before the macro was used to: open the .tif files; duplicate images; subtract the background from the duplicates (rolling ball radius 25 pixels); impose an intensity threshold (set threshold: (22, 255)); and create a binary mask but from this point onwards the macro was modified to include further image-processing steps, as follows.

The first step was to "fill holes" in the binary mask. This was followed by a step to "despeckle" the image. According to the User Guide (https://imagej.nih.gov/ij/docs/guide/146-29.html) this filter "replaces each pixel with the median value in its 3 × 3 neighbourhood… for each pixel in the selection, the nine pixels in the 3 × 3 neighbourhood [are] sorted and the centre pixel replaced with the median value…" Once the image has been despeckled the 'analyze particles' function in ImageJ (Analyze > Analyze particles) was used to detect all objects larger than 20 pixels. The number of IBA1-positive cells were converted to cells per mm^2 in Excel.

5.2.2.5.2 Quantification of percentage area containing IBA1 signal using Image J/ Fiji

Fiji Image J software was used to determine the percentage area containing positive signal in lamina 9 and in the Rb Tract as described in section 2.5, with the following parameters: background subtraction with rolling ball radius 30 pixels; set threshold (18, 255); percentage area containing IBA1 signal across the whole image was analysed rather than a selected area.

Statistical analyses described in section 5.2.4. Acute: C57BL/6 + Saline n=6, C57BL/6 + LPS n=6, P301S + Saline n=6, P301S + LPS n=6. Chronic: C57BL/6 + Saline n=8, C57BL/6 + LPS n=8, P301S + Saline n=8, P301S + LPS n=7

5.2.2.6 Hyperphosphorylation of tau in the brain

5.2.2.6.1 Quantification

AT8-positive cell counts were conducted using the Zeiss upright A1 microscope with objective 20x. Cells were counted in a grid 0.5 mm width by 1 mm subpial depth using the graticule, with use of a cell counter to keep track. Counts were converted to cells per mm^2 in Excel. Statistical analyses described in section 5.2.4. Acute: C57BL/6 + Saline n=3, C57BL/6 + LPS n=3, P301S + Saline n=6, P301S + LPS n=5 Chronic: C57BL/6 + Saline n=3, C57BL/6 + LPS n=3, P301S + Saline n=7, P301S + LPS n=6

5.2.2.7 Hyperphosphorylation of tau in the spinal cord

5.2.2.7.1 Imaging

Fluorescent images of AT8-stained spinal cord were taken with 20x objective and 1600 ms exposure. Four spinal sections per animal were imaged. Until now only the most lateral part of lamina 9 has been imaged. Here images were taken of the most lateral part of lamina 9 as previously described; the medial ventral horn which includes lamina 9 and lamina 8; and the area adjacent to the central canal comprised of laminae 5-7 (figure 3).

5.2.2.7.2 Quantification

AT8-positive cell counts were conducted using Zen 2011 software across the whole image (444.2 μm x 332.8 μm). Cell counts were converted to cells per mm^2 in Excel.

Statistical analyses described in section 5.2.4. Acute: C57BL/6 + Saline n=3, C57BL/6 + LPS n=5, P301S + Saline n=6, P301S + LPS n=4 Chronic: C57BL/6 + Saline n=4, C57BL/6 + LPS n=4, P301S + Saline n=8, P301S + LPS n=5

5.2.2.8 Chronic Neuronal loss in the brain

5.2.2.8.1 Quantification

NeuN-positive cell counts were conducted using the Zeiss Axiovision microscope at objective 63x using oil. Cells were counted in a grid 152 μm width by 152 μm subpial depth using the graticule, with use of a cell counter. Counts were converted to cells per mm^2 using Microsoft Excel™.

Statistical analyses described in section 5.2.4. C57BL/6 + Saline n=6, C57BL/6 + LPS n=7, P301S + Saline n=4, P301S + LPS n=5

5.2.2.9 Chronic Neuronal loss in the SC

5.2.2.9.1 Imaging

Fluorescent images of lamina 9 of NeuN-stained spinal cord were taken with 20x objective and 1200 ms exposure. Four sections per animal were imaged.

5.2.2.9.2 Quantification

NeuN-positive cell counts were conducted in lamina 9 of the spinal cord using Zen 2011. An area 300 μm x 300 μm was copied across all images and cells counted therein. Cell counts were converted to cells per mm^2 in Excel.

Statistical analyses described in section 5.2.4. C57BL/6 + Saline n=8, C57BL/6 + LPS n=8, P301S + Saline n=8, P301S + LPS n=8

5.2.3 Gene expression analysis

Brain and spinal cord tissue were collected from P301S mice and control mice 4-hours post-injection and gene expression analysis conducted as described in methods section 2.6.

5.2.4 Statistical Analyses

All statistical analyses were conducted in IBM SPSS Statistics Software Version 22. For all stains acute and chronic analysis was separated. Mixed effects linear regression with random intercept for animal ID was used for comparison of C57BL/6 mice and P301S mice treated with either saline or LPS. Custom hypothesis tests were used to generate estimated means and SEMs for graphs. An interaction term was generated to determine whether LPS had a greater effect on P301S mice than controls.

5.3 Results

5.3.1 Acute pathology

Having demonstrated an exaggerated acute behavioural response to LPS in P301S mice compared with C57BL/6 mice (see section 4.3.2.1) astrocyte and microglial status in the cortex and spinal cord were assessed by qPCR 4-hours post-injection and by immunofluorescence 24-hours post-injection. CD11b mRNA levels and IBA1 immunofluorescence were used to assess microglial status; GFAP mRNA levels and immunofluorescence were used to determine the degree of reactive astrogliosis; IL-1β mRNA levels were assessed and finally tau pathology was assessed by AT8-positive immunofluorescence.

5.3.1.1 LPS exacerbates tau pathology in the P301S mouse

In order to investigate the impact of systemic inflammation on the abundance of phosphorylated tau 24-hours after injection (age 16 weeks), AT8 antibody was used. This antibody recognises pathological phospho-epitopes P-Ser202, P-Thr205.

There were no AT8-positive cells in the motor cortex of control mice 24-hours post-injection regardless of LPS exposure (Figure 18). However, AT8-positive cells were detected in the motor cortex of P301S mice, (4.0 cells per mm^2; p=0.193; 95% CI -2.6 to 10.7) and LPS-treatment tripled the number of AT8-positive cells in the motor cortex 24-hours post-injection (additional 9.2 cells per mm^2; p=0.055; 95% CI -0.3 to 18.6) (Figure 18).

As expected there were no AT8-positive cells in lamina 9 of the spinal cord of control mice either (Figure 18). There were AT8-positive cells in lamina 9 of the spinal cord of P301S mice (22.7 cells per mm^2; p=0.005; 95% CI 8.9 to 36.4) and LPS exposure increased AT8-positive cell counts although this was not statistically significant at α=0.05 (additional 15.2 cells per mm^2 compared with P301S + saline group; p=0.147; 95% CI -6.6 to 36.9) (Figure 18).

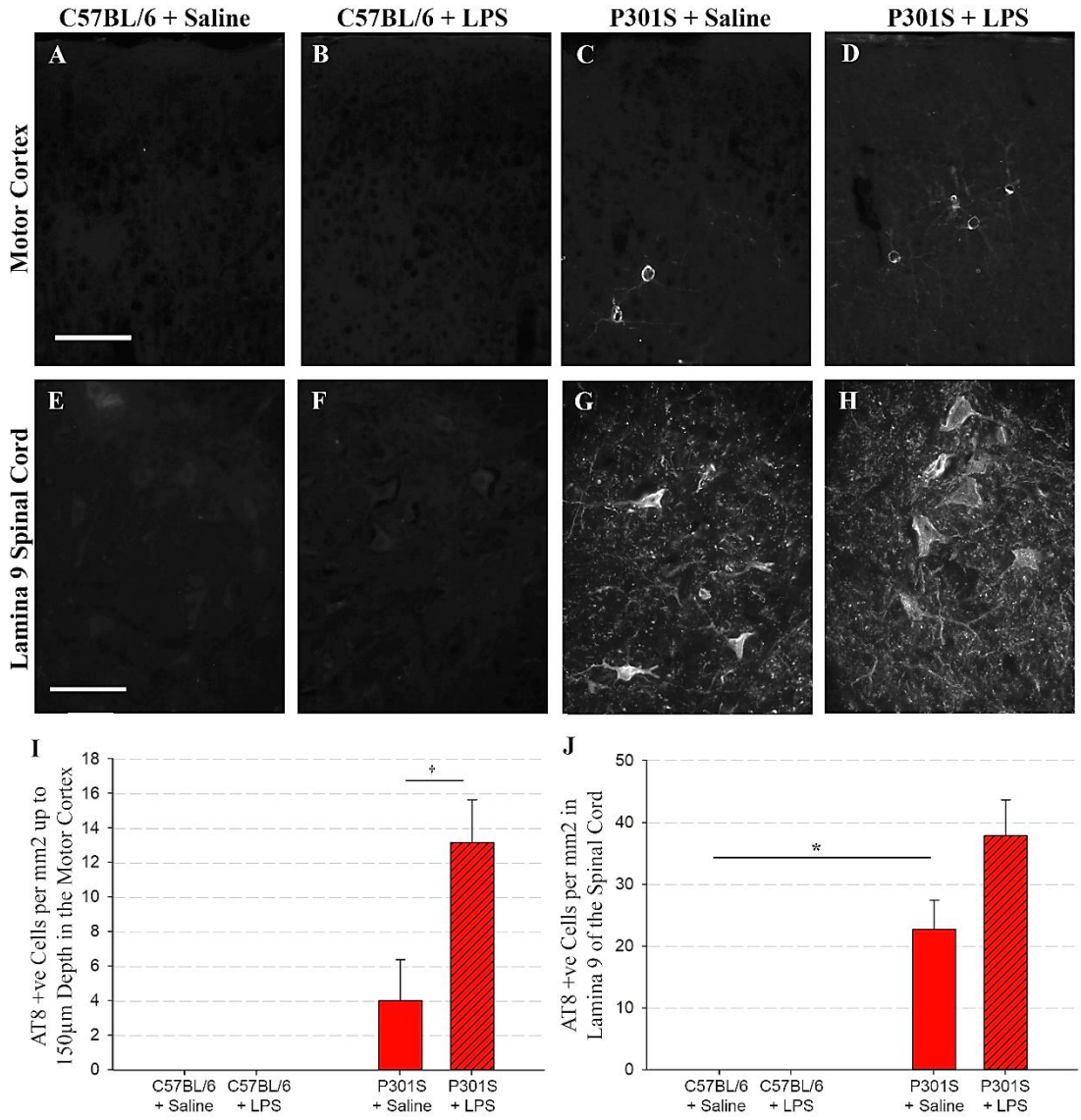

Figure 18 - Acute impact of systemic LPS on AT8-positive tau in the brain and spinal cord. A-D; *Representative examples of AT8 stained cortical tissue collected 24h post-injection from C57BL/6 + Saline* ***(A)****, C57BL/6 + LPS* ***(B)****, P301S + Saline* ***(C)****, P301S + LPS* ***(D)****.* ***E-H****; Representative examples of AT8 stained spinal cord (lamina 9 of c5-c7) from C57BL/6 + Saline* ***(E)****, C57BL/6 + LPS* ***(F)****, P301S + Saline* ***(G)****, P301S + LPS* ***(H)****. Scale bar 100 µm.* ***I)*** *AT8-positive cell counts in the motor cortex (to sub-pial depth of 150 µm) from C57BL/6 (blue) and P301S (red) mice collected 24-hours post-injection with either saline (no pattern) or LPS (patterned) indicated that LPS increased tau hyperphosphorylation detected by AT8 (mixed effects linear regression, indicated by †p=0.055) (C57BL/6 + Saline n=3, C57BL/6 + LPS n=5, P301S + Saline n=6, P301S + LPS n=4).* ***J)*** *AT8-positive cell counts in lamina 9 of spinal cord of C57BL/6 and P301S mice suggest no significant impact of LPS on AT8-positive tau accumulation in the lamina 9 of the spinal cord. (C57BL/6 + Saline n=3, C57BL/6 + LPS n=5, P301S + Saline n=6, P301S + LPS n=4).*

5.3.1.2 LPS-injection did not increase cortical CD11b mRNA levels in C57BL/6 or P301S mice

Cortical tissue was collected 4-hours post-injection with saline or LPS, for gene expression analysis. No difference in cortical CD11b mRNA levels was observed between groups. Following sensitivity analysis to take into account 3 outliers (see Figure 19): one in the C57BL/6 + Saline group (-4.7 SD from the mean), one in P301S + Saline group (-3.2 SD from the mean) and one in the P301S + LPS group (-3.4 SD from the mean) – still no independent effect was seen between the groups thus confirming the absence of an effect for genotype and no differential effect of LPS on the P301S mice (see Figure 19 and Table 23 for details).

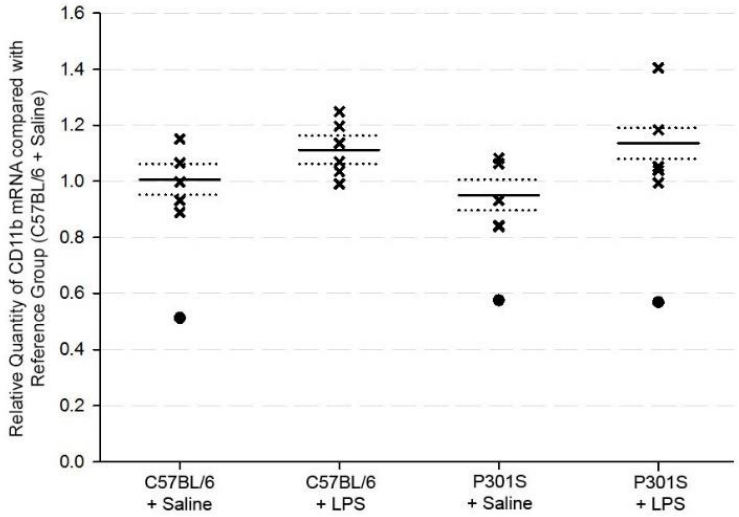

Figure 19 – Systemic LPS does not impact cortical CD11b mRNA levels. *The relative quantity of CD11b mRNA in the motor cortex of groups compared with the C57BL/6 + Saline reference group 4h post-injection indicated neither genotype nor systemic LPS treatment significantly impacted CD11b mRNA in the cortex (mixed effects linear regression). (C57BL/6 + Saline n=5, C57BL/6 + LPS n=6, P301S + Saline n=4, P301S + LPS n=5).*

Condition	Relative Quantity	Δ Relative Quantity	p-value	95% CI	
Reference C57BL/6 + Saline	1.0	-	-	-	-
LPS	1.1	+0.1	0.175	-0.1	0.3
P301S	1.0	-0.1	0.487	-0.2	0.1
P301S + LPS (interaction term)	1.1	+0.1	0.480	-0.1	0.3

Table 23 - ***Systemic LPS does not impact cortical CD11b mRNA levels.*** *The first term represents relative quantity of CD11b mRNA for the reference group: C57BL/6 mice receiving saline. The following two terms test for an independent effect of genotype and intervention. The fourth term tests for a difference in the independent effect of LPS between genotypes.*

5.3.1.3 LPS-injection did not increase IBA1-positive cortical microgliosis in C57BL/6 or P301S mice

Tissue collected 24-hours post-injection was stained for pan-microglial marker IBA1. In agreement with CD11b gene expression analysis IBA1-positive cell counts in the superficial layers of the cortex indicated no significant difference between any of the groups (see Figure 20 and Table 24 for details).

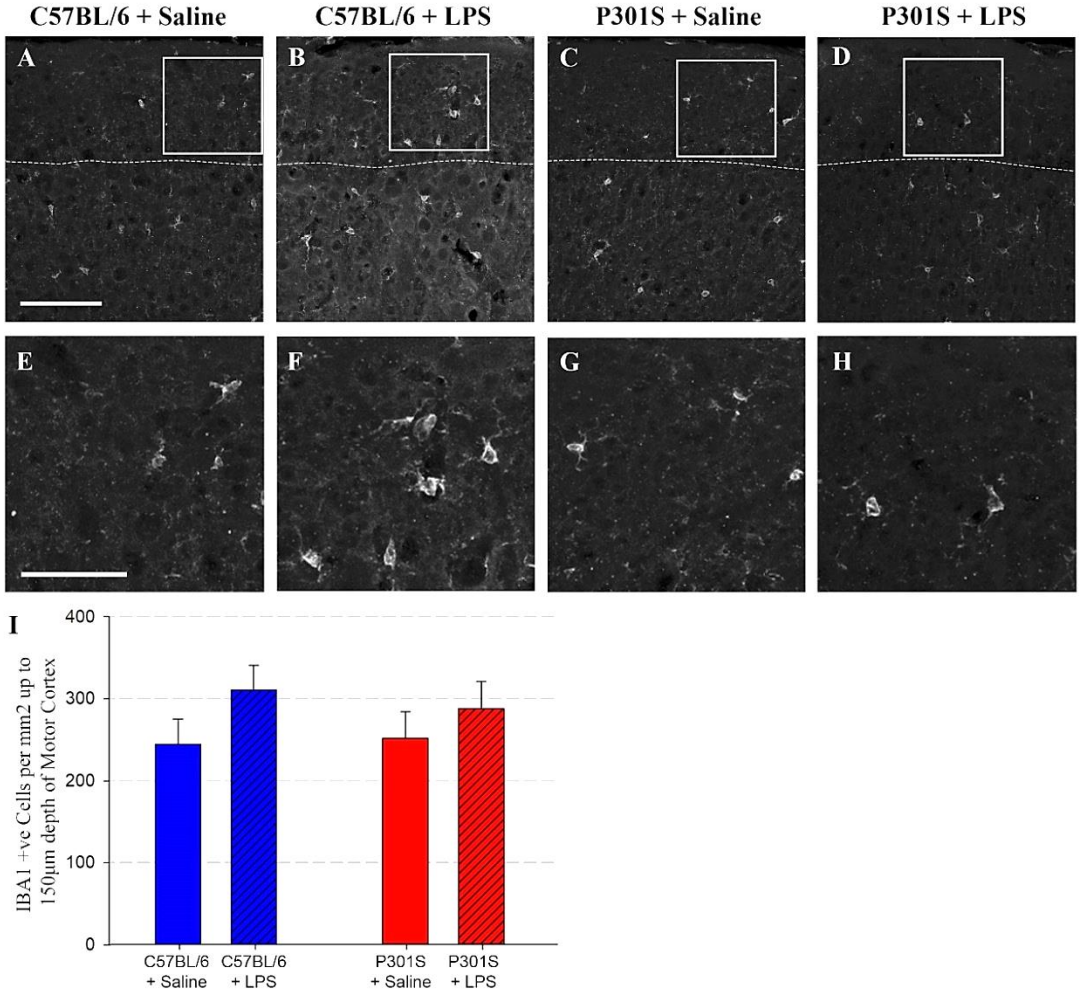

Figure 20 – Systemic LPS injection does not influence numbers of cortical microglia measured by IBA1. ***A-D;*** *Representative examples of IBA1 stained cortical tissue collected 24h post-injection from C57BL/6 + Saline* ***(A),*** *C57BL/6 + LPS* ***(B),*** *P301S + Saline* ***(C),*** *P301S + LPS* ***(D)****.* ***E-H****; Close-up of microglial morphology;* ***(E),*** *C57BL/6 + LPS* ***(F)****, P301S + Saline (G), P301S + LPS (H). I; IBA1-positive cell counts in the superficial layers of the motor cortex of C57BL/6 (blue) and P301S (red) mice collected 24-hours post-injection with either saline (no pattern) or LPS (patterned) indicated that neither genotype nor systemic LPS treatment significantly impacted IBA1-positive microglial cell counts in the motor cortex (mixed effects linear regression). (C57BL/6 + Saline n=5, C57BL/6 + LPS n=6, P301S + Saline n=4, P301S + LPS n=4).*

Condition	Cells per mm²	Δ Cells per mm²	p-value	95% CI	
Reference Cells per mm² (C57BL/6 + Saline)	244.6	-	0.000	179.3	309.8
LPS	310.7	+66.1	0.145	-25.5	157.8
P301S	251.4	+6.9	0.881	-89.7	103.4
P301S + LPS (interaction term)	287.8	-29.8	0.647	-166.0	106.4

*Table 24 - **Systemic LPS injection does not influence numbers of cortical microglia measured by IBA1** The first term represents IBA1-positive cells per mm² for the reference group: C57BL/6 mice receiving saline. The following two terms test for an independent effect of genotype and intervention. The fourth term tests for a difference in the independent effect of LPS between genotypes. Post hoc analysis to compare P301S + LPS with P301S + Saline: indicated additional 36.3; p=0.461; 95% CI -76.6 to 149.2.*

5.3.1.4 **LPS injection results in an increase in cortical IL-1β mRNA levels**

Gene expression assay for IL-1β mRNA in the cortex showed that there was no effect of genotype (Figure 21 and Table 25). There was a 23-fold increase in the relative abundance of IL-1β in LPS-injected C57BL/6 mice (Figure 21 and Table 25). There was a 16-fold increase in IL-1β expression in the brain of LPS-injected P301S compared with saline-injected counterparts (p=0.001; 95% CI 8.3 to 21.7). The differential effect of LPS in P301S mice compared with LPS-injected C57BL/6 mice was significant when formally tested (see interaction term Table 25).

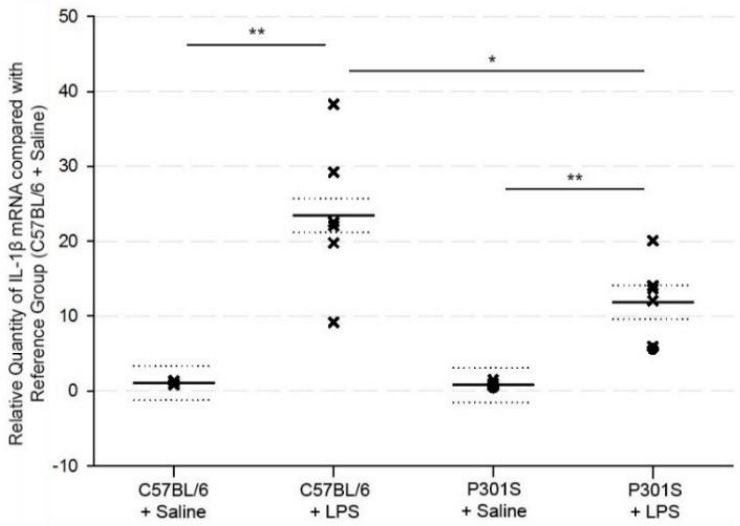

Figure 21 – Systemic LPS induces an acute increase in cortical IL-1β mRNA levels. *The relative quantity of IL-1β mRNA in the motor cortex of groups compared with the C57BL/6 + Saline reference group 4h post-injection indicated no effect of genotype. Systemic LPS treatment significantly impacted IL-1β mRNA levels in the cortex (mixed effects linear regression, indicated by *p<0.05, **p<0.001). (C57BL/6 + Saline n=6, C57BL/6 + LPS n=6, P301S + Saline n=6, P301S + LPS n=6).*

Condition	Relative Quantity	Δ Relative Quantity	p-value	95% CI	
Reference C57BL/6 + Saline	1.0	-	-	-	-
LPS	23.4	**+22.4**	**<0.001**	**15.7**	**29.1**
P301S	0.8	-0.3	0.938	-7.0	6.5
P301S + LPS (interaction term)	11.8	**-11.3**	**0.022**	**-20.8**	**-1.8**

Table 25 - ***Systemic LPS induces an acute increase in cortical IL-1β mRNA levels.*** *The first term represents relative quantity of IL-1β mRNA for the reference group: C57BL/6 mice receiving saline. The following two terms test for an independent effect of genotype and intervention. The fourth term tests for a difference in the independent effect of LPS between genotypes.*

5.3.1.5 LPS-injection increased CD11b mRNA levels in the spinal cord in C57BL/6 and P301S mice

Whole spinal cord tissue (C5-C7) was collected 4-hours post-injection for gene expression analysis. LPS induced a 40% increase in CD11b mRNA levels in the C57BL/6 spinal cord (Figure 22 and Table 26). The effect of genotype on CD11b mRNA levels was not significant and there was no additional differential effect of LPS in P301S mice (Figure 22 and Table 26).

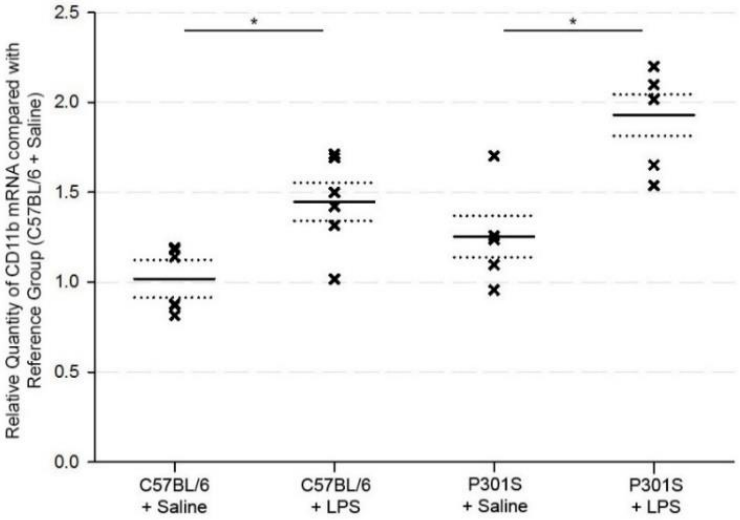

Figure 22 - Systemic LPS induces an acute increase in CD11b mRNA levels in the spinal cord. *The relative quantity of CD11b mRNA in c5-c7 of the spinal cord of groups compared with the C57BL/6 + Saline reference group 4h post-injection indicated no effect of genotype. Systemic LPS treatment significantly impacted IL-1β mRNA levels in the cortex (mixed effects linear regression, indicated by *p<0.05). (C57BL/6 + Saline n=6, C57BL/6 + LPS n=6, P301S + Saline n=5, P301S + LPS n=5).*

Condition	Relative Quantity	Δ Relative Quantity	p-value	95% CI	
Reference C57BL/6 + Saline	1.0	-	-	-	-
LPS	1.4	**+0.4**	**0.010**	**0.1**	**0.7**
P301S	1.3	+0.2	0.149	-0.1	0.6
P301S + LPS (interaction term)	1.9	+0.2	0.278	-0.2	0.7

Table 26 - ***Systemic LPS induces an acute increase in CD11b mRNA levels in the spinal cord.*** *The first term represents relative quantity of CD11b mRNA for the reference group: C57BL/6 mice receiving saline. The following two terms test for an independent effect of genotype and intervention. The fourth term tests for a difference in the independent effect of LPS between genotypes.*

The relative quantity of CD11b mRNA in the spinal cord of C57BL/6 mice was 1.5-fold the levels found in the cortex. In the LPS-injected C57BL/6 mice CD11b levels in the spinal cord were 1.7-fold the levels in the cortex (Table 27). In P301S mice CD11b mRNA levels were 2.0-fold higher in the spinal cord than in the cortex and following LPS-injection spinal cord levels of mRNA were 2.6-fold greater than in the cortex (Table 27).

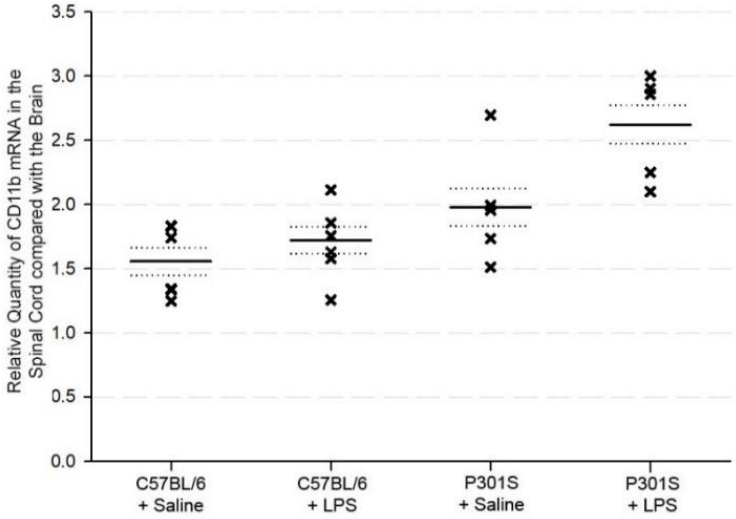

Figure 23 – Regional differences in CD11b mRNA levels. *The relative quantity of CD11b mRNA in c5-c7 of the spinal cord compared with the motor cortex (C57BL/6 + Saline n=6, C57BL/6 + LPS n=6, P301S + Saline n=5, P301S + LPS n=5).*

Group	Relative quantity	Δ Relative Quantity	p-value	95% CI	
C57BL/6 + Saline	1.5	**+0.5**	**0.006**	**0.2**	**0.9**
C57BL/6 + LPS	1.7	**+0.7**	**0.001**	**0.4**	**1.0**
P301S + Saline	2.0	**+0.9**	**0.002**	**0.5**	**1.4**
P301S + LPS	2.6	**+1.7**	**>0.001**	**1.2**	**2.2**

Table 27 – Regional differences in CD11b mRNA levels. *The first term represents the relative quantity of CD11b mRNA in C5-C7 of the spinal cord of C57BL/6 compared with brain, 4-hours post-saline-injection. The following three terms can be interpreted the same way for each of the different groups.*

5.3.1.6 LPS-injection increased IBA1-positive signal in the spinal cord of C57BL/6 and P301S mice

Immunofluorescence for microglial marker IBA1, in lamina 9 of the spinal cord 24-hours post-injection, confirmed the trend shown by CD11b mRNA levels. IBA1-positive cell counts indicate the presence of microglial cells in saline-injected C57BL/6 mice (Figure 24 and Table 28). An increase in the number of microglial cells was seen in P301S mice although this did not reach statistical significance. Against this, LPS induced an increase in IBA1-positive cell counts in both C57BL/6 mice and in P301S mice although post-hoc analysis indicated that this effect of LPS was not statistically significant in P301S mice (additional 45.7 cells per mm2; p=0.227; 95% CI -33.4 to 124.7) (Figure 24 and Table 28).

Densitometric analysis showed no difference in the percentage area containing IBA1 signal between C57BL/6 mice and P301S mice (Figure 24 and Table 28). LPS induced a 2-fold increase in the total area containing IBA1 signal in C57BL/6 mice. Unlike the non-statistically significant change seen for cell counts, post hoc analysis indicated that LPS induced a significant increase in IBA1 signal among P301S mice (additional 1.3% area containing IBA1 signal; p=0.027; 95% CI 0.2 to 2.5) (Figure 24 and Table 28).

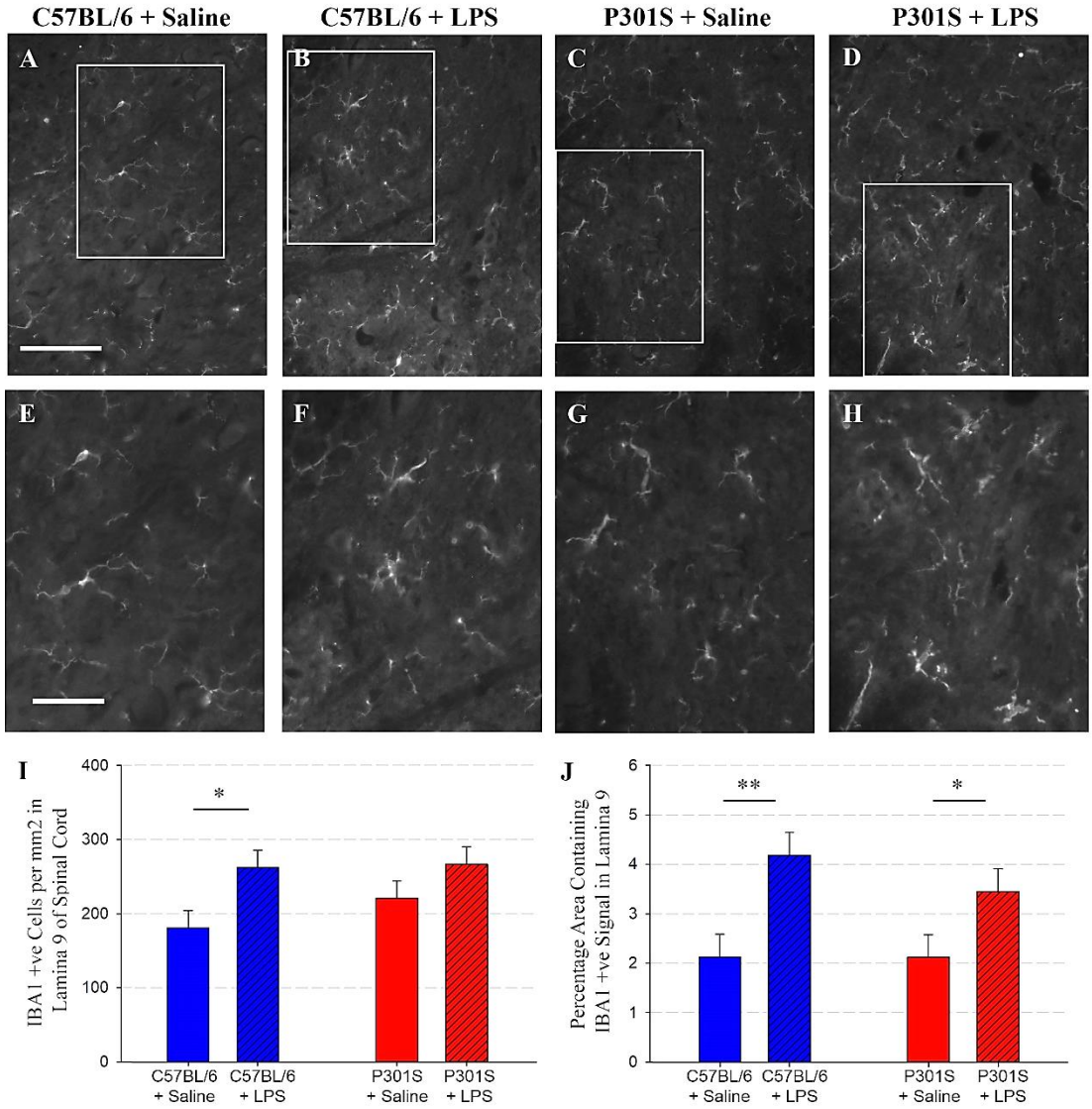

Figure 24 - Systemic LPS induces acute increase in IBA1-positive microglia in the spinal cord. ***A-D)*** *Representative examples of IBA1 stained spinal cord (lamina 9 of c5-c7) from C57BL/6 + Saline (**A**), C57BL/6 + LPS (**B**), P301S + Saline (**C**), P301S + LPS (**D**).* ***E-H)*** *Close-up of microglial morphology; C57BL/6 + Saline (**E**), C57BL/6 + LPS (**F**), P301S + Saline (**G**), P301S + LPS (**H**).* ***I)*** *IBA1-positive cell counts in lamina 9 of the spinal cord indicated that there was no difference between P301S mice (red) and control mice (blue) and that LPS (patterned) induced an increase in IBA1-positive cells in control mice but not P301S mice (*p<0.05).* ***J)*** *Densitometric analysis of lamina 9 indicated no difference between P301S and control mice but LPS induced an increase in the percentage area containing IBA1-positive signal in C57BL/6 and P301S mice (mixed effects linear regression, indicated by *p<0.05, **p<0.005). (C57BL/6 + Saline n=6, C57BL/6 + LPS n=6, P301S + Saline n=6, P301S + LPS n=6).*

Condition	Cells per mm²	Δ Cells per mm²	p-value	95% CI		% Area IBA1 signal	Δ % Area IBA1 signal	p-value	95% CI	
Reference (C57BL/6 + Saline)	181.0	-	0.000	132.3	229.8	2.1	-	0.000	1.2	3.1
LPS	262.4	**+81.4**	**0.023**	**12.4**	**150.3**	4.2	**+2.1**	**0.005**	**0.7**	**3.4**
P301S	220.9	+39.9	0.242	-29.1	108.8	2.1	0.0	0.997	-1.4	1.3
P301S + LPS (interaction term)	266.6	-35.7	0.454	-133.2	61.8	3.4	-0.7	0.431	-2.6	1.2

*Table 28 - **Systemic LPS induces acute increase in IBA1-positive microglia in the spinal cord.** The first term represents IBA1-positive cells per mm² or percentage area containing IBA1 signal for the reference group: C57BL/6 mice receiving saline. The following two terms test for an independent effect of genotype and intervention. The fourth term tests for a difference in the independent effect of LPS between genotypes.*

5.3.1.7 LPS-injection increased IL-1β mRNA levels in the spinal cord of C57BL/6 and P301S mice

In the spinal cord, there was no significant difference in IL-1β expression in P301S mice compared with C57BL/6 mice (Figure 25 and Table 29). There was an estimated 74-fold increase in IL-1β mRNA levels in LPS-injected C57BL/6 mice compared with saline-injected counterparts (Table 29). As was seen in the brain, IL-1β mRNA production was a relatively smaller in LPS-injected P301S mice compared with LPS-injected C57BL/6 mice, although when formally tested this differential impact was not significant at α=0.05 (see interaction term Table 29).

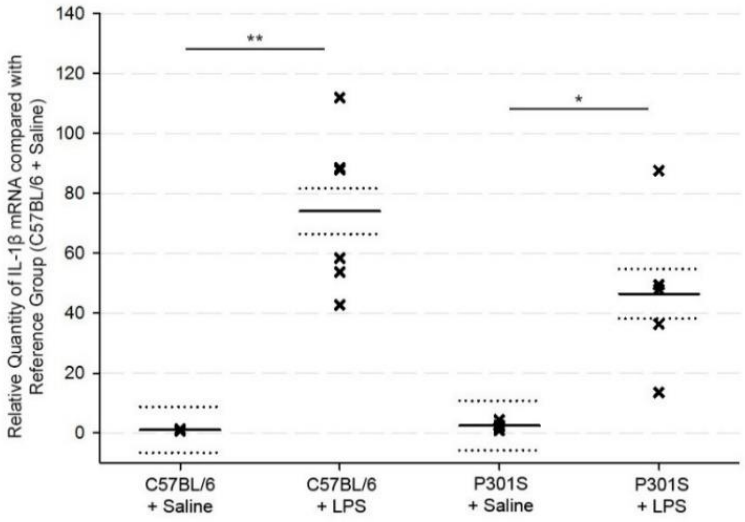

Figure 25 - Systemic LPS induces an acute increase in IL-1β mRNA levels in the spinal cord. *The relative quantity of IL-1β mRNA in c5-c7 of the spinal cord of groups compared with the C57BL/6 + Saline reference group 4h post-injection indicated no effect of genotype. Systemic LPS treatment significantly impacted IL-1β mRNA levels in the spinal cord (mixed effects linear regression, indicated by *p<0.01, **p<0.001). (C57BL/6 + Saline n=6, C57BL/6 + LPS n=6, P301S + Saline n=6, P301S + LPS n=6).*

Condition	Relative Quantity	Δ Relative Quantity	p-value	95% CI	
Reference C57BL/6 + Saline	1.0	-	-	-	-
LPS	74.1	**+73.0**	**<0.001**	**50.9**	**95.2**
P301S	2.5	+1.5	0.897	-21.7	24.6
P301S + LPS (interaction term)	46.9	-28.6	0.077	-60.7	3.4

Table 29 - ***Systemic LPS induces an acute increase in IL-1β mRNA levels in the spinal cord.*** *The first term represents relative quantity of IL-1β mRNA for the reference group: C57BL/6 mice receiving saline. The following two terms test for an independent effect of genotype and intervention. The fourth term tests for a difference in the independent effect of LPS between genotypes.*

IL-1β mRNA levels were equivalent in the cortex and spinal cord of saline-injected C57BL/6 mice (Table 30). LPS-injected C57BL/6 mice demonstrated a 3.8-fold increase in IL-1β mRNA levels in the spinal cord compared with the cortex (Table 30). Saline-injected P301S mice have a 3.5-fold increase in IL-1β mRNA levels in the spinal cord compared to the cortex (Table 30). Following LPS-treatment there IL-1β mRNA levels were 4.9-fold higher in P301S spinal cord compared to cortex (Table 30).

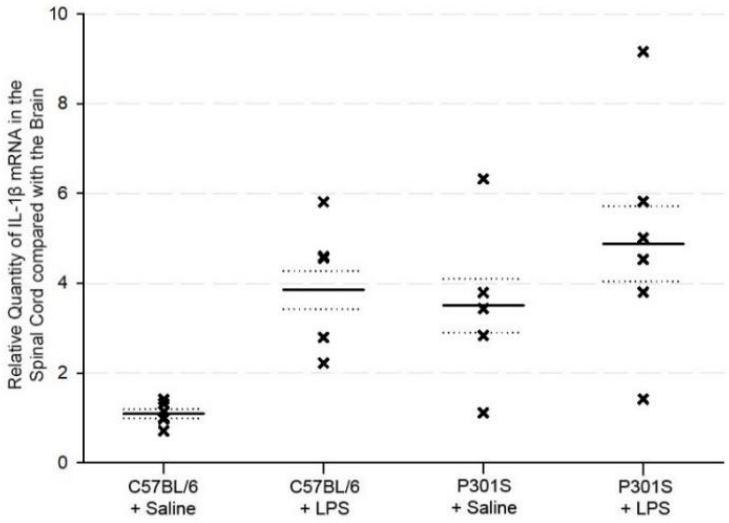

Figure 26 – Regional differences in IL-1β mRNA levels. *The relative quantity of IL-1β mRNA in c5-c7 of the spinal cord compared with the motor cortex. (C57BL/6 + Saline n=6, C57BL/6 + LPS n=5, P301S + Saline n=5, P301S + LPS n=6).*

Group	Relative quantity	Δ Relative Quantity	p-value	95% CI	
C57BL/6 + Saline	1.1	+0.1	0.716	-0.3	0.4
C57BL/6 + LPS	3.8	**+2.7**	**0.001**	**1.4**	**4.0**
P301S + Saline	3.5	**+2.5**	**0.019**	**0.5**	**4.5**
P301S + LPS	4.9	**3.7**	**0.01**	**1.1**	**6.3**

*Table 30 –**Regional differences in IL-1β mRNA levels.** The first term represents the relative quantity of IL-1β mRNA in C5-C7 of the spinal cord of C57BL/6 compared with brain, 4-hours post-saline-injection. The following three terms can be interpreted the same way for each of the different groups*

5.3.1.8 LPS-injection increased cortical GFAP mRNA levels in C57BL/6 and P301S mice

Cortical GFAP mRNA levels were assessed 4-hours post-injection. Primary analysis of the complete dataset indicated no difference in the relative abundance of GFAP mRNA between groups (Figure 27 and Table 31). However, given the potential influence of an extreme outlier in the C57BL/6 + saline reference group (14 SD from the mean) a sensitivity analysis was performed with exclusion of that sample (Figure 27). In this analysis, LPS induced a 2-fold increase in the relative abundance of GFAP mRNA in cortical brain tissue. No independent effect was seen for genotype, or any differential effect of LPS on the P301S mice (Figure 27 and Table 31 for details).

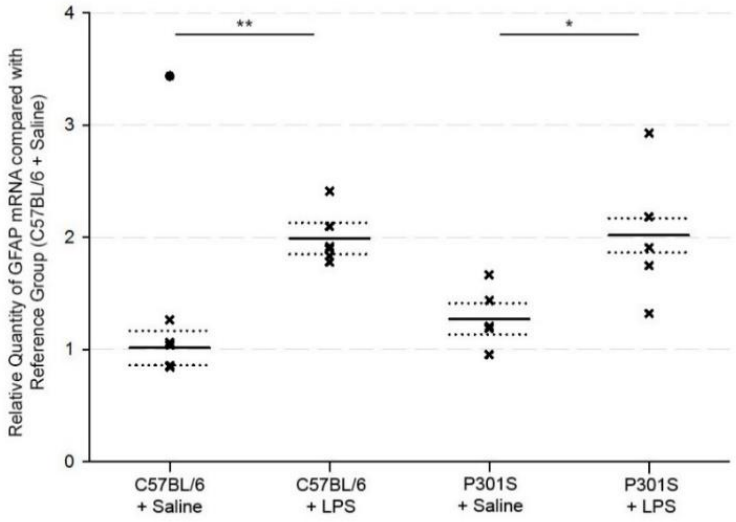

*Figure 27 - **Systemic LPS induces an acute increase in cortical GFAP mRNA levels.** The relative quantity of GFAP mRNA in the cortex of groups compared with the C57BL/6 + Saline reference group 4h post-injection indicated no effect of genotype. Systemic LPS treatment significantly impacted GFAP mRNA levels in the cortex (mixed effects linear regression, indicated by *p<0.01, **p=0.001). (C57BL/6 + Saline n=5, C57BL/6 + LPS n=6, P301S + Saline n=6, P301S + LPS n=5).*

Condition	Relative Quantity	Δ Relative Quantity	p-value	95% CI	
Reference C57BL/6 + Saline	1.0	-	-	-	-
LPS	2.0	**+1.0**	**0.001**	**0.5**	**1.4**
P301S	1.3	+0.3	0.226	-0.2	0.7
P301S + LPS (interaction term)	2.0	-0.2	0.439	-0.9	0.4

*Table 31 - **Systemic LPS induces an acute increase in cortical GFAP mRNA levels.** The first term represents relative quantity of GFAP mRNA for the reference group: C57BL/6 mice receiving saline. The following two terms test for an independent effect of genotype and intervention. The fourth term tests for a difference in the independent effect of LPS between genotypes.*

5.3.1.9 GFAP immunohistochemistry indicated astrogliosis in the motor cortex of P301S mice but no impact of systemic LPS

GFAP-positive cell counts in the superficial layers of the motor cortex indicated a 2-fold increase in the number of astrocytes in P301S mice compared with C57BL/6 (Figure 28 and Table 32). 24-hours post-injection LPS did not significantly impact the number of astrocytes in C57BL/6 mice and post hoc analysis indicted no impact of LPS in P301S mice (additional 55.0 cells per mm2; p=0.506; 95% CI 122.3 to 232.3).

Densitometric analysis indicated little or no GFAP-positive signal in the motor cortex of C57BL/6 mice (Figure 28 and Table 32). The percentage area containing GFAP signal in P301S mice was approximately 4-fold higher than in controls. The impact of LPS on C57BL/6 mice was not significant (Figure 28 and Table 32). Post hoc analysis indicated the impact of LPS on the percentage area GFAP signal in P301S mice compared with saline-injected counterparts was also not quite significant (additional 2.1%; p=0.200; 95% CI 1.3 to 5.4).

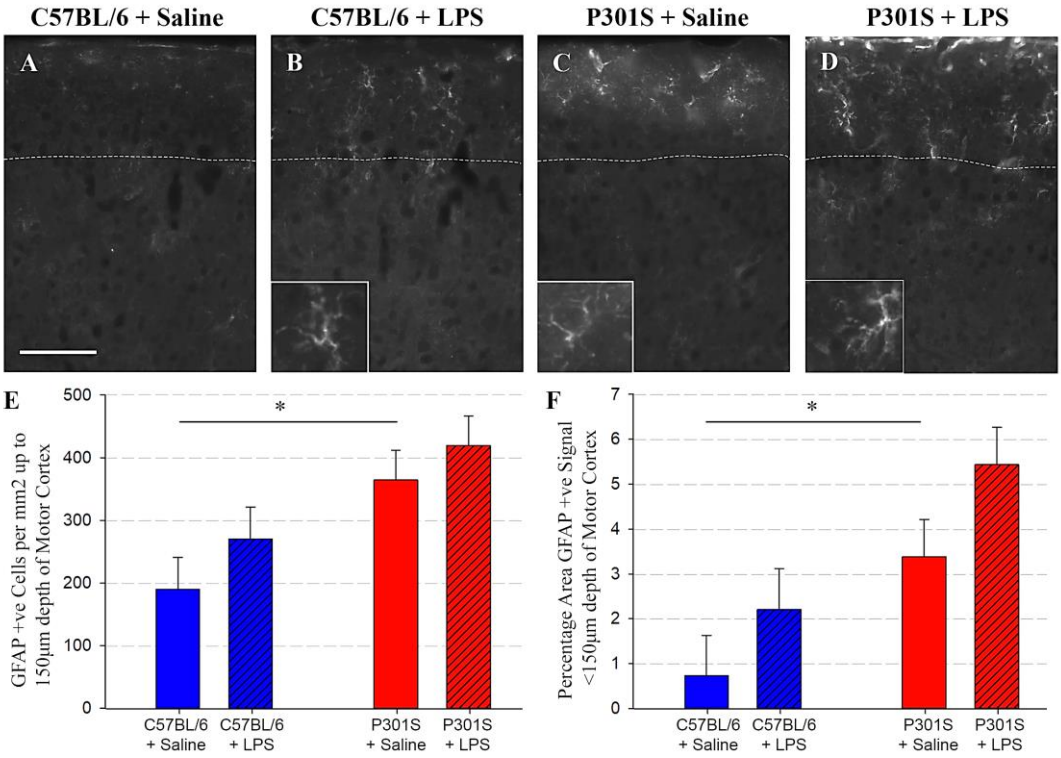

Figure 28 -Systemic LPS has no significant impact on GFAP-positive reactive astrocytes in the brain 24-hours post-injection. A-D; *Representative examples of GFAP stained cortical tissue collected 24h post-injection from C57BL/6 + Saline (**A**), C57BL/6 + LPS (**B**), P301S + Saline (**C**), P301S + LPS (**D**). Scale bar 100 µm.* ***E)*** *GFAP-positive cell counts in the motor cortex (to sub-pial depth of 150 µm) from C57BL/6 (blue) and P301S (red) mice 24h-post-injection with either saline (no pattern) or LPS (patterned) indicated astrogliosis in P301S mice compared with controls but no significant impact of LPS in either controls or P301S mice (mixed effects linear regression, indicated by *p<0.05). (C57BL/6 + Saline n=4, C57BL/6 + LPS n=6, P301S + Saline n=5, P301S + LPS n=6).* ***F)*** *Densitometric analysis supported these results (mixed effects linear regression, indicated by *p<0.05) (C57BL/6 + Saline n=5, C57BL/6 + LPS n=5, P301S + Saline n=6, P301S + LPS n=6).*

Condition	Cells per mm2	Δ Cells per mm2	p-value	95% CI		% Area GFAP signal	Δ % Area GFAP signal	p-value	95% CI	
Reference (C57BL/6 + Saline)	190.0	-	0.002	82.1	298.0	0.7	-	0.431	-1.2	2.6
LPS	270.0	+80.0	0.285	72.6	232.6	2.2	+1.5	0.264	1.2	4.2
P301S	364.3	**+174.3**	**0.023**	**27.4**	**321.3**	3.4	**+2.7**	**0.044**	**0.1**	**5.2**
P301S + LPS (interaction term)	419.4	-24.9	0.804	-232.1	182.4	5.4	+0.6	0.747	-3.1	4.2

Table 32 - **Systemic LPS has no significant impact on GFAP-positive reactive astrocytes in the brain 24-hours post-injection.** The first term represents GFAP-positive cells per mm^2 or percentage area containing GFAP signal for the reference group: C57BL/6 mice receiving saline. The following two terms test for an independent effect of genotype and intervention. The fourth term tests for a difference in the independent effect of LPS between genotype

5.3.1.10 **No influence of LPS injection on GFAP mRNA levels**

Gene expression analysis demonstrated a 130.0% increase in the relative abundance of GFAP mRNA in the spinal cord of P301S mice compared with C57BL/6 mice (Figure 29 and Table 33). LPS had no impact on GFAP mRNA levels in the C57BL/6 mice and although there was a 60% increase in the relative abundance of GFAP mRNA in LPS-injected P301S mice, the differential effect was not significant (Figure 29 and Table 33).

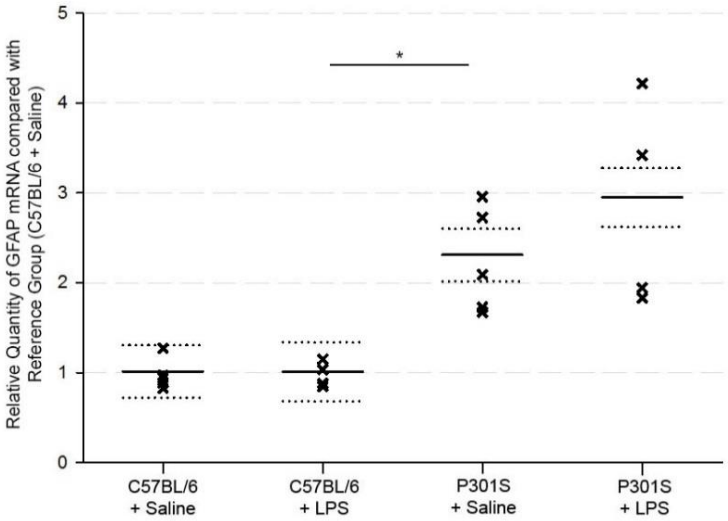

Figure 29 – ***Systemic LPS has no significant impact on GFAP mRNA levels in the spinal cord.*** *The relative quantity of GFAP mRNA in c5-c7 of the spinal cord of groups compared with the C57BL/6 + Saline reference group 4h post-injection indicated no effect of systemic LPS treatment. Genotype significantly impacted GFAP mRNA levels in the spinal cord (mixed effects linear regression, indicated by *p<0.01). (C57BL/6 + Saline n=6, C57BL/6 + LPS n=5, P301S + Saline n=5, P301S + LPS n=4).*

Condition	Relative Quantity	Δ Relative Quantity	p-value	95% CI	
Reference C57BL/6 + Saline	1.0	-	-	-	-
LPS	1.0	0.0	0.926	-0.9	0.8
P301S	2.3	**+1.3**	**0.005**	**0.4**	**2.1**
P301S + LPS (interaction term)	2.9	+0.7	0.269	-0.6	2.0

Table 33 - ***Systemic LPS has no significant impact on GFAP mRNA levels in the spinal cord.*** *The first term represents relative quantity of GFAP mRNA for the reference group: C57BL/6 mice receiving saline. The following two terms test for an independent effect of genotype and intervention. The fourth term tests for a difference in the independent effect of LPS between genotypes.*

5.3.1.11 LPS increased acute GFAP-positive astrogliosis in the spinal cord of P301S mice

Densitometric analysis of GFAP stained tissue detected very low levels of GFAP signal in lamina 9 of the spinal cord of saline-injected C57BL/6 mice (Figure 30 and Table 34). There was no independent effect of genotype. LPS had no effect on acute astrogliosis in the spinal cord of control mice. The percentage area containing GFAP signal was higher in LPS-injected P301S mice than all other groups; post hoc analysis indicated there was a significant increase in astrogliosis in LPS-injected P301S mice compared with saline-injected counterparts (additional 3.4%; p=0.049; 95% CI 0.0 to 6.7) (Figure 30 and Table 34) however the differential impact of LPS on P301S mice compared with controls was not significant at α=0.05 (Figure 30 and Table 34).

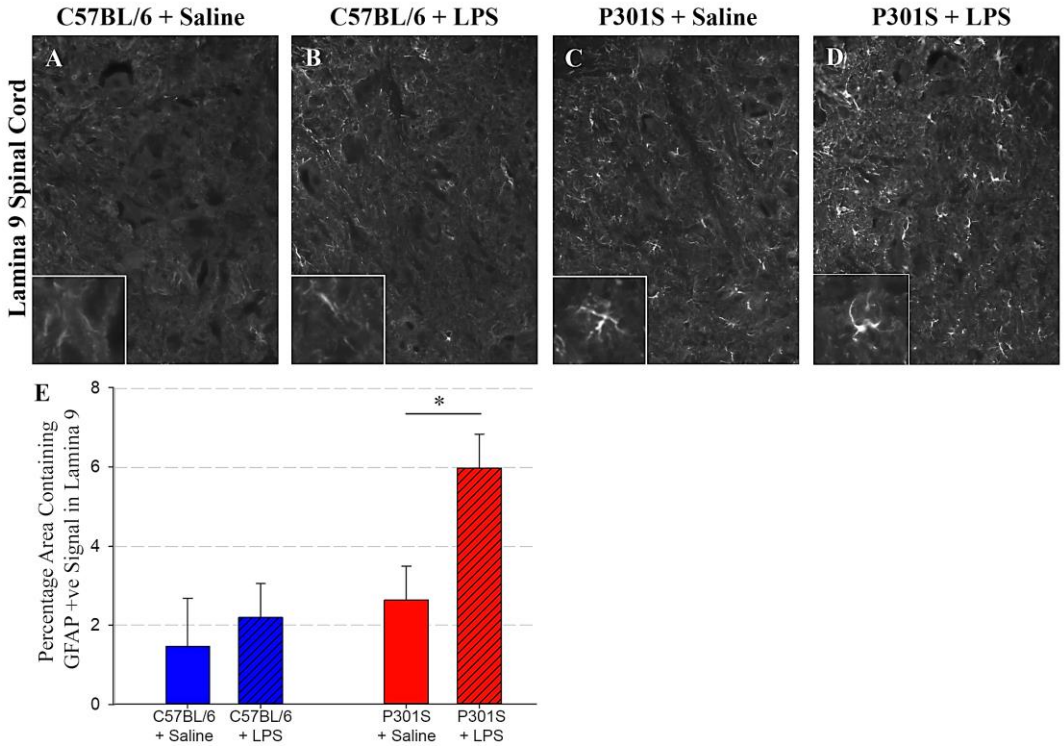

Figure 30 - Systemic LPS induced significant GFAP-positive reactive astrogliosis in the spinal cord of P301S mice 24-hours post-injection. A-D; *Representative examples of GFAP stained spinal cord (lamina 9 of c5-c7) from C57BL/6 + Saline* ***(A)****, C57BL/6 + LPS* ***(B)****, P301S + Saline* ***(C)****, P301S + LPS* ***(D)****. Scale bar 100 µm.* ***E)*** *Densitometric analysis of lamina 9 of the spinal cord showed no significant difference between P301S mice and no impact of LPS in control mice however LPS caused an increase in astrogliosis in P301S mice (mixed effects regression, indicated by *p<0.05). (C57BL/6 + Saline n=3, C57BL/6 + LPS n=6, P301S + Saline n=6, P301S + LPS n=6).*

Condition	% Area GFAP signal	Δ % Area GFAP signal	p-value	95% CI	
Reference (C57BL/6 + Saline)	1.5	-	0.247	-1.1	4.0
LPS	2.2	0.7	0.628	-2.4	3.9
P301S	2.6	1.2	0.442	-2.0	4.3
P301S + LPS (interaction term)	6.0	2.6	0.191	-1.4	6.7

Table 34 - ***Systemic LPS induced significant GFAP-positive reactive astrogliosis in the spinal cord of P301S mice 24-hours post-injection.*** *The first term represents percentage area containing GFAP signal for the reference group: C57BL/6 mice receiving saline. The following two terms test for an independent effect of genotype and intervention. The fourth term tests for a difference in the independent effect of LPS between genotypes.*

5.3.2 Summary of acute pathology

Acutely LPS-injection significantly increased the number of AT8-positive cells in the brains of P301S mice. LPS-treatment had no impact on microglia in the cortices but induced microgliosis in the spinal cord of P301S and C57BL/6 mice. LPS increased IL-1β mRNA levels in the brains and spinal cords of C57BL/6 mice and P301S mice. LPS-injection increased GFAP expression in the brains of C57BL/6 and P301S mice and in the spinal cord of P301S mice.

Tissue	Pathological hallmark	C57BL/6 + Saline	C57BL/6 + LPS	P301S + Saline	P301S + LPS
Cortex	AT8-positive cells per mm²	0	0	4.0	**13.2**
	CD11b (mRNA Relative Quantity)	1.0	1.1	1.0	1.1
	IBA1-positive cells per mm²	244.6	310.7	251.4	287.8
	IL-1β (mRNA Relative Quantity)	1	**23.4**	0.8	**11.8**
	GFAP (mRNA Relative Quantity)	1.0	**2.0**	1.3	**2.0**
	% Area containing GFAP +ve Signal	0.7	2.2	**3.4**	5.4
Spinal cord	AT8-positive cells per mm²	0	0	**22.7**	37.8
	CD11b (mRNA Relative Quantity)	1	**1.4**	1.3	**1.9**
	% Area containing IBA1 +ve Signal	3.6	**7.1**	3.1	**5.5**
	IL-1β (mRNA Relative Quantity)	1.0	**74.1**	2.5	**46.9**
	GFAP (mRNA Relative Quantity)	1.0	1.0	**2.3**	2.9
	% Area containing GFAP +ve Signal	1.5	2.2	2.6	**6.0**

Table 35 – Summary table of acute impact of LPS on pathological markers. *Values refer to estimated means of pathological markers for each group. Bold black font is used to indicate a significant effect of LPS or genotype compared with C57BL/6 mice given saline ($p < 0.05$), except in the final column where bold black font indicates significance compared with saline-injected P301S mice ($p < 0.05$).*

5.3.3 Chronic Pathology

The horizontal bar task indicated an advanced decline in the P301S mice exposed to LPS. These mice were sacrificed at 22 weeks of age to investigate the neuropathological consequences at end stage.

5.3.3.1 No effect of LPS-injection on AT8-positive cell counts in P301S mice at end stage

There were no AT8-positive cells in the motor cortex of C57BL/6 mice regardless of LPS exposure (Figure 31). However, AT8-positive cells were detected in the motor cortex of P301S mice, (65.8 cells per mm^2; $p<0.001$; 95% CI 48.6 to 83.1) (Figure 31) and LPS treatment had no impact on the number of AT8-positive cells at 22 weeks of age (-1.8 cells per mm^2; $p=0.876$; 95% CI -27.5 to 23.8) (Figure 31).

There were no AT8-positive cells in lamina 9 of the spinal cord of C57BL/6 mice regardless of LPS exposure (Figure 31). AT8-positive cells were seen in P301S mice (123.8 cells per mm^2; $p<0.001$; 95% CI 101.2 to 146.4) and LPS exposure did not significantly impact numbers (additional 26.3 cells per mm^2; $p=0.143$; 95% CI -10.5 to 63.1) (Figure 31).

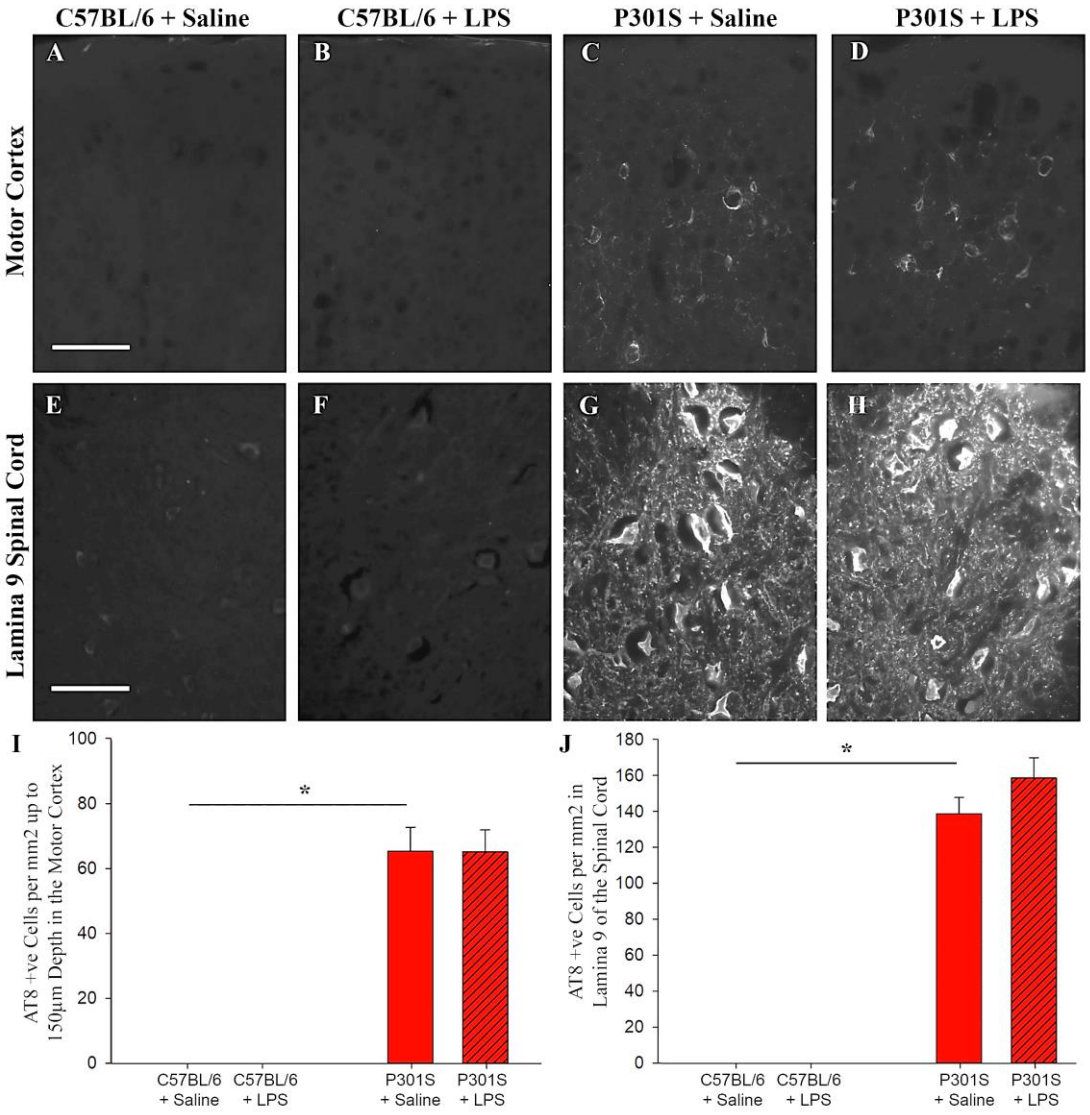

Figure 31 - Chronic impact of systemic LPS on AT8-positive tau in the brain and spinal cord. A-D; *Representative examples of AT8 stained cortical tissue collected 24h post-injection from C57BL/6 + Saline (**A**), C57BL/6 + LPS (**B**), P301S + Saline (**C**), P301S + LPS (**D**).* ***E-H;*** *Representative examples of AT8 stained spinal cord (lamina 9 of c5-c7) from C57BL/6 + Saline (**E**), C57BL/6 + LPS (**F**), P301S + Saline (**G**), P301S + LPS (**H**). Scale bar 100 µm* ***I)*** *AT8-positive cell counts in the motor cortex (to sub-pial depth of 150 µm) from C57BL/6 (blue) and P301S (red) mice collected at age 22weeks following injection at 16 weeks with either saline (no pattern) or LPS (patterned) indicate no significant impact of LPS (mixed effects linear regression) (C57BL/6 + Saline n=3, C57BL/6 + LPS n=3, P301S + Saline n=7, P301S + LPS n=6).* ***J)*** *AT8-positive cell counts conducted in lamina 9 of spinal cord indicate no lasting impact of LPS (C57BL/6 + Saline n=4, C57BL/6 + LPS n=4, P301S + Saline n=8, P301S + LPS n=5).*

5.3.3.2 LPS-injection results in cortical neuronal loss in both P301S and C57BL/6 mice

NeuN-positive cell counts in the superficial layers of the cortex showed marked neuronal loss in P301S mice compared with C57BL/6 mice (Figure 32 and Table 36). LPS-injection reduced the number of NeuN-positive cells in C57BL/6 mice (Figure 32 and Table 36) and in P301S mice (post hoc analysis: -164.1 cells per mm^2; p=0.016; 95% CI -286.9 to -41.3). LPS had no differential impact on neuronal counts in P301S mice compared with C57BL/6 mice (Figure 32 and interaction term Table 36).

Condition	Cells per mm2	Δ Cells per mm2	p-value	95% CI	
Reference Cells per mm^2 (C57BL/6 + Saline)	1089.3	-	<0.001	982.0	1196.6
LPS	915.6	**-173.6**	**0.023**	**-320.0**	**-27.4**
P301S	806.1	**-283.1**	**0.003**	**-452.8**	**-113.5**
P301S + LPS (interaction term)	642.0	9.5	0.931	-219.5	238.6

*Table 36 - **NeuN-positive cell counts indicate significant long term LPS-induced neuronal loss in the brain of C57BL/6 and P301S mice** The first term represents NeuN-positive cells per mm2 for the reference group: C57BL/6 mice receiving saline. The following two terms test for an independent effect of genotype and intervention. The fourth term tests for a difference in the independent effect of LPS between genotypes.*

5.3.3.3 No effect of LPS-injection on spinal cord NeuN-positive cell counts in P301S mice

There was significant neuronal loss in the spinal cord of P301S mice compared with C57BL/6 mice at 22 weeks of age (Figure 32 and **Table 37**). LPS had no effect on NeuN cell counts in C57BL/6 or P301S mice (Figure 32 and **Table 37**).

Condition	Cells per mm2	Δ Cells per mm2	p-value	95% CI	
Reference Cells per mm^2 (C57BL/6 + Saline)	93.7	-	<0.001	76.0	111.3
LPS	86.4	-7.3	0.554	-32.2	17.6
P301S	27.7	**-65.9**	**<0.001**	**-90.8**	**-41.0**
P301S + LPS (interaction term)	24.2	3.7	0.833	-32.1	39.6

Table 37 - NeuN-positive cell counts indicate no significant long term LPS-induced neuronal loss in the spinal cord of C57BL/6 or P301S mice. *The first term represents NeuN-positive cells per mm^2 for the reference group: C57BL/6 mice receiving saline. The following two terms test for an independent effect of genotype and intervention. The fourth term tests for a difference in the independent effect of LPS between genotypes.*

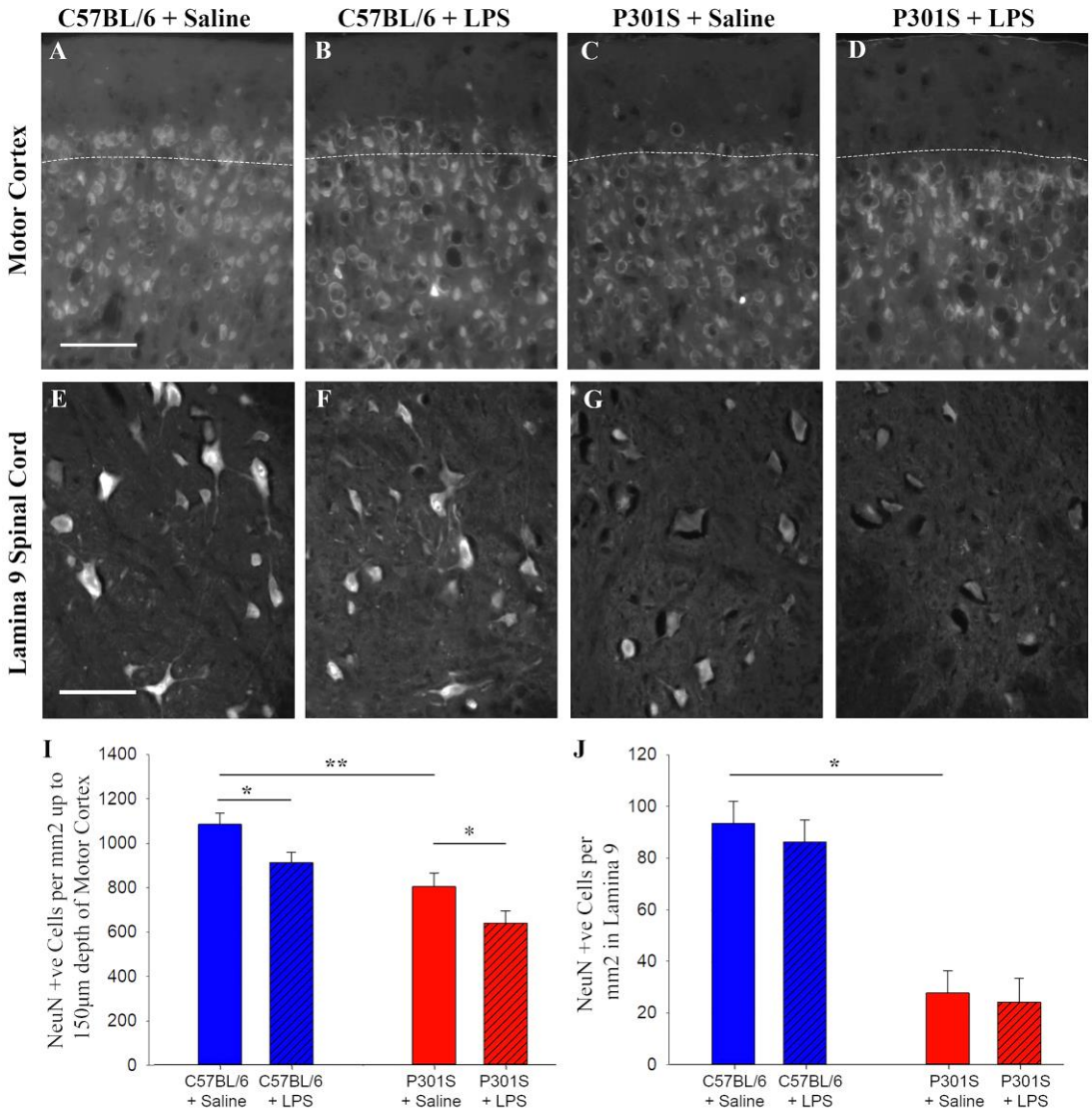

Figure 32 - NeuN-positive cell counts indicate significant long term LPS-induced neuronal loss in the brain but not spinal cord of C57BL/6 and P301S mice. A-D; *Representative examples of NeuN stained cortical tissue collected at 22 weeks of age from C57BL/6 + Saline (**A**), C57BL/6 + LPS (**B**), P301S + Saline (**C**), P301S + LPS (**D**).* ***E-H;*** *Representative examples of NeuN stained spinal cord (lamina 9 of c5-c7) from C57BL/6 + Saline (**E**), C57BL/6 + LPS (**F**), P301S + Saline (**G**), P301S + LPS (**H**). Scale bar 100 µm (**A-H**).* ***I;*** *NeuN-positive cell counts in the motor cortex (to sub-pial depth of 150 µm) from C57BL/6 (blue) and P301S (red) mice injected with either saline (no pattern) or LPS (patterned) indicated significant neuronal loss in P301S mice compared with controls (mixed effects linear regression, **p<0.005). LPS impacted NeuN-positive cell counts in C57BL/6 mice, and P301S mice (*p<0.05) (C57BL/6 + Saline n=6, C57BL/6 + LPS n=7, P301S + Saline n=4, P301S + LPS n=5).* ***J****) NeuN-positive cell counts in lamina 9 of the spinal cord indicated significant neuronal loss in P301S mice compared with controls (*p<0.0001) but no effect of LPS NeuN-positive cell counts. (C57BL/6 + Saline n=8, C57BL/6 + LPS n=8, P301S + Saline n=8, P301S + LPS n=8).*

5.3.3.4 **LPS has no long-term impacts on IBA1-positive cortical microgliosis**

Tissue collected at 22 weeks of age was stained for pan-microglial marker IBA1. As before, IBA1-positive cell counts in the superficial layers of the cortex indicated no significant difference between any of the groups (Figure 33 and Table 38).

Condition	Cells per mm²	Δ Cells per mm²	p-value	95% CI	
Reference Cells per mm² (C57BL/6 + Saline)	181.3	-	0.000	138.4	224.2
LPS	239.2	57.9	0.068	-4.8	120.5
P301S	221.6	40.3	0.149	-15.9	96.6
P301S + LPS (interaction term)	213.6	-66.5	0.114	-150.7	17.6

*Table 38 - **Systemic LPS has no impact on IBA1-positive microglia in the cortex at end stage** The first term represents IBA1-positive cells per mm² for the reference group: C57BL/6 mice receiving saline. The following two terms test for an independent effect of genotype and intervention. The fourth term tests for a difference in the independent effect of LPS between genotypes. Post hoc analysis to compare P301S + LPS with P301S + Saline: indicated additional 36.3; p=0.461; 95% CI -76.6 to 149.2.*

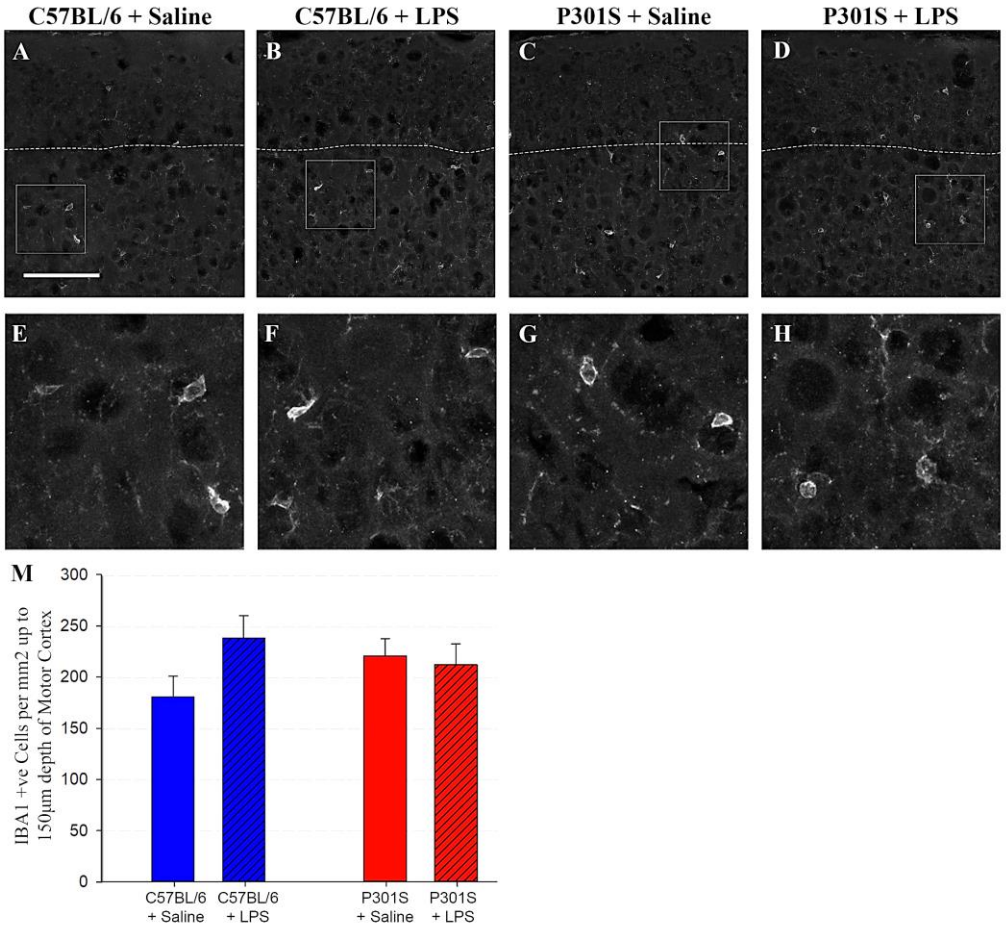

Figure 33 *- **Systemic LPS has no impact on IBA1-positive microglia in the cortex at end stage. A-D;** Representative examples of IBA1 stained cortical tissue collected 24h post-injection from C57BL/6 + Saline (**A**), C57BL/6 + LPS (**B**), P301S + Saline (**C**), P301S + LPS (**D**). **E-H;** Close-up of microglial morphology; C57BL/6 + Saline (**E**), C57BL/6 + LPS (**F**), P301S + Saline (**G**), P301S + LPS (**H**). Scale bar 100 µm (**A-H**). **I** IBA1-positive cell counts in the motor cortex (to sub-pial depth of 150 µm) from C57BL/6 (blue) and P301S (red) mice collected 24-hours post-injection with either saline (no pattern) or LPS (patterned) indicate that neither genotype nor LPS exposure significantly impacted IBA1-positive microglial cell counts in the motor cortex. (mixed effects linear regression) (C57BL/6 + Saline n=6, C57BL/6 + LPS n=7, P301S + Saline n=6, P301S + LPS n=6).*

5.3.3.5 LPS-treatment significantly increases IBA1-positive microgliosis in Lamina 9 of the spinal cord of P301S mice at end stage

IBA1-positive cell counts in lamina 9 of the spinal cord indicate significant microgliosis in P301S mice (Figure 34 and Table 39). LPS did not impact IBA1-positive cell density in C57BL/6 mice at 22 weeks (Figure 34 and Table 39). There was a significant increase in the number of IBA1-positive cells in the spinal cord of P301S mice and LPS significantly increased the number of microglial cells in P301S mice (additional 133.6 cells per mm^2; p=0.003; 95% CI 52.7 to 214.6). The differential impact of LPS was also greater in P301S mice than control mice (Figure 34 and interaction term Table 39).

Densitometric analysis confirmed these results. There was a disease-associated increase in the percentage area containing IBA1 signal in lamina 9 of P301S mice (Figure 34 and Table 39). LPS induced an increase in the percentage area containing IBA1-positive signal in C57BL/6 mice and a further increase in P301S mice (Figure 34 and Table 39). Again, the differential effect of LPS was greater in P301S mice than control mice (Figure 34 and Table 39).

Condition	Cells per mm²	Δ Cells per mm²	p-value	95% CI		% Area IBA1 signal	Δ % Area IBA1 signal	p-value	95% CI	
Reference (C57BL/6 + Saline)	198.6	-	<0.001	151.1	246.0	1.7	-	<0.001	0.9	2.4
LPS	244.8	+46.2	0.156	-18.8	111.1	3.1	**1.4**	**0.012**	**0.3**	**2.5**
P301S	417.3	**+218.7**	**<0.001**	**153.7**	**283.7**	3.9	**2.3**	**0.001**	**1.2**	**3.3**
P301S + LPS (interaction term)	550.9	+87.5	0.061	-4.4	179.3	7.0	**1.7**	**0.036**	**0.1**	**3.2**

Table 39 - Systemic LPS has a differential impact on IBA1-positive microglia in lamina 9 of the spinal cord of P301S mice. *The first term represents IBA1-positive cells per mm² or percentage area containing IBA1 signal for the reference group: C57BL/6 mice receiving saline. The following two terms test for an independent effect of genotype and intervention. The fourth term tests for a difference in the independent effect of LPS between genotypes.*

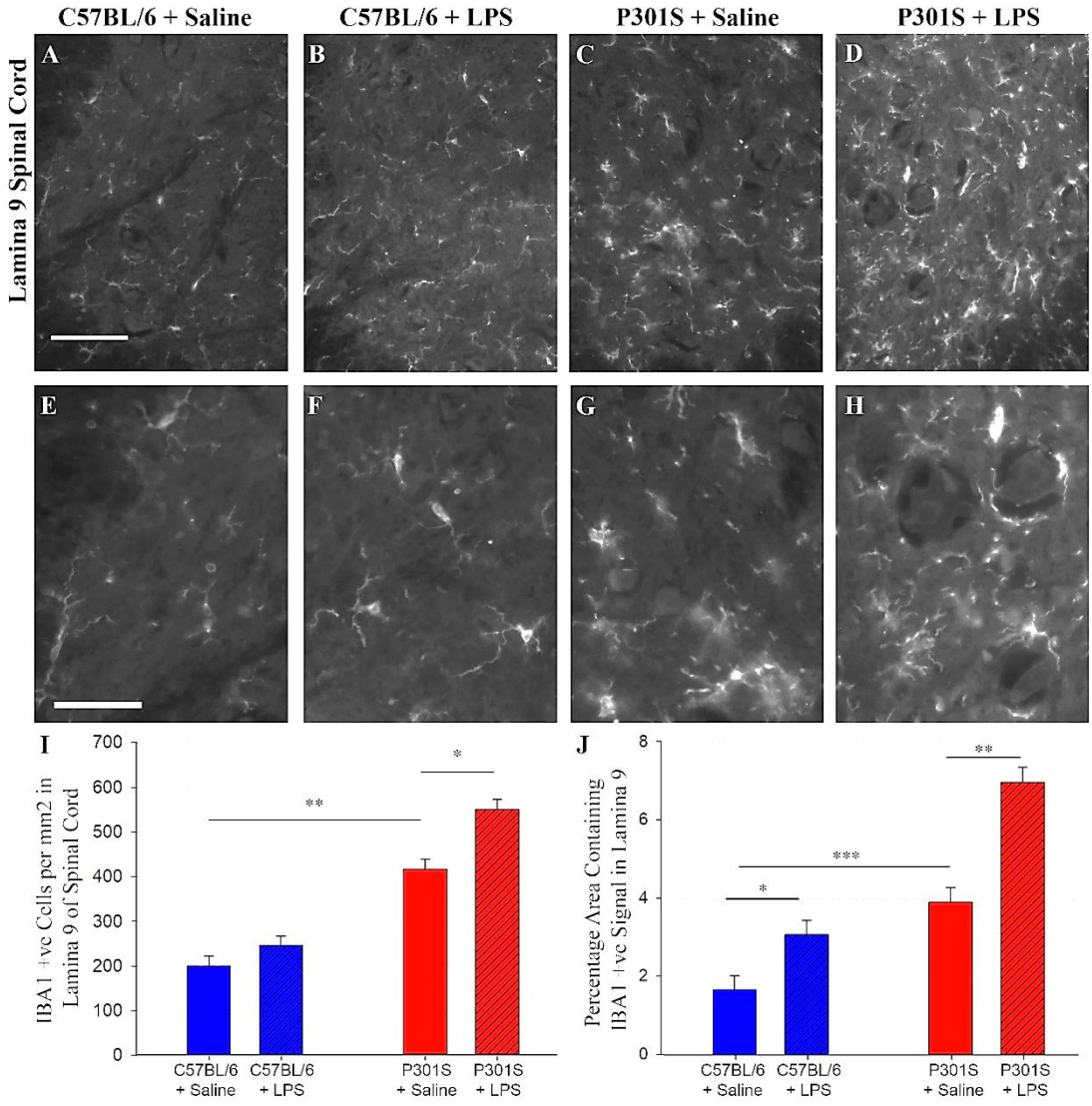

***Figure 34** - **Systemic LPS has a differential impact on IBA1-positive microglia in lamina 9 of the spinal cord of P301S mice. A-D)** Representative examples of IBA1 stained spinal cord (lamina 9 of c5-c7) from C57BL/6 + Saline (**A**), C57BL/6 + LPS (**B**), P301S + Saline (**C**), P301S + LPS (**D**). **E-H)** Close up of microglial morphology from C57BL/6 + Saline (**E**), C57BL/6 + LPS (**F**), P301S + Saline (**G**), P301S + LPS (**H**). **I)** IBA1-positive cell counts in lamina 9 of the spinal cord indicate that P301S mice have more IBA1-positive cells than controls (indicated by **p<0.0001) and LPS induced a further increase (indicated by *p<0.001) (C57BL/6 + Saline n=8, C57BL/6 + LPS n=8, P301S + Saline n=8, P301S + LPS n=7). **J)** Densitometric analysis indicated more IBA1 signal in P301S mice compared with controls (mixed effects linear regression, indicated by ***p<0.0001) and LPS induced an increase in the area containing IBA1 signal in both controls and P301S mice (indicated by *p<0.05, **p=0.001).*

5.3.3.6 LPS-treatment significantly increases IBA1-positive microgliosis in the rubrospinal tract of P301S mice at end stage

Previous analyses have focussed on lamina 9 of the spinal cord since this area is enriched with AT8-positive motor neurons which degenerate and contribute to the hind limb pathology of P301S mice. However there was striking microgliosis in the rubrospinal tract at 22 weeks of age. This area contains axon fibres which descend from the red nucleus, combining information from the motor cortex and the cerebellum and synapse with interneurons and motor neurons hence this system establishes rudimental motor skills that are refined by further corticospinal input (Martinez-Lopez et al., 2015) (see **Figure 3** for anatomical schematic).

Densitometric analysis of the rubrospinal tract indicated an increase in the percentage area containing IBA1 signal in P301S mice (Figure 35 and Table 40). LPS exposure caused a significant increase in IBA1 signal in P301S mice (additional 2.6% compared with saline-injected P301S; p<0.001; 95% CI 1.5 to 3.8) but not C57BL/6 mice (Figure 35). The effect of LPS was also greater in P301S mice than control mice when formally tested (Figure 35 and Table 40).

Condition	% Area IBA1 signal	Δ % Area IBA1 signal	p-value	95% CI	
Reference (C57BL/6 + Saline)	1.1	-	<0.001	0.6	1.7
LPS	1.9	**+0.7**	**0.069**	**-0.1**	**1.5**
P301S	2.4	**+1.3**	**0.002**	**0.5**	**2.1**
P301S + LPS (interaction term)	5.1	**+1.9**	**0.002**	**0.7**	**3.1**

Table 40 - Systemic LPS has a differential impact on IBA1-positive microglia in the rubrospinal tract of the spinal cord of P301S mice. *The first term represents IBA1-positive cells per mm² or percentage area containing IBA1 signal for the reference group: C57BL/6 mice receiving saline. The following two terms test for an independent effect of genotype and intervention. The fourth term tests for a difference in the independent effect of LPS between genotypes.*

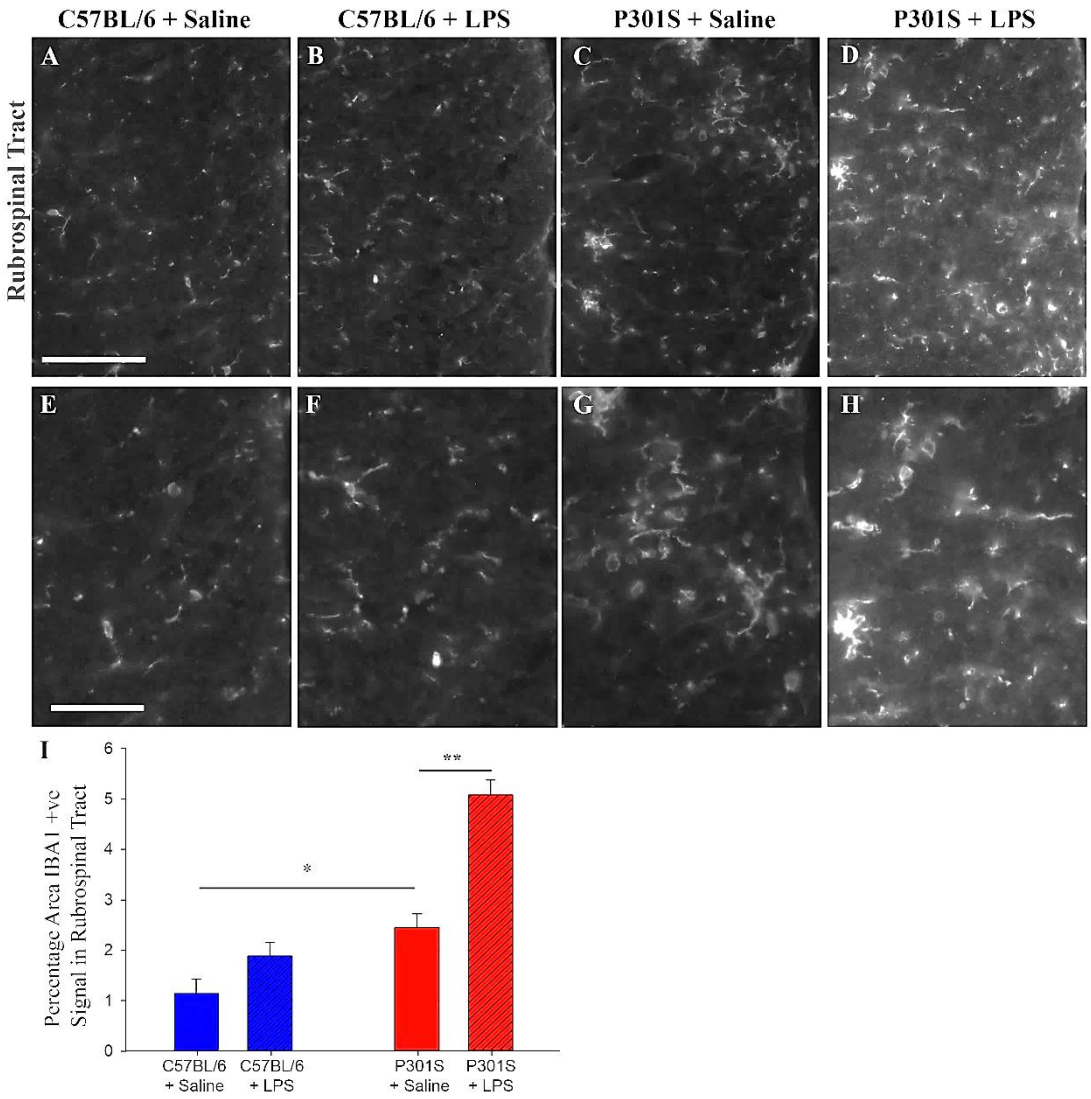

Figure 35 - Systemic LPS has a differential impact on IBA1-positive microglia in the rubrospinal tract of the spinal cord of P301S mice. A-D; *Representative examples of IBA1 stained spinal cord rubrospinal tract (of c5-c7) from C57BL/6 + Saline (**A**), C57BL/6 + LPS (**B**), P301S + Saline (**C**), P301S + LPS (**D**).* ***E-H)*** *Close-up of microglial morphology from C57BL/6 + Saline (**E**), C57BL/6 + LPS (**F**), P301S + Saline (**G**), P301S + LPS (**H**).* ***I)*** *Densitometric analysis indicated more IBA1 signal in P301S mice compared with controls (mixed effects linear regression, indicated by *p<0.005) and LPS induced an increase in the area containing IBA1 signal in P301S mice (indicated by **p<0.001).*

5.3.3.7 LPS-treatment reduced GFAP-positive cortical astrogliosis in P301S mice at end-stage

As expected, by end stage there was significant disease-associated cortical astrogliosis in P301S mice compared to C57BL/6 mice (Figure 36 and Table 41). Acutely LPS exposure increased astrogliosis, however, LPS had no lasting impact on cortical astrogliosis in C57BL/6 mice (Figure 36 and Table 41). At 22 weeks there was an apparent *reduction* in the number of GFAP-positive cells in the cortex of LPS-injected P301S mice compared with saline-injected counterparts (-81.4 cells per mm^2; p=0.088; 95% CI -146.3 to 29.6) (Figure 36 and Table 41).

Densitometric analysis of the motor cortex confirmed the disease-associated increase in the percentage area containing GFAP signal in P301S mice compared with C57BL/6 mice (Figure 36 and Table 41). Exposure to LPS had no effect on percentage area containing GFAP signal in control mice and again resulted in an apparent reduction in GFAP signal in P301S mice compared with saline-injected counterparts (Figure 36 and Table 41).

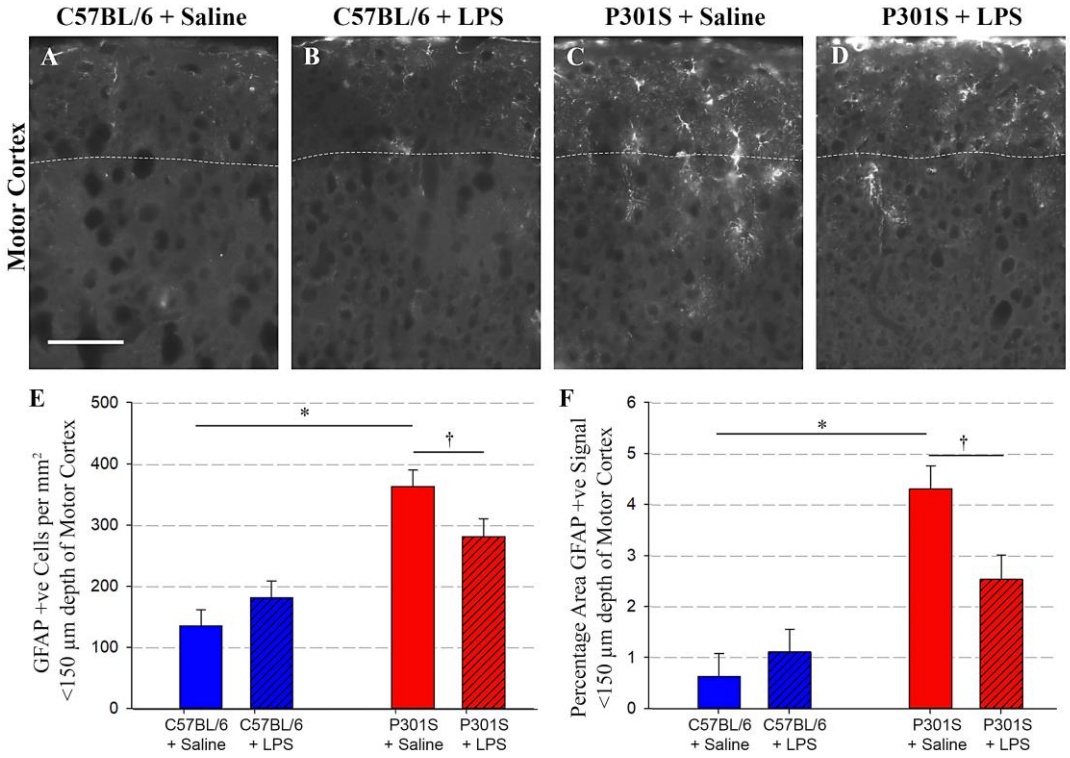

***Figure 36** - **No chronic impact of systemic LPS on GFAP-positive reactive astrocytes in the brain. A-D;** Representative examples of GFAP stained cortical tissue collected at 22 weeks of age from C57BL/6 + Saline (**A**), C57BL/6 + LPS (**B**), P301S + Saline (**C**), P301S + LPS (**D**). **E-H;** Scale bar 100 µm. **E)** GFAP-positive cell counts in the motor cortex (to sub-pial depth of 150 µm) from C57BL/6 (blue) and P301S (red) mice injected with either saline (no pattern) or LPS (patterned) indicate significant astrogliosis in P301S mice compared with controls but no significant long term impact of LPS (mixed effects linear regression, indicated by †p=0.088 *p<0.0001). **F)** Densitometric analysis in the same area support these results (mixed effects linear regression, indicated by †p=0.070, *p<0.0001) (C57BL/6 + Saline n=8, C57BL/6 + LPS n=8, P301S + Saline n=8, P301S + LPS n=8).*

Condition	Cells per mm²	Δ Cells per mm²	p-value	95% CI		% Area IBA1 signal	Δ % Area IBA1 signal	p-value	95% CI	
Reference (C57BL/6 + Saline)	135.4	-	<0.001	80.1	190.7	0.6	-	0.166	-0.3	1.6
LPS	181.9	+46.5	0.232	-31.7	124.7	1.1	0.5	0.457	-0.8	1.8
P301S	363.8	**+228.4**	**<0.001**	**150.1**	**306.8**	4.3	**3.7**	**<0.001**	**2.4**	**5.0**
P301S + LPS (interaction term)	282.2	**-128.1**	**0.028**	**-241.2**	**-15.0**	2.5	**-2.3**	**0.020**	**-4.1**	**-0.4**

Table 41 - No chronic impact of systemic LPS on GFAP-positive reactive astrocytes in the brain. *The first term represents GFAP-positive cells per mm² or percentage area containing GFAP signal for the reference group: C57BL/6 mice receiving saline. The following two terms test for an independent effect of genotype and intervention. The fourth term tests for a difference in the independent effect of LPS between genotypes.*

5.3.3.8 LPS-treatment reduced GFAP-positive astrogliosis in lamina 9 of the spinal cord of P301S mice at end-stage

The morphology of astrocytes in the spinal cord at end stage made it very difficult to count cells. Densitometric analysis of lamina 9 of the spinal cord indicated significant disease-associated astrogliosis in P301S mice compared with C57BL/6 mice (Figure 37 and Table 42). LPS had no significant effect on acute astrogliosis in the spinal cord of control mice (Figure 37 and Table 42). Acutely LPS caused an increase in astrogliosis in P301S mice, however at end stage there was an apparent reduction in GFAP signal in the spinal cord of P301S mice as seen in the cortical tissue, although not significant at α=0.05 (-1.8%; p=0.254; CI 95% -5.1 to 1.5) (Figure 37).

Condition	% Area GFAP signal	Δ % Area GFAP signal	p-value	95% CI	
Reference (C57BL/6 + Saline)	0.9	-	0.217	-0.6	2.5
LPS	0.7	-0.2	0.856	-2.3	2.0
P301S	9.9	**9.0**	**<0.001**	**6.8**	**11.1**
P301S + LPS (interaction term)	8.1	-1.6	0.289	-4.7	1.5

Table 42 - No chronic impact of systemic LPS on GFAP-positive reactive astrocytes in the spinal cord. *The first term represents percentage area containing GFAP signal for the reference group: C57BL/6 mice receiving saline. The following two terms test for an independent effect of genotype and intervention. The fourth term tests for a difference in the independent effect of LPS between genotypes.*

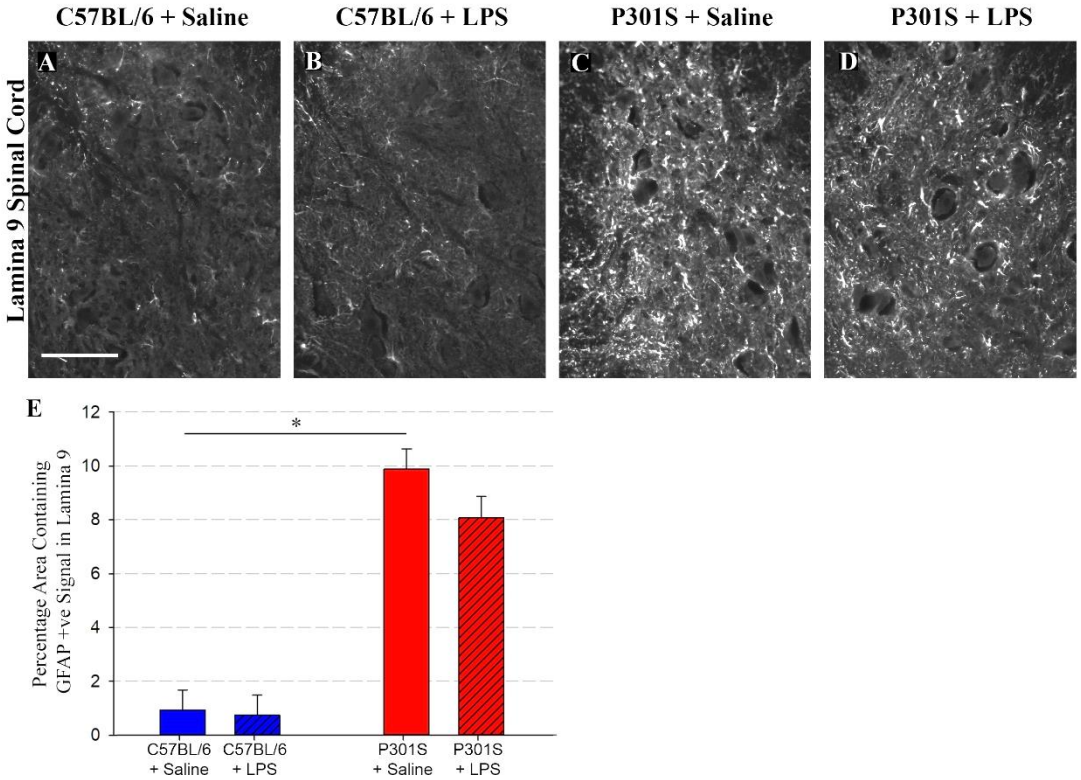

Figure 37 - No chronic impact of systemic LPS on GFAP-positive reactive astrocytes in the spinal cord. ***A-D;*** *Representative examples of GFAP stained spinal cord (lamina 9 of c5-c7) from C57BL/6 + Saline (**A**), C57BL/6 + LPS (**B**), P301S + Saline (**C**), P301S + LPS (**D**). Scale bar 100 µm* ***E)*** *Densitometric analysis of lamina 9 of the spinal cord showed significant astrogliosis in P301S mice but no lasting effect of LPS on GFAP-positive reactive astrocytes (*p<0.0001). (C57BL/6 + Saline n=8, C57BL/6 + LPS n=8, P301S + Saline n=8, P301S + LPS n=8).*

5.3.4 Summary of chronic pathology

At end stage, there was significant tau pathology and neuronal loss in the cortex and lamina 9 of the spinal cord of P301S mice. LPS-injection had no lasting impact on AT8-positive tau pathology in the cortex or spinal cord. LPS-injection induced additional cortical neuronal loss which was equivalent in C57BL/6 and P301S mice but LPS-injection did not impact neuronal counts in the spinal cord. There was no cortical microgliosis in P301S or C57BL/6 mice at end stage regardless of LPS exposure. There was, however, significant microgliosis in the spinal cord of P301S mice and LPS-exposure increased that microgliosis further still. There was also significant reactive astrogliosis in the brain and spinal cord of P301S mice which was *reduced* in LPS-injected P301S mice compared with saline-treated mice.

Tissue	Pathological hallmark	C57BL/6 + Saline	C57BL/6 + LPS	P301S + Saline	P301S + LPS
Cortex	AT8-positive cells per mm²	0	0	**65.8**	63.8
	NeuN-positive cells per mm²	1089.3	**915.6**	**806.1**	**642.0**
	IBA1-positive cells per mm²	181.3	239.2	221.6	213.6
	% Area containing GFAP +ve Signal	0.6	1.1	**4.3**	**2.5**
Spinal cord	AT8-positive cells per mm²	0	0	**123.8**	149.9
	NeuN-positive cells per mm²	93.7	86.4	**27.7**	24.2
	% Area containing IBA1 +ve Signal	1.7	**3.1**	**3.9**	**7.0**
	% Area containing GFAP +ve Signal	0.9	0.7	**9.9**	8.1

Table 43– Summary table of impact of LPS on pathological markers at end stage. *Values refer to estimated mean measures of pathological markers for each group. Bold black font is used to indicate a significant effect of LPS or genotype compared with C57BL/6 mice given saline ($p < 0.05$) except in the final column where bold black font indicates significance compared with saline-injected P301S mice ($p < 0.05$). Underlined font indicates a differential effect of LPS in P301S mice compared with C57BL/6 mice ($p < 0.05$).*

5.4 Discussion

LPS-injection exacerbated AT8-positive tau pathology in the brain and spinal cord of P301S mice when assessed 24-hours post-injection (Figure 18). Although this acute increase in tau pathology did not persist to end stage, there was evidence of increased neuronal death at end stage.

That is to say, there is already significant superficial cortical neuronal loss in P301S mice compared with C57BL/6 mice at end stage (22 weeks) but the data presented here demonstrate that a single dose of intraperitoneal LPS (500 μg/kg) at 16 weeks of age is sufficient to cause additional cortical neuronal loss in P301S mice, as well as C57BL/6 mice (Figure 32).

Analysis of whether glial cells might contribute to this exacerbation of pathology did not yield conclusive results. IBA1-positive cell counts and CD11b mRNA levels indicated a lack of cortical microgliosis in P301S mice, regardless of age and there was no observed increase in cortical microgliosis following LPS-injection (Figure 19, Figure 20, and Figure 33). Nonetheless, there was a robust increase in IL-1β mRNA levels in the cortex and spinal cord of P301S mice and C57BL/6 mice 4-hours post-LPS-injection (Figure 21 and Figure 25) which could conceivably contribute to the observed LPS-induced pathology.

In the spinal cord, where there is disease-associated microgliosis, LPS acutely induced IBA-1 labelling in both P301S mice and C57BL/6 mice (Figure 24). These cells did not show exaggerated IL-1β responses to LPS in P301S mice and do not appear to be primed. Nonetheless, when examined at end stage there was increased disease-associated microgliosis and further exacerbation in LPS-injected P301S mice (Figure 34 -Figure 35).

LPS also caused an acute increase in GFAP signal in P301S mice and C57BL/6 mice but in the long-term LPS-injection reduced disease-associated GFAP-positive astrogliosis in the brain and spinal cord (Figure 36 Figure 37).

Therefore, LPS has acute impacts on tau pathology and has lasting impacts on cortical neuronal death and spinal cord microgliosis. The contribution of microglia, astrocytes or IL-1β in the pathological deficits observed remain undetermined.

5.4.1 Systemic inflammation exacerbated tau pathology in P301S mice and caused cortical neuronal loss in C57BL/6 and P301S mice

In chapter 3 progressive neuronal loss and astrogliosis were demonstrated in the superficial layers of the cortex in the absence of apparent microgliosis. Meanwhile there was significant progressive microgliosis in lamina 9 of the spinal cord. The same disease-relevant areas were studied in this chapter to investigate the acute and long-term impacts of systemic inflammation on these key pathological hallmarks and the potential interactions between systemic inflammation and disease pathology.

LPS-injection at 16 weeks of age acutely increased AT8-positive hyperphosphorylated tau pathology in the motor cortex and spinal cord of P301S mice, but not C57BL/6 mice, (Figure 18) and yet LPS-injection induced significant cortical neuronal loss in both P301S *and* C57BL/6 mice and failed to induce neuronal loss in the spinal cord of either. This poses interesting questions regarding the mechanisms of LPS-induced tau phosphorylation and neuronal loss and whether the two are related.

It remains to be determined whether the increase in AT8-staining represents an increase in overall transgene expression and therefore total tau or an increase in *phosphorylation* of tau. Tau expression in the P301S mouse is driven by the Thy 1.2 promoter. Thy 1 expression is developmentally and dynamically regulated and there is evidence to suggest that Thy 1 is upregulated by cytokines including IL-1β and TNF-α (Ishizu et al., 1997). However, Kitazawa et al. (2005) used a chronic systemic LPS protocol (500 μg/kg twice per week for 6 weeks) to investigate the effects of systemic inflammation in 3xTgAD mice which express mutant tau under the same Thy 1.2 promoter. They demonstrated markedly increased tau pathology following peripheral LPS injection but total human tau levels remained constant indicating that

the increased tau pathology was not due to increased transgene expression, but there was a 2-fold increase in AT8 and AT180 immunoreactivity in the hippocampus. From this work, we might infer that the increase in AT8 staining shown here in P301S mice is unlikely due to an increase in transgene expression since 3xTgAD and P301S mice share the same Thy 1.2 promoter although this still must be verified.

How, then, did LPS increase tau phosphorylation in P301S mice and not C57BL/6 mice? It has previously been demonstrated that intraperitoneal LPS-injection (100 μg/kg) into young, healthy C57BL/6 mice was sufficient to induce a transient increase in tau hyperphosphorylation in the hippocampus (visualised by AT8 and PHF) which returned to baseline levels by 4-hours post LPS (Roe et al., 2011). Tau phosphorylation status is dependent on the balance between kinase and phosphatase activity; LPS-injection induced the transient activation of tau kinases, GSK-3 and cyclin-dependent kinase-5 (CDK5) activator proteins p25 and p35 (Roe et al., 2011). Thus, transient tau hyperphosphorylation is a known response to systemic inflammation in wild-type mice and the absence of AT8-positive pathology in C57BL/6 mice 24-hours post-LPS-injection is likely due to restoration of baseline phosphorylation status due to the proper balance of kinase and phosphatase reactions in C57BL/6 mice.

It is likely that the over-expression of human P301S tau increases the propensity for the hyperphosphorylation of tau protein in neurons and delays, or perhaps prevents totally, the restoration of the normal phosphorylation status via several mechanisms: first, over-expression of human mutant tau protein provides abundant substrate for the LPS-induced kinases and in doing so shifts the reaction kinetics in favour of hyperphosphorylation; second, there is increased disease-associated activation of tau kinases, including GSK-3, in P301S mice (Allen et al., 2002); third, there is evidence that phosphorylation of tau occurs sequentially such that phosphorylation by CDK5 is required for further phosphorylation by GSK-3β (Li et al., 2006), hence it is plausible that disease-associated tau phosphorylation prior to LPS-injection allows progressive accumulation of increasingly irreversible hyperphosphorylation. These factors likely

contribute to the tau pathology observed in LPS-injected P301S mice but not C57BL/6 mice 24-hours post-injection.

Alternatively, LPS induces transient hypothermia in C57BL/6 mice (Combrinck et al., 2002) and hypothermia is associated with increased tau phosphorylation due to inhibition of temperature-sensitive tau phosphatase, protein phosphatase 2A (PP2A) (Planel et al., 2007). According to data presented in chapter 3 LPS-induced hypothermia might be exaggerated in P301S mice thus potentially influencing tau phosphorylation.

At 22 weeks of age there was a profound disease-associated increase in AT8-positive cell counts in the superficial cortex and the spinal cord of saline-injected P301S mice compared with C57BL/6 mice (Figure 31). In contrast to the acute LPS-induced increase in tau pathology, there was no lasting impact of LPS on tau pathology in P301S mice compared with saline-injected counterparts at end stage (Figure 31). First and foremost, it is worth mentioning that AT8 is just one marker of pathological tau phosphorylated at Ser-202 and Thr-205. Early studies in the P301S mouse showed that human tau in the brain and spinal cord of P301S mouse at end stage is strongly immunoreactive for the following phosphoepitopes: AT8, AT270 (Thr181), pT212 (Thr212), CP3 (Thr214) AT100 (Thr212 and Thr214) AT180 (Thr 231), 12E8 (Ser262 and Ser356), AD2 (Ser395, Ser404), PG5 (Ser 409), and AP422 (Ser 422) (Allen et al., 2002). More than 40 phospho-epitopes have been discovered on tau protein and they are phosphorylated in a hierarchical manner such that there are early and late markers of pathology (Augustinack et al., 2002). AT8 stained the most cells in the P301S mouse compared with alternative markers, and it stains soluble and insoluble tau and does not give information regarding the severity of tau hyperphosphorylation, aggregation or NFT formation. Hence it is plausible that the ubiquitous disease-related AT8 pathology masks any impact of LPS and at this late stage in disease it is possible that alternative markers might better identify LPS-induced differences in phosphorylation status. Silver staining, thioflavin-S immunofluorescence or conformational antibodies Alz50 or anti-NFT antibodies ought to be used to further

characterise the impact of LPS on the severity of tau pathology following LPS injection.

Alternatively, it is plausible that the increased cortical neuronal loss of LPS-treated P301S mice might account for the absence of additional AT8-positive cells at end-stage. In agreement with previously published work there was significant disease-associated neuronal loss in the superficial layers of the motor cortex and lamina 9 of the spinal cord of P301S mice at 22 weeks of age (Figure 32) and importantly, data presented here indicate that LPS induced additional superficial cortical neuronal loss in P301S mice as well as C57BL/6 mice (Figure 32). Interestingly, in lamina 9 of the spinal cord where LPS failed to induce significant neuronal loss of C57BL/6 or P301S mice there was a trend towards LPS-induced increase in tau pathology although this did not reach significance ($p=0.143$) (Figure 31).

Due to the nature of the experiment, tissue was collected at end stage and there were no longitudinal data. Hence, it is unclear when neuronal loss occurred relative to the appearance of tau pathology, that is, whether there was acute or gradual, progressive neuronal loss and whether there was transient tau hyperphosphorylation which rapidly returned to saline-injected levels, or whether LPS-induced tau pathology persisted and was eventually masked by disease associated tau pathology.

The magnitude of LPS-induced neuronal loss in C57BL/6 mice was equivalent to that of P301S mice suggesting that this neuronal loss was not disease-specific or dependent on the LPS-induced tau pathology observed exclusively in P301S mice 24-hours post-injection. A mechanism has not been determined for LPS-induced neuronal loss or increased tau pathology in this instance, however, previously described mechanisms causing acute LPS-induced neuronal loss and LPS-induced tau phosphorylation converge on one molecule; the pro-inflammatory cytokine IL-1β.

Peripheral LPS administration (200 μg/kg) can induce cortical apoptosis in otherwise healthy male Wistar rats as demonstrated by an increased proportion of TUNEL-positive cells from cortical tissue of LPS-injected rats (Nolan et al., 2003). This LPS-induced apoptosis is mediated by IL-1β via IL-1 type 1 receptor (IL-1R1) signalling which causes downstream p38 and JNK activation, cytochrome-c translocation, caspase-3 activation, accumulation of reactive oxygen species (ROS) and DNA-fragmentation (Lynch et al., 2002, Martin et al., 2002, Nolan et al., 2003, Lynch et al., 2004, Xie et al., 2004). LPS-induced apoptosis, cytochrome c translocation and caspase 3 activation can be reversed by IL-1β receptor inhibition and p38 inhibition (Martin et al., 2002, Nolan et al., 2003, Xie et al., 2004). Hence IL-1β can induce acute cortical neuronal loss.

In addition, in vitro studies have shown that microglial IL-1β production can cause an increase in tau hyperphosphorylation (Li et al., 2003). Primary rat microglia or N9 microglial cells were stimulated with either amyloid-β or LPS to produce IL-1α, IL-1β and TNF-α. When co-cultured with primary rat neurons within 30 minutes activated microglia caused an increase in tau phosphorylation (AT8 antibody), and p38-MAPK phosphorylation, i.e. activation. The same effect was shown on incubation with IL-1β alone. Neuronal cultures were pre-treated with IL-1 receptor antagonist (IL-1ra), anti-IL-1β antibody, or anti-TNFα antibody prior to co-culture with activated microglia. Tau phosphorylation was attenuated by IL-1ra as well as anti-IL-1β antibody but not anti-TNF-α antibody. p38-MAPK inhibition reversed the influence of IL-1β on tau phosphorylation (Li et al., 2003).

Previous studies in the 3xTgAD mouse model of AD demonstrated that peripheral LPS-injection increased microgliosis, increased IL-1β mRNA levels and increased tau pathology, however no mechanistic studies were conducted to determine a causative link (Kitazawa et al., 2005, Sy et al., 2011).

Studies in C57BL/6 mice showed that systemic LPS-injection induced apoptosis (4-hours post-injection) and tau pathology (24-hours post-injection) in the dentate gyrus

(Cardona et al., 2006, Bhaskar et al., 2010). These effects were exacerbated in fractalkine deficient (Cx3cr1$^{-/-}$) mice suggesting microglial involvement (Cardona et al., 2006, Bhaskar et al., 2010). Intraperitoneal LPS-injection (1 mg/kg) into 2-month-old hTau mice (where the endogenous mouse tau gene is replaced by the human wild-type tau gene) induced early tau hyperphosphorylation at TG3 (phospho-thr231) and AT8 epitopes 24-hours post-injection (Bhaskar et al., 2010). Fractalkine deficient hTau mice (hTau-*Cx3cr1*$^{-/-}$ mice) were then used to demonstrate that increased microgliosis in hTau-*Cx3cr1*$^{-/-}$ mice was associated with increased tau hyperphosphorylation (AT8, AT180 and PHF1) and increased aggregation of insoluble tau. Authors went on to generate *Tlr4*$^{-/-}$ and *Il-1r1*$^{-/-}$ mice which were used to demonstrate that LPS increases tau phosphorylation and p38-MAPK activation via the TLR4 signalling pathway and that IL-1 is key in mediating this effect (Bhaskar et al., 2010). Together these experiments indicate that LPS-induced microglial activation leads to IL-1β production which causes increased tau phosphorylation.

Importantly the hTau studies focussed on the dentate gyrus (Bhaskar et al., 2010), a region where there is disease-associated microgliosis and where IL-1R1 expression is highest (Ban, 1994), whereas my studies have focussed on the superficial cortex where there is no apparent microgliosis and where IL-1R1 expression is minimal. However, the potential role of IL-1β and p38-MAPK in tau phosphorylation and neuronal loss is particularly interesting in the case of P301S mice because previously published work showed that p38-MAPK family members (MAP kinase, phospho-JNK, and phospho-p38) labelled tau-positive neurons in the P301S mouse (Allen et al., 2002) hence these neurons might be sensitive to LPS-induced increases in IL-1β.

None of the studies investigating the effects of systemic inflammation in a pure model of tauopathy have directly compared the levels of LPS-induced hyperphosphorylated tau pathology, microglial activation or IL-1β production between models of tauopathy and wild-type mice. This is an important concept since studies in alternative models of neurodegeneration demonstrate disease-associated microglial priming (section 1.2.9) whereby microglia in the disease context exist in an alternative

state of activation, and subsequent inflammatory challenge results in the over-production of proinflammatory cytokines, including IL-1β, with deleterious downstream consequences (Cunningham et al., 2007). It is important to understand whether the increased pathology in P301S mice is the result of an exaggerated neuroinflammatory response or perhaps due to increased neuronal vulnerability to an equivalent inflammatory environment.

5.4.2 There is no apparent microglial priming in the brain or spinal cord of P301S mice, but systemic inflammation induced IL-1β expression

The data presented here demonstrate the absence of any detectable cortical microgliosis. CD11b, a component of complement receptor 3, is a microglial marker known to be upregulated in the brainstem of P301S mice at end stage (Bellucci et al., 2004) and was therefore used for a gene expression assay 4-hours post-injection at 16 weeks of age. The CD11b expression assay and IBA1-positive cell counts in the cortex 24-hours post-injection confirmed the absence of disease-associated microgliosis in the cortex of P301S mice compared with C57BL/6 mice.

There was no impact of LPS on CD11b mRNA transcript levels or IBA1-positive cell counts in the cortex of C57BL/6 mice or P301S mice and there were no obvious morphological differences between groups, although no formal morphological studies were undertaken (Figure 19 and Figure 20). Importantly there was no difference in the magnitude of LPS-induced microglial response between C57BL/6 mice and P301S mice, as measured by either of these markers at either time point (Figure 19 and Figure 20).

The apparent absence of cortical microgliosis persisted until end stage (Figure 33); despite the significant disease-associated neuronal loss, abundant tau pathology and astrogliosis in the cortex. When mice were sacrificed at 22 weeks of age, IBA1 staining indicated that there was still no microgliosis in this area in P301S mice compared with C57BL/6 mice. LPS had no impact on IBA1-positive cell counts or microglial

morphology in either P301S mice or C57BL/6 mice (Figure 33). These data further reaffirm the notion that there is, remarkably, no disease-associated microgliosis in the cortex of P301S mice and microglia in the cortex of P301S mice are still subject to the same stringent regional immune regulation as control mice.

There is, however, known disease-associated microgliosis in the spinal cord of P301S mice at end stage (Bellucci et al., 2004) and this progressive microgliosis becomes significant in lamina 9 at 10 weeks of age (section 3.3.2.5).

At 16 weeks of age the disease-associated increase in IBA1-positive cells detected in lamina 9 of the spinal cord of P301S mice did not reach significance ($p=0.242$) (Figure 24). This contrasts with work in Chapter 3 which demonstrated a clear progressive increase in microglial counts in the spinal cord of P301S mice which became significant compared with controls at 10 weeks of age using the same microglial marker, IBA1. There are several plausible explanations which might account for this failure to detect microgliosis in P301S mice.

In chapter 3 IBA1-positive cells were visualised using 3′,3′-diaminobenzidine (DAB) as the chromagen, whereas in chapter 5 they were visualised using immunofluorescence. DAB-staining depends on the oxidation of DAB into a dark brown or black, alcohol-insoluble reaction product. The reaction can be run until optimal staining is achieved, thus improving signal-to noise ratio. In chapter 5 however IBA1 was visualised by immunofluorescence; which does not allow this type of optimal staining and produces more background staining.

IBA1 cells in chapter 3 were stained using anti-IBA1 antibody (MP-290-CR05) from A. Menarini Diagnostics, however, the antibody expired and due to timing and cost-effectiveness, in Chapter 5 IBA1-positive cells were stained using anti-IBA1 antibody (Ab5076) from AbCam. It is possible that the different results are due to problems with the AbCam IBA1 antibody which has since reported inconsistent results in mouse tissue especially at relatively mild levels of microgliosis (abcam_datasheet).

Alternatively, it is possible that the discrepancy is a result of variation in the tissue either due to the fixative or due to genuine biological variation between cohorts. Although statistically significant, the microgliosis demonstrated in 16-week-old P301S mice in chapter 3 represented only a 1.6-fold change in IBA1-positive cell counts compared with controls. The results in Chapter 5 represent a 1.2-fold change in IBA1-positive cell counts – a difference which might realistically be attributed to biological variation. It is worth noting that there was also relatively mild astrogliosis in the spinal cord of the same mice used in Chapter 5 (Figure 30), although again, astrogliosis in this chapter was detected by immunofluorescence and not DAB staining as before.

LPS caused a subtle but significant increase in IBA1-positive signal detected in the spinal cord of C57BL/6 and P301S mice 24-hours post-injection (Figure 24). There was no difference in the magnitude of the IBA1 response between genotypes. In agreement with these results qPCR data indicated a significant LPS-induced increase in CD11b transcripts in both C57BL/6 and P301S mice and there was no difference in the magnitude of the response (Figure 22).

Interestingly there were regional differences in CD11b mRNA levels; the relative quantity of CD11b mRNA in the spinal cord of saline-treated C57BL/6 mice is 1.5-fold higher than in the cortex, as might be expected since microglia are more densely packed in white matter than grey (Mittelbronn et al., 2001). This ratio is unchanged in LPS-injected C57BL/6 mice indicating an equivalent response to LPS in the brain and spinal cord of control mice (Table 27). Saline-injected P301S mice have 2-fold CD11b expression in the spinal cord compared with the brain suggesting perhaps some degree of microglial activation in the spinal cord at baseline and LPS-injection increased the relative quantity to 2.6-fold in the spinal cord compared with the brain, further supporting the notion that there is a differential microglial response in the spinal cord of P301S mice compared with the brain.

These data highlight a microglial response to LPS in the spinal cord which is absent in the cortex – whether this is due to differential exposure to systemically administered LPS and circulating proinflammatory mediators perhaps due to differences in tissue perfusion or whether it is the result of different regional microglial properties is unclear. These data perhaps support the theory that there are sub-populations of microglia which exist on a spectrum of immune-vigilance along the rostral-caudal axis, such that cortical microglia are subject to stringent immune-regulation, whereas more caudal microglia are considered "immune-vigilant" by comparison (Kim et al., 2000, Grabert et al., 2016). There are opposing regional differences in the expression patterns of ITIM-containing and ITAM-associating immunoreceptors such that ITAM-associating receptors were found in the cerebellum and ITIM-containing inhibitory members were predominantly found in the cortex. In future studies it will be interesting to investigate the regional expression pattern of genes involved in restricting over-activation of microglia including *Cx3cr1*, *Trem2*, *Cd33*, *Siglech* and *Fcgr2b,* which are all usually expressed at greater levels in the striatum and cortex than the cerebellum (Grabert et al., 2016).

IBA1 and CD11b are generic, widely expressed markers and do not always detect subtle changes in microglial sub-populations or phenotype switching, hence, a gene expression assay for IL-1β was conducted 4-hours post-injection. According to the microglial priming hypothesis, following an inflammatory stimulus, IL-1β is over-produced by microglia which are primed by the disease context and this IL-1β over-production is implicated in the observed exaggerated LPS-induced sickness behaviour (Sly et al., 2001, Cunningham et al., 2005, Perry et al., 2007, Chen et al., 2008).

Gene expression analysis indicated negligible IL-1β mRNA in the brains of saline-injected C57BL/6 and P301S mice. IL-1β mRNA levels in the spinal cord of saline-injected C57BL/6 were also negligible but IL-1β expression in the spinal cord of P301S mice was approximately 3.5-fold IL-1β expression in the brain (Table 30). This is in line with studies by Bellucci et al (2004) which failed to detect IL-1β staining in the

cortex of P301S mice at end stage but showed IL-1β staining in the brainstem and spinal cord. Following LPS-exposure there was a 3.8-fold increase in IL-1β mRNA levels in the spinal cord of C57BL/6 mice compared with the brain and a 4.9-fold increase in the spinal cord of P301S mice compared with brain tissue (Table 30) – again, this is in line with the hypotheses that there are microglial sub-populations with different immune-vigilance (Grabert et al., 2016) and that there is microglial activation in the spinal cord of P301S mice.

LPS induced a robust increase in IL-1β mRNA in the cortices of C57BL/6 and P301S mice but there was no evidence of an exaggerated IL-1β response in P301S mice compared with C57BL/6 mice (Figure 21). The absence of an exaggerated LPS-induced IL-1β response in P301S compared with C57BL/6 mice supports the notion that there is no disease-related microglial priming.

In a recent review, Cunningham explains that the term "microglial priming" arose independently from the concept of "inflammasome priming" whereby a priming stimulus is required to induce expression of components and assembly of the NLRP3-inflammasome complex and accumulation of pro-IL-1β. A secondary stimulus is required to activate the NLRP3-inflammasome complex resulting in cleavage of pro-IL-1β into the active form of IL-1β (Cunningham, 2013). Despite the distinction between microglial priming and inflammasome priming there may well be some overlap. It is certainly of interest that animal models which demonstrate over-production of IL-1β associated with microglial priming have some disease-associated microglial IL-1β expression prior to LPS-exposure (Sly et al., 2001, Lee et al., 2002, Kitazawa et al., 2005, Chen et al., 2008) whereas here I demonstrate negligible cortical IL-1β mRNA in saline-injected P301S mice. Post-transcriptional modifications and the post-translational cleavage of pro-IL-1β to IL-1β by the inflammasome complex are key steps in regulating IL-1β protein levels hence it remains to be seen whether the secreted, active IL-1β protein levels reflect mRNA levels demonstrated here.

Unexpectedly, not only was there no exaggerated IL-1β response but a relatively *smaller* IL-1β response in P301S mice; the LPS-induced increase in IL-1β mRNA in the cortex and spinal cord of P301S mice was approximately half that of C57BL/6 mice.

There are several possible explanations for a reduced IL-1β response in P301S mice. Firstly, it is possibly a matter of timing; IL-1β mRNA levels were only assessed at one time point 4-hours post-LPS-injection. This time point was chosen based on similar studies showing exaggerated IL-1β expression in alternative models of neurodegeneration at this time point (Godbout et al., 2005, Chen et al., 2008, Henry et al., 2009, Sy et al., 2011, Murray et al., 2012). It is possible however that there was a difference in the peak of IL-1β expression in P301S mice which was not apparent at 4-hours post-LPS. Intraperitoneal LPS (100 μg/kg) was shown by others to induce IL-1β expression in the C57BL/6 brain (Murray et al., 2012). IL-1β mRNA transcript levels peaked 1-hour post-injection, and were equivalent to IL-1β mRNA in the ME7 prion diseased brain at this time. IL-1β transcript levels in C57BL/6 mice gradually returned to baseline (Murray et al., 2012) however IL-1β transcript levels were still elevated in the ME7 prion diseased brain compared with C57BL/6 brain at 2- and 4-hours post LPS injection. Both groups had returned to baseline levels by 8 hours (Murray et al., 2012). Detailed temporal analysis of central cytokine mRNA and protein levels are required to better understand the impact of LPS injection on the neuropathology in the P301S mouse.

In addition, there is evidence that the presence of the meninges and choroid plexus dramatically increase the apparent LPS-induced increase in IL-1β mRNA (Garabedian et al., 2000). Although effort was made to remove the meninges, mice were not perfused prior to extraction of fresh tissue for gene expression assays and hence it is plausible that the contribution of IL-1β mRNA from circulating cells in the blood might lead to erroneous interpretations.

Alternatively, reduced IL-1β expression in P301S mice might indicate a different microglial phenotype with limited IL-1β capacity. In a study using rTg4510 mice,

which overexpress human mutant P301L tau under an inducible CaMKIIα promoter, expression of microglial markers CD45, MHCII and an "alternative activation marker" YM1 were assessed at 1, 5, and 9 months of age in the anterior cortex and hippocampus of rTg4510 mice (Lee et al., 2010). There was an age-related increase in CD45 expression, a small increase in MHCII expression and no change in YM-1 expression over time. Intracerebral LPS-injection (2 μl of LPS at 5 μg/μl) dramatically induced CD45 and arginase-1 expression in rTg4510 mice and control mice but interestingly there was an exaggerated increase in YM-1-positive microgliosis in rTg4510 mice compared with LPS-injected controls. YM-1 is a mouse-specific chitinase-like protein associated with "alternative" or "M2" microglial activation (Lee et al., 2010). YM1 is thought to interact with, and protect extracellular matrix components (Jin et al., 1998) and is associated with the development of Th2 inflammation (Lee et al., 2011).

To date there have been no investigations of the microglial expression profile of P301S mice and the absence of an exaggerated IL-1β response alone is insufficient to characterise the phenotype of these cells. The expression data of rTg4510 mice were compared with that of primed microglia and there was considerable overlap between the consensus transcriptional signature of primed microglia and the rTg4510 dataset (Holtman et al., 2015). Thus, conceptually tau pathology seems capable of inducing microglial priming, hence gene expression assays and immunohistochemistry are required to determine the relative abundance of markers associated with microglial priming in the P301S model, including CD14, Axl, Clec7a, CD11c, Cybb and Cfs1 (Chiu et al., 2013, Holtman et al., 2015). Several of the markers associated with microglial priming are involved in phagocytosis and endocytosis – it will be interesting to determine whether these markers are elevated in the P301S mouse with its mostly intracellular deposits compared with the extracellular deposits associated with amyloidopathies.

It is possible that the intracellular localisation of tau pathology in P301S mice induces an alternative microglial phenotype compared with the primed microglia seen in instances of extracellular amyloid and prion pathology.

In innate immunology, there are intracellular and extracellular PRRs which recognise different PAMPs and initiate different types of immune response, as discussed in section 1.2.3.2 (Akira et al., 2006). Extracellular receptors tend to be associated with bacterial, fungal and protozoan infections and initiate an inflammatory response that serves to opsonize, phagocytose and destroy the pathogen (Akira et al., 2006). Intracellular receptors tend to be associated with viral immunity. When intracellular PAMPs are detected PRRs initiate complex signalling pathways which induce expression of type 1 interferons (IFN) (Akira et al., 2006).

IFNs and IFN-inducible genes are upregulated in aging, in AD and in ALS (Lee et al., 2000, Colangelo et al., 2002, Ricciarelli et al., 2004, Wang et al., 2011, Baruch et al., 2014); a type 1 IFN signature is associated with the common gene expression signature of primed microglia (Holtman et al., 2015); and transcriptome analysis of rats overexpressing the longest isoform of wild type tau demonstrated a vast increase in IFN-inducible genes (Wang et al., 2010a). Importantly, type 1 IFNs can have an anti-inflammatory role in the CNS: they can increase anti-inflammatory cytokine production, such as IL-10 (Field et al., 2010); limit pro-inflammatory cytokine production, including TNF-α, IFN-γ and IL-12 (Castiglia et al., Teige et al., 2003, Makar et al., 2008); and have been shown to reduce IL-1β-induced IL-1β production (Schindler et al., 1990). Hence intracellular tau protein deposits might be recognised as non-self by intracellular receptors and might initiate a different arm of the immune system dominated by IFNs such that LPS-induced IL-1β expression is limited. Increased IFN-γ signalling is associated with increased tau pathology (Mastrangelo et al., 2009) hence in future it will be interesting to see if IFN signalling might contribute to the acute increase in tau pathology seen here.

Alternatively, there is evidence of inflammation-induced preconditioning associated with reduced inflammation. Exposure of naïve macrophages to cytokines such as IFN-γ, IL-12, and IL-10, alone or in combination had different effects on the response to subsequent LPS-exposure (Shnyra et al., 1998) and preconditioning with LPS resulted in neuroprotection during subsequent ischemia caused by transient middle cerebral artery occlusion (Rosenzweig et al., 2004); however, this was associated with reduced microglial activation measured by CD11b expression and since there was equivalent microgliosis, if not more, in the spinal cords of P301S mice compared with control mice, this seems an unlikely explanation for the reduced IL-1β response.

Alternatively again, there are suggestions that microglia associated with tau pathology are dystrophic or senescent (Streit et al., 2009) potentially due to phagocytosis of pathological tau protein (Rodriguez-Callejas et al., 2016). Hence this attenuated IL-1β response might represent failure of microglia to respond appropriately due to microglial cell death. However, dystrophic microglia are identified based on morphological changes, including cytorrhexis and membrane blebbing (Streit et al., 2009) features which are not apparent 24-hours post-LPS-injection in the P301S mouse.

5.4.3 Systemic inflammation increased microgliosis in the spinal cord of P301S mice at end stage

By 22 weeks of age, there was profound microgliosis in the spinal cord of P301S mice detected by IBA1 staining, in agreement with data from Chapter 3 and previously published work which showed MHCII and CD11b-positive microgliosis in the brainstem and spinal cord at end stage (Bellucci et al., 2004). The increase in IBA1-positive cell numbers in P301S mice at 22 weeks was associated with clear morphological changes; cells did not exist in ramified resting morphology as seen at 16 weeks (Figure 24) or in 22-week-old C57BL/6 mice (Figure 34E) but adopted a bushy morphology (Figure 34G) associated with microglial activation. In several instances, microglial cells also appeared to cluster around swollen dying motor

neurons (Figure 34H) (Allen et al., 2002). This might be indicative of phagocytosis of dying neurons as has been reported elsewhere (Zilka et al., 2009, Asai et al., 2015).

During the acute phase (24-hours post-injection) there was an equivalent LPS-induced increase in IBA1-positive microgliosis in C57BL/6 and P301S groups. However, at end stage there was a differential increase in microgliosis in the LPS-treated P301S group compared with C57BL/6 mice which indicates an interaction between systemic inflammatory insult and disease-related pathology. Investigation of alternative markers of microgliosis acutely, at end stage and at intervening time points might be required to determine whether there was an LPS-induced phenotypic switch during the acute stages which was not detected using the chosen markers or whether there was a progressive and acquired change in microglial phenotype.

It is plausible that the differential effect of LPS on microgliosis in the spinal cord of P301S mice was acquired over time, for example, the LPS-induced increase in tau pathology seen 24-hours post-injection may have persisted and exacerbated microgliosis over time. There is plenty of evidence that tau pathology results in microgliosis in humans and in animal models of tauopathy, as discussed in chapter 3 (Kida et al., 1992, Paulus et al., 1993, Sheng et al., 1997, Ishizawa et al., 2001, Ikeda et al., 2005, Sasaki et al., 2008, Morales et al., 2013); the current data and others have shown that overexpression of P301S tau is sufficient to cause microgliosis in these mice (Bellucci et al., 2004). In addition, there is evidence that microgliosis drives tau pathology (Bhaskar et al., 2010, Maphis et al., 2015b) hence it is conceivable that an acute increase in tau pathology resulted in a self-exacerbating loop between microgliosis and increasing tau pathology.

Not only was there clear disease-associated microgliosis in lamina 9 of the spinal cord where there is also known loss of motor neurons, but at end stage there was also striking microgliosis in the rubrospinal tract of P301S mice. The rubrospinal tract carries information which originates from the red nucleus, which integrates inputs from the motor cortex and the cerebellum. The tract synapses with motor neurons

and enables refinement of motor coordination by corticospinal inputs (Martinez-Lopez et al., 2015) (see **Figure 3** for orientation within spinal cord). This tract is rich in axons and thus tau protein is abundant in this area. Disease-associated tau pathology is likely to result in axonal degeneration with extreme pathological consequences in this area. Indeed, at 22 weeks of age there was abundant microgliosis in the rubrospinal tract of P301S mice and significant LPS-induced changes on top of the disease-associated microgliosis.

There were large bushy microglia but also smaller fragments of IBA1 staining with no clear cell body. The staining in the rubrospinal tract is reminiscent of the dystrophic (senescent) microglia apparently associated with tau pathology in Down's Syndrome and AD post-mortem tissue at end stage (Streit et al., 2009, Xue et al., 2011). Dystrophic microglia are characterised by fragmentation or "cytorrhexis", beading, blebbing and formation of spheroids (Xue et al., 2011). Confocal imaging is required to determine the 3-dimensional structure of microglia in this case to establish whether there is indeed cytorrhexis or whether the apparent fragmentation might be better explained by bushy processes of microglia which cross the 1-dimensional plane imaged here. Dystrophic microglia have not been studied in detail however they are associated with loss of neuroprotective functions in healthy ageing (Streit et al., 2004).

5.4.4 Systemic inflammation caused an acute increase in GFAP signal but a long term decrease in GFAP signal

In agreement with previous chapters there was disease-associated astrogliosis in the superficial layers of the cortex of 16-week old P301S mice by GFAP immunohistochemistry (Figure 28 and Table 32). In contrast, immunofluorescence failed to demonstrate significant astrogliosis in lamina 9 of the spinal cord of P301S mice, compared with control mice at 16 weeks of age (Figure 30). There are several plausible explanations for the failure to detect disease-associated astrogliosis at this time point. First, as with IBA1 staining, in chapter 3 GFAP-positive cells were visualised by DAB staining whereas here they were visualised using

immunofluorescence which brings with it the variations previously discussed. Second, in chapter 3 GFAP-positive cells were counted whereas in chapter 5 the percentage area containing GFAP signal was quantified – this method used in conjunction with the use of fluorescence staining rather than DAB, may introduce more variability in the results. Third, the discrepancies might arise from differences in the tissue rather than the staining or quantification methods, in which case they might be caused by differences in fixation or genuine biological variability. Despite the failure to detect disease-associated astrogliosis by immunofluorescence gene expression analysis of c5-c7 of the spinal cord showed an increase in the relative abundance of GFAP mRNA in P301S mice compared with C57BL/6 mice (Figure 29).

Gene expression analysis indicated a 2-fold increase in cortical GFAP expression 4-hours post-LPS and the magnitude of the LPS-induced response was equivalent in C57BL/6 and P301S mice (Figure 7). Immunofluorescence failed to detect a significant impact of LPS on GFAP-positive astrogliosis in the cortex (Figure 8). This is in line with detailed time course studies in the hippocampus of BALB/c mice which indicate that GFAP immunoreactivity does not change with systemic LPS-injection despite changes in the astrocyte expression profile and hence this measure alone is inadequate as an informant of the proinflammatory state astrocytes following systemic LPS (0.33 mg/kg) (Norden et al., 2016).

In contrast, there was a large LPS-induced increase in reactive astrogliosis in the spinal cords of P301S mice but not C57BL/6 mice by immunohistochemistry (Figure 30). It is of course possible that this could be a false-positive due to the peculiar absence of astrogliosis in the saline-treated P301S group, however, importantly the qPCR data, from a separate cohort of mice, confirmed the LPS-induced increase in GFAP expression in P301S mice but not C57BL/6 mice (Figure 29). These data thus indicate an impact of LPS on GFAP-positive reactive-astrogliosis in the spinal cord of P301S mice and not C57BL/6 mice.

It is unclear at this stage what caused the LPS-induced differential increase in GFAP expression in the spinal cord of P301S mice compared with C57BL/6 mice but not in the brain.

The differential astrogliosis in the spinal cord might be microglia-mediated. Detailed time course studies from BALB/c mice injected intraperitoneally with LPS (0.33 mg/kg) demonstrated sequential LPS-induced expression of cytokines and chemokines in microglia (2-4 hours post-LPS) followed by cytokine, chemokine and GFAP expression in astrocytes (peaked around 12-hours post-injection) (Norden et al., 2016). Evidence from the Barres lab showed that A1-astrocytes were not induced by LPS or IL-1β directly; instead the A1-reactive astrocyte profile was induced by microglia-derived IL-1α, TNF-α and complement component C1q, (Liddelow et al., 2017). LPS induction of A1-astrocytes required microglial activation. It is plausible that the differential increase in GFAP-positive reactive astrogliosis in LPS-injected P301S mice is microglia-dependent and reflects an exaggerated inflammatory environment in P301S mice compared with control mice which is not detected with the chosen microglial markers.

On the contrary, a study in the ME7 prion disease model demonstrated "astrocyte priming"; there was disease-associated astrogliosis in the brains of ME7 mice, visualised by GFAP staining, and subsequent inflammatory insult with intracerebral IL-1β or TNF-α altered the expression profile of astrocytes. There was an exaggerated astrocyte response in ME7 mice compared with control mice characterised by increased NFκB activation due to nuclear localisation of p65 and increased expression of chemokines (CCL2, CXCL1, RANTES, CXCL10) and markers of reactive astrogliosis (PTX3 and STEAP4) (Hennessy et al., 2015). Astrocyte activation was assessed 2-hours post intracerebral cytokine injection hence these astrocytic responses were unlikely to be microglia-dependent.

Recently published work identified a host of astrocytic genes which are differentially regulated when astrocytes are co-cultured with neurons rather than grown in mono-

culture (Hasel et al., 2017). There were nine neuronally-regulated astrocyte genes which were assessed in P301S spinal cord tissue. There was a reduced expression of astrocyte-specific genes involved in glutamate and GABA transport (Metabotropic Glutamate Receptor 3, GABA Transporter 3) and in metabolism in 20-week-old P301S mice compared with age-matched control mice (Hasel et al., 2017). This is of interest since LPS-administration is known to induce hypoglycaemia (del Rey et al., 1987, Oguri et al., 2002) and in this context altered astrocyte metabolism might be deleterious.

Far more significant than the amount of GFAP in the brain or spinal cord is the functional output of those GFAP-positive cells. As discussed in the introduction, astrocytes are abundant cells which play an essential role in maintaining brain homeostasis; they provide structural, metabolic and trophic support to neurons and remove waste products, they participate in the tripartite synapse where they recycle neurotransmitters, regulate synaptogenesis, synaptic pruning and participate in synaptic transmission and they maintain the BBB and regulate blood flow (Martinez-Hernandez et al., 1977, Zhou et al., 1994, Friedman et al., 1998, Hirase, 2005, Stevens et al., 2007, Fuller et al., 2010).

GFAP is a generic marker of reactive astrocytes and does not distinguish between different profiles of these cells. GeneChip expression profiling of astrocytes demonstrated that reactive gliosis is dependent on the transient expression of networks of genes and those networks are dependent on the stimulus. Astrocytes isolated following i.p. LPS-injection (5 mg/kg) expressed proteins involved in the antigen presentation pathway and complement pathway initiation, as well as cytokine and chemokine production – hence LPS-induced astrocytes adopt a damaging, proinflammatory phenotype whereas astrocytes isolated following ischemia (induced by middle cerebral artery occlusion (MCAO)) express neurotrophic factors and cytokines, and thrombospondins which help to rebuild lost synapses therefore seem to be neuroprotective (Zamanian et al., 2012). These two phenotypes were later referred to as “A1” and “A2” phenotypes respectively

(Liddelow et al., 2017). This terminology refers to the now out-dated "M1 vs. M2" microglial/macrophage phenotypes (Martinez et al., 2014) and while it is inevitably an over-simplification, it will prove to be a necessary step in shifting the field away from thinking of only reactive, GFAP-positive astrogliosis towards thinking about different types of astrogliosis (neuroprotective vs deleterious astrogliosis) and ultimately towards a more refined understanding the spectrum of astrocyte profiles.

A1-reactive-astrocytes lose their neuroprotective functions and are neurotoxic (Liddelow et al., 2017) hence in future experiments, it will be interesting to use a transcriptomic approach to determine the baseline profile of astrocytes in the P301S model compared with controls and in addition to investigate whether systemic LPS has a differential impact on the astrocyte expression profile in P301S mice compared with C57BL/6 mice.

At 22 weeks of age there was robust disease-associated GFAP-positive astrogliosis in the superficial layers of the cortex and lamina 9 of the spinal cord of P301S mice (Figure 36 and Figure 37) in agreement with data shown in chapter 3 and previously published data (Allen et al., 2002, Hampton et al., 2010).

LPS-injection at 16 weeks of age had no lasting impact on astrogliosis in the brain or spinal cord of C57BL/6 mice, yet unexpectedly LPS caused a *reduction* in GFAP signal in P301S mice at 22 weeks of age compared with saline-injected counterparts (Figure 36 and Figure 37). Reduced astrogliosis has previously been associated with increased neuronal loss and increased disease severity (Broe et al., 2004). Given the role of astrocytes in maintaining homeostasis it is possible that loss of astrocytes might lead to loss of neuroprotective function.

Without a pan-astrocyte marker such as Aldh1l1 it is unclear whether this apparent decrease in astrogliosis at end stage results from down-regulation of GFAP expression or an overall reduction in the number of GFAP-positive cells in the LPS-treated group.

There is evidence from *in vitro* studies that treatment of astrocyte cultures with LPS-activated microglial conditioned medium stimulates astrocyte proliferation but decreases GFAP protein and mRNA levels (Röhl et al., 2007). This effect has been shown by treatment of astrocyte cultures with proinflammatory cytokines such as IL-1β and TNF-α (Selmaj et al., 1991, Oh et al., 1993, Murphy et al., 1995). Studies in CSF-1 deficient op/op mice showed that deficits in microgliosis increased GFAP expression in astrocytes in response to trauma (Bruccoleri et al., 2000). Swiss Webster mice expressing eGFP in astrocytes under the pan-astrocyte Aldh1l1 promoter exposed to i.p. LPS (5 mg/kg) showed an acute increase in GFAP 24-hours post-LPS which returned to baseline 30-days post-injection. There was no corresponding loss of e-GFP expression indicating that there was a down-regulation of GFAP rather than astrocyte cell death on resolution of inflammation (Zamanian et al., 2012). It is plausible that the acute inflammatory insult at 16 weeks might cause long-term down-regulation of GFAP in P301S mice which persists until 22 weeks of age.

LPS-induced microgliosis can also cause astrocyte cell death. Several in vitro studies have shown that inflammatory mediators IL-1β and nitric oxide, which are often produced by microglia and astrocytes following LPS-injection, can induce apoptosis in astrocytes in culture (Hu et al., 1996, Ehrlich et al., 1999, Suk et al., 2002). Hence it is possible that the exacerbated microgliosis with associated increase in proinflammatory cytokine production in the spinal cord of LPS-treated P301S mice at end stage might either cause a decrease in GFAP expression in astrocytes or apoptosis. However, this cannot explain the loss of astrogliosis in the cortex where there was no microgliosis even at end stage.

At end stage, there was disease-associated astrogliosis and microgliosis in the spinal cord of P301S mice. LPS induced a further increase in microgliosis in lamina 9 and in the rubrospinal tract of P301S mice compared with saline-injected counterparts, but a decrease in GFAP-positive astrogliosis in P301S mice compared with saline-injected counterparts.

Despite these LPS-induced glial changes, there was no impact of LPS on the NeuN-positive cell counts conducted in Lamina 9 of the spinal cord. This might have been because at such a late stage in disease motor neuron loss is so severe (~75% loss) there is a floor effect and any LPS-induced neuronal loss is masked by disease-associated neuron loss.

We have seen previously that the over-expression of human mutant tau protein is sufficient to cause astrogliosis with altered astrocyte gene expression (Hampton et al., 2010, Hasel et al., 2017) and microgliosis (Bellucci et al., 2004) hence it is possible that the exacerbated tau pathology in LPS-injected mice caused the acute increase in reactive astrogliosis and long term increase in microgliosis in P301S mice and not the other way around.

5.5 Conclusions

In conclusion, peripheral LPS-injection (500 μg/kg) at 16 weeks of age was sufficient to acutely increase AT8-positive tau pathology in P301S mice but not C57BL/6 mice and cause equivalent cortical neuronal loss in both genotypes, apparent at end stage. There was no evidence of microglial priming in P301S mice. LPS-injection induced an increase in IL-1β mRNA levels in the cortex and spinal cord of P301S and C57BL/6 mice 4-hours post-injection, which although reduced in P301S mice, might have been sufficient to induce the observed tau pathology in neurons which express human mutant tau protein and have activated kinases, including p38 and JNK (Allen et al., 2002). IL-1β might also have induced neuronal loss in P301S mice and C57BL/6 mice. Mechanistic studies with IL-1 receptor antagonists and downstream kinase inhibitors are required to confirm or deny the potential involvement of IL-1β in the observed pathological changes.

Interestingly, LPS-injection at 16-weeks-of-age advanced the chronic decline in horizontal bar performance (between 16-22 weeks of age) in P301S mice. The precise neurocircuitry involved in this declining performance is unknown, however, LPS-injection failed to induce additional neuronal loss in lamina 9 of the spinal cord of

P301S mice. Neuronal loss in this area might not be the correct biological correlate for motor dysfunction: tau protein is known to influence synaptic changes and axonal degeneration. LPS caused a long-term increase in microgliosis in lamina 9 and in the rubrospinal (Rb) tract. The Rb tract carries information from the motor cortex and cerebellum to interneurons and motor neurons (Martinez-Lopez et al., 2015) hence exaggerated microgliosis in this area might indicate axonal degeneration associated with worse horizontal bar performance. LPS also reduced GFAP-positive astrogliosis in the cortex and spinal cord which might be associated with loss of neuroprotective function.

In future, it will be interesting to investigate the impact of systemic inflammation on axonal degeneration and synaptic changes in areas relevant for sickness behaviours and horizontal bar performance.

6 Chapter 6 - Discussion

The overarching aim of this study was to explore the effect of systemic inflammation on disease progression in a mouse model of tauopathy neurodegeneration, with both pathological and non-invasive, behavioural outcomes.

It had previously been demonstrated that over-expression of human mutant P301S tau protein under the Thy 1.2 promoter was sufficient to cause regional neuronal loss, astrogliosis and microgliosis (Allen et al., 2002, Bellucci et al., 2004, Hampton et al., 2010). Here I built on that knowledge and determined a detailed time course for these pathological markers. I showed that there was progressive superficial cortical neuronal loss which occurred between 10-12 weeks of age, there was progressive astrogliosis in the same area and in the cervical spinal cord, significant already at 8 weeks of age. Importantly I demonstrated that disease-associated microgliosis was regional; there was progressive microgliosis in lamina 9 of the spinal cord but microgliosis was absent in the cortex even at very late stages of disease.

The lack of microgliosis in the cortex despite the neuronal loss and astrogliosis in the same area was surprising. A recent study isolated microglia from different regions of the brain for transcriptomic studies and demonstrated that there are regional sub-populations of microglia which exist on a spectrum of immune vigilance (Grabert et al., 2016). It would be fascinating to apply these transcriptomic techniques to microglia isolated from the cortex and spinal cord of C57BL/6 and P301S mice in order to investigate the regional differences in microglial activation in tauopathy dementia. Given the relatively limited microglial activation and the failure to demonstrate microglial priming it is now essential to perform a more detailed analysis of the microglial phenotype in this model and to compare it to transcriptomics performed in other tau pathology models (Holtman et al., 2015).

In addition, this study identified the horizontal bar task as a reliable tool with which to reproducibly and non-invasively monitor disease progression. Together with

pathological read-outs, this task provided essential information for identifying when neurological function begins to become vulnerable, thus identifying potential tipping points at which acute inflammatory insults might alter the trajectory of disease. The precise neurocircuitry which is required for good horizontal bar performance and which is impaired during the chronic decline phase remains to be determined. Tau is known to cause synaptic changes, axonal degeneration and neuronal cell death hence precisely how that neurocircuitry is impaired also requires further study.

The horizontal bar task is a measure of motor strength and coordination. Attempts to identify an appropriate assay of *cognitive* decline which reflected the progressive nature of the disease failed. In the case of burrowing it was impossible to determine whether the chronic decline phase was due to motor or cognitive impairments and in the case of T-maze alternation, at 22 weeks of age P301S mice were still able to attain 80% successful alternation so working memory deficits are not occurring even relatively late in disease.

This dominant hind limb phenotype, is in line with previously published data, and pathological data from Chapter 3 demonstrating worse tau pathology and microgliosis in the spinal cord than in the cortex or hippocampus (Allen et al., 2002, Bellucci et al., 2004). The hind limb paralysis is one of the major limitations of this and other tau models, as it means mice must be humanely sacrificed before pathology in the forebrain has had a chance to fully develop. However, as discussed in Chapter 3 this regional pathology should not be dismissed as merely an artefact of Thy 1.2 driven expression of mutant tau protein since tau is expressed at two-fold endogenous mouse tau levels in the brain and spinal cord (Allen et al., 2002) hence the variations in pathology might reflect true and important regional vulnerability to tau pathology. Although tau expression levels are equivalent in the brain and spinal cord, it is also worth considering whether there are different types of tau pathologies in different regions, perhaps due to regional or cell-specific expression of kinase and phosphatase enzymes.

Initially we set out to model aspects of delirium caused by systemic inflammation superimposed onto dementia. Clinical studies show that in someone with pre-existing dementia, acute systemic inflammation (for example, in the context of a peripheral infection) frequently results in delirium (Cunningham et al., 2013). Additionally, delirium and systemic inflammatory illness are associated with increased risk of dementia, and can exacerbate or accelerate pre-existing dementia (Rockwood et al., 1999, Engelhart et al., 2004, Yaffe et al., 2004, Perry et al., 2007, Tobinick, 2008, Fong et al., 2009). Failure to detect cognitive decline in this model limits its usefulness as a tool for modelling dementia or indeed delirium superimposed onto dementia. However, there is no *a priori* reason to believe that the disease exacerbation has to be cognitive. The prediction is that systemic inflammation will exacerbate impaired function in tasks that become impaired in the underlying disease and that the inflammatory stress unmasks this circuit vulnerability and the data presented here are consistent with that hypothesis.

In this case the vulnerable circuitry in the P301S model is predominantly involved in motor coordination, thus, the horizontal bar task offers an excellent tool for tracking the progression of disease pathology in P301S mice and detecting inflammation induced acute impairments in the same functions. Using this task, I demonstrated that a single dose of LPS (500 μg/kg) early in disease was sufficient to induce exaggerated acute impairments of motor strength and coordination in P301S tau mice compared with LPS-injected control mice. P301S mice injected at 16 weeks of age were more impaired and took longer to recover from the systemic inflammatory insult compared with mice injected with the same dose of LPS at 10 weeks of age. This indicates that the disease severity determines the level of vulnerability to the effects of a secondary stressor.

In P301S mice injected at 16 weeks of age systemic inflammation was sufficient to increase the rate of the chronic decline in horizontal bar performance which is thought to be associated with neurodegeneration. It remains to be determined whether there is a change in the *rate* of neurodegeneration or whether injury causes acute damage

to the brain and then the disease continues at the same rate, but reaches the threshold for a measurable functional deficit sooner.

In this study, the systemic inflammatory insult was modelled by LPS – a chemical moiety found on gram negative bacteria, however studies in alternative animal models of neurodegeneration and ageing demonstrate that other secondary inflammatory insults such as poly I:C or mouse hepatitis virus, both viral mimetics, osteoarthritis and obesity can influence disease pathology (Sriram et al., 2002, Field et al., 2010, Kyrkanides et al., 2011, Sy et al., 2011). There is also evidence that psychosocial stress can exacerbate tau pathology, neurodegeneration and chronic decline in alternative models of tauopathy (Carroll et al., 2011).

Here I also showed that as the disease severity of P301S mice progresses, the animals become more vulnerable both acutely and in the long-term. If this is true of patients with on-going tau pathology the clinical consequences could be very significant.

6.1 Potential mechanisms

In order to better understand the pathological consequences of LPS-injection, brain and spinal cord tissue were collected acutely after LPS-injection and at end stage and the same pathological hallmarks were assessed.

Previous studies investigating the impact of systemic inflammation on models of ageing or neurodegeneration have demonstrated microglial priming whereby the microglia are activated or disinhibited by some aspect of the diseased or aged brain and a subsequent inflammatory insult stimulates an exaggerated inflammatory response with deleterious effects (discussed in detail in section 1.2.9), however in P301S mice there was no evidence of microglial priming.

The superficial cortex and spinal cord are relevant areas for investigating regional differences between the microglia, asking whether microglia are primed by the disease pathology and whether they are differentially responsive to systemic

inflammation. However, these regions are largely irrelevant neurocircuitry when it comes to identifying biological substrates of the exaggerated sickness response seen in chapter 4 and the focus has been on these areas as a result of prior knowledge regarding disease pathology in the P301S tau model.

The focus has been on CD11b and IBA1 as they are classical markers of microglial populations and IL-1β because it has been the classical descriptor of further activation associated with primed microglia. Taken together the evidence presented here fails to demonstrate the presence of microglial priming with the archetypal exaggerated IL-1β response. LPS-treatment induced equivalent microgliosis in P301S and C57BL/6 mice and LPS-induced IL-1β mRNA levels were relatively reduced in P301S mice compared with C57BL/6 mice. In future studies, it would be interesting to confirm these results with the transcriptomic studies previously mentioned and perhaps identify an alternative microglial profile. Although binary classifications of microglial phenotype are still referred to in the literature, known as "classically activated, M1" or "alternatively activated, M2", it is becoming clear that there are very many microglial activation phenotypes (Ransohoff, 2016), influenced by ageing, regional heterogeneity, and the timing, dose, duration and type of pathology they are exposed to. The microglial phenotype in the current model certainly merits full analysis.

In the absence of microglial priming, it remains to be understood what drives the exaggerated acute response to LPS in P301S mice compared with control mice. Despite the reduced IL-1β response, peripheral LPS-injection at 16 weeks of age was sufficient to increase AT8-positive tau pathology in the motor cortex and the spinal cord of P301S mice but not C57BL/6 mice at 24-hours post-injection which might indicate that over-expression of tau by neurons renders them more vulnerable to equivalent neuroinflammation.

It is unclear at this stage whether the LPS-induced increase in acute AT8 staining represents an increase in transgene expression or tau phosphorylation. To resolve this, the most obvious next step would be to collect further tissue 24-hours post-

injection, in order to run Western blots to determine whether there is a change in the amount of total tau protein as well as investigating the impact of LPS on other phospho-tau epitopes.

Neurons in P301S mice are likely to be sensitised to the effects of LPS-induced IL-1β production since they contain tau pathology as well as elevated levels of activated p38 and JNK (Allen et al., 2002). Mechanistic studies using IL-1 receptor agonists and specific kinase inhibitors are required to determine whether this is indeed the mechanism of neuronal loss and increased tau pathology in LPS-injected P301S mice as has been suggested in alternative models of tauopathy (Kitazawa et al., 2005, Bhaskar et al., 2010).

Indeed research showed that endogenous mouse tau mediated the neurotoxic effects of LPS in $Cx3cr1^{-/-}$ mice (Maphis et al., 2015a). In $Cx3cr1^{-/-}$ mice AT8-positive tau pathology co-localised with markers of neuronal death including cleaved caspase (CC3) but when $Cx3cr1^{-/-}$ mice were crossed with tau deficient mice to generate $Cx3cr1^{-/-}/Mapt^{-/-}$ mice; tau deficiency was neuroprotective and following LPS-injection there were fewer CC3-positive cells and fewer NeuN-positive-TUNEL-positive cells in $Cx3cr1^{-/-}/Mapt^{-/-}$ mice compared with $Cx3cr1^{-/-}$ mice (Maphis et al., 2015a).

It would be interesting to conduct similar studies to these in a knock-in mutant tau mouse model (Gilley et al., 2012) where mutant tau levels are equivalent to normal endogenous mouse tau levels in order to determine whether the LPS-induced increase in phospho-tau observed in P301S mice is in fact an artefact of over-expression of tau, that is there is LPS-induced tau phosphorylation compared with C57BL/6 mice because of increased substrate availability, or whether mutation induced tau pathology might also be sufficient to yield similar results.

Peripheral LPS is known to induce transient pathology in the hippocampus, where IL-1β receptor type 1 expression is greatest (Cunningham et al., 1992, Parnet et al.,

1994) and Roe et al. (2011) demonstrated a transient LPS-induced increase in tau pathology in the dentate gyrus and CA3 of the hippocampus of C57BL/6 mice which returned to baseline by 24-hours post-injection. Given that there is evidence of tau pathology in the hippocampus of P301S mice as early as 2.5 months of age (Xu et al., 2014) it might be interesting to investigate the possibility of a differential response in this area since it is relevant for sickness behaviours as well as disease pathology and thus a differential response in this area might account for the exaggerated sickness behaviour.

Astrocytes can also have beneficial or detrimental roles in a pathological context (Zamanian et al., 2012). LPS-injection caused an acute increase in GFAP signal in the spinal cord of P301S mice and not C57BL/6 and a decrease in GFAP signal in P301S mice at end stage hence it would be interesting to first use Aldh1l1 stain to determine whether the increase in GFAP signal is due to upregulation or proliferation. In the absence of microglial priming and given the known disease-associated astrogliosis in the cortex of P301S mice it would be interesting to conduct further transcriptomic studies akin to those of Zamanian et al. (2012) to investigate the beneficial or detrimental role of astrocytes in the P301S mouse following LPS-injection.

It is possible that the major change in microglia is not a pro-inflammatory switch but rather a loss of support functions, as has been demonstrated in alternative models associated with neurodegeneration (Holtman et al., 2015). LPS-induced inflammation impairs hippocampal neurogenesis in the sub-granular zone of rodents and is thought to do so via microglial activation; suppression of neuroinflammation using minocycline or indomethacin treatment restored this neurogenesis (Ekdahl et al., 2003, Monje et al., 2003). This discovery was followed by the observation that LPS is associated with reduced production of neurotrophins – BDNF, NGF and NT-3 – in the frontal cortex (Guan et al., 2006) which are involved in neurogenesis during development but also neuroprotection during adulthood (Tandon et al., 1999, Yanamoto et al., 2004), and which are reduced in dementia (Phillips et al., 1991), hence

LPS might not only induce neuronal death directly but might also reduce neuroprotection.

This study is the first of its kind to show that systemic inflammation, modelled by LPS has an exaggerated acute impact on motor control in a mouse model of tauopathy dementia and can affect the long-term trajectory of chronic decline associated with neurodegeneration, and importantly that these outcomes are not necessarily dependent on microglial status.

6.2 Implications of these results

The notion that systemic inflammation advances the onset of decline of neurodegeneration and can exacerbate disease-associated pathology might provide us with exciting therapeutic targets out-with the CNS, which might significantly delay the onset of dementia.

There is a possibility of acute interventions in high risk populations; if it becomes clear in clinical research that an inflammatory insult is sufficient to exacerbate neurodegeneration, for example in the context of an acute infection or hip fracture, this provides a rationale for trials of anti-inflammatory agents used at the time of the insult.

Researchers who showed that systemic inflammatory events and specifically increased TNF-α plasma levels predict increased rate of cognitive decline went on to test the effectiveness of Etanercept, an anti-TNF treatment, at preventing cognitive decline in a randomised, placebo-controlled clinical trial. Although the trial was too small to draw conclusions on efficacy, Etanercept was well tolerated and trends indicated cognitive benefits (Butchart et al., 2015). There are similar, promising trials underway to determine whether minocycline is superior to placebo in affecting the rate of decline in cognitive and functional outcomes, measured by standardised cognitive testing and Bristol Activities of Daily Living Scale over a 2-year period in patients with very early Alzheimer's Disease (Howard, 2017).

There might be opportunities to influence the risk of dementia and rate of cognitive decline via important lifestyle changes. There is a known inflammatory component to numerous preventable medical conditions including hypertension, hypercholesterolaemia and obesity (Dunn et al., 2005) and there are suggestions that prevention and treatment of vascular and chronic conditions and attention to optimum health early in life might reduce the incidence of dementia and improve cognitive health later in life (Wu et al., 2016).

The impact of treatments like this could be enormous. It is estimated that if we could delay the onset of Alzheimer's disease by five years, then over the following 15 years there would be 425,000 fewer people with dementia and accumulated savings of around £100 billion.

7 References

(2015). Prime Minister's challenge on dementia 2020. D. o. Health. Cabinet Office, Department of Health, Prime Minister's Office, 10 Downing Street.

abcam_datasheet (ab5076). "Anti-Iba1 antibody (ab5076) Datasheet."

Ahmed, S., B. Leurent and E. L. Sampson (2014). "Risk factors for incident delirium among older people in acute hospital medical units: a systematic review and meta-analysis." Age Ageing **43**(3): 326-333.

Akira, S., S. Uematsu and O. Takeuchi (2006). "Pathogen Recognition and Innate Immunity." Cell **124**(4): 783-801.

Akiyama, H., S. Barger, S. Barnum, B. Bradt, J. Bauer, G. M. Cole, N. R. Cooper, P. Eikelenboom, M. Emmerling, B. L. Fiebich, C. E. Finch, S. Frautschy, W. S. Griffin, H. Hampel, M. Hull, G. Landreth, L. Lue, R. Mrak, I. R. Mackenzie, P. L. McGeer, M. K. O. Banion, J. Pachter, G. Pasinetti, C. Plata-Salaman, J. Rogers, R. Rydel, Y. Shen, W. Streit, R. Strohmeyer, I. Tooyoma, F. L. V. Muiswinkel, R. Veerhuis, D. Walker, S. Webster, B. Wegrzyniak, G. Wenk and T. Wyss-Coray (2000). "Inflammation and Alzheimer's disease." Neurobiology of aging **21**(3): 383-421.

Alldred, M. J., K. E. Duff and S. D. Ginsberg (2012). "Microarray analysis of CA1 pyramidal neurons in a mouse model of tauopathy reveals progressive synaptic dysfunction." Neurobiology of Disease **45**(2): 751-762.

Allen, B., E. Ingram, M. Takao, M. J. Smith, R. Jakes, K. Virdee, H. Yoshida, M. Holzer, M. Craxton and P. C. Emson (2002). "Abundant tau filaments and nonapoptotic neurodegeneration in transgenic mice expressing human P301S tau protein." The journal of neuroscience **22**(21): 9340-9351.

Allgaier, M. and C. Allgaier (2013). "An update on drug treatment options of Alzheimer's disease." Frontiers in bioscience (Landmark edition) **19**: 1345-1354.

American_Psychiatric_Association (2013). Diagnostic and Statistical Manual of Mental Disorders, Fifth Edition (DSM-5), . Arlington, VA

Anderson, C. T., P. L. Sheets, T. Kiritani and G. M. G. Shepherd (2010). "Sublayer-specific microcircuits of corticospinal and corticostriatal neurons in motor cortex." Nat Neurosci **13**(6): 739-744.

Andorfer, C., C. M. Acker, Y. Kress, P. R. Hof, K. Duff and P. Davies (2005). "Cell-cycle reentry and cell death in transgenic mice expressing nonmutant human tau isoforms." J Neurosci **25**(22): 5446-5454.

Andorfer, C., Y. Kress, M. Espinoza, R. De Silva, K. L. Tucker, Y.-A. Barde, K. Duff and P. Davies (2003). "Hyperphosphorylation and aggregation of tau in mice expressing normal human tau isoforms." Journal of Neurochemistry **86**(3): 582-590.

Arendt, T., M. Holzer and U. Gärtner (1998). "Neuronal expression of cycline dependent kinase inhibitors of the INK4 family in Alzheimer's disease." Journal of Neural Transmission **105**(8): 949-960.

Arendt, T., J. Stieler, A. M. Strijkstra, R. A. Hut, J. Rüdiger, E. A. Van der Zee, T. Harkany, M. Holzer and W. Härtig (2003). "Reversible Paired Helical Filament-Like Phosphorylation of Tau Is an Adaptive Process Associated with Neuronal Plasticity in Hibernating Animals." The Journal of Neuroscience **23**(18): 6972.

Arriagada, P. V. M. G., John H. MD; Hedley-Whyte, E. Tessa MD; Hyman, Bradley T. MD, PhD (1992). "Neurofibrillary tangles but not senile plaques parallel duration and severity of Alzheimer's disease." Neurology **42**(3): 631-639.

ARUK (2014). Defeat Dementia: The evidence and a vision for action Cambridge, Alzheimer's Research UK.

Asai, H., S. Ikezu, S. Tsunoda, M. Medalla, J. Luebke, T. Haydar, B. Wolozin, O. Butovsky, S. Kugler and T. Ikezu (2015). "Depletion of microglia and inhibition of exosome synthesis halt tau propagation." Nat Neurosci **18**(11): 1584-1593.

Aspelund, A., S. Antila, S. T. Proulx, T. V. Karlsen, S. Karaman, M. Detmar, H. Wiig and K. Alitalo (2015). "A dural lymphatic vascular system that drains brain interstitial fluid and macromolecules." The Journal of Experimental Medicine **212**(7): 991.

Atzori, C., B. Ghetti, R. Piva, A. N. Srinivasan, P. Zolo, M. B. Delisle, S. S. Mirra and A. Migheli (2001). "Activation of the JNK/p38 pathway occurs in diseases characterized by tau protein pathology and is related to tau phosphorylation but not to apoptosis." J Neuropathol Exp Neurol **60**(12): 1190-1197.

Augustinack, J. C., A. Schneider, E. M. Mandelkow and B. T. Hyman (2002). "Specific tau phosphorylation sites correlate with severity of neuronal cytopathology in Alzheimer's disease." Acta Neuropathol **103**(1): 26-35.

Babine, R. L., K. E. Hyrkas, D. A. Bachand, J. L. Chapman, V. J. Fuller, C. A. Honess and H. R. Wierman (2016). "Falls in A Tertiary Care Hospital-Association With Delirium: A Replication Study." Psychosomatics **57**(3): 273-282.

Ban, E. M. (1994). "Interleukin-1 receptors in the brain: characterization by quantitative in situ autoradiography." Immunomethods **5**(1): 31-40.

Bancher, C., H. Braak, P. Fischer and K. A. Jellinger (1993). "Neuropathological staging of Alzheimer lesions and intellectual status in Alzheimer's and Parkinson's disease patients." Neuroscience Letters **162**(1–2): 179-182.

Banks, W. A. and S. M. Robinson (2010). "Minimal penetration of lipopolysaccharide across the murine blood–brain barrier." Brain, behavior, and immunity **24**(1): 102-109.

Barclay, A. N., G. J. Wright, G. Brooke and M. H. Brown (2002). "CD200 and membrane protein interactions in the control of myeloid cells." Trends in Immunology **23**(6): 285-290.

Baruch, K., A. Deczkowska, E. David, J. M. Castellano, O. Miller, A. Kertser, T. Berkutzki, Z. Barnett-Itzhaki, D. Bezalel, T. Wyss-Coray, I. Amit and M. Schwartz (2014). "Aging-induced type I interferon response at the choroid plexus negatively affects brain function." Science **346**(6205): 89-93.

Baudier, J. and R. D. Cole (1987). "Phosphorylation of tau proteins to a state like that in Alzheimer's brain is catalyzed by a calcium/calmodulin-dependent kinase and modulated by phospholipids." Journal of Biological Chemistry **262**(36): 17577-17583.

Baumann, K., E. M. Mandelkow, J. Biernat, H. Piwnica-Worms and E. Mandelkow (1993). "Abnormal Alzheimer-like phosphorylation of tau-protein by cyclin-dependent kinases cdk2 and cdk5." FEBS Letters **336**(3): 417-424.

Bellelli, G., S. Speciale, S. Morghen, T. Torpilliesi, R. Turco and M. Trabucchi (2011). "Are Fluctuations in Motor Performance a Diagnostic Sign of Delirium?" Journal of the American Medical Directors Association **12**(8): 578-583.

Bellucci, A., O. Bugiani, B. Ghetti and M. G. Spillantini (2011). "Presence of Reactive Microglia and Neuroinflammatory Mediators in a Case of Frontotemporal Dementia with P301S Mutation." Neurodegenerative Diseases **8**(4): 221-229.

Bellucci, A., Westwood, Ingram Esther, Casamenti Fiorella, M. Goedert and G. Spillantini Maria (2004). "Induction of inflammatory mediators and microglial activation in mice transgenic for mutant human P301S tau protein." The American journal of pathology **165**(5): 1643-1652.

Bennett, D. A., J. A. Schneider, Z. Arvanitakis, J. F. Kelly, N. T. Aggarwal, R. C. Shah and R. S. Wilson (2006). "Neuropathology of older persons without cognitive impairment from two community-based studies." Neurology **66**(12): 1837-1844.

Betmouni, S., V. H. Perry and J. L. Gordon (1996). "Evidence for an early inflammatory response in the central nervous system of mice with scrapie." Neuroscience **74**(1): 1-5.

Bhaskar, K., M. Konerth, O. N. Kokiko-Cochran, A. Cardona, R. M. Ransohoff and B. T. Lamb (2010). "Regulation of Tau Pathology by the Microglial Fractalkine Receptor." Neuron **68**(1): 19-31.

Bierer, L. M., P. R. Hof, D. P. Purohit, L. Carlin, J. Schmeidler, K. L. Davis and D. P. Perl (1995). "Neocortical neurofibrillary tangles correlate with dementia severity in Alzheimer's disease." Archives of neurology **52**(1): 81-88.

Biernat, J., N. Gustke, G. Drewes, E. Mandelkow and E. Mandelkow (1993). "Phosphorylation of Ser262 strongly reduces binding of tau to microtubules: Distinction between PHF-like immunoreactivity and microtubule binding." Neuron **11**(1): 153-163.

Blatteis, C. M., S. Bealer, W. Hunter, J.-Q. Llanos, R. Ahokas and T. Mashburn (1983). "Suppression of fever after lesions of the anteroventral third ventricle in guinea pigs." Brain research bulletin **11**(5): 519-526.

Blatteis, C. M., E. Sehic and S. Li (1998). "Afferent Pathways of Pyrogen Signalinga." Annals of the New York Academy of Sciences **856**(1): 95-107.

Bohnen, N. I., D. I. Kaufer, R. Hendrickson, L. S. Ivanco, B. Lopresti, J. G. Davis, G. Constantine, C. A. Mathis, R. Y. Moore and S. T. DeKosky (2005). "Cognitive correlates of alterations in acetylcholinesterase in Alzheimer's disease." Neuroscience Letters **380**(1–2): 127-132.

Bolivar, V. J. (2009). "Intrasession and Intersession Habituation in Mice: From Inbred Strain Variability to Linkage Analysis." Neurobiology of learning and memory **92**(2): 206-214.

Braak, H., I. Alafuzoff, T. Arzberger, H. Kretzschmar and K. Del Tredici (2006). "Staging of Alzheimer disease-associated neurofibrillary pathology using paraffin sections and immunocytochemistry." Acta Neuropathologica **112**(4): 389-404.

Braak, H. and E. Braak (1989). "Cortical and subcortical argyrophilic grains characterize a disease associated with adult onset dementia." Neuropathol Appl Neurobiol **15**(1): 13-26.

Brambilla, R., V. Bracchi-Ricard, W.-H. Hu, B. Frydel, A. Bramwell, S. Karmally, E. J. Green and J. R. Bethea (2005). "Inhibition of astroglial nuclear factor κB reduces inflammation and improves functional recovery after spinal cord injury." The Journal of Experimental Medicine **202**(1): 145-156.

Breitner, M. D. M. P. H. J. C. S. (1996). "The Role Of Anti-Inflammatory Drugs In The Prevention And Treatment Of Alzheimer's Disease." Annual Review of Medicine **47**(1): 401-411.

Brion, J.-P., C. Smith, A.-M. Couck, J.-M. Gallo and B. H. Anderton (1993). "Developmental Changes in τ Phosphorylation: Fetal τ Is Transiently Phosphorylated in a Manner Similar to Paired Helical Filament-τ Characteristic of Alzheimer's Disease." Journal of Neurochemistry **61**(6): 2071-2080.

Brion, J. P., J. N. Octave and A. M. Couck (1994). "Distribution of the phosphorylated microtubule-associated protein tau in developing cortical neurons." Neuroscience **63**(3): 895-909.

Broe, M., J. Kril and G. M. Halliday (2004). "Astrocytic degeneration relates to the severity of disease in frontotemporal dementia." Brain **127**(Pt 10): 2214-2220.

Bruccoleri, A. and G. J. Harry (2000). "Chemical-induced hippocampal neurodegeneration and elevations in TNFα, TNFβ, IL-1α, IP-10, and MCP-1 mRNA in osteopetrotic (op/op) mice." Journal of Neuroscience Research **62**(1): 146-155.

Buchman, A. S. and D. A. Bennett (2011). "Loss of motor function in preclinical Alzheimer's disease." Expert review of neurotherapeutics **11**(5): 665-676.

Buée, L., T. Bussière, V. Buée-Scherrer, A. Delacourte and P. R. Hof (2000). "Tau protein isoforms, phosphorylation and role in neurodegenerative disorders1." Brain Research Reviews **33**(1): 95-130.

Bugiani, O., J. R. Murrell, G. Giaccone, M. Hasegawa, G. Ghigo, M. Tabaton, M. Morbin, A. Primavera, F. Carella, C. Solaro, M. Grisoli, M. Savoiardo, M. G. Spillantini, F. Tagliavini, M. Goedert and B. Ghetti (1999). "Frontotemporal Dementia and Corticobasal Degeneration in a Family with a P301S Mutation in Tau." Journal of Neuropathology & Experimental Neurology **58**(6): 667.

Butchart, J., L. Brook, V. Hopkins, J. Teeling, U. Puntener, D. Culliford, R. Sharples, S. Sharif, B. McFarlane, R. Raybould, R. Thomas, P. Passmore, V. H. Perry and C. Holmes (2015). "Etanercept in Alzheimer disease: A randomized, placebo-controlled, double-blind, phase 2 trial." Neurology **84**(21): 2161-2168.

Cagnin, A., M. Rossor, E. L. Sampson, T. MacKinnon and R. B. Banati (2004). "In vivo detection of microglial activation in frontotemporal dementia." Annals of Neurology **56**(6): 894-897.

Cardona, A. E., E. P. Pioro, M. E. Sasse, V. Kostenko, S. M. Cardona, I. M. Dijkstra, D. Huang, G. Kidd, S. Dombrowski, R. Dutta, J. C. Lee, D. N. Cook, S. Jung, S. A. Lira, D. R. Littman and R. M. Ransohoff (2006). "Control of microglial neurotoxicity by the fractalkine receptor." Nat Neurosci **9**(7): 917-924.

Carroll, J. C., M. Iba, D. A. Bangasser, R. J. Valentino, M. J. James, K. R. Brunden, V. M. Y. Lee and J. Q. Trojanowski (2011). "Chronic stress exacerbates tau pathology,

neurodegeneration, and cognitive performance through a corticotropin-releasing factor receptor-dependent mechanism in a transgenic mouse model of tauopathy." The Journal of neuroscience : the official journal of the Society for Neuroscience **31**(40): 14436-14449.

Castiglia, V., A. Piersigilli, F. Ebner, M. Janos, O. Goldmann, U. Damböck, A. Kröger, S. Weiss, S. Knapp, Amanda M. Jamieson, C. Kirschning, U. Kalinke, B. Strobl, M. Müller, D. Stoiber, S. Lienenklaus and P. Kovarik "Type I Interferon Signaling Prevents IL-1β-Driven Lethal Systemic Hyperinflammation during Invasive Bacterial Infection of Soft Tissue." Cell Host & Microbe **19**(3): 375-387.

Chai, Z., S. Gatti, C. Toniatti, V. Poli and T. Bartfai (1996). "Interleukin (IL)-6 gene expression in the central nervous system is necessary for fever response to lipopolysaccharide or IL-1 beta: a study on IL-6-deficient mice." J Exp Med **183**.

Chen H, J. E., Schwarzschild MA, McCullough ML, Calle EE, Thun MJ, Ascherio and A. (2005). "Nonsteroidal antiinflammatory drug use and the risk for Parkinson's disease." Annals of neurology **58**(6): 963-967.

Chen, J., J. B. Buchanan, N. L. Sparkman, J. P. Godbout, G. G. Freund and R. W. Johnson (2008). "Neuroinflammation and disruption in working memory in aged mice after acute stimulation of the peripheral innate immune system." Brain, Behavior, and Immunity **22**(3): 301-311.

Chiu, I. M., E. T. A. Morimoto, H. Goodarzi, J. T. Liao, S. O'Keeffe, H. P. Phatnani, M. Muratet, M. C. Carroll, S. Levy, S. Tavazoie, R. M. Myers and T. Maniatis (2013). "A neurodegeneration-specific gene expression signature and immune profile of acutely isolated microglia from an ALS mouse model." Cell reports **4**(2): 385-401.

Clark, L. N., P. Poorkaj, Z. Wszolek, D. H. Geschwind, Z. S. Nasreddine, B. Miller, D. Li, H. Payami, F. Awert, K. Markopoulou, A. Andreadis, I. D'Souza, V. M.-Y. Lee, L. Reed, J. Q. Trojanowski, V. Zhukareva, T. Bird, G. Schellenberg and K. C. Wilhelmsen (1998). "Pathogenic implications of mutations in the tau gene in pallido-ponto-nigral degeneration and related neurodegenerative disorders linked to chromosome 17." Proceedings of the National Academy of Sciences **95**(22): 13103-13107.

Clavaguera, F., T. Bolmont, R. A. Crowther, D. Abramowski, S. Frank, A. Probst, G. Fraser, A. K. Stalder, M. Beibel, M. Staufenbiel, M. Jucker, M. Goedert and M. Tolnay (2009). "Transmission and spreading of tauopathy in transgenic mouse brain." Nat Cell Biol **11**(7): 909-913.

Colangelo, V., J. Schurr, M. J. Ball, R. P. Pelaez, N. G. Bazan and W. J. Lukiw (2002). "Gene expression profiling of 12633 genes in Alzheimer hippocampal CA1: Transcription and neurotrophic factor down-regulation and up-regulation of

apoptotic and pro-inflammatory signaling." Journal of Neuroscience Research **70**(3): 462-473.

Combrinck, M. I., V. H. Perry and C. Colm (2002). "Peripheral infection evokes exaggerated sickness behaviour in pre-clinical murine prion disease." Peripheral infection evokes exaggerated sickness behaviour in pre-clinical murine prion disease.

Costello, D. A., A. Lyons, S. Denieffe, T. C. Browne, F. F. Cox and A. M. Lynch (2011). "Long term potentiation is impaired in membrane glycoprotein CD200-deficient mice: a role for Toll-like receptor activation." The Journal of biological chemistry **286**(40): 34722-34732.

Cuchillo-Ibanez, I., A. Seereeram, H. L. Byers, K. Y. Leung, M. A. Ward, B. H. Anderton and D. P. Hanger (2008). "Phosphorylation of tau regulates its axonal transport by controlling its binding to kinesin." Faseb j **22**(9): 3186-3195.

Cunningham, C. (2013). "Microglia and neurodegeneration: the role of systemic inflammation." Glia **61**(1): 71-90.

Cunningham, C., S. Campion, K. Lunnon, C. L. Murray, J. F. C. Woods, R. M. J. Deacon, J. N. P. Rawlins and V. H. Perry (2009). "Systemic Inflammation Induces Acute Behavioral and Cognitive Changes and Accelerates Neurodegenerative Disease." Biological Psychiatry **65**(4): 304-312.

Cunningham, C., S. Campion, J. Teeling, L. Felton and V. H. Perry (2007). "The sickness behaviour and CNS inflammatory mediator profile induced by systemic challenge of mice with synthetic double-stranded RNA (poly I:C)." Brain Behav Immun **21**.

Cunningham, C., R. Deacon, H. Wells, D. Boche, S. Waters, C. P. Diniz, H. Scott, J. N. Rawlins and V. H. Perry (2003). "Synaptic changes characterize early behavioural signs in the ME7 model of murine prion disease." The European journal of neuroscience **17**(10): 2147-2155.

Cunningham, C. and A. Maclullich (2013). "At the extreme end of the psychoneuroimmunological spectrum: delirium as a maladaptive sickness behaviour response." Brain, behavior, and immunity **28**: 1-13.

Cunningham, C., D. C. Wilcockson, S. Campion, K. Lunnon and V. H. Perry (2005). "Central and systemic endotoxin challenges exacerbate the local inflammatory response and increase neuronal death during chronic neurodegeneration." The Journal of Neuroscience **25**(40): 9275-9284.

Cunningham, E. T., Jr., E. Wada, D. B. Carter, D. E. Tracey, J. F. Battey and E. B. De Souza (1992). "In situ histochemical localization of type I interleukin-1 receptor

messenger RNA in the central nervous system, pituitary, and adrenal gland of the mouse." J Neurosci **12**(3): 1101-1114.

Dabir, D. V., M. B. Robinson, E. Swanson, B. Zhang, J. Q. Trojanowski, V. M. Y. Lee and M. S. Forman (2006). "Impaired Glutamate Transport in a Mouse Model of Tau Pathology in Astrocytes." The Journal of Neuroscience **26**(2): 644.

Dallmann, R., S. Steinlechner, S. von Horsten and T. Karl (2006). "Stress-induced hyperthermia in the rat: comparison of classical and novel recording methods." Lab Anim **40**(2): 186-193.

Danbolt, N. C. (2001). "Glutamate uptake." Progress in Neurobiology **65**(1): 1-105.

Dantzer, R. (2001). "Cytokine-induced sickness behavior: where do we stand?" Brain Behav Immun **15**(1): 7-24.

Dantzer, R. (2009). "Cytokine, Sickness Behavior, and Depression." Immunology and allergy clinics of North America **29**(2): 247-264.

Dantzer, R., J. C. O'Connor, G. G. Freund, R. W. Johnson and K. W. Kelley (2008). "From inflammation to sickness and depression: when the immune system subjugates the brain." Nat Rev Neurosci **9**(1): 46-56.

David, D. C., S. Hauptmann, I. Scherping, K. Schuessel, U. Keil, P. Rizzu, R. Ravid, S. Dröse, U. Brandt and W. E. Müller (2005). "Proteomic and functional analyses reveal a mitochondrial dysfunction in P301L tau transgenic mice." Journal of Biological Chemistry **280**(25): 23802-23814.

Davis, D. H., G. Muniz-Terrera, H. A. Keage, T. Rahkonen, M. Oinas, F. E. Matthews, C. Cunningham, T. Polvikoski, R. Sulkava, A. M. MacLullich and C. Brayne (2012). "Delirium is a strong risk factor for dementia in the oldest-old: a population-based cohort study." Brain : a journal of neurology **135**(Pt 9): 2809-2816.

Davis, D. H., G. Muniz-Terrera, H. A. Keage, B. C. Stephan, J. Fleming, P. G. Ince, F. E. Matthews, C. Cunningham, E. W. Ely, A. M. MacLullich and C. Brayne (2017). "Association of Delirium With Cognitive Decline in Late Life: A Neuropathologic Study of 3 Population-Based Cohort Studies." JAMA Psychiatry **74**(3): 244-251.

Davis, D. H., D. T. Skelly, C. Murray, E. Hennessy, J. Bowen, S. Norton, C. Brayne, T. Rahkonen, R. Sulkava and D. J. Sanderson (2015). "Worsening cognitive impairment and neurodegenerative pathology progressively increase risk for delirium." The American journal of geriatric psychiatry **23**(4): 403-415.

de Haas, A. H., H. W. G. M. Boddeke and K. Biber (2008). "Region-specific expression of immunoregulatory proteins on microglia in the healthy CNS." Glia **56**(8): 888-894.

de Calignon, A., M. Polydoro, M. Suárez-Calvet, C. William, David H. Adamowicz, Kathy J. Kopeikina, R. Pitstick, N. Sahara, Karen H. Ashe, George A. Carlson, Tara L. Spires-Jones and Bradley T. Hyman (2012). "Propagation of Tau Pathology in a Model of Early Alzheimer's Disease." Neuron **73**(4): 685-697.

Deacon, R. M. J. (2006). "Burrowing in rodents: a sensitive method for detecting behavioral dysfunction." Nat. Protocols **1**(1): 118-121.

Deacon, R. M. J. (2013). "Measuring Motor Coordination in Mice." Journal of Visualized Experiments : JoVE(75): 2609.

Deacon, R. M. J., A. Croucher and J. N. P. Rawlins (2002). "Hippocampal cytotoxic lesion effects on species-typical behaviours in mice." Behavioural Brain Research **132**(2): 203-213.

Deacon, R. M. J., C. Penny and J. N. P. Rawlins (2003). "Effects of medial prefrontal cortex cytotoxic lesions in mice." Behavioural Brain Research **139**(1–2): 139-155.

Deacon, R. M. J. and J. N. P. Rawlins (2006). "T-maze alternation in the rodent." Nat. Protocols **1**(1): 7-12.

Degens, H. (2007). "Age-related skeletal muscle dysfunction: causes and mechanisms." J Musculoskelet Neuronal Interact **7**(3): 246-252.

del Rey, A. and H. Besedovsky (1987). "Interleukin 1 affects glucose homeostasis." Am J Physiol **253**(5 Pt 2): R794-798.

Delacourte, A., Y. Robitaille, N. Sergeant, L. Buée, P. R. Hof, A. Wattez, A. Laroche-Cholette, J. Mathieu, P. Chagnon and D. Gauvreau (1996). "Specific pathological Tau protein variants characterize Pick's disease." Journal of Neuropathology and Experimental Neurology **55**(2): 159-168.

Delobel, P., I. Lavenir, B. Ghetti, M. Holzer and M. Goedert (2006). "Cell-Cycle Markers in a Transgenic Mouse Model of Human Tauopathy : Increased Levels of Cyclin-Dependent Kinase Inhibitors p21Cip1 and p27Kip1." The American Journal of Pathology **168**(3): 878-887.

Dember, W. N. R., C.L. (1989). "Spontaneous Alternation Behavior " Springer.

Denieffe, S., R. J. Kelly, C. McDonald, A. Lyons and M. A. Lynch (2013). "Classical activation of microglia in CD200-deficient mice is a consequence of blood brain barrier permeability and infiltration of peripheral cells." Brain, Behavior, and Immunity **34**: 86-97.

Derijk, R. H. and F. Berkenbosch (1994). "Hypothermia to endotoxin involves the cytokine tumor necrosis factor and the neuropeptide vasopressin in rats." Am J Physiol **266**(1 Pt 2): R9-14.

DiCarlo, G., D. Wilcock, D. Henderson, M. Gordon and D. Morgan (2001). "Intrahippocampal LPS injections reduce Aβ load in APP+PS1 transgenic mice." Neurobiology of Aging **22**(6): 1007-1012.

Dickstein, D. L., H. Brautigam, S. D. Stockton, J. Schmeidler and P. R. Hof (2010). "Changes in dendritic complexity and spine morphology in transgenic mice expressing human wild-type tau." Brain structure & function **214**(2-3): 161-179.

Dinkel, P. D., A. Siddiqua, H. Huynh, M. Shah and M. Margittai (2011). "Variations in Filament Conformation Dictate Seeding Barrier between Three- and Four-Repeat Tau." Biochemistry **50**(20): 4330-4336.

Divac, I., R. G. E. Wikmark and A. Gade (1975). "Spontaneous alternation in rats with lesions in the frontal lobes: An extension of the frontal lobe syndrome." Physiological Psychology **3**(1): 39-42.

Dixit, R., J. L. Ross, Y. E. Goldman and E. L. Holzbaur (2008). "Differential regulation of dynein and kinesin motor proteins by tau." Science **319**(5866): 1086-1089.

Douglas, R. J. and A. C. Raphelson (1966). "Spontaneous alternation and septal lesions." Journal of Comparative and Physiological Psychology **62**(2): 320-322.

Drechsel, D. N., A. A. Hyman, M. H. Cobb and M. W. Kirschner (1992). "Modulation of the dynamic instability of tubulin assembly by the microtubule-associated protein tau." Molecular Biology of the Cell **3**(10): 1141-1154.

Drewes, G., A. Ebneth, U. Preuss, E. M. Mandelkow and E. Mandelkow (1997). "MARK, a novel family of protein kinases that phosphorylate microtubule- associated proteins and trigger microtubule disruption." Cell **89**(2): 297-308.

Drewes, G., B. Lichtenberg-Kraag, F. Döring, E. M. Mandelkow, J. Biernat, J. Goris, M. Dorée and E. Mandelkow (1992). "Mitogen activated protein (MAP) kinase transforms tau protein into an Alzheimer-like state." EMBO Journal **11**(6): 2131-2138.

Duff, K., H. Knight, L. M. Refolo, S. Sanders, X. Yu, M. Picciano, B. Malester, M. Hutton, J. Adamson, M. Goedert, K. Burki and P. Davies (2000). "Characterization of Pathology in Transgenic Mice Over-Expressing Human Genomic and cDNA Tau Transgenes." Neurobiology of Disease **7**(2): 87-98.

Dunn, N., M. Mullee, V. H. Perry and C. Holmes (2005). "Association between Dementia and Infectious Disease: Evidence from a Case-Control Study." Alzheimer Disease & Associated Disorders **19**(2): 91-94.

Eddleston, M. and L. Mucke (1993). "Molecular profile of reactive astrocytes—Implications for their role in neurologic disease." Neuroscience **54**(1): 15-36.

Ehrlich, L. C., P. K. Peterson and S. Hu (1999). "Interleukin (IL)-1 mediated apoptosis of human astrocytes." NeuroReport **10**(9): 1849-1852.

Ekdahl, C. T., J.-H. Claasen, S. Bonde, Z. Kokaia and O. Lindvall (2003). "Inflammation is detrimental for neurogenesis in adult brain." Proceedings of the National Academy of Sciences **100**(23): 13632-13637.

El Khoury, J., T. Michelle, E. H. Suzanne, K. M. Terry, T. Kinya, G. Changiz and D. L. Andrew (2007). "Ccr2 deficiency impairs microglial accumulation and accelerates progression of Alzheimer-like disease." Nature medicine **13**(4): 432-438.

Elkabes, S., E. M. DiCicco-Bloom and I. B. Black (1996). "Brain microglia/macrophages express neurotrophins that selectively regulate microglial proliferation and function." J Neurosci **16**(8): 2508-2521.

Engelhart, M. J., M. I. Geerlings, J. Meijer, A. Kiliaan, A. Ruitenberg, J. C. van Swieten, T. Stijnen, A. Hofman, J. C. Witteman and M. M. Breteler (2004). "Inflammatory proteins in plasma and the risk of dementia: the rotterdam study." Arch Neurol **61**(5): 668-672.

Erkinjuntti, T., J. Wikström, J. Palo and L. Autio (1986). "Dementia among medical inpatients: evaluation of 2000 consecutive admissions." Archives of Internal Medicine **146**(10): 1923-1926.

Fadok, V. A., D. L. Bratton, A. Konowal, P. W. Freed, J. Y. Westcott and P. M. Henson (1998). "Macrophages that have ingested apoptotic cells in vitro inhibit proinflammatory cytokine production through autocrine/paracrine mechanisms involving TGF-beta, PGE2, and PAF." The Journal of clinical investigation **101**(4): 890-898.

Fairchild, K. D., I. S. Singh, S. Patel, B. E. Drysdale, R. M. Viscardi, L. Hester, H. M. Lazusky and J. D. Hasday (2004). "Hypothermia prolongs activation of NF-κB and augments generation of inflammatory cytokines." American Journal of Physiology - Cell Physiology **287**(2): C422-C431.

Fassbender, K., s. Walter, s. Kühl, r. Landmann, k. Ishii, t. Bertsch, a. K. Stalder, f. Muehlhauser, y. Liu, a. J. Ulmer, s. Rivest, a. Lentschat, e. Gulbins, m. Jucker, m. Staufenbiel, k. Brechtel, j. Walter, g. Multhaup, b. Penke, y. Adachi, t. Hartmann and

k. Beyreuther (2004). "The LPS receptor (CD14) links innate immunity with Alzheimer's disease." The FASEB Journal **18**(1): 203-205.

Faulkner, J. R., J. E. Herrmann, M. J. Woo, K. E. Tansey, N. B. Doan and M. V. Sofroniew (2004). "Reactive Astrocytes Protect Tissue and Preserve Function after Spinal Cord Injury." The Journal of Neuroscience **24**(9): 2143-2155.

Feany, M. B. and D. W. Dickson (1995). "Widespread cytoskeletal pathology characterizes corticobasal degeneration." Am J Pathol **146**(6): 1388-1396.

Fick, D. M., J. V. Agostini and S. K. Inouye (2002). "Delirium superimposed on dementia: a systematic review." Journal of the American Geriatrics Society **50**(10): 1723-1732.

Field, R. H., S. Campion, Warren, C. Murray and C. Cunningham (2010). "Systemic challenge with the TLR3 agonist poly I:C induces amplified IFNalpha/beta and IL-1beta responses in the diseased brain and exacerbates chronic neurodegeneration." Brain, behavior, and immunity **24**(6): 996-1007.

Fitch, M. T. and J. Silver (2008). "CNS injury, glial scars, and inflammation: Inhibitory extracellular matrices and regeneration failure." Experimental Neurology **209**(2): 294-301.

Fletcher, D. A. and R. D. Mullins (2010). "Cell mechanics and the cytoskeleton." Nature **463**(7280): 485-492.

Flunkert, S., M. Hierzer, T. Loffler, R. Rabl, J. Neddens, S. Duller, E. L. Schofield, M. A. Ward, M. Posch, H. Jungwirth, M. Windisch and B. Hutter-Paier (2013). "Elevated levels of soluble total and hyperphosphorylated tau result in early behavioral deficits and distinct changes in brain pathology in a new tau transgenic mouse model." Neurodegener Dis **11**(4): 194-205.

Fong, T., R. Jones, P. Shi, E. Marcantonio, L. Yap, J. Rudolph, F. M. Yang, D. Kiely and S. Inouye (2009). "Delirium accelerates cognitive decline in Alzheimer disease." Neurology **72**(18): 1570-1575.

Francis, P. T., C. G. Parsons and R. W. Jones (2012). "Rationale for combining glutamatergic and cholinergic approaches in the symptomatic treatment of Alzheimer's disease." Expert Review of Neurotherapeutics **12**(11): 1351-1365.

Friedman, W. J., I. B. Black and D. R. Kaplan (1998). "Distribution of the neurotrophins brain-derived neurotrophic factor, neurotrophin-3, and neurotrophin-4/5 in the postnatal rat brain: an immunocytochemical study." Neuroscience **84**(1): 101-114.

Frost, B., R. L. Jacks and M. I. Diamond (2009). "Propagation of tau misfolding from the outside to the inside of a cell." The Journal of biological chemistry **284**(19): 12845-12852.

Fuller, K. G., J. K. Olson, L. M. Howard, J. L. Croxford and S. D. Miller (2004). "Mouse models of multiple sclerosis: experimental autoimmune encephalomyelitis and Theiler's virus-induced demyelinating disease." Methods Mol Med **102**: 339-361.

Fuller, S., M. Steele and G. Münch (2010). "Activated astroglia during chronic inflammation in Alzheimer's disease—Do they neglect their neurosupportive roles?" Mutation Research/Fundamental and Molecular Mechanisms of Mutagenesis **690**(1–2): 40-49.

Furman, J. L. and C. M. Norris (2014). "Calcineurin and glial signaling: neuroinflammation and beyond." Journal of Neuroinflammation **11**(1): 158.

Garabedian, B. V.-d., Y. Lemaigre-Dubreuil and J. Mariani (2000). "Central origin of IL-1β produced during peripheral inflammation: role of meninges." Molecular Brain Research **75**(2): 259-263.

Gerhard, A., I. Trender-Gerhard, F. Turkheimer, N. P. Quinn, K. P. Bhatia and D. J. Brooks (2006). "In vivo imaging of microglial activation with [11C](R)-PK11195 PET in progressive supranuclear palsy." Movement Disorders **21**(1): 89-93.

Gerlai, R. (1998). "A new continuous alternation task in T-maze detects hippocampal dysfunction in mice: a strain comparison and lesion study." Behavioural brain research **95**(1): 91-101.

Giannakopoulos, P., F. R. Herrmann, T. Bussiere, C. Bouras, E. Kovari, D. P. Perl, J. H. Morrison, G. Gold and P. R. Hof (2003). "Tangle and neuron numbers, but not amyloid load, predict cognitive status in Alzheimer's disease." Neurology **60**(9): 1495-1500.

Gilley, J., A. Seereeram, K. Ando, S. Mosely, S. Andrews, M. Kerschensteiner, T. Misgeld, J.-P. Brion, B. Anderton, D. P. Hanger and M. P. Coleman (2012). "Age-dependent axonal transport and locomotor changes and tau hypophosphorylation in a "P301L" tau knockin mouse." Neurobiology of Aging **33**(3): 621.e621-621.e615.

Giulian, D., L. J. Haverkamp, J. H. Yu, W. Karshin, D. Tom, J. Li, J. Kirkpatrick, L. M. Kuo and A. E. Roher (1996). "Specific domains of beta-amyloid from Alzheimer plaque elicit neuron killing in human microglia." J Neurosci **16**(19): 6021-6037.

Gleckman, A. M., Z. Jiang, Y. Liu and T. W. Smith (1999). "Neuronal and glial DNA fragmentation in Pick's disease." Acta Neuropathologica **98**(1): 55-61.

Godbout, J. P., J. Chen, J. Abraham, A. F. Richwine, B. M. Berg, K. W. Kelley and R. W. Johnson (2005). "Exaggerated neuroinflammation and sickness behavior in aged mice following activation of the peripheral innate immune system." FASEB journal : official publication of the Federation of American Societies for Experimental Biology **19**(10): 1329-1331.

Goedert, M. (1998). "Neurofibrillary pathology of Alzheimer's disease and other tauopathies." Prog Brain Res **117**: 287-306.

Goedert, M., M. Hasegawa, R. Jakes, S. Lawler, A. Cuenda and P. Cohen (1997). "Phosphorylation of microtubule-associated protein tau by stress-activated protein kinases." FEBS Letters **409**(1): 57-62.

Goedert, M. and R. Jakes (1990). "Expression of separate isoforms of human tau protein: correlation with the tau pattern in brain and effects on tubulin polymerization." Expression of separate isoforms of human tau protein: correlation with the tau pattern in brain and effects on tubulin polymerization.

Goedert, M., M. G. Spillantini, N. J. Cairns and R. A. Crowther (1992). "Tau proteins of alzheimer paired helical filaments: Abnormal phosphorylation of all six brain isoforms." Neuron **8**(1): 159-168.

Goedert, M., M. G. Spillantini, R. Jakes, D. Rutherford and R. A. Crowther (1989a). "Multiple isoforms of human microtubule-associated protein tau: sequences and localization in neurofibrillary tangles of Alzheimer's disease." Neuron **3**(4): 519-526.

Goedert, M., M. G. Spillantini, M. C. Potier, J. Ulrich and R. A. Crowther (1989b). "Cloning and sequencing of the cDNA encoding an isoform of microtubule-associated protein tau containing four tandem repeats: differential expression of tau protein mRNAs in human brain." The EMBO journal **8**(2): 393-399.

Goehler, L. E., J. K. Relton, D. Dripps, R. Kiechle, N. Tartaglia, S. F. Maier and L. R. Watkins (1997). "Vagal paraganglia bind biotinylated interleukin-1 receptor antagonist: a possible mechanism for immune-to-brain communication." Brain Res Bull **43**(3): 357-364.

Gomez-Isla, T., R. Hollister, H. West, S. Mui, J. H. Growdon, R. C. Petersen, J. E. Parisi and B. T. Hyman (1997). "Neuronal loss correlates with but exceeds neurofibrillary tangles in Alzheimer's disease." Ann Neurol **41**(1): 17-24.

Gong, C. X., S. Shaikh, J. Z. Wang, T. Zaidi, I. Grundke-Iqbal and K. Iqbal (1995). "Phosphatase Activity Toward Abnormally Phosphorylated τ: Decrease in Alzheimer Disease Brain." Journal of Neurochemistry **65**(2): 732-738.

Götz, J., F. Chen, R. Barmettler and R. M. Nitsch (2001). "Tau Filament Formation in Transgenic Mice Expressing P301L Tau." Journal of Biological Chemistry **276**(1): 529-534.

Gotz, J., A. Probst, M. G. Spillantini, T. Schafer, R. Jakes, K. Burki and M. Goedert (1995). "Somatodendritic localization and hyperphosphorylation of tau protein in transgenic mice expressing the longest human brain tau isoform." Embo j **14**(7): 1304-1313.

Gould, T. D., D. T. Dao and C. E. Kovacsics (2009). The Open Field Test. Mood and Anxiety Related Phenotypes in Mice: Characterization Using Behavioral Tests. T. D. Gould. Totowa, NJ, Humana Press**:** 1-20.

Grabert, K., T. Michoel, M. H. Karavolos, S. Clohisey, J. K. Baillie, M. P. Stevens, T. C. Freeman, K. M. Summers and B. W. McColl (2016). "Microglial brain region-dependent diversity and selective regional sensitivities to aging." Nat Neurosci **19**(3): 504-516.

Grand, J. H. G., S. Caspar and S. W. S. MacDonald (2011). "Clinical features and multidisciplinary approaches to dementia care." Journal of Multidisciplinary Healthcare **4**: 125-147.

Greenwood, J. A., C. W. Scott, R. C. Spreen, C. B. Caputo and G. V. W. Johnson (1994). "Casein kinase II preferentially phosphorylates human tau isoforms containing an amino-terminal insert: Identification of threonine 39 as the primary phosphate acceptor." Journal of Biological Chemistry **269**(6): 4373-4380.

Greer, G. G. and E. T. Rietschel (1978). "Lipid A-induced tolerance and hyperreactivity to hypothermia in mice." Infection and Immunity **19**(2): 357-368.

Gross, A. L., R. N. Jones, D. A. Habtemariam, T. Fong, D. Tommet, L. Quach, E. Schmitt, L. Yap and S. K. Inouye (2012). "Delirium and Long-term Cognitive Trajectory Among Persons With Dementia." Archives of internal medicine **172**(17): 1324-1331.

Grossberg, A. J. (2011). "Inflammatory regulation of hypothalamic neurons in sickness behavior."

Grundke-Iqbal, I., K. Iqbal, Y. C. Tung, M. Quinlan, H. M. Wisniewski and L. I. Binder (1986). "Abnormal phosphorylation of the microtubule-associated protein tau (tau) in Alzheimer cytoskeletal pathology." Proc Natl Acad Sci U S A **83**(13): 4913-4917.

Guan, Z. and J. Fang (2006). "Peripheral immune activation by lipopolysaccharide decreases neurotrophins in the cortex and hippocampus in rats." Brain, Behavior, and Immunity **20**(1): 64-71.

Guenther, K., R. M. J. Deacon, V. H. Perry and J. N. P. Rawlins (2001). "Early behavioural changes in scrapie-affected mice and the influence of dapsone." European Journal of Neuroscience **14**(2): 401-409.

Guerreiro, R., A. Wojtas, J. Bras, M. Carrasquillo, E. Rogaeva, E. Majounie, C. Cruchaga, C. Sassi, J. S. K. Kauwe, S. Younkin, L. Hazrati, J. Collinge, J. Pocock, T. Lashley, J. Williams, J.-C. Lambert, P. Amouyel, A. Goate, R. Rademakers, K. Morgan, J. Powell, P. St. George-Hyslop, A. Singleton and J. Hardy (2012). "TREM2 Variants in Alzheimer's Disease." New England Journal of Medicine **368**(2): 117-127.

Guillozet, A. L., S. Weintraub, D. C. Mash and M. Mesulam (2003). "NEurofibrillary tangles, amyloid, and memory in aging and mild cognitive impairment." Archives of Neurology **60**(5): 729-736.

Gutierrez, E. G., W. A. Banks and A. J. Kastin (1993). "Murine tumor necrosis factor alpha is transported from blood to brain in the mouse." Journal of Neuroimmunology **47**(2): 169-176.

Gutierrez, E. G., W. A. Banks and A. J. Kastin (1994). "Blood-borne interleukin-1 receptor antagonist crosses the blood-brain barrier." Journal of Neuroimmunology **55**(2): 153-160.

Halliday, G. M., R. Tan and H. Cartwright (2013). "Neuroanatomy for the Movement Disorder Specialist." Oxford Textbook of Movement Disorders: 11.

Hampton, D. W., D. J. Webber, B. Bilican, M. Goedert, M. G. Spillantini and S. Chandran (2010). "Cell-mediated neuroprotection in a mouse model of human tauopathy." The Journal of neuroscience : the official journal of the Society for Neuroscience **30**(30): 9973-9983.

Hanger, D. P., K. Hughes, J. R. Woodgett, J. P. Brion and B. H. Anderton (1992). "Glycogen synthase kinase-3 induces Alzheimer's disease-like phosphorylation of tau: Generation of paired helical filament epitopes and neuronal localisation of the kinase." Neuroscience Letters **147**(1): 58-62.

Hanisch, U.-K. and H. Kettenmann (2007). "Microglia: active sensor and versatile effector cells in the normal and pathologic brain." Nat Neurosci **10**(11): 1387-1394.

Hardy, J. and D. J. Selkoe (2002). "The amyloid hypothesis of Alzheimer's disease: progress and problems on the road to therapeutics." Science **297**(5580): 353-356.

Harris, J. A., A. Koyama, S. Maeda, K. Ho, N. Devidze, D. B. Dubal, G.-Q. Yu, E. Masliah and L. Mucke (2012). "Human P301L-Mutant Tau Expression in Mouse Entorhinal-Hippocampal Network Causes Tau Aggregation and Presynaptic Pathology but No Cognitive Deficits." PLOS ONE **7**(9): e45881.

Harrison, J. K., Y. Jiang, S. Chen, Y. Xia, D. Maciejewski, R. K. McNamara, W. J. Streit, M. N. Salafranca, S. Adhikari, D. A. Thompson, P. Botti, K. B. Bacon and L. Feng (1998). "Role for neuronally derived fractalkine in mediating interactions between neurons and CX3CR1-expressing microglia." Proceedings of the National Academy of Sciences **95**(18): 10896-10901.

Hart, B. L. (1988). "Biological basis of the behavior of sick animals." Neuroscience & Biobehavioral Reviews **12**(2): 123-137.

Hasel, P., O. Dando, Z. Jiwaji, P. Baxter, A. C. Todd, S. Heron, N. M. Markus, J. McQueen, D. W. Hampton, M. Torvell, S. S. Tiwari, S. McKay, A. Eraso-Pichot, A. Zorzano, R. Masgrau, E. Galea, S. Chandran, D. J. A. Wyllie, T. I. Simpson and G. E. Hardingham (2017). "Neurons and neuronal activity control gene expression in astrocytes to regulate their development and metabolism." Nat Commun **8**: 15132.

Hauss-Wegrzyniak, B., M. A. Lynch, P. D. Vraniak and G. L. Wenk (2002). "Chronic Brain Inflammation Results in Cell Loss in the Entorhinal Cortex and Impaired LTP in Perforant Path-Granule Cell Synapses." Experimental Neurology **176**(2): 336-341.

Henkel, K., J. Karitzky, M. Schmid, I. Mader, G. Glatting, J. W. Unger, B. Neumaier, A. C. Ludolph, S. N. Reske and G. B. Landwehrmeyer (2004). "Imaging of activated microglia with PET and [11C]PK 11195 in corticobasal degeneration." Movement Disorders **19**(7): 817-821.

Hennessy, E., É. W. Griffin and C. Cunningham (2015). "Astrocytes Are Primed by Chronic Neurodegeneration to Produce Exaggerated Chemokine and Cell Infiltration Responses to Acute Stimulation with the Cytokines IL-1β and TNF-α." The Journal of Neuroscience **35**(22): 8411.

Henry, C. J., Y. Huang, A. M. Wynne and J. P. Godbout (2009). "Peripheral lipopolysaccharide (LPS) challenge promotes microglial hyperactivity in aged mice that is associated with exaggerated induction of both pro-inflammatory IL-1beta and anti-inflammatory IL-10 cytokines." Brain Behav Immun **23**(3): 309-317.

Herber, D. L., L. M. Roth, D. Wilson, N. Wilson, J. E. Mason, D. Morgan and M. N. Gordon (2004). "Time-dependent reduction in Aβ levels after intracranial LPS administration in APP transgenic mice." Experimental Neurology **190**(1): 245-253.

Herrera, A. J., A. Castano, J. L. Venero, J. Cano and A. Machado (2000). "The single intranigral injection of LPS as a new model for studying the selective effects of inflammatory reactions on dopaminergic system." Neurobiol Dis **7**(4): 429-447.

Higuchi, M., T. Ishihara, B. Zhang, M. Hong, A. Andreadis, J. Q. Trojanowski and V. M. Y. Lee (2002). "Transgenic Mouse Model of Tauopathies with Glial Pathology and Nervous System Degeneration." Neuron **35**(3): 433-446.

Hirase, H. (2005). "A multi-photon window onto neuronal–glial–vascular communication." Trends in Neurosciences **28**(5): 217-219.

Ho, L., Z. Xiang, P. Mukherjee, W. Zhang, N. De Jesus, M. Mirjany, S. Yemul and G. M. Pasinetti (2001). "Gene expression profiling of the tau mutant (P301L) transgenic mouse brain." Neuroscience Letters **310**(1): 1-4.

Ho, S., N. Clipstone, L. Timmermann, J. Northrop, I. Graef, D. Fiorentino, J. Nourse and G. R. Crabtree (1996). "The Mechanism of Action of Cyclosporin A and FK506." Clinical Immunology and Immunopathology **80**(3): S40-S45.

Hoffmann, N. A., M. M. Dorostkar, S. Blumenstock, M. Goedert and J. Herms (2013). "Impaired plasticity of cortical dendritic spines in P301S tau transgenic mice." Acta Neuropathologica Communications **1**(1): 82.

Holmes, C., C. Colm, E. Zotova, J. Woolford, C. Dean, S. Kerr, D. Culliford and V. H. Perry (2009). "Systemic inflammation and disease progression in Alzheimer disease." Neurology **73**(10): 768-774.

Holmes, C., M. El-Okl, A. L. Williams, C. Cunningham, D. Wilcockson and V. H. Perry (2003). "Systemic infection, interleukin 1β, and cognitive decline in Alzheimer's disease." Journal of Neurology, Neurosurgery & Psychiatry **74**(6): 788.

Holtman, I. R., D. D. Raj, J. A. Miller, W. Schaafsma, Z. Yin, N. Brouwer, P. D. Wes, T. Möller, M. Orre, W. Kamphuis, E. M. Hol, E. W. G. M. Boddeke and B. J. L. Eggen (2015). "Induction of a common microglia gene expression signature by aging and neurodegenerative conditions: a co-expression meta-analysis." Acta Neuropathologica Communications **3**(1): 31.

Hoover, B. R., M. N. Reed, J. Su, R. D. Penrod, L. A. Kotilinek, M. K. Grant, R. Pitstick, G. A. Carlson, L. M. Lanier, L.-L. Yuan, K. H. Ashe and D. Liao (2010). "Tau Mislocalization to Dendritic Spines Mediates Synaptic Dysfunction Independently of Neurodegeneration." Neuron **68**(6): 1067-1081.

Hosoi, T., Y. Okuma and Y. Nomura (2000). "Electrical stimulation of afferent vagus nerve induces IL-1beta expression in the brain and activates HPA axis." Am J Physiol Regul Integr Comp Physiol **279**(1): R141-147.

Howard, R. Z., O. (2017). "Clinical Trials: Minocycline in Alzheimer's Disease (MADE)." Retrieved 1st September 2017, 2017, from https://www.kcl.ac.uk/ioppn/depts/oldage/research/Medication-studies/Clinical-Trials/minocycline-in-alzheimers-disease-(MADE).aspx.

Hrnkova, M., N. Zilka, Z. Minichova, P. Koson and M. Novak (2007). "Neurodegeneration caused by expression of human truncated tau leads to

progressive neurobehavioural impairment in transgenic rats." Brain Research **1130**: 206-213.

Hu, J. and L. J. Van Eldik (1996). "S100β induces apoptotic cell death in cultured astrocytes via a nitric oxide-dependent pathway." Biochimica et Biophysica Acta - Molecular Cell Research **1313**(3): 239-245.

Huang, S.-W., W.-T. Wang, L.-C. Chou, C.-D. Liao, T.-H. Liou and H.-W. Lin (2015). "Osteoarthritis Increases the Risk of Dementia: A Nationwide Cohort Study in Taiwan." Scientific Reports **5**: 10145.

Hutton, M., C. L. Lendon, P. Rizzu, M. Baker, S. Froelich, H. Houlden, S. Pickering-Brown, S. Chakraverty, A. Isaacs, A. Grover, J. Hackett, J. Adamson, S. Lincoln, D. Dickson, P. Davies, R. C. Petersen, M. Stevens, E. d. Graaff, E. Wauters, J. v. Baren, M. Hillebrand, M. Joosse, J. M. Kwon, P. Nowotny, L. K. Che, J. Norton, J. C. Morris, L. A. Reed, J. Trojanowski, H. Basun, L. Lannfelt, M. Neystat, S. Fahn, F. Dark, T. Tannenberg, P. R. Dodd, N. Hayward, J. B. Kwok, P. R. Schofield, A. Andreadis, J. Snowden, D. Craufurd, D. Neary, F. Owen, B. A. Oostra, J. Hardy, A. Goate, J. v. Swieten, D. Mann, T. Lynch and P. Heutink (1998). "Association of missense and 5'-splice-site mutations in tau with the inherited dementia FTDP-17." Nature **393**(6686): 702-705.

Huynh, M.-L. N., V. A. Fadok and P. M. Henson (2002). "Phosphatidylserine-dependent ingestion of apoptotic cells promotes TGF-β1 secretion and the resolution of inflammation." The Journal of Clinical Investigation **109**(1): 41-50.

Ikeda, M., T. Kawarai, T. Kawarabayashi, E. Matsubara, T. Murakami, A. Sasaki, Y. Tomidokoro, Y. Ikarashi, H. Kuribara, K. Ishiguro, M. Hasegawa, S.-H. Yen, M. A. Chishti, Y. Harigaya, K. Abe, K. Okamoto, P. St. George-Hyslop, D. Westaway and M. Shoji (2005). "Accumulation of Filamentous Tau in the Cerebral Cortex of Human Tau R406W Transgenic Mice." The American Journal of Pathology **166**(2): 521-531.

Illenberger, S., Q. Zheng-Fischhöfer, U. Preuss, K. Stamer, K. Baumann, B. Trinczek, J. Biernat, R. Godemann, E.-M. Mandelkow and E. Mandelkow (1998). "The Endogenous and Cell Cycle-dependent Phosphorylation of tau Protein in Living Cells: Implications for Alzheimer's Disease." Molecular Biology of the Cell **9**(6): 1495-1512.

Ingelsson, M., H. Fukumoto, K. L. Newell, J. H. Growdon, E. T. Hedley-Whyte, M. P. Frosch, M. S. Albert, B. T. Hyman and M. C. Irizarry (2004). "Early Abeta accumulation and progressive synaptic loss, gliosis, and tangle formation in AD brain." Neurology **62**(6): 925-931.

Inouye, S. K., S. T. Bogardus, P. A. Charpentier, L. Leo-Summers, D. Acampora, T. R. Holford and L. M. Cooney (1999). "A Multicomponent Intervention to Prevent

Delirium in Hospitalized Older Patients." New England Journal of Medicine **340**(9): 669-676.

Irwin, S. (1968). "Comprehensive observational assessment: Ia. A systematic, quantitative procedure for assessing the behavioral and physiologic state of the mouse." Psychopharmacologia **13**(3): 222-257.

Ishihara, T., M. Hong, B. Zhang, Y. Nakagawa, M. K. Lee, J. Q. Trojanowski and V. M. Y. Lee (1999). "Age-Dependent Emergence and Progression of a Tauopathy in Transgenic Mice Overexpressing the Shortest Human Tau Isoform." Neuron **24**(3): 751-762.

Ishihara, T., B. Zhang, M. Higuchi, Y. Yoshiyama, J. Q. Trojanowski and V. M. Y. Lee (2001). "Age-Dependent Induction of Congophilic Neurofibrillary Tau Inclusions in Tau Transgenic Mice." The American Journal of Pathology **158**(2): 555-562.

Ishizawa, K. and D. W. Dickson (2001). "Microglial Activation parallels System Degeneration in progressive Supranuclear palsy and Corticobasal Degeneration." Journal of Neuropathology & Experimental Neurology **60**(6): 647.

Ishizu, A., H. Ishikura, Y. Nakamaru, K. Kikuchi, T. Koike and T. Yoshiki (1997). "Interleukin-1α Regulates Thy-1 Expression on Rat Vascular Endothelial Cells." Microvascular Research **53**(1): 73-78.

Itagaki, S., P. L. McGeer and H. Akiyama (1988). "Presence of T-cytotoxic suppressor and leucocyte common antigen positive cells in Alzheimer's disease brain tissue." Neuroscience Letters **91**(3): 259-264.

Ito, D., Y. Imai, K. Ohsawa, K. Nakajima, Y. Fukuuchi and S. Kohsaka (1998). "Microglia-specific localisation of a novel calcium binding protein, Iba1." Molecular Brain Research **57**(1): 1-9.

Jin, H., N. Copeland, D. Gilbert, N. Jenkins, R. Kirkpatrick and M. Rosenberg (1998). "Genetic characterization of the murine Ym1 gene and identification of a cluster of highly homologous genes." Genomics **54**(2): 316-322.

Johnson, G. V. W. (1992). "Differential Phosphorylation of τ by Cyclic AMP-Dependent Protein Kinase and Ca2+/Calmodulin-Dependent Protein Kinase II: Metabolic and Functional Consequences." Journal of Neurochemistry **59**(6): 2056-2062.

Jonsson, T., H. Stefansson, S. Steinberg, I. Jonsdottir, P. V. Jonsson, J. Snaedal, S. Bjornsson, J. Huttenlocher, A. I. Levey, J. J. Lah, D. Rujescu, H. Hampel, I. Giegling, O. A. Andreassen, K. Engedal, I. Ulstein, S. Djurovic, C. Ibrahim-Verbaas, A. Hofman, M. A. Ikram, C. M. van Duijn, U. Thorsteinsdottir, A. Kong and K. Stefansson (2013).

"Variant of TREM2 associated with the risk of Alzheimer's disease." N Engl J Med **368**(2): 107-116.

Kahlson, M. A. and K. J. Colodner (2015). "Glial Tau Pathology in Tauopathies: Functional Consequences." Journal of Experimental Neuroscience **9**(Suppl 2): 43-50.

Kaneko, T., R.-H. Cho, Y.-Q. Li, S. Nomura and N. Mizuno (2000). "Predominant information transfer from layer III pyramidal neurons to corticospinal neurons." The Journal of Comparative Neurology **423**(1): 52-65.

Kanemaru, K., K. Takio, R. Miura, K. Titani and Y. Ihara (1992). "Fetal-Type Phosphorylation of the τ in Paired Helical Filaments." Journal of Neurochemistry **58**(5): 1667-1675.

Kfoury, N., B. B. Holmes, H. Jiang, D. M. Holtzman and M. I. Diamond (2012). "Trans-cellular propagation of Tau aggregation by fibrillar species." J Biol Chem **287**(23): 19440-19451.

Kida, E., M. Barcikowska and M. Niemczewska (1992). "Immunohistochemical study of a case with progressive supranuclear palsy without ophthalmoplegia." Acta Neuropathol **83**(3): 328-332.

Kim, W. G., R. P. Mohney, B. Wilson, G. H. Jeohn, B. Liu and J. S. Hong (2000). "Regional difference in susceptibility to lipopolysaccharide-induced neurotoxicity in the rat brain: role of microglia." J Neurosci **20**(16): 6309-6316.

Kirby, K. A., B. A. Rothenburg, W. Victery, A. J. Vander and M. J. Kluger (1982). "Urinary excretion of zinc and iron following injection of bacteria in the unanesthetized rabbit." Mineral and electrolyte metabolism **7**(5): 250-256.

Kitazawa, M., S. Oddo, T. R. Yamasaki, K. N. Green and F. M. LaFerla (2005). "Lipopolysaccharide-induced inflammation exacerbates tau pathology by a cyclin-dependent kinase 5-mediated pathway in a transgenic model of Alzheimer's disease." The Journal of neuroscience : the official journal of the Society for Neuroscience **25**(39): 8843-8853.

Kluger, M. J. (1991). "Fever: Role of pyrogens and cryogens." Physiological Reviews **71**(1): 93-127.

Komori, T. (1999). "Tau-positive dial Inclusions in Progressive Supranuclear Palsy, Corticobasal Degeneration and Pick's Disease." Brain Pathology **9**(4): 663-679.

Koning, N., D. F. Swaab, R. M. Hoek and I. Huitinga (2009). "Distribution of the immune inhibitory molecules CD200 and CD200R in the normal central nervous

system and multiple sclerosis lesions suggests neuron-glia and glia-glia interactions." Journal of Neuropathology and Experimental Neurology **68**(2): 159-167.

Konsman, J. P., P. Parnet and R. Dantzer (2002). "Cytokine-induced sickness behaviour: mechanisms and implications." Trends in neurosciences **25**(3): 154-159.

Kopeikina, K. J., M. Polydoro, H.-C. Tai, E. Yaeger, G. A. Carlson, R. Pitstick, B. T. Hyman and T. L. Spires-Jones (2013). "Synaptic alterations in the rTg4510 mouse model of tauopathy." The Journal of comparative neurology **521**(6): 1334-1353.

Koss, D. J., L. Robinson, B. D. Drever, K. Plucińska, S. Stoppelkamp, P. Veselcic, G. Riedel and B. Platt (2016). "Mutant Tau knock-in mice display frontotemporal dementia relevant behaviour and histopathology." Neurobiology of Disease **91**: 105-123.

Kraemer, B. C., B. Zhang, J. B. Leverenz, J. H. Thomas, J. Q. Trojanowski and G. D. Schellenberg (2003). "Neurodegeneration and defective neurotransmission in a Caenorhabditis elegans model of tauopathy." Proceedings of the National Academy of Sciences **100**(17): 9980-9985.

Ksiezak-Reding, H., W. K. Liu and S. H. Yen (1992). "Phosphate analysis and dephosphorylation of modified tau associated with paired helical filaments." Brain Research **597**(2): 209-219.

Ksiezak-Reding, H., K. Morgan, L. A. Mattiace, P. Davies, W. K. Liu, S. H. Yen, K. Weidenheim and D. W. Dickson (1994). "Ultrastructure and biochemical composition of paired helical filaments in corticobasal degeneration." American Journal of Pathology **145**(6): 1496-1508.

Kumagae, Y., Y. Zhang, O. J. Kim and C. A. Miller (1999). "Human c-Jun N-terminal kinase expression and activation in the nervous system." Molecular Brain Research **67**(1): 10-17.

Kyrkanides, S., R. H. Tallents, J.-n. H. Miller, M. E. Olschowka, R. Johnson, M. Yang, J. A. Olschowka, S. M. Brouxhon and M. K. O'Banion (2011). "Osteoarthritis accelerates and exacerbates Alzheimer's disease pathology in mice." Journal of Neuroinflammation **8**(1): 112.

Ladner, C. J., J. Czech, J. Maurice, S. A. Lorens and J. M. Lee (1996). "Reduction of calcineurin enzymatic activity in Alzheimer's disease: Correlation with neuropathologic changes." Journal of Neuropathology and Experimental Neurology **55**(8): 924-931.

Laflamme, N., S. Lacroix and S. Rivest (1999). "An essential role of interleukin-1beta in mediating NF-kappaB activity and COX-2 transcription in cells of the blood-brain

barrier in response to a systemic and localized inflammation but not during endotoxemia." J Neurosci **19**(24): 10923-10930.

Laurent, C., G. Dorothée, S. Hunot, E. Martin, Y. Monnet, M. Duchamp, Y. Dong, F.-P. Légeron, A. Leboucher, S. Burnouf, E. Faivre, K. Carvalho, R. Caillierez, N. Zommer, D. Demeyer, N. Jouy, V. Sazdovitch, S. Schraen-Maschke, C. Delarasse, L. Buée and D. Blum (2016). "Hippocampal T cell infiltration promotes neuroinflammation and cognitive decline in a mouse model of tauopathy." Brain.

Lawson, L. J., V. H. Perry, P. Dri and S. Gordon (1990). "Heterogeneity in the distribution and morphology of microglia in the normal adult mouse brain." Neuroscience **39**(1): 151-170.

Layé, S., G. Gheusi, S. Cremona, C. Combe, K. Kelley, R. Dantzer and P. Parnet (2000). "Endogenous brain IL-1 mediates LPS-induced anorexia and hypothalamic cytokine expression." American Journal of Physiology - Regulatory, Integrative and Comparative Physiology **279**(1): R93-R98.

Lee, C.-K., R. Weindruch and T. A. Prolla (2000). "Gene-expression profile of the ageing brain in mice." Nat Genet **25**(3): 294-297.

Lee, C. G., C. A. Da Silva, C. S. Dela Cruz, F. Ahangari, B. Ma, M.-J. Kang, C.-H. He, S. Takyar and J. A. Elias (2011). "Role of Chitin and Chitinase/Chitinase-Like Proteins in Inflammation, Tissue Remodeling, and Injury." Annual review of physiology **73**: 10.1146/annurev-physiol-012110-142250.

Lee, D. C., J. Rizer, M.-L. B. Selenica, P. Reid, C. Kraft, A. Johnson, L. Blair, M. N. Gordon, C. A. Dickey and D. Morgan (2010). "LPS- induced inflammation exacerbates phospho-tau pathology in rTg4510 mice." Journal of Neuroinflammation **7**(1): 56.

Lee, H.-g., G. Casadesus, X. Zhu, R. J. Castellani, A. McShea, G. Perry, R. B. Petersen, V. Bajic and M. A. Smith (2009). "Cell cycle re-entry mediated neurodegeneration and its treatment role in the pathogenesis of Alzheimer's disease." Neurochemistry International **54**(2): 84-88.

Lee, J., S. L. Chan and M. P. Mattson (2002). "Adverse effect of a presenilin-1 mutation in microglia results in enhanced nitric oxide and inflammatory cytokine responses to immune challenge in the brain." NeuroMolecular Medicine **2**(1): 29-45.

Lee, J. W., Y. K. Lee, D. Y. Yuk, D. Y. Choi, S. B. Ban, K. W. Oh and J. T. Hong (2008). "Neuro-inflammation induced by lipopolysaccharide causes cognitive impairment through enhancement of beta-amyloid generation." Journal of Neuroinflammation **5**(1): 37.

Leon, L. R., W. Kozak, K. Rudolph and M. J. Kluger (1999). "An antipyretic role for interleukin-10 in LPS fever in mice." Am J Physiol **276**(1 Pt 2): R81-89.

Leon, L. R., A. A. White and M. J. Kluger (1998). "Role of IL-6 and TNF in thermoregulation and survival during sepsis in mice." American Journal of Physiology - Regulatory, Integrative and Comparative Physiology **275**(1): R269-R277.

Lewis, J., E. McGowan, J. Rockwood, H. Melrose, P. Nacharaju, M. Van Slegtenhorst, K. Gwinn-Hardy, M. P. Murphy, M. Baker, X. Yu, K. Duff, J. Hardy, A. Corral, W.-L. Lin, S.-H. Yen, D. W. Dickson, P. Davies and M. Hutton (2000). "Neurofibrillary tangles, amyotrophy and progressive motor disturbance in mice expressing mutant (P301L) tau protein." Nat Genet **25**(4): 402-405.

Li, H.-L., H.-H. Wang, S.-J. Liu, Y.-Q. Deng, Y.-J. Zhang, Q. Tian, X.-C. Wang, X.-Q. Chen, Y. Yang and J.-Y. Zhang (2007). "Phosphorylation of tau antagonizes apoptosis by stabilizing β-catenin, a mechanism involved in Alzheimer's neurodegeneration." Proceedings of the National Academy of Sciences **104**(9): 3591-3596.

Li, T., C. Hawkes, H. Y. Qureshi, S. Kar and H. K. Paudel (2006). "Cyclin-Dependent Protein Kinase 5 Primes Microtubule-Associated Protein Tau Site-Specifically for Glycogen Synthase Kinase 3β." Biochemistry **45**(10): 3134-3145.

Li, Y., L. Liu, S. W. Barger and W. S. T. Griffin (2003). "Interleukin-1 Mediates Pathological Effects of Microglia on Tau Phosphorylation and on Synaptophysin Synthesis in Cortical Neurons through a p38-MAPK Pathway." The Journal of neuroscience : the official journal of the Society for Neuroscience **23**(5): 1605-1611.

Liddelow, S. A., K. A. Guttenplan, L. E. Clarke, F. C. Bennett, C. J. Bohlen, L. Schirmer, M. L. Bennett, A. E. Münch, W.-S. Chung, T. C. Peterson, D. K. Wilton, A. Frouin, B. A. Napier, N. Panicker, M. Kumar, M. S. Buckwalter, D. H. Rowitch, V. L. Dawson, T. M. Dawson, B. Stevens and B. A. Barres (2017). "Neurotoxic reactive astrocytes are induced by activated microglia." Nature **541**(7638): 481-487.

Lim, F., F. Hernández, J. J. Lucas, P. Gómez-Ramos, M. A. Morán and J. Ávila (2001). "FTDP-17 Mutations in tau Transgenic Mice Provoke Lysosomal Abnormalities and Tau Filaments in Forebrain." Molecular and Cellular Neuroscience **18**(6): 702-714.

Limatola, C. and R. M. Ransohoff (2014). "Modulating neurotoxicity through CX3CL1/CX3CR1 signaling." Frontiers in Cellular Neuroscience **8**(229).

Lin, W.-L., C. Zehr, J. Lewis, M. Hutton, S.-H. Yen and D. W. Dickson (2005). "Progressive white matter pathology in the spinal cord of transgenic mice expressing mutant (P301L) human tau." Journal of Neurocytology **34**(6): 397-410.

Liu, G.-P., W. Wei, X. Zhou, Y. Zhang, H.-H. Shi, J. Yin, X.-Q. Yao, C.-X. Peng, J. Hu and Q. Wang (2012a). "I 2 PP2A regulates p53 and Akt correlatively and leads the neurons to abort apoptosis." Neurobiology of aging **33**(2): 254-264.

Liu, L., V. Drouet, J. W. Wu, M. P. Witter, S. A. Small, C. Clelland and K. Duff (2012b). "Trans-synaptic spread of tau pathology in vivo." PloS one **7**(2).

Liu, S., Y. Liu, W. Hao, L. Wolf, A. J. Kiliaan, B. Penke, C. E. Rube, J. Walter, M. T. Heneka, T. Hartmann, M. D. Menger and K. Fassbender (2012c). "TLR2 is a primary receptor for Alzheimer's amyloid beta peptide to trigger neuroinflammatory activation." J Immunol **188**(3): 1098-1107.

Liu, W. K., R. T. Williams, F. L. Hall, D. W. Dickson and S. H. Yen (1995). "Detection of a Cdc2-related kinase associated with Alzheimer paired helical filaments." American Journal of Pathology **146**(1): 228-238.

Liu, Y., S. Walter, M. Stagi, D. Cherny, M. Letiembre, W. Schulz-Schaeffer, H. Heine, B. Penke, H. Neumann and K. Fassbender (2005). "LPS receptor (CD14): a receptor for phagocytosis of Alzheimer's amyloid peptide." Brain **128**(8): 1778-1789.

Lively, S. and L. C. Schlichter (2013). "The microglial activation state regulates migration and roles of matrix-dissolving enzymes for invasion." Journal of Neuroinflammation **10**: 75-75.

Lodish, Berk, Zipursky., Matsudaira, Baltimore and Darnell (2000). Molecular Cell Biology Section 19.2, Microtubule Dynamics and Associated Proteins. Molecular Cell Biology New York, W. H. Freeman.

Louveau, A., I. Smirnov, T. J. Keyes, J. D. Eccles, S. J. Rouhani, J. D. Peske, N. C. Derecki, D. Castle, J. W. Mandell, K. S. Lee, T. H. Harris and J. Kipnis (2015). "Structural and functional features of central nervous system lymphatic vessels." Nature **523**(7560): 337-341.

Lu, Y.-C., W.-C. Yeh and P. S. Ohashi (2008). "LPS/TLR4 signal transduction pathway." Cytokine **42**(2): 145-151.

Lyman, M., D. Lloyd, X. Ji, M. Vizcaychipi and D. Ma (2013). "Neuroinflammation: The role and consequences." Neuroscience research.

Lynch, A. M. and M. A. Lynch (2002). "The age-related increase in IL-1 type I receptor in rat hippocampus is coupled with an increase in caspase-3 activation." European Journal of Neuroscience **15**(11): 1779-1788.

Lynch, A. M., C. Walsh, A. Delaney, Y. Nolan, V. A. Campbell and M. A. Lynch (2004). "Lipopolysaccharide-induced increase in signalling in hippocampus is abrogated by IL-10 – a role for IL-1β?" Journal of Neurochemistry **88**(3): 635-646.

Maeda, S., N. Sahara, Y. Saito, M. Murayama, Y. Yoshiike, H. Kim, T. Miyasaka, S. Murayama, A. Ikai and A. Takashima (2007). "Granular tau oligomers as intermediates of tau filaments." Biochemistry **46**(12): 3856-3861.

Magnus, T., A. Chan, O. Grauer, K. V. Toyka and R. Gold (2001). "Microglial phagocytosis of apoptotic inflammatory T cells leads to down-regulation of microglial immune activation." J Immunol **167**(9): 5004-5010.

Makar, T. K., D. Trisler, C. T. Bever, J. E. Goolsby, K. T. Sura, S. Balasubramanian, S. Sultana, N. Patel, D. Ford, I. S. Singh, A. Gupta, R. M. Valenzuela and S. Dhib-Jalbut (2008). "Stem cell based delivery of IFN-β reduces relapses in experimental autoimmune encephalomyelitis." Journal of Neuroimmunology **196**(1-2): 67-81.

Maphis, N., G. Xu, O. N. Kokiko-Cochran, A. E. Cardona, R. M. Ransohoff, B. T. Lamb and K. Bhaskar (2015a). "Loss of tau rescues inflammation-mediated neurodegeneration." Frontiers in Neuroscience **9**(196).

Maphis, N., G. Xu, O. N. Kokiko-Cochran, S. Jiang, A. Cardona, R. M. Ransohoff, B. T. Lamb and K. Bhaskar (2015b). "Reactive microglia drive tau pathology and contribute to the spreading of pathological tau in the brain." Brain **138**(Pt 6): 1738-1755.

Martin, D. S. D., P. E. Lonergan, B. Boland, M. P. Fogarty, M. Brady, D. F. Horrobin, V. A. Campbell and M. A. Lynch (2002). "Apoptotic Changes in the Aged Brain Are Triggered by Interleukin-1β-induced Activation of p38 and Reversed by Treatment with Eicosapentaenoic Acid." Journal of Biological Chemistry **277**(37): 34239-34246.

Martinez-Hernandez, A., K. Bell and M. Norenberg (1977). "Glutamine synthetase: glial localization in brain." Science **195**(4284): 1356-1358.

Martinez-Lopez, J. E., J. A. Moreno-Bravo, M. P. Madrigal, S. Martinez and E. Puelles (2015). "Red nucleus and rubrospinal tract disorganization in the absence of Pou4f1." Front Neuroanat **9**: 8.

Martinez, F. O. and S. Gordon (2014). "The M1 and M2 paradigm of macrophage activation: time for reassessment." F1000Prime Reports **6**: 13.

Mastrangelo, M. A., K. L. Sudol, W. C. Narrow and W. J. Bowers (2009). "Interferon-g; Differentially Affects Alzheimer's Disease Pathologies and Induces Neurogenesis in Triple Transgenic-AD Mice." The American Journal of Pathology **175**(5): 2076-2088.

Matsumura, K. and S. Kobayashi (2004). "Signaling the brain in inflammation: the role of endothelial cells." Front Biosci **9**: 2819-2826.

McDonald, D. R., M. E. Bamberger, C. K. Combs and G. E. Landreth (1998). "β-Amyloid Fibrils Activate Parallel Mitogen-Activated Protein Kinase Pathways in Microglia and THP1 Monocytes." The Journal of Neuroscience **18**(12): 4451.

McKeon, R. J., R. C. Schreiber, J. S. Rudge and J. Silver (1991). "Reduction of neurite outgrowth in a model of glial scarring following CNS injury is correlated with the expression of inhibitory molecules on reactive astrocytes." Journal of Neuroscience **11**(11): 3398-3411.

McShea, A., P. L. R. Harris, K. R. Webster, A. F. Wahl and M. A. Smith (1997). "Abnormal expression of the cell cycle regulators P16 and CDK4 in Alzheimer's disease." American Journal of Pathology **150**(6): 1933-1939.

McShea, A., H.-g. Lee, R. B. Petersen, G. Casadesus, I. Vincent, N. J. Linford, J.-O. Funk, R. A. Shapiro and M. A. Smith (2007). "Neuronal cell cycle re-entry mediates Alzheimer disease-type changes." Biochimica et Biophysica Acta (BBA) - Molecular Basis of Disease **1772**(4): 467-472.

Mekada, K., K. Abe, A. Murakami, S. Nakamura, H. Nakata, K. Moriwaki, Y. Obata and A. Yoshiki (2009). "Genetic Differences among C57BL/6 Substrains." Experimental Animals **58**(2): 141-149.

Mittelbronn, M., K. Dietz, H. J. Schluesener and R. Meyermann (2001). "Local distribution of microglia in the normal adult human central nervous system differs by up to one order of magnitude." Acta Neuropathol **101**(3): 249-255.

Monje, M. L., H. Toda and T. D. Palmer (2003). "Inflammatory Blockade Restores Adult Hippocampal Neurogenesis." Science **302**(5651): 1760-1765.

Moore, K. W., R. D. Malefyt, R. L. Coffman and A. O'Garra (2001). "Interleukin-10 and the interleukin-10 receptor." Annual Review of Immunology **19**: 683-765.

Morales, I., J. M. Jimenez, M. Mancilla and R. B. Maccioni (2013). "Tau oligomers and fibrils induce activation of microglial cells." J Alzheimers Dis **37**(4): 849-856.

Morfini, G. A., M. Burns, L. I. Binder, N. M. Kanaan, N. LaPointe, D. A. Bosco, R. H. Brown, Jr., H. Brown, A. Tiwari, L. Hayward, J. Edgar, K. A. Nave, J. Garberrn, Y. Atagi, Y. Song, G. Pigino and S. T. Brady (2009). "Axonal transport defects in neurodegenerative diseases." J Neurosci **29**(41): 12776-12786.

Mori, H., J. Kondo and Y. Ihara (1987). "Ubiquitin is a component of paired helical filaments in Alzheimer's disease." Science **235**(4796): 1641-1644.

Mudher, A., D. Shepherd, T. A. Newman, P. Mildren, J. P. Jukes, A. Squire, A. Mears, S. Berg, D. MacKay, A. A. Asuni, R. Bhat and S. Lovestone (2004). "GSK-3[beta] inhibition reverses axonal transport defects and behavioural phenotypes in Drosophila." Mol Psychiatry **9**(5): 522-530.

Mullen, R. J., C. R. Buck and A. M. Smith (1992). "NeuN, a neuronal specific nuclear protein in vertebrates." Development **116**(1): 201-211.

Murakami, T., E. Paitel, T. Kawarabayashi, M. Ikeda, M. A. Chishti, C. Janus, E. Matsubara, A. Sasaki, T. Kawarai, A. L. Phinney, Y. Harigaya, P. Horne, N. Egashira, K. Mishima, A. Hanna, J. Yang, K. Iwasaki, M. Takahashi, M. Fujiwara, K. Ishiguro, C. Bergeron, G. A. Carlson, K. Abe, D. Westaway, P. St. George-Hyslop and M. Shoji (2006). "Cortical Neuronal and Glial Pathology in TgTauP301L Transgenic Mice: Neuronal Degeneration, Memory Disturbance, and Phenotypic Variation." The American Journal of Pathology **169**(4): 1365-1375.

Murphy, G. M., Jr., Y. L. Lee, X. C. Jia, A. C. H. Yu, A. Majewska, Y. Song, K. Schmidt and L. F. Eng (1995). "Tumor Necrosis Factor-α and Basic Fibroblast Growth Factor Decrease Glial Fibrillary Acidic Protein and Its Encoding mRNA in Astrocyte Cultures and Glioblastoma Cells." Journal of Neurochemistry **65**(6): 2716-2724.

Murray, C., D. J. Sanderson, C. Barkus, R. M. Deacon, J. N. Rawlins, D. M. Bannerman and C. Cunningham (2012). "Systemic inflammation induces acute working memory deficits in the primed brain: relevance for delirium." Neurobiol Aging **33**(3): 603-616.e603.

Murray, C. L., D. T. Skelly and C. Cunningham (2011). "Exacerbation of CNS inflammation and neurodegeneration by systemic LPS treatment is independent of circulating IL-1β and IL-6." Journal of Neuroinflammation **8**(1): 50.

Nagy, Z., M. M. Esiri, A. M. Cato and A. D. Smith (1997a). "Cell cycle markers in the hippocampus in Alzheimer's disease." Acta Neuropathologica **94**(1): 6-15.

Nagy, Z., M. M. Esiri and A. D. Smith (1997b). "Expression of cell division markers in the hippocampus in Alzheimer's disease and other neurodegenerative conditions." Acta Neuropathologica **93**(3): 294-300.

Neve, R. L., P. Harris, K. S. Kosik, D. M. Kurnit and T. A. Donlon (1986). "Identification of cDNA clones for the human microtubule-associated protein tau and chromosomal localization of the genes for tau and microtubule-associated protein 2." Brain Research **387**(3): 271-280.

Nimmerjahn, A., F. Kirchhoff and F. Helmchen (2005). "Resting microglial cells are highly dynamic surveillants of brain parenchyma in vivo." Science **308**(5726): 1314-1318.

Nolan, Y., E. Vereker, A. M. Lynch and M. A. Lynch (2003). "Evidence that lipopolysaccharide-induced cell death is mediated by accumulation of reactive oxygen species and activation of p38 in rat cortex and hippocampus." Experimental Neurology **184**(2): 794-804.

Norden, D. M., P. J. Trojanowski, E. Villanueva, E. Navarro and J. P. Godbout (2016). "Sequential activation of microglia and astrocyte cytokine expression precedes increased Iba-1 or GFAP immunoreactivity following systemic immune challenge." Glia **64**(2): 300-316.

Oguri, S., K. Motegi, Y. Iwakura and Y. Endo (2002). "Primary Role of Interleukin-1α and Interleukin-1β in Lipopolysaccharide-Induced Hypoglycemia in Mice." Clinical and Diagnostic Laboratory Immunology **9**(6): 1307-1312.

Oh, Y. J., G. J. Markelonis and T. H. Oh (1993). "Effects of interleukin-1β and tumor necrosis factor-α on the expression of glial fibrillary acidic protein and transferrin in cultured astrocytes." Glia **8**(2): 77-86.

Ohsawa, K., Y. Imai, Y. Sasaki and S. Kohsaka (2004). "Microglia/macrophage-specific protein Iba1 binds to fimbrin and enhances its actin-bundling activity." Journal of Neurochemistry **88**(4): 844-856.

ONS (2016). "Statistical bulletin: Deaths registered in England and Wales: 2015." The National Archives.

Palin, K., C. Cunningham, P. Forse, V. H. Perry and N. Platt (2008). "Systemic inflammation switches the inflammatory cytokine profile in CNS Wallerian degeneration." Neurobiology of disease **30**(1): 19-29.

Pandharipande, P. P., T. D. Girard, J. C. Jackson, A. Morandi, J. L. Thompson, B. T. Pun, N. E. Brummel, C. G. Hughes, E. E. Vasilevskis, A. K. Shintani, K. G. Moons, S. K. Geevarghese, A. Canonico, R. O. Hopkins, G. R. Bernard, R. S. Dittus and E. W. Ely (2013). "Long-Term Cognitive Impairment after Critical Illness." New England Journal of Medicine **369**(14): 1306-1316.

Parnet, P., S. Amindari, C. Wu, D. Brunke-Reese, E. Goujon, J. A. Weyhenmeyer, R. Dantzer and K. W. Kelley (1994). "Expression of type I and type II interleukin-1 receptors in mouse brain." Brain Res Mol Brain Res **27**(1): 63-70.

Patrick, G. N., L. Zukerberg, M. Nikolic, S. de la Monte, P. Dikkes and L.-H. Tsai (1999). "Conversion of p35 to p25 deregulates Cdk5 activity and promotes neurodegeneration." Nature **402**(6762): 615-622.

Paulus, W., C. Bancher and K. Jellinger (1993). "Microglial reaction in Pick's disease." Neuroscience Letters **161**(1): 89-92.

Pavlides, C., E. Miyashita and H. Asanuma (1993). "Projection from the sensory to the motor cortex is important in learning motor skills in the monkey." J Neurophysiol **70**(2): 733-741.

Pearson Education, I. (2016). Periplasm Peptidoglycan Cell wall Lipopolysaccharide Lipid A Protein Porin protein Lipoprotein Phospholipid Outer membrane Plasma membrane Lipid A Core polysaccharide O polysaccharide Parts of the LPS Core polysaccharide O polysaccharide. B. c. walls.

Pennanen, L., H. Welzl, P. D'Adamo, R. M. Nitsch and J. Götz (2004). "Accelerated extinction of conditioned taste aversion in P301L tau transgenic mice." Neurobiology of Disease **15**(3): 500-509.

Pennanen, L., D. P. Wolfer, R. M. Nitsch and J. Götz (2006). "Impaired spatial reference memory and increased exploratory behavior in P301L tau transgenic mice." Genes, Brain and Behavior **5**(5): 369-379.

Perry, V. H., C. Cunningham and C. Holmes (2007). "Systemic infections and inflammation affect chronic neurodegeneration." Nature reviews. Immunology **7**(2): 161-167.

Phillips, H. S., J. M. Hains, M. Armanini, G. R. Laramee, S. A. Johnson and J. W. Winslow (1991). "BDNF mRNA is decreased in the hippocampus of individuals with Alzheimer's disease." Neuron **7**(5): 695-702.

Planel, E., A. Bretteville, L. Liu, L. Virag, A. L. Du, W. H. Yu, D. W. Dickson, R. A. Whittington and K. E. Duff (2009). "Acceleration and persistence of neurofibrillary pathology in a mouse model of tauopathy following anesthesia." The FASEB Journal **23**(8): 2595-2604.

Planel, E., K. E. G. Richter, C. E. Nolan, J. E. Finley, L. Liu, Y. Wen, P. Krishnamurthy, M. Herman, L. Wang, J. B. Schachter, R. B. Nelson, L.-F. Lau and K. E. Duff (2007). "Anesthesia Leads to Tau Hyperphosphorylation through Inhibition of Phosphatase Activity by Hypothermia." The Journal of Neuroscience **27**(12): 3090-3097.

Pocock, J. M. and H. Kettenmann (2007). "Neurotransmitter receptors on microglia." Trends in Neurosciences **30**(10): 527-535.

Poorkaj, P., T. D. Bird, E. Wijsman, E. Nemens, R. M. Garruto, L. Anderson, A. Andreadis, W. C. Wiederholt, M. Raskind and G. D. Schellenberg (1998). "Tau is a candidate gene for chromosome 17 frontotemporal dementia." Annals of Neurology **43**(6): 815-825.

Pope, W. B., M. P. Lambert, B. Leypold, R. Seupaul, L. Sletten, G. Krafft and W. L. Klein (1994). "Microtubule-Associated Protein Tau Is Hyperphosphorylated during

Mitosis in the Human Neuroblastoma Cell Line SH-SY5Y." Experimental Neurology **126**(2): 185-194.

Previll, L. A., M. E. Crosby, R. J. Castellani, R. Bowser, G. Perry, M. A. Smith and X. Zhu (2007). "Increased Expression of p130 in Alzheimer Disease." Neurochemical Research **32**(4): 639-644.

Price, J. L. and J. C. Morris (1999). "Tangles and plaques in nondemented aging and "preclinical" Alzheimer's disease." Ann Neurol **45**(3): 358-368.

Probst, A., J. Götz, K. H. Wiederhold, M. Tolnay, C. Mistl, A. L. Jaton, M. Hong, T. Ishihara, V. M. Lee, J. Q. Trojanowski, R. Jakes, R. A. Crowther, M. G. Spillantini, K. Bürki and M. Goedert (2000). "Axonopathy and amyotrophy in mice transgenic for human four-repeat tau protein." Acta neuropathologica **99**(5): 469-481.

Prusiner, S. B. (1982). "Novel proteinaceous infectious particles cause scrapie." Science **216**(4542): 136.

Quan, N., E. L. Stern, M. B. Whiteside and M. Herkenham (1999). "Induction of pro-inflammatory cytokine mRNAs in the brain after peripheral injection of subseptic doses of lipopolysaccharide in the rat." Journal of Neuroimmunology **93**(1): 72-80.

Quimby, J. M., F. Olea-Popelka and M. R. Lappin (2009). "Comparison of Digital Rectal and Microchip Transponder Thermometry in Cats." Journal of the American Association for Laboratory Animal Science : JAALAS **48**(4): 402-404.

Raftery, A. E. (1995). "Bayesian model selection in social research." Sociological methodology: 111-163.

Raina, A. K., M. J. Monteiro, A. McShea and M. A. Smith (1999). "The role of cell cycle-mediated events in Alzheimer's disease." International Journal of Experimental Pathology **80**(2): 71-76.

Raina, A. K., P. Pardo, C. A. Rottkamp, X. Zhu, O. M. Pereira-Smith and M. A. Smith (2001). "Neurons in Alzheimer disease emerge from senescence." Mechanisms of Ageing and Development **123**(1): 3-9.

Raina, A. K., X. Zhu, M. Monteiro, A. Takeda and M. A. Smith (2000). Abortive oncogeny and cell cycle-mediated events in Alzheimer disease. Progress in Cell Cycle Research. L. Meijer, A. Jézéquel and B. Ducommun. Boston, MA, Springer US**:** 235-242.

Ramsden, M., L. Kotilinek, C. Forster, J. Paulson, E. McGowan, K. SantaCruz, A. Guimaraes, M. Yue, J. Lewis, G. Carlson, M. Hutton and K. H. Ashe (2005). "Age-Dependent Neurofibrillary Tangle Formation, Neuron Loss, and Memory

Impairment in a Mouse Model of Human Tauopathy (P301L)." The Journal of Neuroscience **25**(46): 10637.

Ransohoff, R. M. (2016). "A polarizing question: do M1 and M2 microglia exist?" Nature neuroscience **19**(8): 987-991.

Ren, L., B. Lubrich, K. Biber and P. J. Gebicke-Haerter (1999). "Differential expression of inflammatory mediators in rat microglia cultured from different brain regions." Brain Res Mol Brain Res **65**(2): 198-205.

Reynolds, C. H., M. A. Utton, G. M. Gibb, A. Yates and B. H. Anderton (1997). "Stress-activated protein kinase/c-Jun N-terminal kinase phosphorylates τ protein." Journal of Neurochemistry **68**(4): 1736-1744.

Ricciarelli, R., C. d'Abramo, S. Massone, U. M. Marinari, M. A. Pronzato and M. Tabaton (2004). "Microarray Analysis in Alzheimer's Disease and Normal Aging." IUBMB Life **56**(6): 349-354.

Roberts, W. W., W. N. Dember and M. Brodwick (1962). "Alternation and exploration in rats with hippocampal lesions." Journal of Comparative and Physiological Psychology **55**(5): 695-700.

Robertsson, B., K. Blennow, C. G. Gottfries and A. Wallin (1998). "Delirium in dementia." Int J Geriatr Psychiatry **13**(1): 49-56.

Rockwood, K., S. Cosway, D. Carver, P. Jarrett, K. Stadnyk and J. Fisk (1999). "The risk of dementia and death after delirium." Age Ageing **28**(6): 551-556.

Rodriguez-Callejas, J. D., E. Fuchs and C. Perez-Cruz (2016). "Evidence of tau hyperphosphorylation and dystrophic microglia in the common marmoset." Frontiers in Aging Neuroscience **8**(DEC).

Roe, A. D., M. A. Staup, J. Serrats, P. E. Sawchenko and R. A. Rissman (2011). "Lipopolysaccharide-induced tau phosphorylation and kinase activity – modulation, but not mediation, by corticotropin-releasing factor receptors." European Journal of Neuroscience **34**(3): 448-456.

Rogers, J., L. C. Kirby, S. R. Hempelman, D. L. Berry, P. L. McGeer, A. W. Kaszniak, J. Zalinski, M. Cofield, L. Mansukhani and P. Willson (1993). "Clinical trial of indomethacin in Alzheimer's disease." Neurology **43**(8): 1609-1611.

Rogers, J., J. Luber-Narod, S. D. Styren and W. H. Civin (1988). "Expression of immune system-associated antigens by cells of the human central nervous system: Relationship to the pathology of Alzheimer's disease." Neurobiology of Aging **9**: 339-349.

Röhl, C., R. Lucius and J. Sievers (2007). "The effect of activated microglia on astrogliosis parameters in astrocyte cultures." Brain Research **1129**: 43-52.

Romanovsky, A. A. (2000). "Thermoregulatory manifestations of systemic inflammation: lessons from vagotomy." Auton Neurosci **85**(1-3): 39-48.

Romanovsky, A. A. (2004). "Signaling the brain in the early sickness syndrome: are sensory nerves involved." Front Biosci **9**: 494-504.

Rosenmann, H., N. Grigoriadis, H. Eldar-Levy, A. Avital, L. Rozenstein, O. Touloumi, L. Behar, T. Ben-Hur, Y. Avraham, E. Berry, M. Segal, I. Ginzburg and O. Abramsky (2008). "A novel transgenic mouse expressing double mutant tau driven by its natural promoter exhibits tauopathy characteristics." Experimental Neurology **212**(1): 71-84.

Rosenzweig, H. L., N. S. Lessov, D. C. Henshall, M. Minami, R. P. Simon and M. P. Stenzel-Poore (2004). "Endotoxin Preconditioning Prevents Cellular Inflammatory Response During Ischemic Neuroprotection in Mice." Stroke **35**(11): 2576-2581.

Rőszer, T. (2015). "Understanding the Mysterious M2 Macrophage through Activation Markers and Effector Mechanisms." Mediators of Inflammation **2015**: 16.

Roth, J. and G. E. P. De Souza (2001). "Fever induction pathways: Evidence from responses to systemic or local cytokine formation." Brazilian Journal of Medical and Biological Research **34**(3): 301-314.

Rotshenker, S. (2009). "The Role of Galectin-3/MAC-2 in the Activation of the Innate-Immune Function of Phagocytosis in Microglia in Injury and Disease." Journal of Molecular Neuroscience **39**(1): 99-103.

Roubenoff, R. (2000). "Sarcopenia and its implications for the elderly." Eur J Clin Nutr **54 Suppl 3**: S40-47.

Rudaya, A. Y., A. A. Steiner, J. R. Robbins, A. S. Dragic and A. A. Romanovsky (2005). "Thermoregulatory responses to lipopolysaccharide in the mouse: dependence on the dose and ambient temperature." American Journal of Physiology - Regulatory, Integrative and Comparative Physiology **289**(5): R1244-R1252.

Sahara, N., S. Maeda, M. Murayama, T. Suzuki, N. Dohmae, S. H. Yen and A. Takashima (2007). "Assembly of two distinct dimers and higher-order oligomers from full-length tau." Eur J Neurosci **25**(10): 3020-3029.

Sajja, V. S. S. S., N. Hlavac and P. J. VandeVord (2016). "Role of Glia in Memory Deficits Following Traumatic Brain Injury: Biomarkers of Glia Dysfunction." Frontiers in Integrative Neuroscience **10**(7).

Sakamoto, T., K. Arissian and H. Asanuma (1989). "Functional role of the sensory cortex in learning motor skills in cats." Brain Research **503**(2): 258-264.

SantaCruz, K., J. Lewis, T. Spires, J. Paulson, L. Kotilinek, M. Ingelsson, A. Guimaraes, M. DeTure, M. Ramsden, E. McGowan, C. Forster, M. Yue, J. Orne, C. Janus, A. Mariash, M. Kuskowski, B. Hyman, M. Hutton and K. H. Ashe (2005). "Tau Suppression in a Neurodegenerative Mouse Model Improves Memory Function." Science **309**(5733): 476.

Sasaki, A., T. Kawarabayashi, T. Murakami, E. Matsubara, M. Ikeda, H. Hagiwara, D. Westaway, P. S. George-Hyslop, M. Shoji and Y. Nakazato (2008). "Microglial activation in brain lesions with tau deposits: Comparison of human tauopathies and tau transgenic mice TgTauP301L." Brain Research **1214**: 159-168.

Sasaki, N., R. Fukatsu, K. Tsuzuki, Y. Hayashi, T. Yoshida, N. Fujii, T. Koike, I. Wakayama, R. Yanagihara, R. Garruto, N. Amano and Z. Makita (1998). "Advanced glycation end products in Alzheimer's disease and other neurodegenerative diseases." American Journal of Pathology **153**(4): 1149-1155.

Sastre, M., I. Dewachter, G. E. Landreth, T. M. Willson, T. Klockgether, F. van Leuven and M. T. Heneka (2003). "Nonsteroidal Anti-Inflammatory Drugs and Peroxisome Proliferator-Activated Receptor-γ Agonists Modulate Immunostimulated Processing of Amyloid Precursor Protein through Regulation of β-Secretase." The Journal of Neuroscience **23**(30): 9796.

Scattoni, M. L., J. Crawley and L. Ricceri (2009). "Ultrasonic vocalizations: a tool for behavioural phenotyping of mouse models of neurodevelopmental disorders." Neuroscience and biobehavioral reviews **33**(4): 508-515.

Scattoni, M. L., L. Gasparini, E. Alleva, M. Goedert, G. Calamandrei and M. G. Spillantini (2010). "Early behavioural markers of disease in P301S tau transgenic mice." Behavioural brain research **208**(1): 250-257.

Schindelin, J., I. Arganda-Carreras, E. Frise, V. Kaynig, M. Longair, T. Pietzsch, S. Preibisch, C. Rueden, S. Saalfeld and B. Schmid (2012). "Fiji: an open-source platform for biological-image analysis." Nature methods **9**(7): 676-682.

Schindler, R., P. Ghezzi and C. A. Dinarello (1990). "IL-1 induces IL-1. IV. IFN-gamma suppresses IL-1 but not lipopolysaccharide-induced transcription of IL-1." The Journal of Immunology **144**(6): 2216-2222.

Schindowski, K., K. Belarbi, A. Bretteville, K. Ando and L. Buee (2008). "Neurogenesis and cell cycle-reactivated neuronal death during pathogenic tau aggregation." Genes Brain Behav **7 Suppl 1**: 92-100.

Schindowski, K., A. Bretteville, K. Leroy, S. Bégard, J.-P. Brion, M. Hamdane and L. Buée (2006). "Alzheimer's Disease-Like Tau Neuropathology Leads to Memory Deficits and Loss of Functional Synapses in a Novel Mutated Tau Transgenic Mouse without Any Motor Deficits." The American Journal of Pathology **169**(2): 599-616.

Schneider, C. A. R., W. S. & Eliceiri, K. W. (2012). "NIH Image to ImageJ: 25 years of image analysis." Nature methods **9**(7): 671-675.

Schwab, C., A. Klegeris and P. L. McGeer (2010). "Inflammation in transgenic mouse models of neurodegenerative disorders." Biochimica et Biophysica Acta (BBA) - Molecular Basis of Disease **1802**(10): 889-902.

Selkoe, D. J. (2002). "Alzheimer's disease is a synaptic failure." Science **298**(5594): 789-791.

Selmaj, K., B. Shafit-Zagardo, D. A. Aquino, M. Farooq, C. S. Raine, W. T. Norton and C. F. Brosnan (1991). "Tumor Necrosis Factor-Induced Proliferation of Astrocytes from Mature Brain Is Associated with Down-Regulation of Glial Fibrillary Acidic Protein mRNA." Journal of Neurochemistry **57**(3): 823-830.

Semmler, A., T. Okulla, M. Sastre, L. Dumitrescu-Ozimek and M. T. Heneka (2005). "Systemic inflammation induces apoptosis with variable vulnerability of different brain regions." Journal of Chemical Neuroanatomy **30**(2–3): 144-157.

Sheng, J. G., S. H. Bora, G. Xu, D. R. Borchelt, D. L. Price and V. E. Koliatsos (2003). "Lipopolysaccharide-induced-neuroinflammation increases intracellular accumulationof amyloid precursor protein and amyloid beta peptide in APPswe transgenic mice." Neurobiol Dis **14**.

Sheng, J. G., R. E. Mrak and W. S. T. Griffin (1997). "Glial-Neuronal Interactions in Alzheimer Disease: Progressive Association of IL-1α Microglia and S100β Astrocytes with Neurofibrillary Tangle Stages." Journal of Neuropathology & Experimental Neurology **56**(3): 285.

Shnyra, A., R. Brewington, A. Alipio, C. Amura and D. C. Morrison (1998). "Reprogramming of Lipopolysaccharide-Primed Macrophages Is Controlled by a Counterbalanced Production of IL-10 and IL-12." The Journal of Immunology **160**(8): 3729-3736.

Simon, M. M., S. Greenaway, J. K. White, H. Fuchs, V. Gailus-Durner, S. Wells, T. Sorg, K. Wong, E. Bedu, E. J. Cartwright, R. Dacquin, S. Djebali, J. Estabel, J. Graw, N. J. Ingham, I. J. Jackson, A. Lengeling, S. Mandillo, J. Marvel, H. Meziane, F. Preitner, O. Puk, M. Roux, D. J. Adams, S. Atkins, A. Ayadi, L. Becker, A. Blake, D. Brooker, H. Cater, M. F. Champy, R. Combe, P. Danecek, A. di Fenza, H. Gates, A. K. Gerdin, E. Golini, J. M. Hancock, W. Hans, S. M. Holter, T. Hough, P. Jurdic, T. M. Keane, H.

Morgan, W. Muller, F. Neff, G. Nicholson, B. Pasche, L. A. Roberson, J. Rozman, M. Sanderson, L. Santos, M. Selloum, C. Shannon, A. Southwell, G. P. Tocchini-Valentini, V. E. Vancollie, H. Westerberg, W. Wurst, M. Zi, B. Yalcin, R. Ramirez-Solis, K. P. Steel, A. M. Mallon, M. H. de Angelis, Y. Herault and S. D. Brown (2013). "A comparative phenotypic and genomic analysis of C57BL/6J and C57BL/6N mouse strains." Genome Biol **14**(7): R82.

Singaraja, R. R. (2013). "TREM2: a new risk factor for Alzheimer's disease." Clinical Genetics **83**(6): 525-526.

Sly, L. M., R. F. Krzesicki, J. R. Brashler, A. E. Buhl, D. D. McKinley, D. B. Carter and J. E. Chin (2001). "Endogenous brain cytokine mRNA and inflammatory responses to lipopolysaccharide are elevated in the Tg2576 transgenic mouse model of Alzheimer's disease." Brain Res Bull **56**(6): 581-588.

Smith, A. M., H. M. Gibbons, R. L. Oldfield, P. M. Bergin, E. W. Mee, M. A. Curtis, R. L. Faull and M. Dragunow (2013). "M-CSF increases proliferation and phagocytosis while modulating receptor and transcription factor expression in adult human microglia." J Neuroinflammation **10**: 85.

Smith, T. W. and C. F. Lippa (1995). "Ki-67 Immunoreactivity in Alzheimer's Disease and Other Neurodegenerative Disorders." Journal of Neuropathology & Experimental Neurology **54**(3): 297.

Snowden, J. S., D. Neary and M. M. D (2002). "Frontotemporal dementia." Frontotemporal dementia.

Sofroniew, M. V. (2009). "Molecular dissection of reactive astrogliosis and glial scar formation." Trends Neurosci **32**(12): 638-647.

Sofroniew, M. V. and H. V. Vinters (2010). "Astrocytes: biology and pathology." Acta Neuropathologica **119**(1): 7-35.

Solà, C., J. M. Tusell and J. Serratosa (1999). "Comparative study of the distribution of calmodulin kinase II and calcineurin in the mouse brain." Journal of Neuroscience Research **57**(5): 651-662.

Sorger, P. K., M. Dobles, R. Tournebize and A. A. Hyman (1997). "Coupling cell division and cell death to microtubule dynamics." Current opinion in cell biology **9**(6): 807-814.

Sparkman, N. L., L. A. Martin, W. S. Calvert and G. W. Boehm (2005). "Effects of intraperitoneal lipopolysaccharide on Morris maze performance in year-old and 2-month-old female C57BL/6J mice." Behav Brain Res **159**.

Spillantini, M. G. and M. Goedert (2013). "Tau pathology and neurodegeneration." The Lancet Neurology **12**(6): 609-622.

Spillantini, M. G., J. R. Murrell, M. Goedert, M. R. Farlow, A. Klug and B. Ghetti (1998). "Mutation in the tau gene in familial multiple system tauopathy with presenile dementia." Proceedings of the National Academy of Sciences **95**(13): 7737-7741.

Spires-Jones, T. L., J. Attems and D. R. Thal (2017). "Interactions of pathological proteins in neurodegenerative diseases." Acta Neuropathol **134**(2): 187-205.

Spittaels, K., C. Van den Haute, J. Van Dorpe, K. Bruynseels, K. Vandezande, I. Laenen, H. Geerts, M. Mercken, R. Sciot, A. Van Lommel, R. Loos and F. Van Leuven (1999). "Prominent Axonopathy in the Brain and Spinal Cord of Transgenic Mice Overexpressing Four-Repeat Human tau Protein." The American Journal of Pathology **155**(6): 2153-2165.

Sriram, K., S. A. Benkovic, D. B. Miller and J. P. O'Callaghan (2002). "Obesity exacerbates chemically induced neurodegeneration." Neuroscience **115**(4): 1335-1346.

Sriram, K., J. M. Matheson, S. A. Benkovic, D. B. Miller, M. I. Luster and J. P. O'Callaghan (2006). "Deficiency of TNF receptors suppresses microglial activation and alters the susceptibility of brain regions to MPTP-induced neurotoxicity: role of TNF-α." The FASEB Journal **20**(6): 670-682.

Stephens Devalle, J. M. (2005). "Comparison of tympanic, transponder, and noncontact infrared laser thermometry with rectal thermometry in strain 13 guinea pigs (Cavia porcellus)." Contemp Top Lab Anim Sci **44**(5): 35-38.

Stevens, B., N. J. Allen, L. E. Vazquez, G. R. Howell, K. S. Christopherson, N. Nouri, K. D. Micheva, A. K. Mehalow, A. D. Huberman, B. Stafford, A. Sher, A. M. Litke, J. D. Lambris, S. J. Smith, S. W. John and B. A. Barres (2007). "The classical complement cascade mediates CNS synapse elimination." Cell **131**(6): 1164-1178.

Streit, W. J., H. Braak, Q. S. Xue and I. Bechmann (2009). "Dystrophic (senescent) rather than activated microglial cells are associated with tau pathology and likely precede neurodegeneration in Alzheimer's disease." Acta Neuropathol **118**(4): 475-485.

Streit, W. J., N. W. Sammons, A. J. Kuhns and D. L. Sparks (2004). "Dystrophic microglia in the aging human brain." Glia **45**(2): 208-212.

Suk, K., S. Y. Kim and H. Kim (2002). "Essential role of caspase-11 in activation-induced cell death of rat astrocytes." Journal of Neurochemistry **80**(2): 230-238.

Suntharalingam, G., M. R. Perry, S. Ward, S. J. Brett, A. Castello-Cortes, M. D. Brunner and N. Panoskaltsis (2006). "Cytokine Storm in a Phase 1 Trial of the Anti-CD28 Monoclonal Antibody TGN1412." New England Journal of Medicine **355**(10): 1018-1028.

Sy, M., M. Kitazawa, R. Medeiros, L. Whitman, D. Cheng, T. E. Lane and F. M. Laferla (2011). "Inflammation induced by infection potentiates tau pathological features in transgenic mice." Am J Pathol **178**(6): 2811-2822.

Szekely, C. A., J. E. Thorne, P. P. Zandi, M. Ek, E. Messias, J. C. S. Breitner and S. N. Goodman (2004). "Nonsteroidal Anti-Inflammatory Drugs for the Prevention of Alzheimer's Disease: A Systematic Review." Neuroepidemiology **23**(4): 159-169.

Takata, K., Y. Kitamura, D. Yanagisawa, S. Morikawa, M. Morita, T. Inubushi, D. Tsuchiya, S. Chishiro, M. Saeki, T. Taniguchi, S. Shimohama and I. Tooyama (2007). "Microglial transplantation increases amyloid-β clearance in Alzheimer model rats." FEBS Letters **581**(3): 475-478.

Tandon, P., Y. Yang, K. Das, G. L. Holmes and C. E. Stafstrom (1999). "Neuroprotective effects of brain-derived neurotrophic factor in seizures during development." Neuroscience **91**(1): 293-303.

Tanemura, K., T. Akagi, M. Murayama, N. Kikuchi, O. Murayama, T. Hashikawa, Y. Yoshiike, J.-M. Park, K. Matsuda, S. Nakao, X. Sun, S. Sato, H. Yamaguchi and A. Takashima (2001). "Formation of Filamentous Tau Aggregations in Transgenic Mice Expressing V337M Human Tau." Neurobiology of Disease **8**(6): 1036-1045.

Tanemura, K., M. Murayama, T. Akagi, T. Hashikawa, T. Tominaga, M. Ichikawa, H. Yamaguchi and A. Takashima (2002). "Neurodegeneration with Tau Accumulation in a Transgenic Mouse Expressing V337M Human Tau." The Journal of Neuroscience **22**(1): 133-141.

Tatebayashi, Y., T. Miyasaka, D.-H. Chui, T. Akagi, K.-i. Mishima, K. Iwasaki, M. Fujiwara, K. Tanemura, M. Murayama, K. Ishiguro, E. Planel, S. Sato, T. Hashikawa and A. Takashima (2002). "Tau filament formation and associative memory deficit in aged mice expressing mutant (R406W) human tau." Proceedings of the National Academy of Sciences **99**(21): 13896-13901.

Teeling, J. L., C. Cunningham, T. A. Newman and V. H. Perry (2010). "The effect of non-steroidal anti-inflammatory agents on behavioural changes and cytokine production following systemic inflammation: Implications for a role of COX-1." Brain Behav Immun **24**.

Teige, I., A. Treschow, A. Teige, R. Mattsson, V. Navikas, T. Leanderson, R. Holmdahl and S. Issazadeh-Navikas (2003). "IFN-β gene deletion leads to augmented and

chronic demyelinating experimental autoimmune encephalomyelitis." Journal of Immunology **170**(9): 4776-4784.

Terrando, N., L. I. Eriksson, J. K. Ryu, T. Yang, C. Monaco, M. Feldmann, M. Jonsson Fagerlund, I. F. Charo, K. Akassoglou and M. Maze (2011). "Resolving postoperative neuroinflammation and cognitive decline." Ann Neurol **70**(6): 986-995.

Terry, R. D., E. Masliah, D. P. Salmon, N. Butters, R. DeTeresa, R. Hill, L. A. Hansen and R. Katzman (1991). "Physical basis of cognitive alterations in Alzheimer's disease: synapse loss is the major correlate of cognitive impairment." Ann Neurol **30**(4): 572-580.

Terwel, D., R. Lasrado, J. Snauwaert, E. Vandeweert, C. Van Haesendonck, P. Borghgraef and F. Van Leuven (2005). "Changed Conformation of Mutant Tau-P301L Underlies the Moribund Tauopathy, Absent in Progressive, Nonlethal Axonopathy of Tau-4R/2N Transgenic Mice." Journal of Biological Chemistry **280**(5): 3963-3973.

Tobinick, E. L. (2008). "Re: Inflammatory markers and the risk of Alzheimer disease: the Framingham Study." Neurology **70**(14): 1222-1223; author reply 1223.

Togo, T., H. Akiyama, E. Iseki, H. Kondo, K. Ikeda, M. Kato, T. Oda, K. Tsuchiya and K. Kosaka (2002). "Occurrence of T cells in the brain of Alzheimer's disease and other neurological diseases." Journal of Neuroimmunology **124**(1–2): 83-92.

Torvell, M., D. W. Hampton, C. Cunningham, A. M. Maclullich and S. Chandran (2013). "Early Behavioural Differences in P301S Mice which Precede Tau Pathology and Neurodegeneration - MSc by Research in Integrative Neuroscience."

Tsoni, S. V. and G. D. Brown (2008). "β-Glucans and Dectin-1." Annals of the New York Academy of Sciences **1143**(1): 45-60.

Ueno, M., Y. Fujita, T. Tanaka, Y. Nakamura, J. Kikuta, M. Ishii and T. Yamashita (2013). "Layer V cortical neurons require microglial support for survival during postnatal development." Nature neuroscience **16**(5): 543-551.

Ueno, R., S. Narumiya, T. Ogorochi, T. Nakayama, Y. Ishikawa and O. Hayaishi (1982). "Role of prostaglandin D2 in the hypothermia of rats caused by bacterial lipopolysaccharide." Proc Natl Acad Sci U S A **79**(19): 6093-6097.

Vincent, I., G. Jicha, M. Rosado and D. W. Dickson (1997). "Aberrant expression of mitotic cdc2/cyclin B1 kinase in degenerating neurons of Alzheimer's disease brain." Journal of Neuroscience **17**(10): 3588-3598.

Vincent, I., C. I. Pae and J. L. Hallows (2002). "The cell cycle and human neurodegenerative disease." Progress in cell cycle research **5**: 31-41.

Vulliet, R., S. M. Halloran, R. K. Braun, A. J. Smith and G. Lee (1992). "Proline-directed phosphorylation of human Tau protein." Journal of Biological Chemistry **267**(31): 22570-22574.

Wang, D. B., R. D. Dayton, R. M. Zweig and R. L. Klein (2010a). "Transcriptome analysis of a tau overexpression model in rats implicates an early pro-inflammatory response." Experimental Neurology **224**(1): 197-206.

Wang, J.-Z., Z.-H. Wang and Q. Tian (2014). "Tau hyperphosphorylation induces apoptotic escape and triggers neurodegeneration in Alzheimer's disease." Neuroscience Bulletin **30**(2): 359-366.

Wang, R., B. Yang and D. Zhang (2011). "Activation of interferon signaling pathways in spinal cord astrocytes from an ALS mouse model." Glia **59**(6): 946-958.

Wang, Z. F., J. Yin, Y. Zhang, L. Q. Zhu, Q. Tian, X. C. Wang, H. L. Li and J. Z. Wang (2010b). "Overexpression of tau proteins antagonizes amyloid-beta-potentiated apoptosis through mitochondria-caspase-3 pathway in N2a cells." J Alzheimers Dis **20**(1): 145-157.

Weggen, S., J. L. Eriksen, P. Das, S. A. Sagi, R. Wang, C. U. Pietrzik, K. A. Findlay, T. E. Smith, M. P. Murphy, T. Bulter, D. E. Kang, N. Marquez-Sterling, T. E. Golde and E. H. Koo (2001). "A subset of NSAIDs lower amyloidogenic A[beta]42 independently of cyclooxygenase activity." Nature **414**(6860): 212-216.

Weiland, T. J., N. J. Voudouris and S. Kent (2007). "CCK₂ receptor nullification attenuates lipopolysaccharide-induced sickness behavior." American Journal of Physiology - Regulatory, Integrative and Comparative Physiology **292**(1): R112-R123.

Weiler, N., L. Wood, J. Yu, S. A. Solla and G. M. G. Shepherd (2008). "Top-down laminar organization of the excitatory network in motor cortex." Nat Neurosci **11**(3): 360-366.

Weinger, J. G., C. F. Brosnan, O. Loudig, M. F. Goldberg, F. Macian, H. A. Arnett, A. L. Prieto, V. Tsiperson and B. Shafit-Zagardo (2011). "Loss of the receptor tyrosine kinase Axl leads to enhanced inflammation in the CNS and delayed removal of myelin debris during Experimental Autoimmune Encephalomyelitis." Journal of Neuroinflammation **8**(1): 49.

West, M. J. (2012). "Basic stereology for biologists and neuroscientists."

Wimo, A., M. Guerchet, G.-C. Ali, Y.-T. Wu, A. M. Prina, B. Winblad, L. Jönsson, Z. Liu and M. Prince (2017). "The worldwide costs of dementia 2015 and comparisons with 2010." Alzheimer's & Dementia **13**(1): 1-7.

Wisniewski, H. M., M. Barcikowska and E. Kida (1991). "Phagocytosis of β/A4 amyloid fibrils of the neuritic neocortical plaques." Acta Neuropathologica **81**(5): 588-590.

Witlox, J., L. S. Eurelings, J. F. de Jonghe, K. J. Kalisvaart, P. Eikelenboom and W. A. Van Gool (2010). "Delirium in elderly patients and the risk of postdischarge mortality, institutionalization, and dementia: a meta-analysis." Jama **304**(4): 443-451.

Wohlfart, G. (1958). "Collateral regeneration in partially denervated muscles." Neurology **8**(3): 175-180.

Wöhr, M. and R. K. W. Schwarting. (2015). "Ultrasonic vocalizations as a tool for research on emotion and motivation in rodents." 2017, from http://www.avisoft.com/rats.htm.

Wong, D., K. Dorovini-Zis and S. R. Vincent (2004). "Cytokines, nitric oxide, and cGMP modulate the permeability of an in vitro model of the human blood-brain barrier." Exp Neurol **190**(2): 446-455.

Wright, S. D., R. A. Ramos, P. S. Tobias, R. J. Ulevitch and J. C. Mathison (1990). "CD14, a receptor for complexes of lipopolysaccharide (LPS) and LPS binding protein." Science **249**(4975): 1431-1433.

Wright, S. D., P. S. Tobias, R. J. Ulevitch and R. A. Ramos (1989). "Lipopolysaccharide (LPS) binding protein opsonizes LPS-bearing particles for recognition by a novel receptor on macrophages." Journal of Experimental Medicine **170**(4): 1231-1241.

Wu, Y.-T., L. Fratiglioni, F. E. Matthews, A. Lobo, M. M. B. Breteler, I. Skoog and C. Brayne (2016). "Dementia in western Europe: epidemiological evidence and implications for policy making." The Lancet Neurology **15**(1): 116-124.

Wynne, A. M., C. J. Henry, Y. Huang, A. Cleland and J. P. Godbout (2010). "Protracted downregulation of CX3CR1 on microglia of aged mice after lipopolysaccharide challenge." Brain, Behavior, and Immunity **24**(7): 1190-1201.

Xie, Z., C. J. Smith and L. J. Van Eldik (2004). "Activated glia induce neuron death via MAP kinase signaling pathways involving JNK and p38." Glia **45**(2): 170-179.

Xu, H., T. W. Rösler, T. Carlsson, A. de Andrade, J. Bruch, M. Höllerhage, W. H. Oertel and G. U. Höglinger (2014). "Memory deficits correlate with tau and spine pathology in P301S MAPT transgenic mice." Neuropathology and Applied Neurobiology **40**(7): 833-843.

Xue, Q.-S. and W. J. Streit (2011). "Microglial pathology in Down syndrome." Acta Neuropathologica **122**(4): 455.

Yaffe, K., A. Kanaya, K. Lindquist, E. M. Simonsick, T. Harris, R. I. Shorr, F. A. Tylavsky and A. B. Newman (2004). "The metabolic syndrome, inflammation, and risk of cognitive decline." Jama **292**(18): 2237-2242.

Yanamoto, H., J.-H. Xue, S. Miyamoto, I. Nagata, Y. Nakano, K. Murao and H. Kikuchi (2004). "Spreading depression induces long-lasting brain protection against infarcted lesion development via BDNF gene-dependent mechanism." Brain Research **1019**(1–2): 178-188.

Yata, K., S. Oikawa, R. Sasaki, A. Shindo, R. Yang, M. Murata, K. Kanamaru and H. Tomimoto (2011). "Astrocytic neuroprotection through induction of cytoprotective molecules; a proteomic analysis of mutant P301S tau-transgenic mouse." Brain Research **1410**: 12-23.

Yoshiyama, Y., M. Higuchi, B. Zhang, S. Huang, N. Iwata, T. Saido, J. Maedam, T. Suhara, J. Trojanowski and V. Lee (2007). "Synapse loss and microglial activation precede tangles in a P301S tauopathy mouse model." Neuron **53**(3): 337-351.

Zamanian, J. L., L. Xu, L. C. Foo, N. Nouri, L. Zhou, R. G. Giffard and B. A. Barres (2012). "Genomic Analysis of Reactive Astrogliosis." The Journal of Neuroscience **32**(18): 6391-6410.

Zdanys, K. F., A. F. Carvalho, R. R. Tampi and D. C. Steffens (2016). "The Treatment of Behavioral and Psychological Symptoms of Dementia: Weighing Benefits and Risks." Curr Alzheimer Res **13**(10): 1124-1133.

Zhang, B., M. Higuchi, Y. Yoshiyama, T. Ishihara, M. S. Forman, D. Martinez, S. Joyce, J. Q. Trojanowski and V. M.-Y. Lee (2004). "Retarded Axonal Transport of R406W Mutant Tau in Transgenic Mice with a Neurodegenerative Tauopathy." The Journal of Neuroscience **24**(19): 4657-4667.

Zhao, J., Z. Lv, F. Wang, J. Wei, Q. Zhang, S. Li, F. Yang, X. Zeng, X. Wu and Z. Wu (2013). "Ym1, an eosinophilic chemotactic factor, participates in the brain inflammation induced by Angiostrongylus cantonensis in mice." Parasitology Research **112**(7): 2689-2695.

Zheng-Fischhöfer, Q., J. Biernat, E. M. Mandelkow, S. Illenberger, R. Godemann and E. Mandelkow (1998). "Sequential phosphorylation of Tau by glycogen synthase kinase-3β and protein kinase A at Thr212 and Ser214 generates the Alzheimer-specific epitope of antibody AT100 and requires a paired-helical-filament-like conformation." European Journal of Biochemistry **252**(3): 542-552.

Zhou, F., X. Zhu, R. J. Castellani, R. Stimmelmayr, G. Perry, M. A. Smith and K. L. Drew (2001). "Hibernation, a Model of Neuroprotection." The American Journal of Pathology **158**(6): 2145-2151.

Zhou, X.-F. and R. A. Rush (1994). "Localization of neurotrophin-3-like immunoreactivity in the rat central nervous system." Brain Research **643**(1–2): 162-172.

Zilka, N., P. Filipcik, P. Koson, L. Fialova, R. Skrabana, M. Zilkova, G. Rolkova, E. Kontsekova and M. Novak (2006). "Truncated tau from sporadic Alzheimer's disease suffices to drive neurofibrillary degeneration in vivo." FEBS Letters **580**(15): 3582-3588.

Zilka, N., Z. Stozicka, A. Kovac, E. Pilipcinec, O. Bugos and M. Novak (2009). "Human misfolded truncated tau protein promotes activation of microglia and leukocyte infiltration in the transgenic rat model of tauopathy." Journal of Neuroimmunology **209**(1): 16-25.

Zilkova, M., N. Zilka, A. Kovac, B. Kovacech, R. Skrabana, M. Skrabanova and M. Novak (2011). "Hyperphosphorylated truncated protein tau induces caspase-3 independent apoptosis-like pathway in the Alzheimer's disease cellular model." J Alzheimers Dis **23**(1): 161-169.